AD NUMBER: AD0484064

LIMITATION CHANGES

TO:

Approved for public release; distribution is unlimited.

FROM:

Distribution authorized to U.S. Gov't. agencies and their contractors; Export Control; 1 May 1966. Other requests shall be referred to the Air Force Rome Air Development Center, Griffiss AFB, NY 13440.

AUTHORITY

17 SEP 1971, RADC USAF LTR

RADC-TR-66-207
Final Report

TRANSITIONS FOR PERIODIC FILTERS

John P. Rooney
Richard Z. Gerlack
Hans J. Mohr

Varian Associates

TECHNICAL REPORT NO. RADC-TR-66-207

May 1966

Rome Air Development Center
Research and Technology Division
Air Force Systems Command
Griffiss Air Force Base, New York

TRANSITIONS FOR PERIODIC FILTERS

John P. Rooney
Richard Z. Gerlack
Hans J. Mohr

Varian Associates

AFLC, GAFB, N.Y., 20 June 66-173

FOREWARD

This final report was prepared by Varian Associates, 601 California Avenue, Palo Alto, California, on Contract AF 30(602)-3556, Project 4540, Task 454003, for the Rome Air Development Center, Griffiss Air Force Base, New York.

The research program described in this document was begun in December 1964 and was concluded in February 1966. The Varian number designation of this report is 66CA0260-4.

This document is not releasable to the general public because it contains test and evaluation data relative to military systems and subsystems.

RADC Project Engineer is John J. McCabe (EMCVI-1).

This technical report has been reviewed and is approved.

John J. McCabe

Approved: JOHN J. MCCABE
Effort Engineer
Analysis & Prediction Group

Samuel D. Zaccari

Approved: for CHARLES A. STROM, JR.
Acting Chief
Communications Division

FOR THE COMMANDER:

IRVING J. GABELMAN
Chief, Advanced Studies Group

ABSTRACT

This report presents the results of a one year program for improvement of transitions between conventional transmission lines and periodic filters suitable for use on high power radars. General studies of transitions, filter design, and coupled periodic circuits are described. These studies were applied to a variety of filter structures and resulted in:

1. A novel higher order mode helix filter of high power capacity
2. A helix filter that operated satisfactorily in tests on an FPS-6 radar
3. A ladder filter with low loss and VSWR over a wide passband and high power capability.

The validity of the general studies was demonstrated and their conclusions can be extended to several applications of a variety of periodic structures.

EVALUATION

The objective of this effort was to develop transitions to couple slow wave open periodic filters to standard transmission lines, i.e., waveguide and coaxial. The primary design goals of the effort were to increase the transitions power handling capacity, and achieve a full 10% bandwidth by decreasing the transitions VSWR and insertion loss.

As a result of the effort, three very useful transitions were developed; two for the helix circuit and one for the thick ladder circuit. Several other transitions were also investigated for the thin ladder and yagi circuit but each had at least one serious shortcoming.

The transitions developed for the helix circuits exhibited an insertion loss of less than 0.2db, a VSWR less than 1.1 to 1 over more than a 200mc bandwidth at S-band. A breadboard S-band model incorporating the new transitions exhibited a basic filter power handling capacity of 1.3Mw. The filter successfully handled the maximum power output of the FPS-6 (5Mw) when pressurized with a high strength dielectric gas, and completely eliminated all the spurious signals generated by the FPS-6.

Similarly, the transitions developed for the higher order helix (-1 mode) and the ladder circuit exhibited low pass band loss and VSWR as well as very high power handling capacity.

John J. McCabe

JOHN J. MCCABE
Effort Engineer
Analysis & Prediction Group

CONTENTS

ILLUSTRATIONS

I. INTRODUCTION

This report describes the work performed on a one year program sponsored by the Rome Air Development Center under Contract AF 30(602)-3556. The broad objective of the program was to study the design requirements of the transitions connecting standard microwave transmission lines to open periodic transmission circuits functioning as filters. Such filters were studied during a preceding program under Contract AF 30(602)-2955, which was also sponsored by RADC. The filters operate on the principle that a periodic structure can support a propagating surface wave over certain bands of frequencies, while outside of these bands the energy radiates from the structure. Filters were constructed on the previous program which demonstrated the feasibility of the basic principle, but they were somewhat limited with respect to bandwidth, input VSWR, loss, and power handling capability. These limitations resulted in part from the difficulty encountered in making a transition from a closed fast wave transmission line to the open periodic structure. The reductions of these limitations on filter performance was a goal of the program of this report.

The program plan lists the following specific tasks and objectives:

1. Transitions shall be designed for at least the structures developed under Contract AF 30(602)-2955 as below:
   a. Waveguide to
      (1) Helix circuits
      (2) Interdigital ladder circuits
      (3) Open slot circuits
   b. Coaxial line to
      (1) Helix circuits
      (2) Interdigital open slot circuits.
2. The transitions shall have a maximum VSWR of 1.06 and a maximum loss of 0.1 db.

3. The power handling capacity of existing transitions will be surveyed. Research will be conducted to provide a minimum peak power handling capacity of 10 Mw.
4. Coupling to the slow wave rather than the fast wave modes in a transition structure will be investigated.
5. Breadboard models of transition structures designed for useful filter circuits will be tested at their rated power on a high power S-band source for a minimum of 40 hours.
6. One or more breadboard models of specific filters, utilizing the transition designs developed on this program, will be thoroughly tested at low power and then tested at high power in an operational radar. Originally the tests were to be performed on an AN/FPS-27 radar. However, this plan was changed and the testing was performed on an AN/FPS-6 radar. The AN/FPS-6 power level imposes higher peak power handling requirements on its components than almost any other radar, when waveguide size and dielectric strength are taken into consideration. Filters designed for the FPS-6 radar must have about twice the intrinsic or basic power capacity of those that would be used on the FPS-27 radar.

The work of the project was organized into the four phases described below.

Phase I, of six months duration, included the basic study and analysis of transition circuits. Specific areas of study included circuit configurations, mode coupling, and basic slow wave circuit parameters.

Phase II, of six months duration and starting with the beginning of the second quarter, was concerned with circuit configuration feasibility and the optimization of the circuit parameters with respect to power handling, loss, and VSWR. Experimental work in these areas was performed.

Phase III was concerned with transition design and was scheduled for the sixth through the eleventh month of the program. Design data and procedures were compiled and breadboard models were designed and constructed.

Phase IV was the high and low power testing of breadboard models, both in the field and in the laboratory. It was scheduled for the last quarter of the program.

The organization of this report generally follows the project plan. However, it is not strictly chronological. For example, experimental data and findings from the later phases have been incorporated, explicitly and implicitly, in the discussions of the general studies which were largely performed in the earlier phases.

Section II reviews the previous work on open periodic circuit filters. The basic theory is treated briefly and circuits exhibiting useful filter characteristics are illustrated. Periodic circuit parameters and various aspects of practical filter design are discussed.

Section III is a general treatment of transitions to open periodic circuits. The basic concepts which guided the design of specific transitions are discussed. The general transition studies pointed out the need to investigate the nature of open periodic circuits beyond the point achieved on the previous program, particularly in regard to determining the suitability of particular types of periodic circuits for high power filter application. These investigations are treated in Section IV.

Section V treats coupled line junctions which were investigated in some detail.

Section VI describes the experimental work done on helix filters and transitions. Design parameters are developed. The development and testing of breadboard models are described, including the field tests on an operating radar.

Section VII summarizes the design and experimental work performed on filters incorporating periodic structures other than helices.

This program resulted in transition improvements in the helix filter developed under the previous program. An operational filter was constructed which demonstrated satisfactory performance in an FPS-6 radar.

Also, a filter was developed which was novel in two respects: it utilized a higher order helix mode and its transition employed distributed coupling between transmission line modes. This filter demonstrated superior performance with respect to power capacity, bandwidth, passband loss, and VSWR. The requirements for practical high power filter circuits were clarified and basic filter design information for such circuits was developed. In particular, a thick ladder filter with low loss and low VSWR over a wide passband was developed. It demonstrated the highest power capacity of all the filters designed. This power capacity will permit it to operate in the FPS-6 radar without an increase in the pressurization or the use of a high strength gas.

II. OPEN PERIODIC FILTERS – REVIEW

A. BASIC THEORY

The use of open periodic structure as filters was first proposed and demonstrated by Birdsall and White (ref 1). Further studies, made under Contract AF 30(602)-2955, were described by Stone, et al (ref 2). Rather than repeating this material, a few statements will be made which, it is felt, will be sufficient for our purposes.

A metal surface can be corrugated, grooved, slotted, or otherwise altered in a periodic manner so that RF energy can propagate along the structure. This occurs when the corrugations, grooves, etc, appear inductive. The propagating wave has the following characteristics:

1. The propagating wave always has an electric field component in the direction of power flow.

2. The field strength of the wave decreases exponentially away from the surface. The axial electric field can therefore be expressed in cylindrical coordinates as

$$E_z = E_o F(\phi) e^{-\gamma r} e^{j(\omega t - \beta z)} \qquad (2.1)$$

where $F(\phi)$ is the variation of the field with the angular coordinate ϕ and γ is the decay factor or transverse separation constant. γ is related to the phase propagation constant β by

$$\gamma^2 = \beta^2 - \left(\frac{\omega}{c}\right)^2 = \beta^2 - k^2 \qquad (2.2)$$

where c is the velocity of light in the dielectric surrounding the periodic structure.

3. The propagating surface wave has many components of generally different amplitudes whose phase propagation constants are harmonically related by the pitch p of the structure, vis,

$$\beta_m = \beta_o + \frac{2\pi m}{p} \qquad \begin{matrix} m = 0, \pm 1, \pm 2, \ldots \\ p = \text{period or pitch} \end{matrix} \qquad (2.3)$$

β_o is called the fundamental, and the phase constants for $m > 0$ are called spatial harmonics. The transverse separation constants γ_m are given by

$$\gamma_m^2 = \beta_m^2 - k^2 = \left(\beta_o + \frac{2\pi m}{p}\right)^2 - k^2 \qquad (2.4)$$

4. As a consequence of the above statements, a diagram can be constructed as in figure 2-1 to show the regions in which γ is real for all spatial harmonics (unshaded – allowed region for a propagating surface wave) and the regions in which γ is imaginary (shaded – forbidden region).

   Filtering action can be explained on the basis that no propagation can occur in forbidden regions, that is, at frequencies such that $k > \pi/p$, corresponding to a free space wavelength condition $\lambda/2 < p$.

5. The phase velocity, v_p, of the propagating wave is less than the velocity of light in the medium surrounding the structure. Hence, the wave is often referred to as a slow wave, and the open periodic structure as a slow wave structure.

When an open periodic circuit of an integral number of half pitches is short circuited at each end, it will resonate at certain discrete frequencies. All of the spatial harmonics constituting the propagating wave are resonant at these frequencies. By perturbing the field at resonance, one can determine which spatial harmonics are predominant at a particular frequency. When this is known, the appropriate value of β can be calculated and plotted on an ω-β (or k-β where $k = \omega/c$) diagram consisting of one triangular zone representing the allowed region for all spatial harmonics. Figure 2-2 shows the ω-β diagram of a resonated open periodic structure on which the

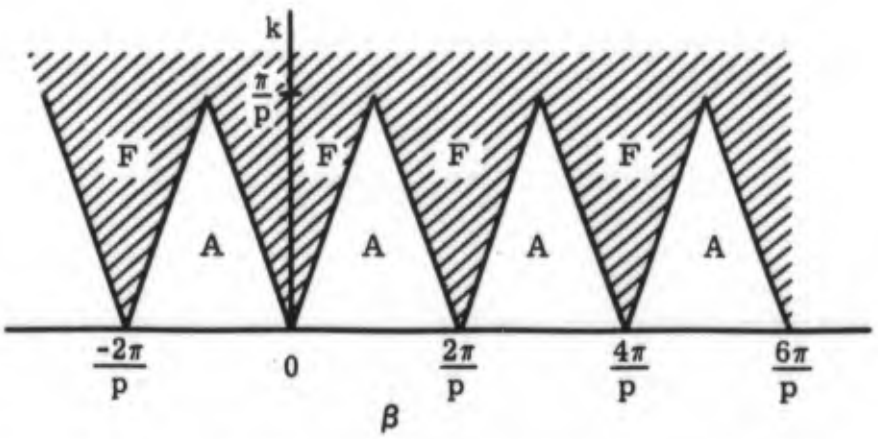

Figure 2-1. k-β diagram showing forbidden regions of an open periodic circuit.

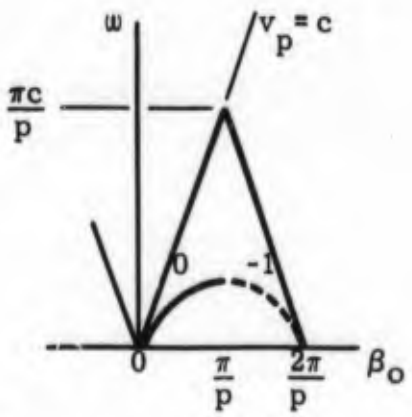

Figure 2-2. ω-β diagram showing point of zero group velocity at $\beta_o = \pi/p$.

waves propagate without transverse phase variation. The solid curve labeled 0 connects points at which a wave having a propagation constant β_o is resonant. The dashed curve connects points of resonance for the m = -1 spatial harmonic. In most cases the m = 0 harmonic, or fundamental, is predominant, and the resonances of the m = -1 harmonic cannot be identified by perturbation of the field. This type of ω-β chart is useful because the phase velocity of a propagating wave at a given frequency is simply ω/β, that is, the slope of the line from the origin to the point on the curve of the predominant spatial harmonic at that frequency. The group velocity is the slope of the curve at a given frequency.

In figure 2-2 the group velocity is zero at $\beta_o = \pi/p$ for both the fundamental and m = -1 harmonic . The frequency at which this occurs is governed by the propagating surface, being usually somewhat below the frequency at which the reactance changes from inductive to capacitive. However, if the structure is so designed that this change of reactance occurs at a frequency higher than that corresponding to $k = \pi/p$, then a point of zero group velocity is obtained just below the peak of the allowed region as shown in figure 2-3. This shows that transmission will indeed decrease markedly at the boundary of an allowed region, even though the surface is still inductive. The frequency at which $v_g = 0$ is of importance in filter design because it is the stopband cutoff frequency.

Figure 2-4 shows the k-β characteristic of an open periodic structure on which there is transverse phase variation – that is, the phase fronts sinuate or spiral along the axis. Now, instead of zero group velocity occurring at $\beta_o = \pi/p$, it occurs near the boundary of the forbidden region. This characteristic is considered to be particularly useful for filters because low phase velocity can be achieved over a broad frequency range without the occurrence of high order passbands within the allowed region. Further, the dispersion or change of v_p can be relatively slight over a wide frequency range.

The suitability of a circuit for filter applications is determined in part by its k-β curve. The k-β characteristics of various structures as functions of their dimensions were reported in reference 2 and will be touched on in

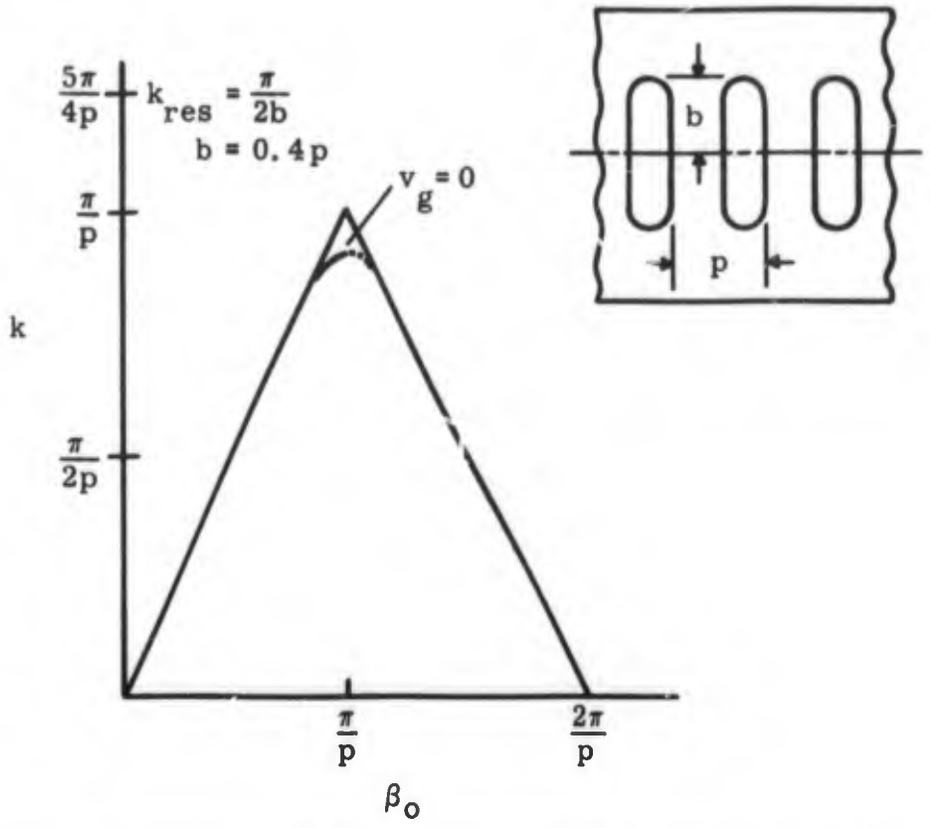

Figure 2-3. k-β diagram of thin ladder with slot resonance in the forbidden region.

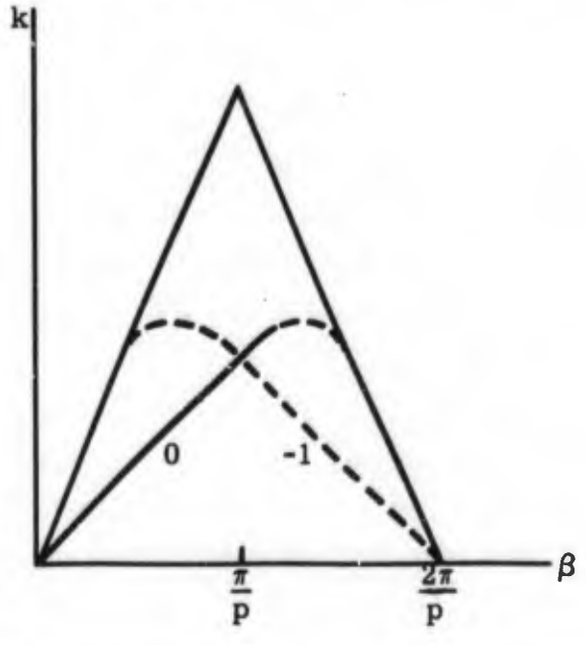

Figure 2-4. k-β diagram of circuit with phase variations transverse to axis; $v_g \neq 0$ at $\beta_o = \pi/p$.

the next part of this section. Further studies of k-β characteristics in relation to filter design will be treated in section IV.

B. TYPICAL OPEN PERIODIC FILTER CIRCUITS

There are many open periodic structures which are possibly suited for use in filters. Some of these circuits were investigated during the previous program and are described briefly in the following paragraphs.

1. THICK LADDER. This circuit consists of a plane conductor with short-circuited slots as shown in figure 2-5. k-β curves for various ladder dimensions are shown in figure 2-6. In general, the slots do not become inductive and therefore capable of supporting a slow wave until $\omega \geq \frac{\pi c}{2b}$, corresponding to the waveguide cutoff frequency of the slots. The frequency at which $v_g = 0$ is determined largely by the depth of the slots, being slightly below the frequency at which the depth is a quarter guide wavelength.

2. THIN LADDER. Consists of holes or slots machined through a plane conductor. The fields of a propagating wave extend outward on both sides of the circuit in contrast to the thick ladder where the wave propagates on only one side of the circuit. A general thin ladder is shown in figure 2-7 together with k-β plots for various circuit dimensions. Thin ladders are capable of propagating a slow wave from zero frequency almost up to the slot resonant frequency which for a narrow slot is approximately $\omega_{res} = \frac{\pi c}{2b}$. It should be noted that this corresponds to the frequency at which the thick ladder begins to propagate.

3. COMB OR OPEN SLOT CIRCUIT. In this structure, shown in figure 2-8, the waves propagate along the edge. It is basically similar to the thin ladder in that the slow wave can propagate from zero frequency almost up to the slot resonance frequency which again is given approximately by $\omega_{res} = \frac{\pi c}{2b}$. Accordingly the k-$\beta$ curves of comb circuits are similar to thin ladder circuits having the same value of b and otherwise similar dimensions.

4. HELIX CIRCUITS. These circuits may be of wire or tape. The phase velocity of the propagating wave is given approximately by $v_p = c \sin \psi$,

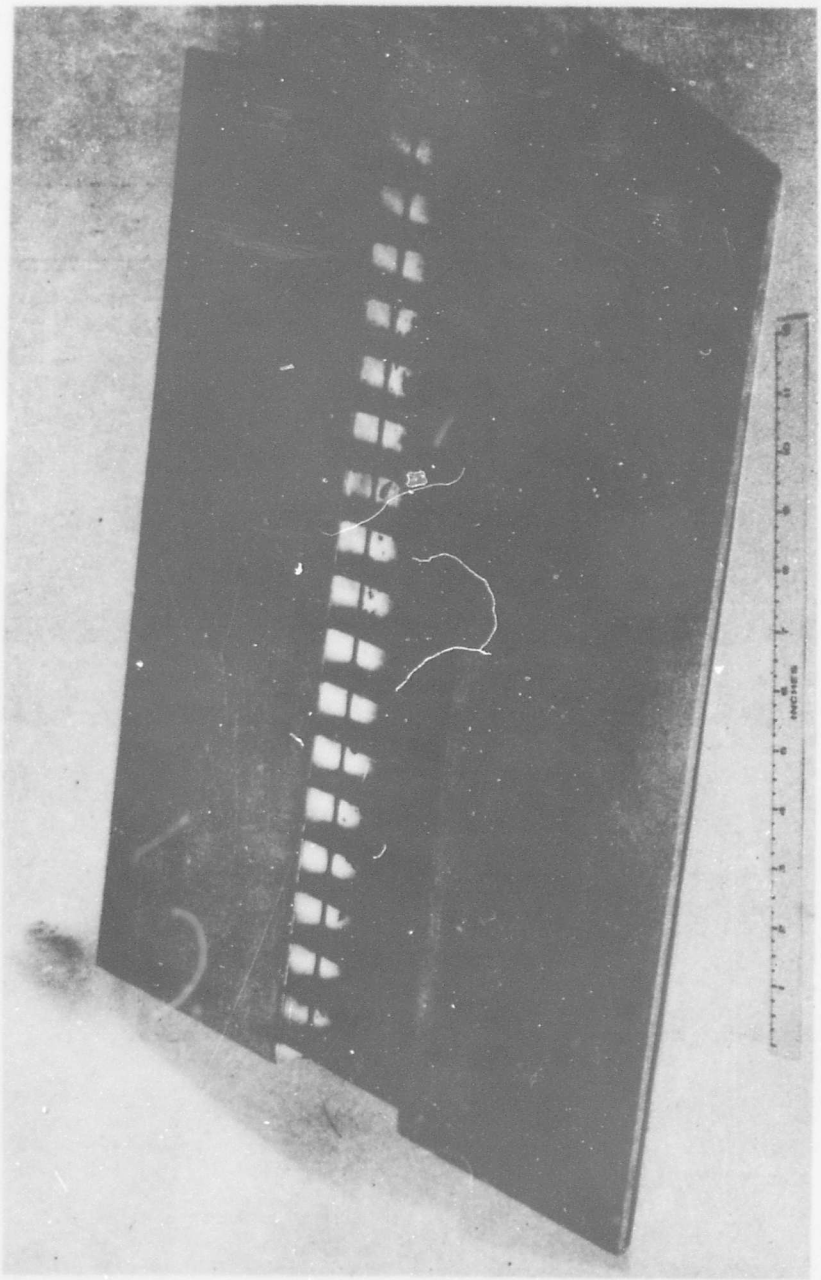

Figure 2-5. Thick ladder filter circuit.

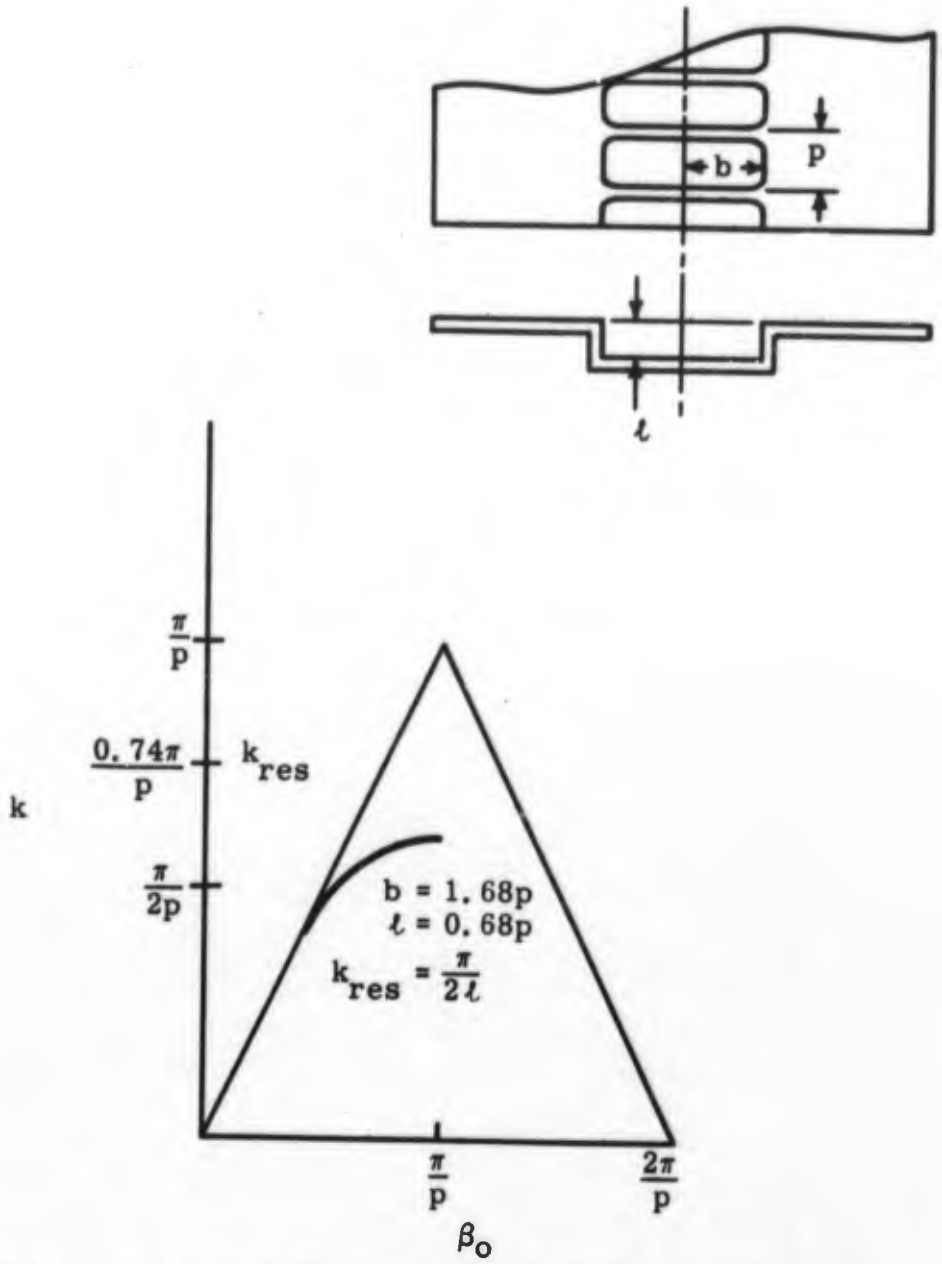

Figure 2-6. k-β curve for typical thick ladder circuit.

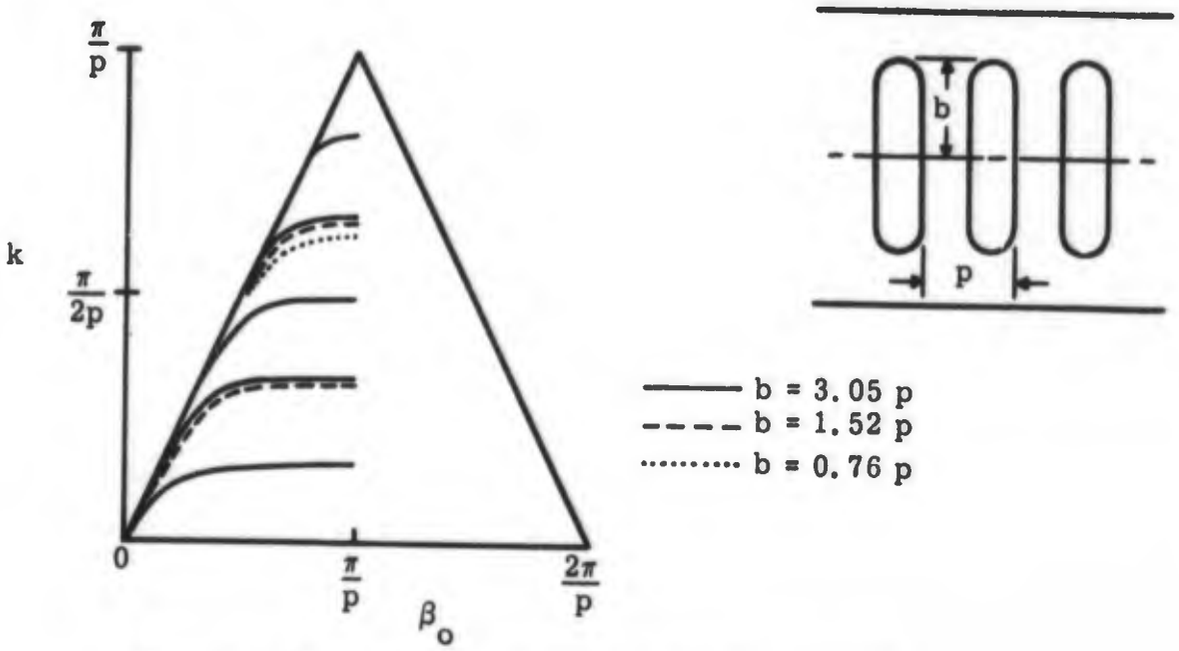

Figure 2-7. k-β diagram of thin ladder circuits.

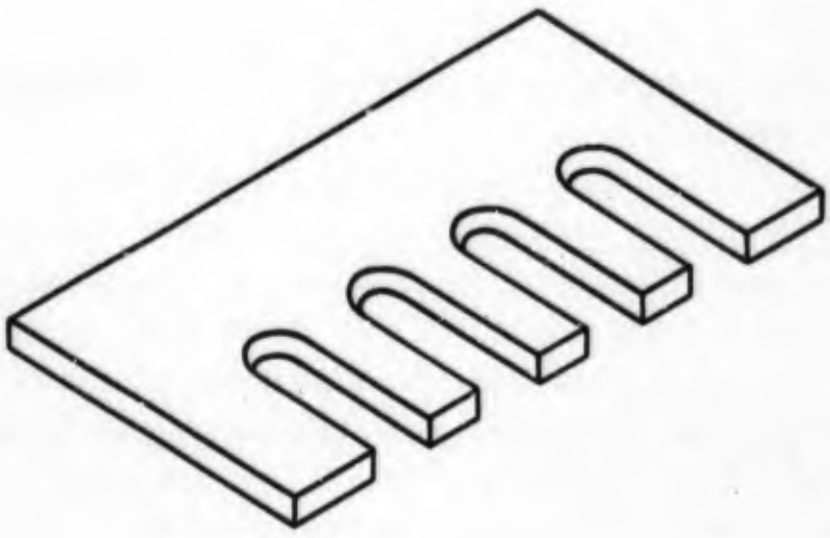

Figure 2-8. Open slot or comb circuit.

where ψ is the pitch angle. This velocity corresponds to the geometric velocity attained by assuming that a plane wave follows the wires of the helix. k-β curves for a typical helix capable of propagating several modes, each with a different spatial harmonic predominant, is shown in figure 2-9(a). Filter applications require that there be no propagating modes in the allowed region at frequencies higher than the operating band; accordingly a helix with relatively large pitch and hence greater phase velocity is usually used. The k-β curve for such a "fast" helix is shown in figure 2-9(b).

The most obvious difference between the k-β curves of helixes and those of the ladder or comb structures previously discussed is the asymmetry of the former with respect to the axis $\beta_o = \pi/p$. This property is due to the variation of phase transverse to the helix axis. A consequence of this property is that the phase velocity and the group velocity are nearly linear over a wide frequency range. Also the transverse separation constant γ is considerably higher over most of this range than comparable ladder or comb circuits.

Helical structures with solid cores, such as those shown in figure 2-10, have electrical properties similar to the wire or tape helix. The central core contributes to strength and rigidity, but in many cases complicates the fabrication of the circuit.

5. INTERDIGITAL LADDER CIRCUITS. When the slots of a ladder circuit are staggered with respect to the axis, a transverse phase variation is introduced and a k-β characteristic such as that shown in figure 2-11 results. Such configurations of both thick ladder and thin ladder circuits were investigated extensively during the previous program because of the apparently more linear k-β characteristic of interdigital structures compared to the uniform ladders. This subject will be dealt with further in section IV of this report.

The characteristics of the interdigital comb or open slot circuit were also investigated under the previous program. Such a circuit, with its k-β curve, is shown in figure 2-12. Like the other interdigital circuits it has

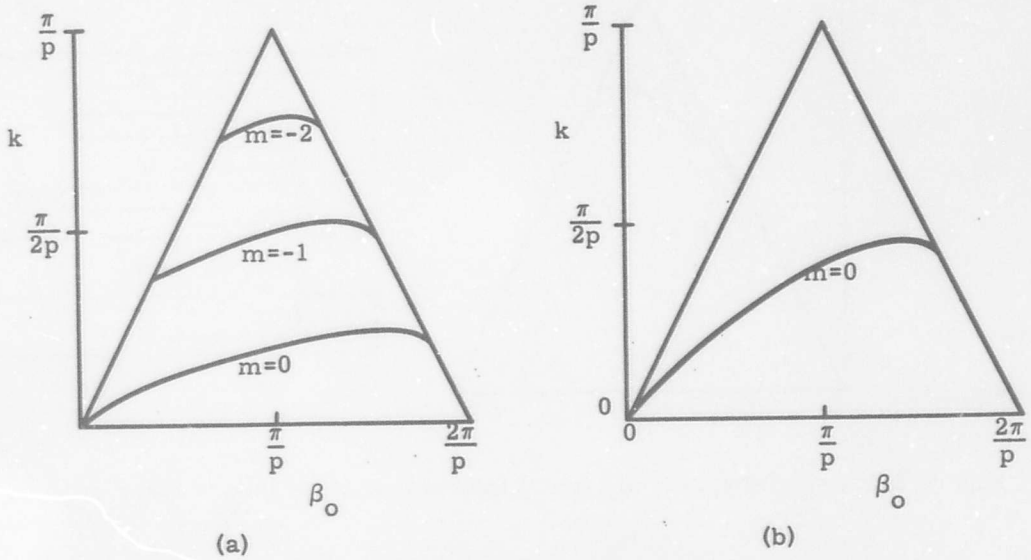

Figure 2-9. k-β diagrams of helices. (a) Typical "slow" helix; (b) "Fast" helix for filter application.

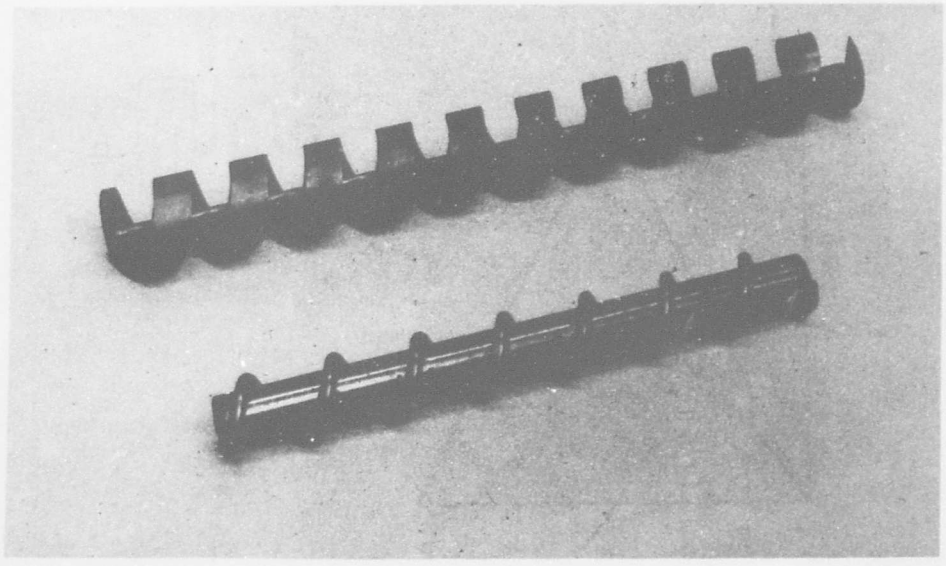

Figure 2-10. Solid core helix circuits.

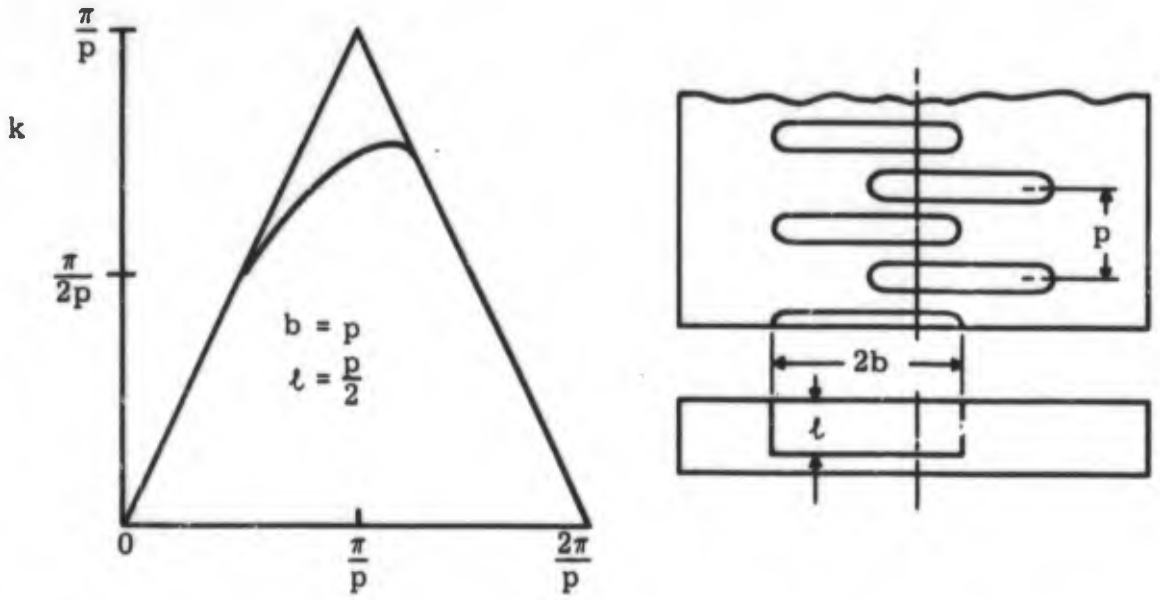

Figure 2-11. k-β diagram of typical interdigital thick ladder filter circuit.

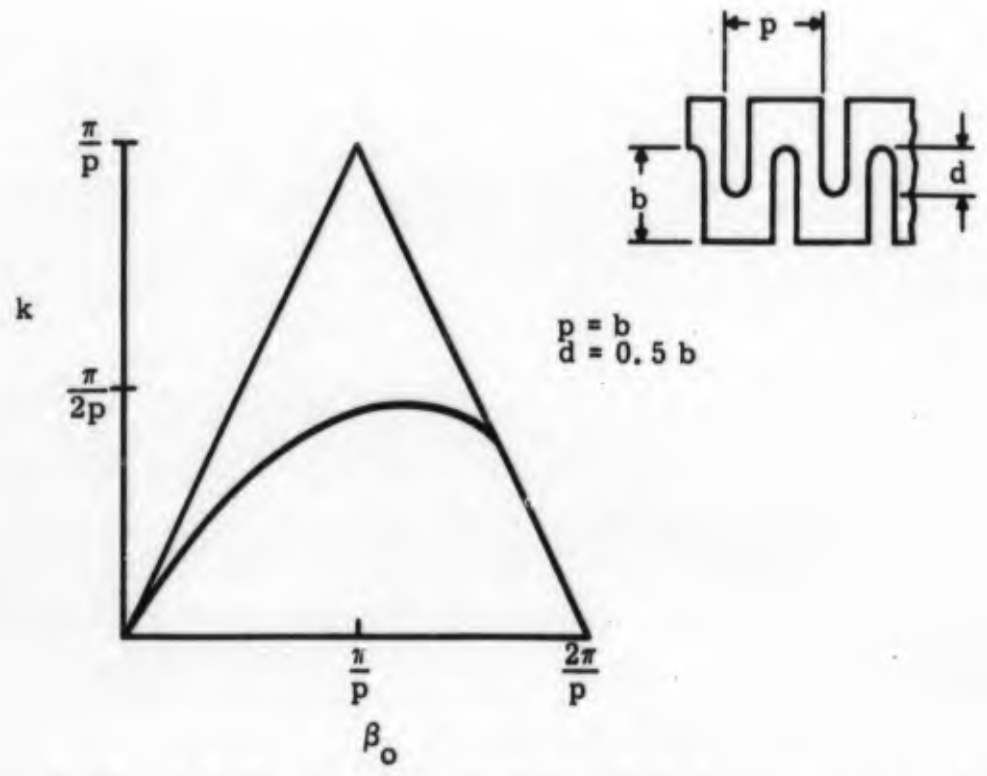

Figure 2-12. k-β diagram of typical interdigital comb or open slot circuit.

transverse phase variation and the k-β curve is more linear than that of a simple comb.

C. FILTER DESIGN CONSIDERATIONS

It was mentioned earlier that the k-β characteristic of a structure helps to determine its suitability for filter applications. Keeping in mind that the function of the open periodic structure is to act as a transmission line or circuit for the operating band and as a radiator in the desired stopband, consider the two characteristics shown in figure 2-13. Both curves attain zero group velocity at the same normalized frequency, however the dashed curve hugs the velocity of light line most of the way as the frequency increases and then bends abruptly, while the solid curve is markedly slower than the velocity of light at low frequencies and bends gradually. Since the transverse separation constant γ , which is a measure of how close the propagating energy hugs the supporting structure, is given by

$$\gamma^2 = \beta^2 - k^2$$

it can be seen that γ is greater for the solid curve than for the dashed curve. As a practical matter, a large value of γ means that the medium required for the absorption of the rejection band energy may be placed close to the structure without absorbing an excessive amount of the energy propagating at passband frequencies, thus reducing the overall cross section of the filter. Therefore, for any frequency up to the frequency of zero group velocity, the filter incorporating the circuit having the solid curve of figure 2-13 will require less space (normalized to the pitch) surrounding the circuit for a given amount of passband attenuation. A large value of γ also renders a circuit less prone to loss by scattering. The scattering can occur from bends intentionally made in the structure or from unintentional discontinuities. The efficiency of transitions between closed and open periodic circuits also depends on the magnitude of γ . If we allow a certain minimum value of γ as permitting a reasonable cross section and efficient transitions, such as point A on the solid curve and point C on the dashed curve, we see that the structure having the solid curve can be used at lower frequencies than the dashed curve structure.

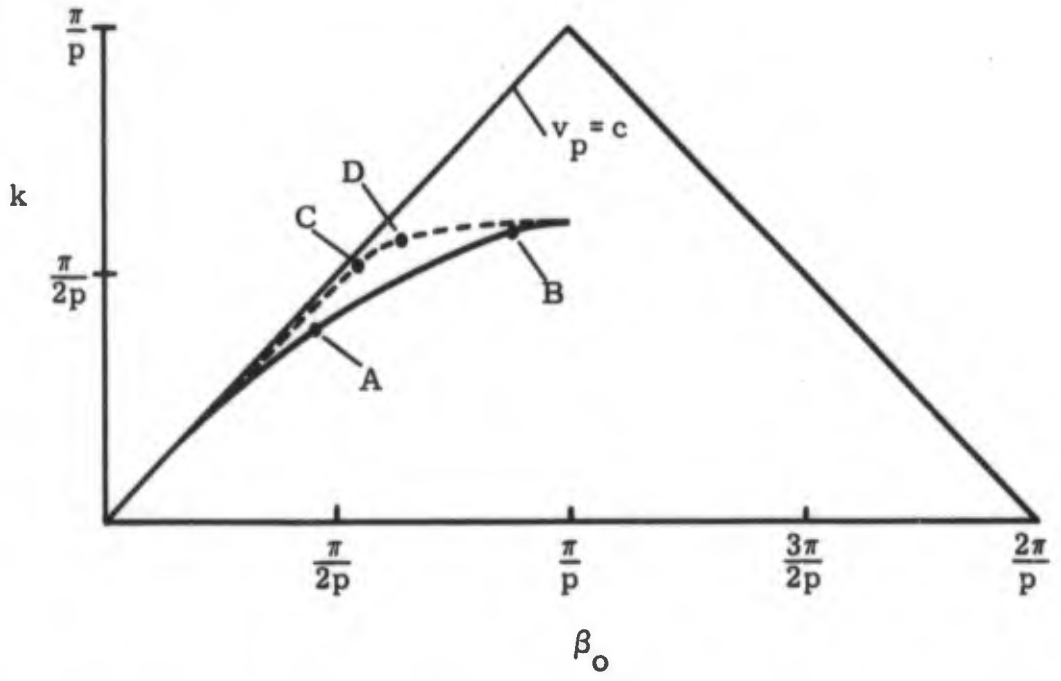

Figure 2-13. Comparison of k-β curves of uniform slow wave circuits.

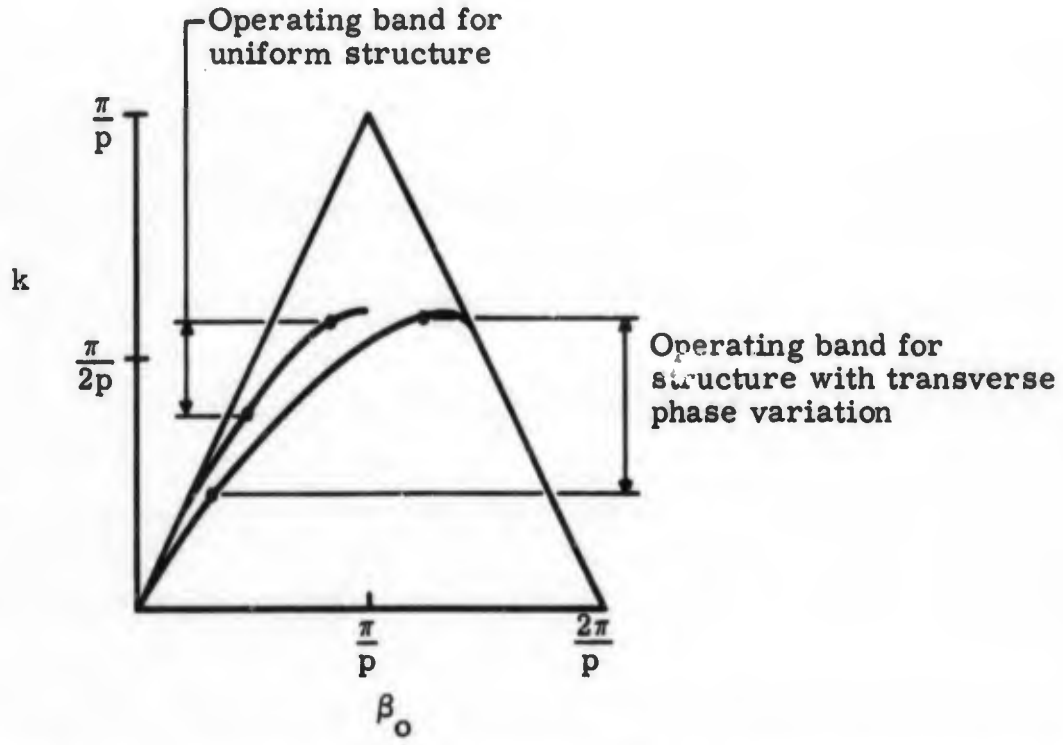

Figure 2-14. Comparison of operating bands of uniform structure and structure with transverse phase variation.

The abrupt bend in the dashed curve implies a sudden decrease in the group velocity, which in turn implies a sudden change in the impedance of the structure, neglecting for the moment just how this impedance is defined. A sudden change in impedance obviously increases the difficulty of achieving an impedance match in a transition from a different transmission circuit.

At frequencies above the abrupt bend in the dashed curve the group velocity, which is proportional to the slope of the curve, is lower than the group velocity of the solid curve at corresponding frequencies. The intrinsic attenuation of a slow wave structure is inversely proportional to the group velocity (ref 2 pp 5-3 to 5-5) and the sudden decrease in group velocity causes a corresponding increase in intrinsic attenuation. It should be noted that the group velocity of the dashed curve is greater than that of the solid curves at frequencies below the abrupt bend in the former. This does not necessarily mean that the intrinsic attenuation of the structure with the dashed curve is lower than that of the structure with the solid curve in this range – intrinsic attenuation is merely <u>proportional</u> to the group velocity. The magnitude of intrinsic attenuation cannot be determined from the ω-β characteristic alone. However, the decrease in group velocity and the consequent increase in intrinsic attenuation imposes an upper frequency limit on the passband range of a given structure. If we allow a certain minimum slope as setting the upper frequency limit, such as point D on the dashed curve and point B on the solid curve, then we see that the operating range of the latter extends slightly higher in frequency. The operating band AB of the structure with the solid curve is therefore seen to be wider than that (CD) of the dashed curve structure.

The above discussion also applies to a comparison of the k-β curves of a uniform ladder and a structure having transverse phase variation, as shown in figure 2-14. The structure with transverse phase variation (a helix, for example) is seen to have a much wider operating band than the ladder structure based on the same minimum values of γ and group velocity. Figure 2-14 also implies that the structure with transverse phase variation should have a much sharper stopband edge since the group velocity goes to zero rather abruptly at the boundary between the allowed and forbidden regions.

While the k-β curve of a structure helps to determine suitability for filter applications, other factors must be considered. Obviously the filter circuit must be capable of handling the peak and average power outputs of the transmitter for which it is intended. The loss in the passband must be low enough that it does not degrade the system performance or damage the filter. Passband loss can to some extent be predicted by the k-β characteristic but measurements or calculations on the specific periodic structure must be made to determine the loss of a practical filter.

In addition to transmitting the passband frequencies without breakdown or excessive loss, the filter must provide the desired stopband attenuation. This attenuation should result, ideally, from radiation from the slow wave structure. In order for radiation to be an effective attenuation mechanism, the radiated energy must be absorbed. This has imposed the practical requirement that the slow wave circuit be bent or otherwise distorted. The need for bending is illustrated by figure 2-15. In figure 2-15(a) some of the stopband energy radiated from a straight periodic structure is directed toward the aperture of the receiving transition, and some energy from the aperture of the input transition is also radiated directly to the receiving transition. In figure 2-15(b) the circuit is bent, and less of the energy radiating from the circuit is directed toward the aperture of the receiving transition. Further, the apertures of the transitions are out of sight of each other so that energy radiated from the input transition aperture cannot reach the receiving transition aperture. However, this is strictly true only if the radiated energy is entirely absorbed. If any of the radiated energy is reflected from the absorbers there will tend to be zones of low attenuation. Accordingly the material and location of the absorbers has an effect on stopband performance. Increasing the amount of bending will make the absorbers more effective in absorbing the radiated power, but this usually involves increased passband loss due to greater circuit length and radiation or scattering from bends. Size is also increased by such measures. The design of a practical filter generally involves a judicious choice between passband loss, stopband attenuation, and physical dimensions.

One of the most important factors in filter design is the subject of this contract, namely, the design of suitable transitions for use between

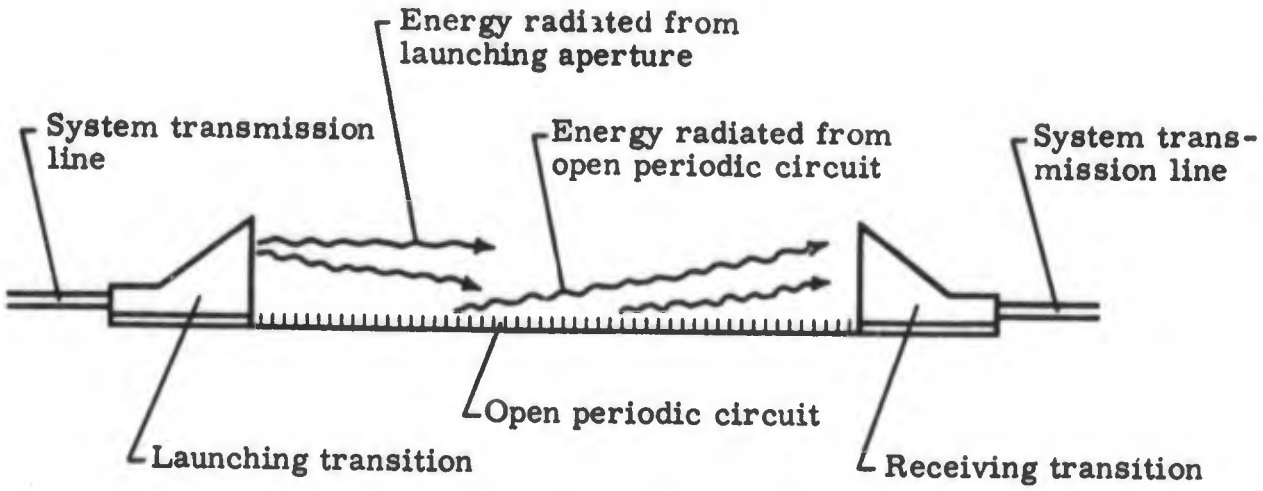

(a) Filter employing straight open periodic circuit.

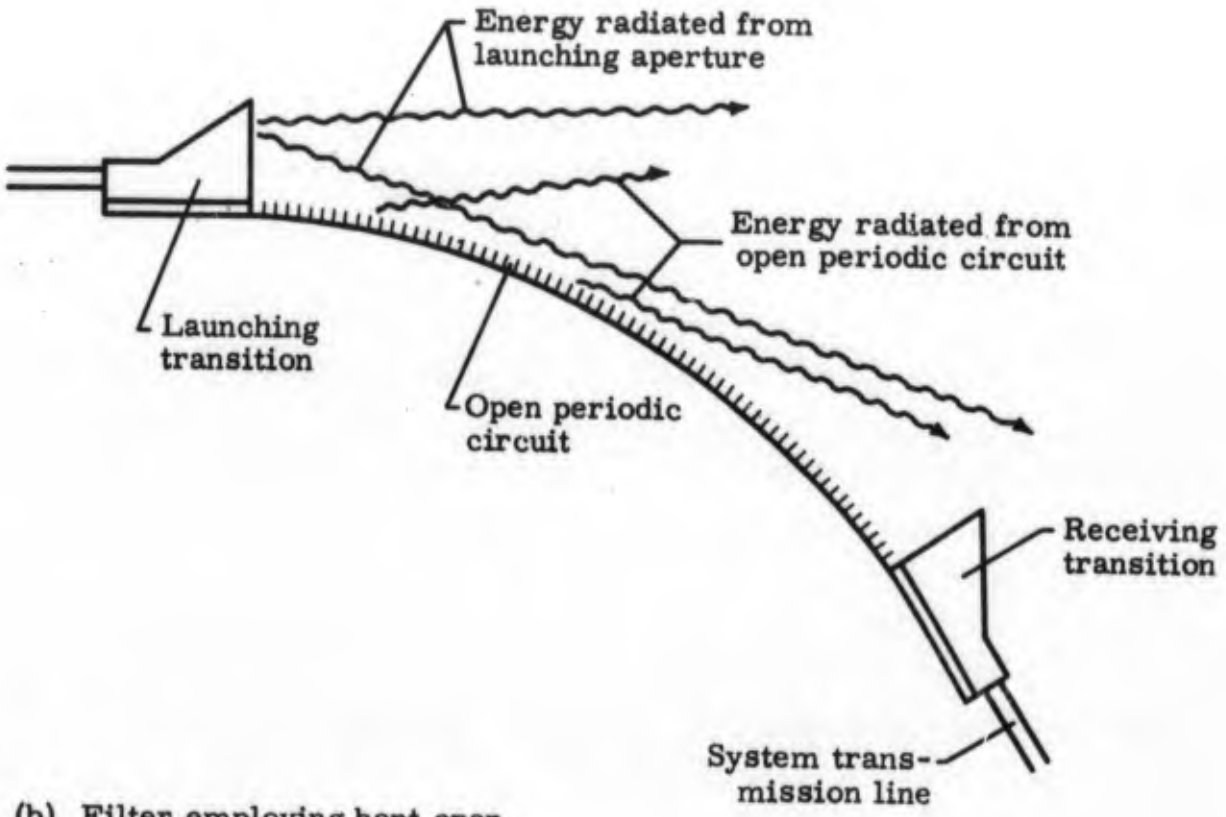

(b) Filter employing bent open periodic circuit.

Figure 2-15. Illustration of need for bending filter slow wave circuit.

system transmission lines and slow wave filter structures. The main function of the transition is to transmit the passband energy from the closed fast wave transmission line to the open slow wave filter structure with little loss while permitting the rejection band energy to pass on to the absorbers.

The main transition design problems encountered on the previous program can be classified as follows:

1. Coupling to a fast mode rather than the desired slow mode.
2. Launching efficiency – transmitting the desired mode through the interface between the closed region and open region of the transition.
3. Achieving an impedance match between the fast mode in the system waveguide and the desired slow mode.
4. Avoiding high reflections of stopband energy from the transition.

Solutions to the above problems should not cause a severe reduction in power handling capacity. The transition configuration should be suitable for incorporation in a filter.

The primary problem areas given above were defined very loosely which indicated a need for a better basic understanding of the transmission circuits employed in transitions, and the junctions between them. At the outset of this program it was decided to try to apply known transmission network principles to the solution of the problems rather than relying on a phenomenological approach.

Accordingly the project work began with general studies in which the various possible transitions were analyzed and the properties of the transmission circuits incorporated in them were clarified.

III. GENERAL TRANSITION STUDIES

A. TRANSITION NETWORKS

The function of the transition is to transmit energy from the system transmission line to the open periodic circuit with minimum loss and reflection. The basic block diagram of a transition is shown in figure 3-1. This simple figure illustrates the important fact that one of the lines is "open", that is, one conductor of that line is at infinity. Therefore, there must be a discontinuity somewhere in the transition circuit. Passband energy must pass through this discontinuity without radiation.

The simple block diagram is expanded in figure 3-2 to show the functional requirements of a general transition. The lines and junctions should be considered lossless. From left to right, the first junction is between the system transmission line and an intermediate fast wave transmission line, the purpose of which is to modify the field configuration so that it can be coupled to a closed slow wave transmission circuit. This coupling is effected at the second junction. The closed slow wave circuit is included as a part of the general transition because it permits the conceptual separation of two functions:

1. Coupling to the desired slow mode, and
2. Passing the desired slow mode through the discontinuity between the circuits with finite and infinite boundaries. The function is often referred to as "launching."

Function (1) is performed at junction 2 while junction 3 performs function (2). The open slow wave structure on which the energy has been launched is shown as being different from the open periodic filter circuit. This has been done to allow for the possibility that it may be either difficult to launch directly onto the filter circuit, or desirable to have an intermediate slow wave circuit for overall filter effectiveness.

Figure 3-1. Basic block diagram of transition.

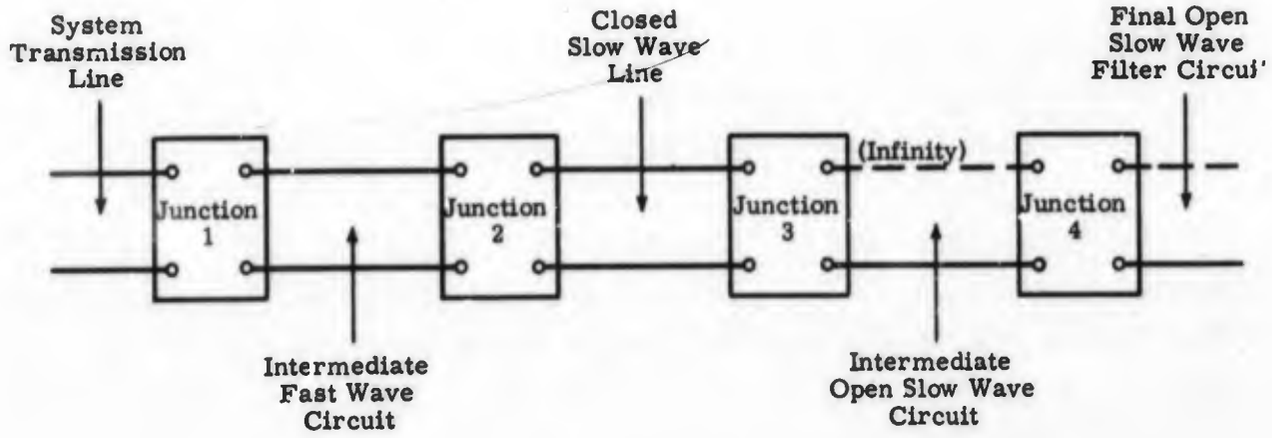

Figure 3-2. Expanded block diagram of transition.

The junctions of figure 3-2 are shown as two port networks. This reflects the desired condition – that incident energy passes from one circuit to the next without loss, provided reflections are minimized. This is not always the case. At junction 3 a third port could be added to represent loss to a free space path, or radiation. Any of the transmission circuits, whether fast or slow, can be considered as possibly capable of multimode transmission. The junctions must therefore couple only the desired pair of modes.

Clearly the design of a transition requires adequate knowledge of the various transmission circuits to be joined. This knowledge should cover the possible modes of propagation and the field configurations, propagation constants, cutoff frequencies, and possibly the impedance of each. This is no problem with the system transmission line which would normally be a standard coaxial line or waveguide operating over a frequency range of single mode propagation. For the open periodic circuits some useful knowledge had been acquired on the previous program particularly in regard to the phase velocities and cutoff frequencies of modes on particular structures. The intermediate transmission circuits can be designed to have the appropriate characteristics.

While the discussion of the general transition of figure 3-2 treated it as the input transition, its development would probably proceed in the reverse direction, i.e., from the open slow wave circuit providing the desired filter characteristic to the open slow wave circuit on which it is relatively easy to launch a surface wave with high efficiency, then to a closed slow wave structure capable of being joined to a type of fast wave transmission line, and next to the system transmission line.

The general network can be applied to almost every type of slow wave filter. In specific applications, some of its complexities might be eliminated by merging the functions of two or more junctions.

It might be argued that figure 3-2 is not sufficiently general to include all practical transitions. For example, one could conceive of a transition in which the fast line opens to free space and the passband energy is beamed

onto the slow wave structure. In fact, many of the transitions described in the literature involve a free space path. However, such transitions can be considered as special cases of figure 3-2, in which the closed slow wave structure is of zero length. It is true that a closed periodic surface can behave as a filter with passbands and stopbands. Energy at stopband frequencies will be reflected, which is not desirable in a filter in which it is desired to absorb stopband energy. However, closed periodic structures, when used as conventional reflective filters at harmonic frequencies, suffer from the fact that the stopbands are based on the dominant mode. Spurious passbands occur within the dominant-mode-defined stopband around the cutoff frequencies of higher order modes. Further, unless one goes to the particular trouble of designing a wide stopband filter (which usually requires that the enclosing conductor be close to the periodic structure) the actual stopbands will be quite narrow. This property of enclosed periodic circuits should be considered in the design and evaluation of a transition.

However, it would be a mistake, for several reasons, to place too much emphasis on the achievement of low reflections in the stopband if such emphasis limits the study of transition configuration. One reason for this statement is that the open periodic filter appears to be unique among filters of all types in its ability to provide a stopband that extends from the passband up to infinitely high frequencies regardless of the type or number of incident modes. Achieving this stopband together with a passband suitable for high power transmission was the primary project goal. Almost any discontinuity such as a bend or an obstacle required at passband frequencies will cause reflections in one or another of the several incident stopband modes. The level of reflection will depend in part on the modal content. System components between the signal source and the transition may have reflections comparable to those occurring at the transition.

Further, if a transition does reflect certain modes at critical stopband frequencies, means are available for the reduction of the level of reflection. For example, a directional coupler can provide padding at low stopband frequencies while transmitting passband energy with negligible loss (ref 3). Still, achieving low stopband reflections is desirable, particularly at the lower harmonics where the power level may be high and if a directional

coupler pad is impractical. Therefore, in addition to considering the stopband reflections from the closed periodic circuits within the transition, the reflections from the various junctions should also be considered. For instance, if the first junction of figure 3-2 involves a right angle between the two transmission lines, together with some reactive obstacles, it could be expected to reflect more stopband energy than an in-line junction in which the higher order modes are only slightly perturbed.

B. JUNCTIONS

In the preceding discussion, the various junctions of the general transition network were described as having particular functions dictated by their location in the network. These junctions will now be treated in turn in order to point out those which were readily conceived and designed and those which, because of novelty or unfamiliarity, required more investigation.

Referring to figure 3-2, the first junction, which is between two fast wave transmission lines, can serve to reorient the fields. As such it would be a transformer or a mode transducer. A change of modes might be required, for example, in making a transition from a rectangular system waveguide to a helix, employing an intermediate coaxial line. The junction would then be some form of waveguide to coaxial line transition. The fast wave lines might be connected in tandem or by distributed coupling. Reactive elements or a non-uniform transmission line may be required to couple the two different field configurations and the frequency range for low reflection may thereby be limited. Properly defined impedances of the desired modes and the orientation of the lines and reactive elements enter into the design of tandem connections. Coupled line junctions require consideration of the phase velocities as well. The design of these junctions is basic to the microwave art, particularly if the transmission line dimensions permit only one mode of propagation. It would appear that such dimensional restrictions are therefore desirable. However, considerations of power handling capacity and overall filter design may prevent this, in which case coupling to the undesired mode must be prevented.

The second junction is similar to the first in that the transmission circuits are closed, i.e., they have finite boundaries. Also, its design depends heavily on whether the propagating modes are unique on either side of the junction, since it has the key function of establishing a mode which can later be transmitted or launched through the aperture of the transition. When the slow mode is unique, that is, when no other mode can propagate, the junction design is relatively simple. However, certain slow wave circuits may not lend themselves to a unique slow mode of propagation when enclosed by a conductor of dimensions suitable for the desired power level. There may be other modes of propagation which interact little with the slow wave structure. These modes could then pass on to the third junction, which is open to space, and be radiated from the aperture. Coupling to these modes must be avoided.

The third junction of necessity requires consideration of multimode conditions since it includes the aperture of the transition which is open to infinity. Launching efficiency, which must be considered in the design of this junction, is treated as a separate topic in section III. C.

The fourth junction, between two open periodic circuits, also appeared to pose problems. Two methods of joining open periodic circuits were studied. The first method, involving tandem junctions of open periodic circuits, is treated in section III. D. The second method is based on the coupling of two open periodic circuits along a portion of their lengths. This method was studied in more detail and experiments with particular filter circuits were performed. In order to present these studies and experiments without loss of continuity they are treated separately in section V.

C. LAUNCHING EFFICIENCY

Launching efficiency can be defined as the ratio of the power transmitted in a surface wave or slow wave to the power transmitted through the launching aperture. Figure 3-3 serves to illustrate this definition which is expressed in the equation

$$\text{Launching Efficiency} = \frac{P_s}{P_r + P_s} \qquad (3.1)$$

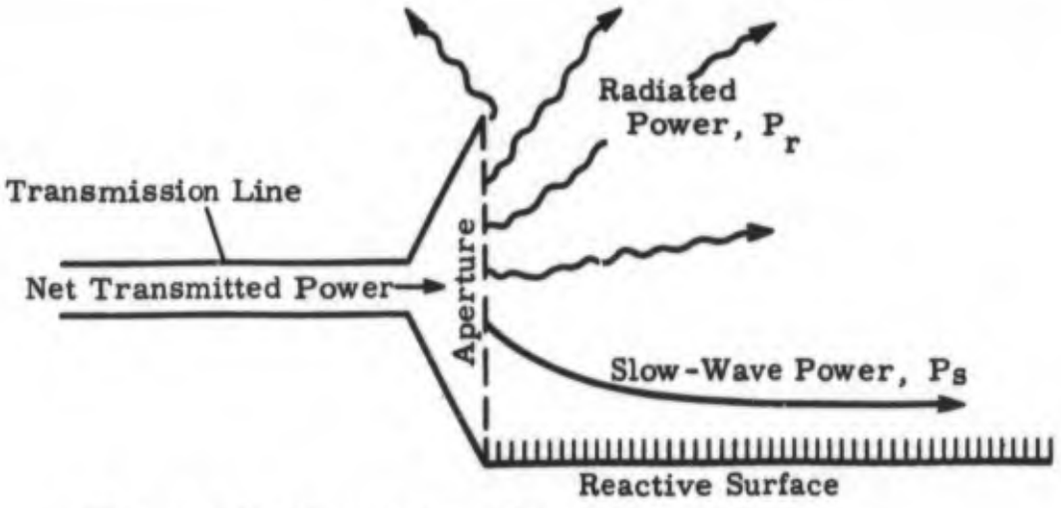

Figure 3-3. Illustration of launching efficiency.

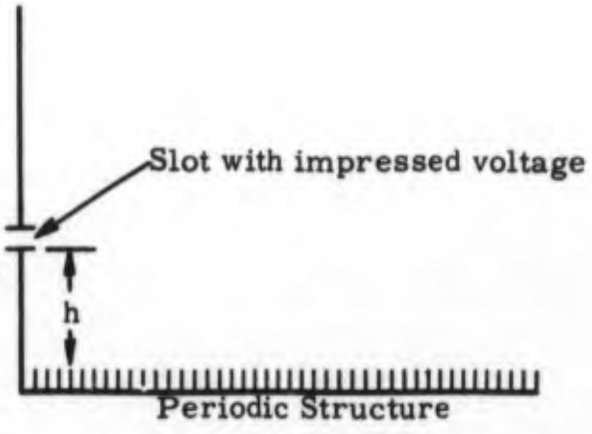

Figure 3-4. Slot launcher for exciting slow wave on plane periodic structure.

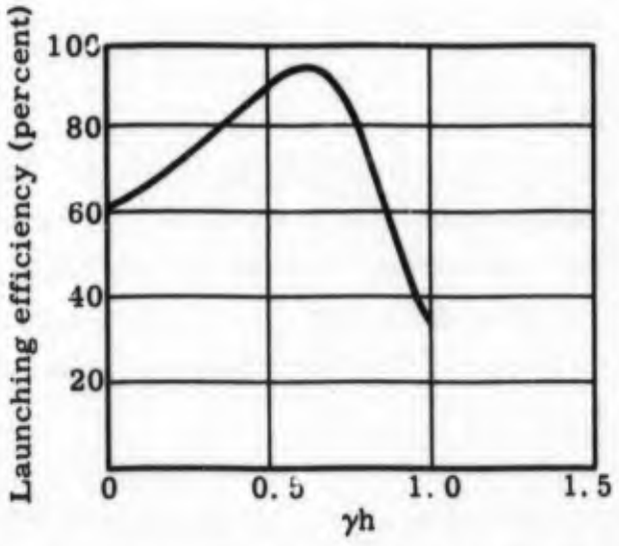

Figure 3-5. Launching efficiency of slot launcher. $\gamma/k = 0.5$.

The problem of launching a surface wave with high efficiency, that is, with little energy radiated into space, has been treated by many workers. Their results were summarized and discussed by Barlow and Brown (ref 4, chapters 10 and 11). A type of launcher that has been studied is the small slot in a conducting plane, shown in figure 3-4. The height h of the slot above the slow wave surface determines the launching efficiency, which can be as high as 90 percent for certain configurations, as shown in figure 3-5. A relative maximum efficiency point arises because of the interference between the direct radiation from the slot and the radiation reflected from the slow wave surface. Assuming that the slot is positioned at an appropriate height, so that at a given frequency the launching efficiency is maximum ($\gamma h = 0.63$ in figure 3-5), then even moderate variation of γ with frequency will cause a decrease in launching efficiency.

Barlow also examined the impedance of the slot launcher just described and concluded that, because of the energy stored in the reactance associated with the launcher, matching of the launcher impedance can only be achieved over a narrow band. This type of launcher is representative of the class employing a free space path, i.e., with no closed slow wave structure. The loss due to radiation is excessive for radar filter application.

However, if the launcher consists of an aperture instead of a small slot, and the fields across the aperture decrease exponentially away from the slow wave surface, then there will be little stored energy associated with the aperture, and a broadband impedance match can be achieved.

Figure 3-6 shows an idealized launcher having an aperture across which the field variation is approximately exponential. The slow wave surface, it should be noted,is continuous through the aperture. Reference 4 concludes that as the size of the aperture increases, the level of reflected power approaches zero while the launching efficiency approaches 100 percent. Furthermore, this desired performance will occur over a broad frequency range.

Figure 3-7 shows the magnitude of reflected power from the aperture as a function of kh, where h is the aperture dimension normal to the slow wave

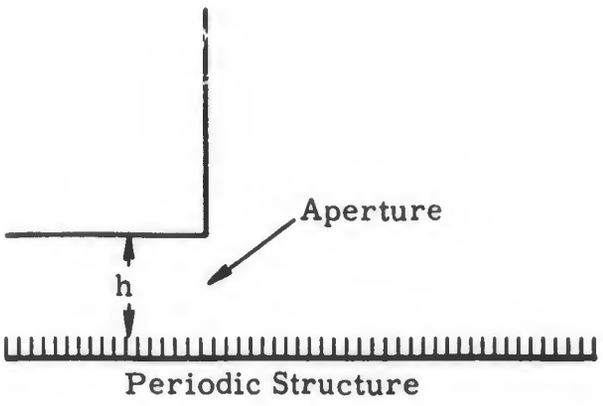

Figure 3-6. Launcher with approximately exponential field variation across the aperture.

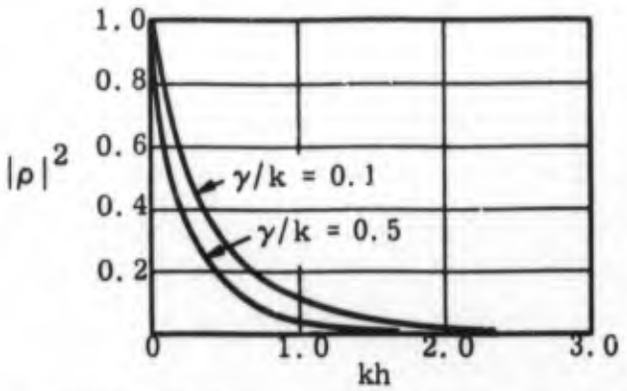

Figure 3-7. Power reflection coefficients for launcher of figure 3-6.

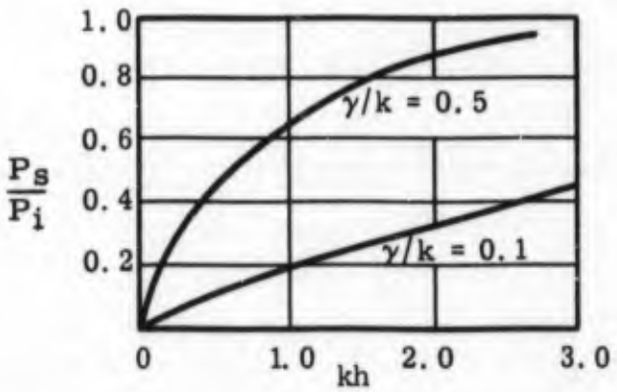

Figure 3-8. Fraction of incident power launched as slow wave by launcher of figure 3-6.

surface. Note that the reflected power is lower for the higher value of γ/k. The overall performance of the junction, i.e., the ratio of the surface wave power to the incident power is shown in figure 3-8.

In designing such a launcher it is necessary to refer to design goals. The present project has design goals of 1.06 VSWR and 0.1 db loss for the transitions, corresponding to a reflected power level of 0.09 percent and a transmitted power level of 97.7 percent, relative to the incident power. These values refer to the whole transition; the performance of any portion of the transition must be better. It appears therefore that kh must be made quite large. However, the curves plotted in figures 3-7 and 3-8 correspond to rather low values of γ/k.

On the previous program the loss due to a horn of finite aperture height was calculated on the premise that all the energy contained in the fields at distances greater than the aperture height was lost. The calculated loss is plotted in figure 3-9 as a function of γ times aperture height. Since reflection was not considered, the loss relates entirely to launching efficiency as defined earlier. Relating figure 3-9 to the values of γ of practical filter structures indicated that the apertures would be of reasonable size. These apertures would also have low reflection.

So far we have treated the aperture as a plane and have shown that high launching efficiency can be achieved if the slow wave circuit is continuous through the aperture and if the aperture is sufficiently large. However, this in a sense avoids the question, because the problem of launching the slow wave in a circuit with a conducting boundary relatively far away remains. In general many transmission modes will exist in addition to the desired slow wave mode.

On the previous program the lowest transition loss was obtained when the slow mode was established on a circuit that was fairly closely encompassed by a conducting boundary. The boundary was then flared out linearly to the aperture dimensions dictated by figure 3-9. The resulting loss was considerably greater than that predicted by figure 3-9, although the dependence on γ could be observed. Decreasing the angle at the flare below

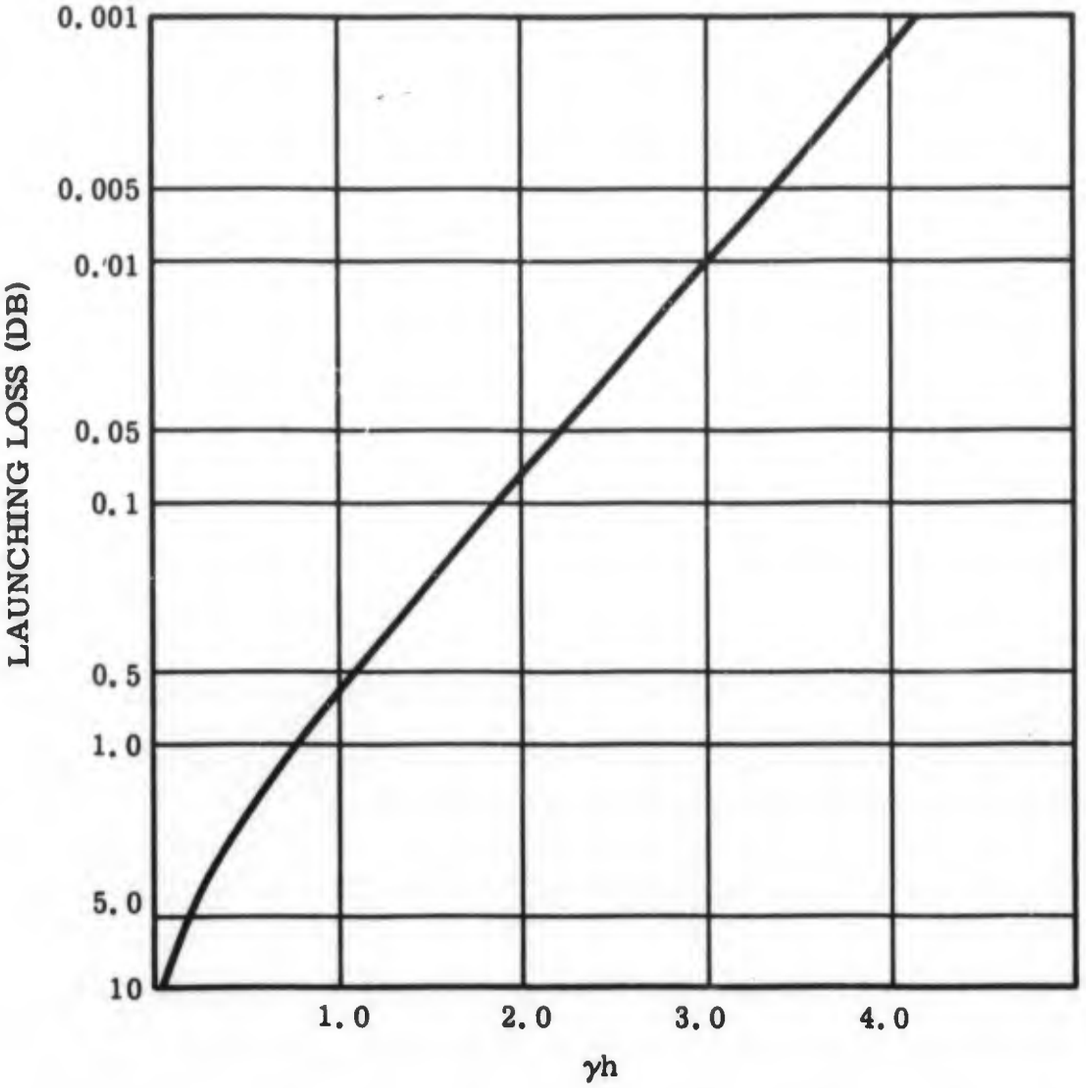

Figure 3-9. Launching loss of aperture with exponential field distribution.

35 deg caused no improvement. The causes of this excessive loss were speculated upon in the transition program. The most probable cause appeared to be failure to couple entirely to the desired slow mode in the uniform closed region. Energy that remained in a fast mode would be radiated out of the horn regardless of how gradually the horn was tapered. The other possible cause was that the radiation came from the horn itself by conversion of the slow wave to fast wave modes or plane waves. This theory seemed to be contradicted by the experiments in which it was found that making the taper angle smaller than 35 deg had little effect. However, the flares used in these experiments were linear, and there was therefore a discontinuity at the beginning of the taper which might have caused much of the scattering. The effect of a discontinuity should be greater when it is close to the surface supporting a slow wave than when it is some distance away.

To eliminate the above possible causes of loss in the junction between the closed and open slow wave circuits, the following design guide lines were set down:

1. The closed slow wave should be established as a unique mode if doing so is consistent with the power requirements and the circuit configuration.
2. The transition to the open slow wave circuit should be gradual, particularly where the enclosing surface is close to the slow wave circuit.
3. The aperture should be as high as required for very low loss (on the order of 0.01 db).

The question of how gradual to make the taper and what shape it should have was deferred for answering until more information about particular structures had been obtained. It was hoped that a properly defined impedance for a closed slow wave structure would assist in the design. It was also recognized that little was known about the required aperture width for plane structures. This would depend on the field configuration on the structure which was not completely determined for the wide variety of structures under consideration.

An important concept concerning the tapered transition from the narrowly closed slow wave circuit to the open circuit is that it does not function as a horn antenna at passband frequencies, even though it resembles one. A horn antenna is designed to have uniform field distribution approaching a plane wave across its aperture. The tapered transition for a slow wave should have a near exponential field distribution across its aperture. This difference of function is illustrated in figure 3-10. Figure 3-10(a) shows a horn antenna from a fast wave line being used to excite a surface wave on the reactive surface to the right of the aperture. Some of the incident energy is launched as a slow wave but a portion is also radiated. In figure 3-10(b) the reactive surface is continuous through the aperture. At the left, where the enclosing conductor is closest, a closed slow wave has been established with a small axial electric field component. By gradually increasing the separation between the reactive surface and the enclosing conductor, the closed slow wave is gradually transformed into the desired slow wave so that at the aperture its field configuration is almost identical with the slow wave on the open reactive surface and there is little radiation. If the horn of figure 3-10(b) is too abrupt, then a source of radiation will occur within the horn.

D. TANDEM JUNCTION OF OPEN PERIODIC CIRCUITS

The fourth junction of figure 3-2 is between open periodic circuits, i.e., the circuits can be connected in tandem, or coupled along a portion of their lengths. The tandem junction is illustrated in figure 3-11.

It might appear that the abrupt junction of two open surface-wave lines could be treated as a simple problem of impedance matching (assuming that the impedances could be properly defined) because both lines at the junction have one terminal at infinity. However, the possibility of radiation occurring at the junction must be taken into account. Reference 4, chapter 12, analyzed the abrupt junction of two plane surface wave structures of infinite extent and different uniform values of γ and β. Reference 4 also calculates the portions of the incident energy which are reflected, radiated, or transmitted. The results are as follows:

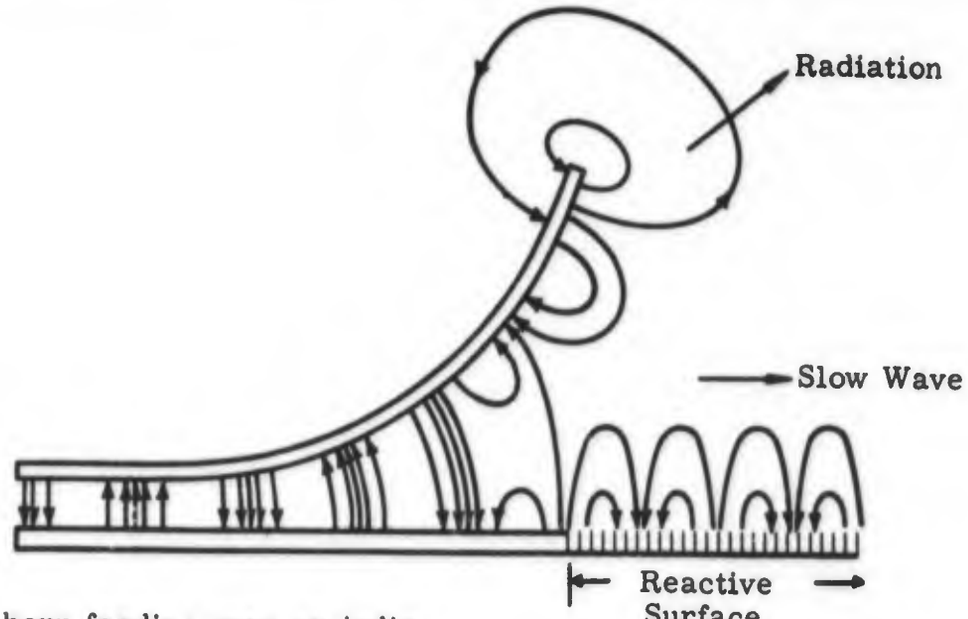

(a) Radiating horn feeding open periodic structure.

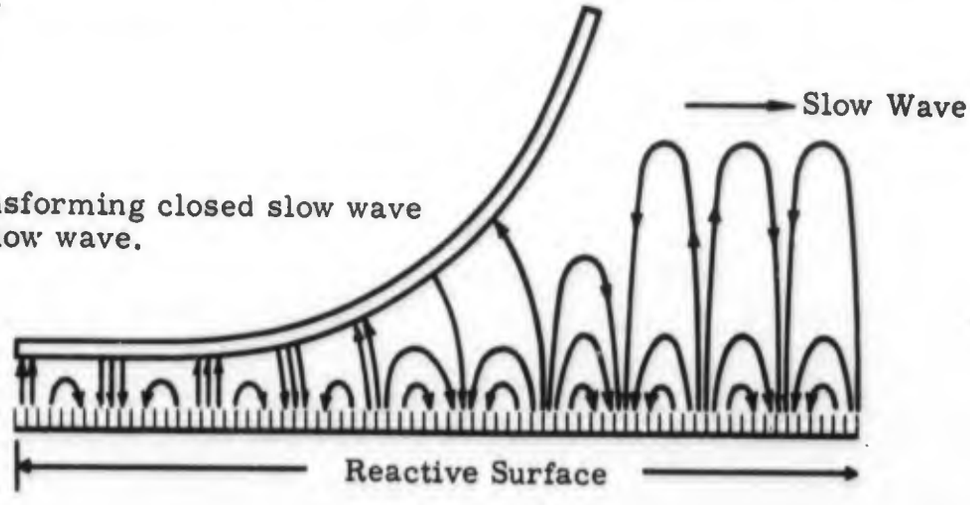

(b) Horn transforming closed slow wave to open slow wave.

Figure 3-10. Comparison of horn antenna (a) and closed to open slow wave transformer horn (b).

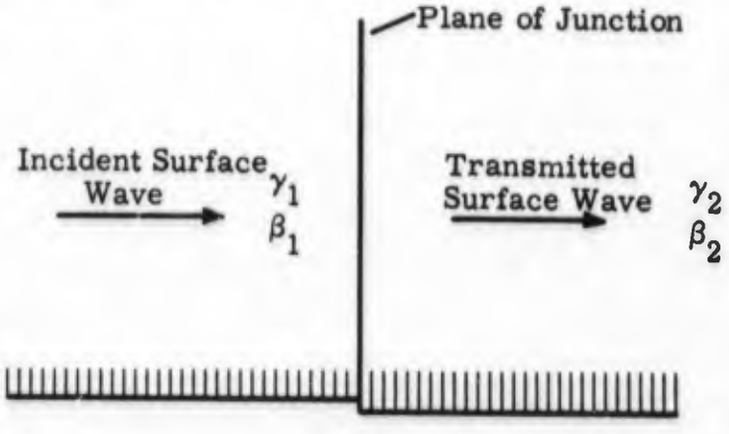

Figure 3-11. Tandem junction of open periodic circuits.

Reflected fraction

$$R = \frac{\gamma_1^2(\gamma_1 - \gamma_2)^2}{\beta_1^2(\beta_1 + \beta_2)^2} \tag{3.2}$$

Radiated fraction

$$Q = \frac{(\gamma_1 - \gamma_2)^2\left[\beta_1^2(\gamma_1 - \gamma_2)^2 - \gamma_1^2(\beta_1 - \beta_2)^2\right]}{\beta_1^2(\beta_1^2 - \beta_2^2)^2} \tag{3.3}$$

Transmitted fraction

$$T = \frac{4\gamma_1\gamma_2}{(\gamma_1 + \gamma_2)^2} \tag{3.4}$$

We are primarily concerned with making the transmitted fraction as large as possible. T is unity when $\gamma_1 = \gamma_2$. It can be shown that the condition $\gamma_1 = \gamma_2$ implies an impedance match. In order to apply the above equations in the design of a practical transition the fields on both sides of the junction should be similar. For example, the width of plane structures should be comparable to each other.

Examination of the equations reveals that for small changes in γ (up to 18 percent) the transmitted fraction T is greater than 0.99. For structures having values of γ/k less than one, which is typical of circuits having no transverse phase variation, the fraction lost through radiation, Q, is much greater than the reflected fraction, R, even for large mismatches in γ. On helices, which may have values of γ/k approaching two, Q and R may be comparable for small mismatches in γ. In general, the higher the values of γ/k, the lower the amount of loss by radiation.

As a practical matter, if it is desired to make a tandem junction between two open periodic circuits having widely different values of γ, equations 3.3 and 3.4 imply that a tapered transition should be used. For example, if $\gamma_2 = 0.5\,\gamma_1$, an abrupt junction will cause 11.1 percent of the incident energy to be lost by radiation or reflection. However, if the transition incorporates five junctions each having a γ mismatch of $(0.5)^{1/5}$ or 0.871, then the total loss will be only 2.45 percent. More steps would tend to

lower the loss. If the amount of energy lost by reflection is comparable to that lost by radiation, as might be the case with helices, then appropriate shaping of the transition may eliminate the loss due to reflection in much the same manner as a well designed waveguide transition.

It was mentioned earlier that two reasons for the inclusion of the fourth junction of figure 3-2 are that it might be difficult to launch directly onto the filter circuit and that an intermediate slow wave circuit may enhance filter effectiveness. Let us consider these reasons as they apply to the design of tandem junctions.

It is shown in section III. C that a high value of γ permits high launching efficiency for a given aperture size. Making γ higher in the launching region than is required (or desired) in the final open periodic filter circuit may aid in achieving high launching efficiency. Taking the uniform thin ladder circuit as an example, γ can be made higher by keeping the slot dimensions fixed while decreasing the period. This is shown in figure 3-12, where the triangle and curve labled "1" represent the final desired filter characteristic, f_r is the slot resonant frequency, f_ℓ and f_h define the design passband. Curves 2, 3, and 4 are for arrays of similar slots with progressively smaller pitch. Now, if curve 4 represents the pitch used in the launching region, the high value of γ associated with this curve will permit high launching efficiency from the closed to the open structure of a given aperture size. In the open region the pitch can be increased gradually through curves 3 and 2 until the filter characteristic, curve 1, is obtained. Of course, the change in pitch must be gradual enough to prevent radiation or reflection. Otherwise the high level of slow wave transmission achieved by the high launching efficiency at the aperture will be negated by the loss in transmission.

A tandem junction might also be used to solve the problem of reflective stopbands in the closed periodic structure. This can be done by making the frequency of zero group velocity high enough to permit stopband energy to pass through the transition aperture onto the open periodic structure. The stopband edge frequency can then be lowered gradually in the open structure so that the undesired frequencies fall into forbidden regions and are

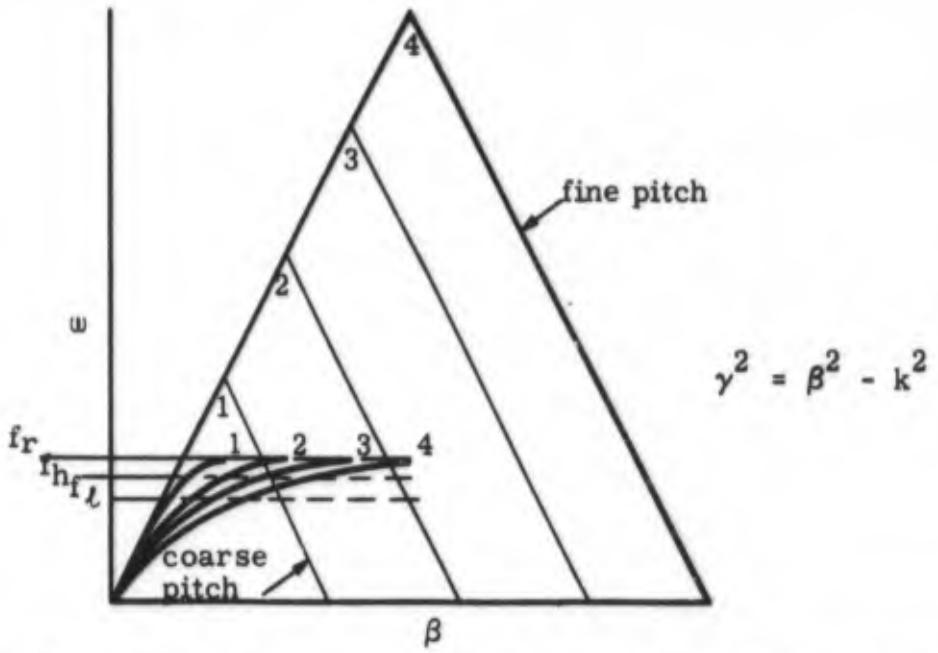

Figure 3-12. ω-β diagram of structure with varying pitch, showing dependence of γ on pitch.

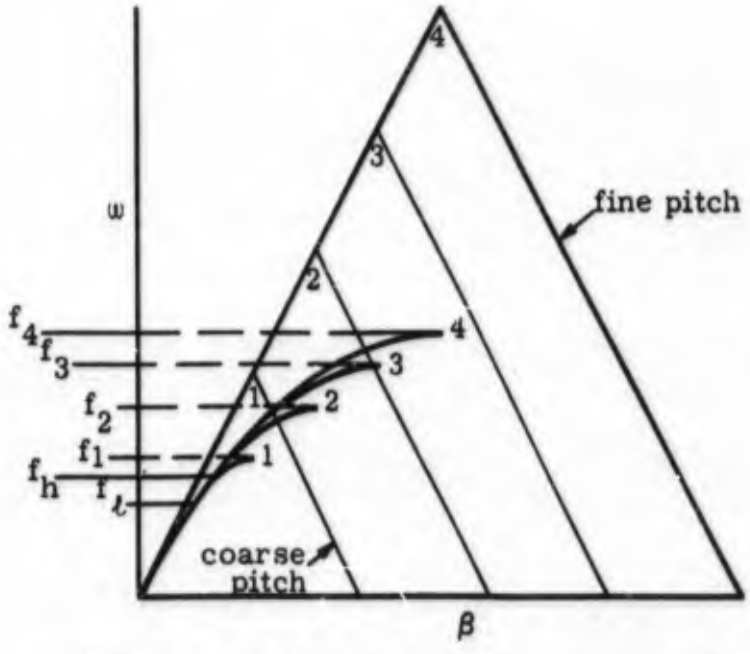

Figure 3-13. ω-β diagram of structure with varying pitch and slot resonance, having γ constant in passband.

radiated from the structure. Figure 3-13 is an ω-β diagram of a tapered tandem junction with these characteristics. Curve 1 and triangle 1 correspond to the final filter characteristic. Curve 4 and triangle 4 represent the characteristic of a slow wave structure having both smaller pitch and a higher $v_g = 0$ point. In a ladder structure this corresponds to a higher resonant frequency for the slots. This structure is continuous through the aperture, so that undesired signals up to f_4 are launched on the open slow wave structure. The pitch is gradually increased and at the same time the $v_g = 0$ point is lowered in frequency, so that the intermediate curve 3 is obtained. In this interval undesired signals from f_4 to f_3 are successively radiated. With continued increase in pitch and decrease of slot resonant frequency, the band from f_3 to f_2 is radiated, and so on until the desired final filter characteristic, curve 1, is achieved and only the passband frequencies from f_h to f_ℓ are propagated by the structure. The structure represented by figure 3-13 will not have as high passband launching efficiency for a given aperture size as would a fine pitch structure in which the resonant frequency is maintained at f_1, such as was shown in figure 3-12, because of the lower values of γ. However, if the values of γ for the passband frequencies are sufficiently high for efficient launching on a structure corresponding to curve 4, and if γ is maintained at this value in the transition from fine pitch to coarse pitch, then little passband energy should be lost through radiation.

IV. GENERAL FILTER STUDIES

A. OVERVIEW

General open periodic filter studies were undertaken on this program in order to determine the roles of the various slow wave circuit parameters in developing transitions.

In the course of phase I work it appeared that the transverse separation constant γ was of great importance to launching efficiency and in tandem junctions of open periodic circuits. The group velocity v_g is of importance in the design of transitions and open periodic filter circuits since $v_g = 0$ defines the edge of a stopband. The phase velocity v_p must be considered in the study and design of coupled line junctions of open periodic circuits. The roles of these parameters are discussed in sections III and V. They are readily calculated for most periodic structures from ω-β diagrams, and a great deal had been learned about them on the previous program.

However, the role of impedance at junctions between open periodic structures was not clear. For instance, the properties of a tapered junction between open periodic circuits were derived from consideration of γ and β, (section III. D, equations 3. 2, 3. 3, and 3. 4). Also, the tapered horn transition between the closed and open regions of a periodic structure is required to transform the slow wave without radiation and no statements were made regarding impedance in section III. C. One of the reasons for this state of affairs is that little was known about the impedance of open periodic filter circuits. Still, it seemed that impedance <u>should</u> be a consideration in the design of transitions. This consideration of impedance was the object of significant effort on the previous program and this effort was continued, with conclusions that are presented in part B of this section.

When particular transition circuits were studied for overall feasiblity and the optimization of circuit parameters, it was found necessary to extend

the previous studies on the application of open periodic circuits to filtering. This was because some of the circuits appeared to be unsatisfactory for high power applications, so designing transitions for these circuits would be unprofitable. The basic design of these circuits was reviewed and general conclusions are presented in section IV. C.

B. IMPEDANCE STUDIES

The general transition studies indicated that while impedances would be an important consideration in the design of the intermediate fast wave line (refer to figure 3-2) and the closed slow wave circuit, as well as the junction between them, no clear-cut role could be assigned to impedance in junctions of open or nearly open periodic circuits. But because impedance is usually an important consideration at transmission circuit junctions it was believed necessary to investigate it.

It should be recognized at the outset that impedance of a guided wave is an artifice; it is an attempt to quantize the fields of the wave so that network calculations can be performed. The impedance concept is useful at a junction of two guided waves only if the two impedances have the same definition in terms of the common fields at the junction.

In lumped element circuits the impedance is clearly defined; it is simply the ratio of the voltage between two points to the current into one of the points. In waveguiding structures current and voltage are seldom readily measured and must be defined in terms of line integrals of electric field or surface integrals of magnetic fields, and the choice of a useful path or surface of integration is not always an obvious one. As with lumped element circuits, it is possible to replace voltage or current by an expression in power and impedance. Doing this leads to the following impedance definitions given by Shelkunoff (ref 5)

$$\text{(a) } Z_{V,\,I} = \frac{V}{I}\,; \quad \text{(b) } Z_{P,\,I} = \frac{2P}{II^*}\,; \quad \text{(c) } Z_{P,\,V} = \frac{VV^*}{2P} \tag{4.1}$$

where I and V are peak values. These impedances are known as the current voltage impedance, the power current impedance, and the power voltage

impedance. In the last two definitions, it is necessary only to define either current or voltage, but not both.

In open surface wave structures the voltage is more readily defined than the current. In general

$$\bar{E} = -\nabla V - \frac{\partial \bar{A}}{\partial t} \tag{4.2}$$

It is possible to pick a direction of electric field for which there is no time varying magnetic vector potential A, and E is the negative gradient of voltage in that direction. The question now arises as to which direction should be used. In the discussion of transitions it was pointed out that the slow wave circuits could be treated as transmission lines with one terminal at the structure and the other at infinity at either end of a section. For tandem junctions the impedance at the terminals is desired. The gradient of voltage should then be taken in the plane perpendicular to the axis of the structure and in the direction in that plane in which electric field strength diminishes. This will be referred to as the transverse or terminal plane impedance.

In rectangular coordinates

$$E_x = -\frac{\partial V}{\partial x} = \gamma V \tag{4.3}$$

Therefore, substituting into equation 4.1(c)

$$Z_{P,\ V(\text{transverse})} = \frac{E_x^2\ (x = 0)}{2\gamma^2 P} \tag{4.4}$$

A longitudinal direction could be chosen for the gradient of voltage which will define the interaction impedance useful in traveling wave tubes.

$$E_z = -\frac{\partial V}{\partial z} = j\beta V \tag{4.5}$$

$$Z_{P,\,V(\text{longitudinal})} = \frac{E_z^2\,(x = 0)}{2\beta^2 P} \tag{4.6}$$

This impedance might be of use in the development of coupled line junctions.

Another open periodic circuit impedance can be defined, which, while it does not relate directly to the guided waves on the structure, and therefore, does not assist network calculations, is still of use in describing the circuit. This impedance concept is the surface impedance, which is the impedance to a plane wave impinging on the surface. The orientation of the plane wave must be such as to permit the existence of an axial electric field. For example, if the open periodic circuit consists of a corrugated conducting surface, as shown in figure 4-1, which supports a surface wave traveling in the z direction, then the surface impedance is defined for a plane wave whose electric fields are in the z direction. Then, following Barlow and Brown (ref 4 pp 19-20) the surface impedance Z_s is found to be

$$Z_s = R_s + j\,X_s = R_s + j\,Z_{groove} \tag{4.7}$$

Assuming a lossless groove and free space

$$j\,Z_{groove} = j\,X_{groove} = j\,377\,\tan\frac{2\pi h}{\lambda} \tag{4.8}$$

and assuming that the ridges have negligible surface impedance

$$Z_s = \frac{d}{D}\,Z_{groove} = j\,377\,\frac{d}{D}\,\tan\frac{2\pi h}{\lambda} \tag{4.9}$$

Collin (ref 6 pp 458-459) gives the following relationships for a general surface

$$\gamma = \gamma' + j\gamma'' = kX_s - j\,k\,R_s \tag{4.10}$$

$$\beta = \beta' + j\beta'' = k\left(1 + X_s^2 - R_s^2 - 2\,j\,R_s\,X_s\right)^{1/2} \tag{4.11}$$

It will probably be recognized that we have been using the surface impedance concept all along when we have stated that the surface must be inductive to support a slow wave. (Examination of equation 4.10 will show that this is so.) The usefulness of surface impedance is that it determines the propagation characteristics of the structure. Of course, it will seldom be as easy to calculate the surface impedance as it was for the simple structure of figure 4-1; but if it is known how to decrease or increase R_s and X_s, the resulting change in propagation characteristics can be predicted.

Several attempts were made to calculate the transverse power voltage impedance of filter structures, both on this program and on the previous program. The basic circuit for these calculations is shown in figure 4-2. What were particularly sought were impedance expressions that related to the easily measured ω-β characteristics of the open structure and the height d of the conducting surface. Then, as the height varies, as in a horn, one could determine the impedance change.

When d is small enough, the impedance of the closed periodic circuit can be calculated from an equivalent circuit of an element of pitch. The equivalent circuit is based on one or more propagating modes whose fields and impedance are defined, and the evanescent modes required to satisfy boundary conditions. In many cases the effect of the evanescent modes has been calculated in terms of reactances and electrical line lengths and is conveniently tabulated.

As dimension d increases we find that the equivalent circuit of a single element no longer holds for the type of surface wave actually encountered, in which interaction between more or less remote elements is required for propagation. Accordingly, the transverse power voltage impedance can no longer be defined by the equivalent circuit.

The equivalent circuit approach is of value at the junction between the fast wave transmission line and a narrowly enclosed slow wave circuit. However, if single mode propagation exists on both sides of the junction, it is often easier to obtain the characteristic impedance of the close slow wave line by measurement. An example is given in reference 2 pp 5-38 ff,

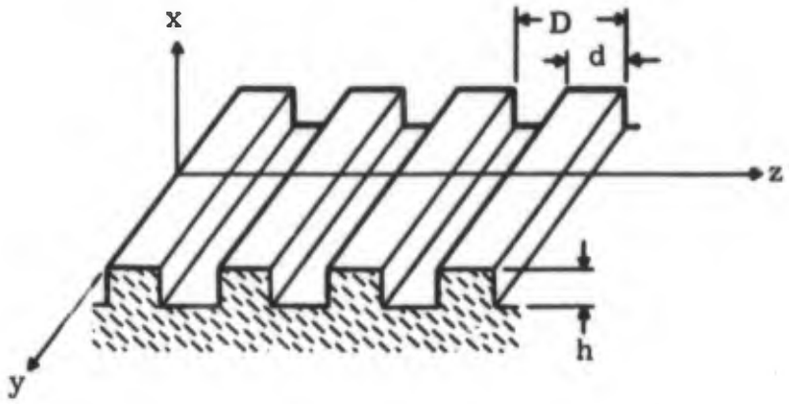

Figure 4-1. Corrugated conducting surface.

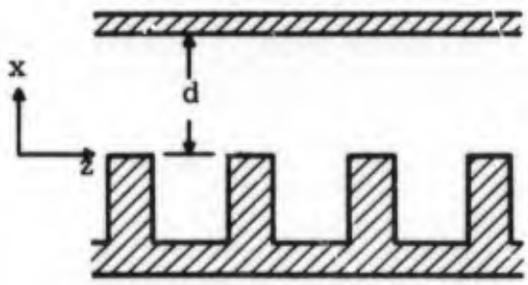

Figure 4-2. Closed slow wave structure.

in which it is pointed out that the characteristic impedance of the structure depends on the definition of its elements. A uniform array of slots can be divided into symmetrical elements at either the center of a web or the center of a slot, and the resulting impedances are inversely related.

Since the impedance at each end of a tapered transition must be defined in the same way to be useful for transition design, it appeared that a definition which was valid for all values of d was required. This approach was started on the previous program (ref 2, pp 5-21 ff). Specifically, for a simple E-mode on the structure of figure 4-2 the axial electric field could be expressed as

$$E_z = E_o \frac{\sinh \gamma (d - x)}{\sinh \gamma d} e^{j(\omega t - \beta z)} \tag{4.12}$$

The fields are postulated as uniform in the y direction, but the condition of the wave extending to infinity is removed by defining

$$E_z = 0 \text{ when } | y | > a \tag{4.13}$$

where a is the distance from the z axis to the edge of the structure. Equation 4.12 reduces to the equation for a simple open slow wave as d approaches infinity:

$$E_z = E_o e^{-\gamma x} e^{j(\omega t - \beta z)} \tag{4.14}$$

The transverse power voltage impedance was calculated by applying Maxwell's laws for guided waves to equation 4.12 and substituting into equation 4.1(c) yielding

$$Z_{P,\ V} = \frac{\beta}{a\omega\epsilon\gamma} \left[\left(\frac{\sinh^2 \gamma d}{\gamma d} \right) \frac{1}{\left(\frac{\sinh^2 \gamma d}{2\gamma d} + 1 \right)} \right] \tag{4.15}$$

This reduces to $Z_{P,\ V} = \beta/\omega\epsilon a\gamma$ as d approaches infinity.

Since this impedance function is continuous as d approaches infinity it would seem to provide insight into the requirements of the tapered transition

between closed and open slow wave structures. However, it suffered from the drawback of being inapplicable to periodic structures. This was a consequence of the basic assumption that the pitch is much smaller than a wavelength, i.e., the surface is smooth. On such a surface the phase velocity is equal to the group velocity whereas on periodic surfaces this is not so.

Since the program was concerned with periodic structures, on which the group velocity may vary radically, a modification of this method was sought which would take periodicity into account.

In the general statements of reference 2 pp 2-27 about periodic structures, the power flow is related to the group velocity and the energy stored in the field per pitch

$$P = \frac{W}{p} v_g = \frac{2 W_E}{p} v_g = \frac{2 W_H}{p} v_g \qquad (4.16)$$

where W is the total average energy per unit length stored in the space surrounding a slow wave structure, and W_E and W_H pertain to the electric and magnetic fields, respectively. Now for an open structure ($d = \infty$) the average energy stored in the electric field per pitch is

$$\frac{W_E}{p} = \frac{\epsilon a}{8\gamma} \left(1 + \frac{\beta^2}{\gamma^2}\right) E_o^2 \qquad (4.17)$$

using equation 4.14 to define the electric field. The transverse power voltage impedance was then found to be

$$Z_{P,V} = \frac{2\beta^2}{\gamma \epsilon a v_g (\gamma^2 + \beta^2)} \qquad (4.18)$$

When d is finite, the transverse power voltage impedance was found to be

$$Z_{P,V} = \frac{2\beta^2}{\gamma \epsilon a v_g (\gamma^2 + \beta^2)} \left[\left(\frac{\sinh^2 \gamma d}{\gamma d} \right) \frac{1}{\left(\frac{\sinh^2 \gamma d}{2\gamma d} + \frac{\beta^2 - \gamma^2}{\beta^2 + \gamma^2} \right)} \right] \qquad (4.19)$$

The bracketed term is similar to the dimensional term in equation 4.15 and likewise approaches unity as d approaches infinity. However, some questions arise as to the usefulness of this approach. First, it is known that the magnitude and frequency variation of impedance when calculated from an equivalent circuit for small values of d depends on the choice of the element terminal planes. This is of practical importance when matching into a closed periodic circuit from a waveguide. Should not the impedance expressions based on field calculations take the choice of terminal planes into account also? And if they do, won't they be radically different in magnitude and frequency variation? One can conceive of an impedance function that goes to zero as the group velocity approaches zero at $\beta = \pi/p$ because the defining voltage approaches zero. The answers to these questions appear to require consideration of the spatial harmonics. At the center of a tooth or boss in figures 4-1 or 4-2 the axial field is always zero, and this represents the sum of the infinite number of spatial harmonics at this point. But the field expressions of equations 4.12 or 4.14 define a traveling wave whose time average amplitude is the same at any point on the axis. Actually these equations are intended to relate to the predominant spatial harmonic when the structure is resonated.

The assumption in all of the above calculations is that a useful impedance can be defined in terms of the predominant spatial harmonic. When the supporting surface is a uniform reactance sheet such a definition will permit one to perform numerical calculations relating to the magnitude of the impedance. But on a true periodic surface, no numerical values of an impedance so defined will be correct at every point on the axis. With the center of a slot or groove as the terminal plane, where the actual field probably bears the most resemblance to the defining field based on the predominant spatial harmonic, the variation of the impedance expression with frequency may not adequately describe the performance of the circuit.

When impedance studies were begun on the previous program, and during much of this program, the aim was to develop impedance expressions that would assist in matching one circuit to another, and the magnitude and frequency dependence of the expression was considered to be of great importance. It has been pointed out that the approaches used could not provide

expressions that were useful for this purpose. However, in the course of the present program it appeared that what was really required was knowledge of how to design the transition from a closed periodic structure to an open periodic structure at a given frequency. Accordingly, the bracketed term of equation 4.19, which relates primarily to the dimensions of the enclosing surface, should be of value.

C. FILTER CIRCUIT DESIGN

Phase II of the program required the determination of the design requirements for transitions to specific types of open periodic circuits which had been investigated on the previous program. One of the first circuits considered for specific transition studies was the interdigital thick ladder filter which appeared to be most suitable for high power purposes and which had been the subject of the greatest effort on the previous program. The filter structure denoted as FTLI-6 and shown in figure 4-3 was the final basic design for this class of filter. The characteristics of typical configurations of FTLI-6 are shown in figure 4-4. Although a good stopband characteristic could be achieved, notably a sharp cutoff, the filter had some shortcomings which tended to lessen its usefulness in operational applications. One such shortcoming was the range of relatively low attenuation in the stopband shown in figure 4-4(a). Bending the open filter circuit as in figure 4-4(b) tended to improve the stopband attenuation but at the cost of increased passband loss, and reduced bandwidth. Even without the bend the passband loss is about 1 db for a fairly short length of circuit. It had been determined that the intrinsic loss of the slow wave circuit increased with frequency, while the launching loss decreased with frequency. The measured values for these loss mechanisms are shown in figure 4-5. It can be seen that even with radically improved launching efficiency (i.e., improved transitions), the overall filter loss will be high.

In an effort to determine whether the interdigital thick ladder could be improved the ω-β chart of the FTLI-6 circuit was examined. This is shown in figure 4-6, together with that of the FTL-13 in which the slots are aligned rather than interdigitally offset. It can be seen that the FTL-13 has a higher order slow wave mode. Further, the apex of the FTL-13

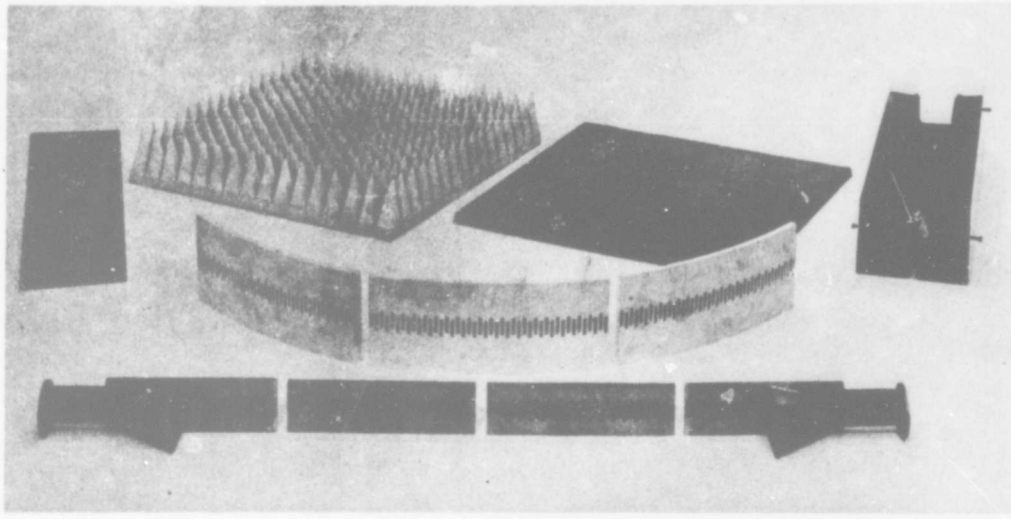

(a) Photograph of the elements.

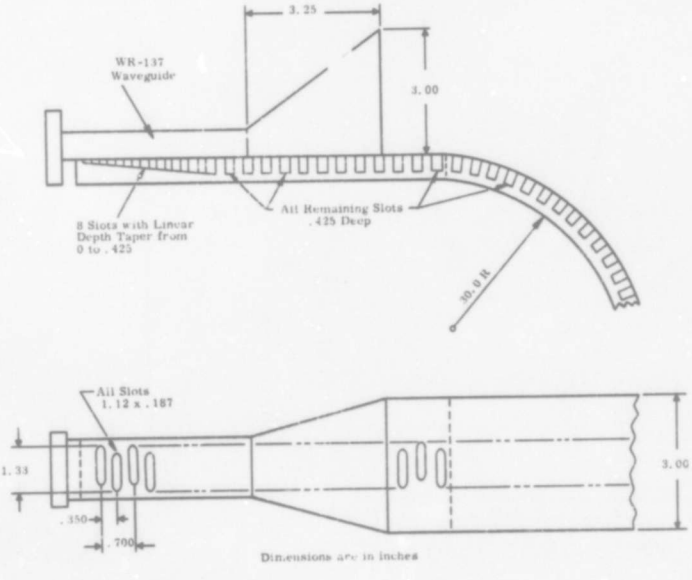

(b) Schematic drawing with dimensions.

(b) Schematic drawing with dimensions.

Figure 4-3. Interdigital thick ladder filter FTLI-6.

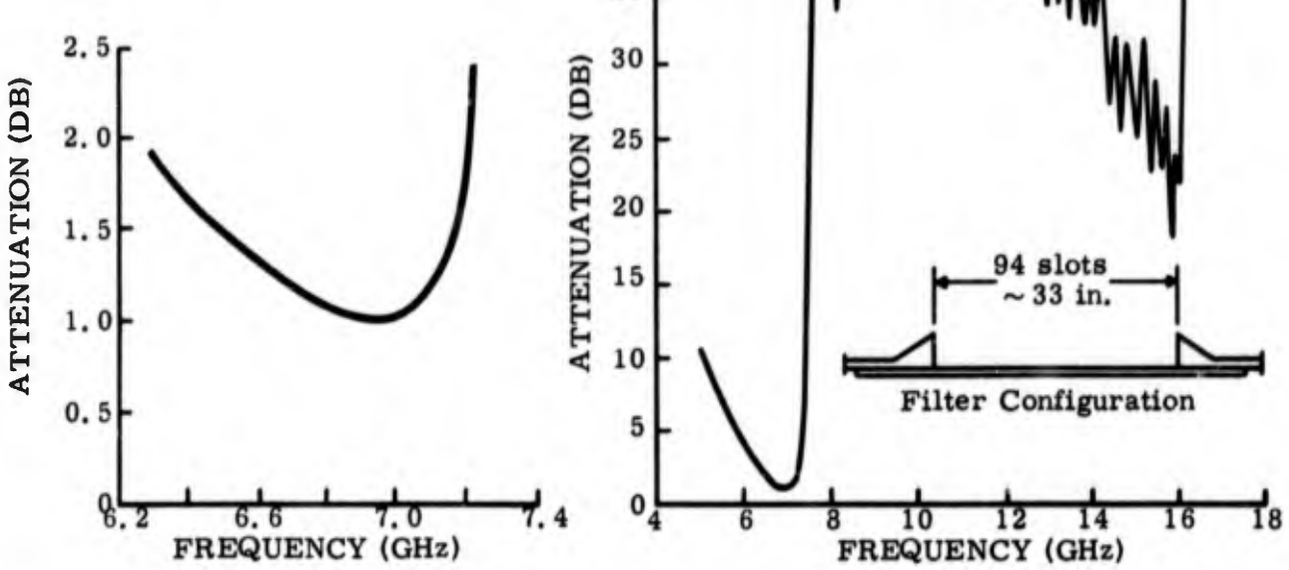

(a) Straight configuration.

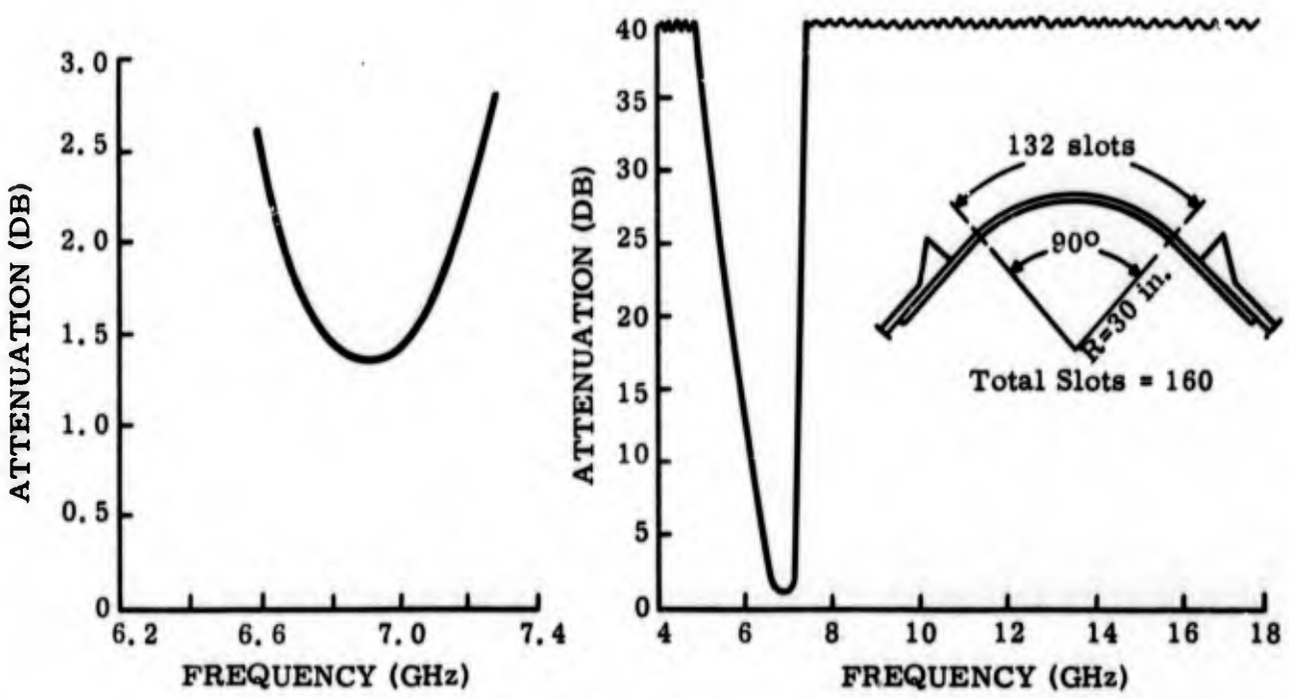

(b) 90° bend.

Figure 4-4. Attenuation of FTLI-6 in two configurations.

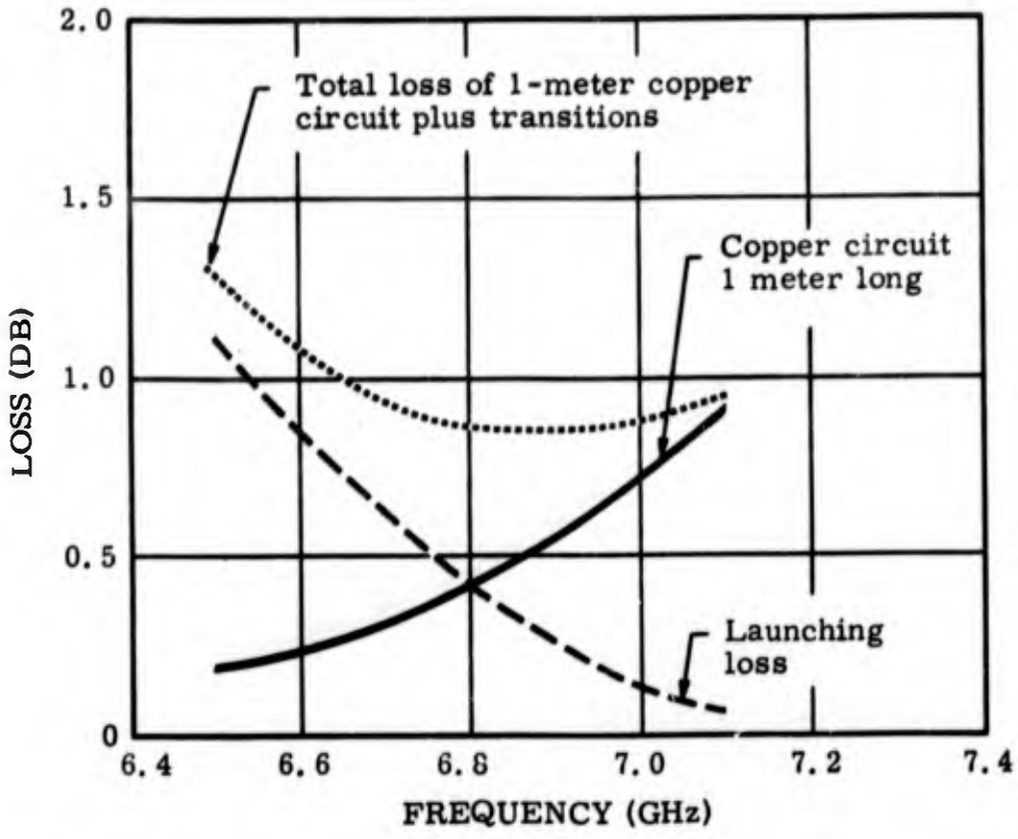

Figure 4-5. Loss mechanisms of FTLI-6.

triangle corresponds to the upper edge of the zone of low attenuation noted for a straight FTLI-6, figure 4-4(a).

There seemed to be a possibility that the filter performance did not depend entirely on the FTLI-6 ω-β diagram. The only difference between the two triangles of figure 4-6 is the arbitrary definition of pitch, which in the case of the FTLI-6 is the interdigital pitch, while in the FTL-13 diagram the pitch is the center-to-center spacing of adjacent slots. Since the FTLI-6 has the same spacing of adjacent slots, it was not surprising that it supported the higher order slow mode. In other words, the designation of the region outside of the FTLI-6 triangle as forbidden is of doubtful validity from consideration of all aspects of circuit performance. That it does have some validity is indicated by the sharper cutoff characteristic of the FTLI-6 at the beginning of the stopband as compared to the FTL-13; this sharper cutoff characteristic can be explained by the forbidden region corresponding to the interdigital pitch. The relatively high loss in the spurious passband of FTLI-6 can also be explained by the scattering which the interdigital pitch introduces.

It was clear, however, that attenuation should not be concentrated solely on the ω-β diagram corresponding to interdigital pitch. What was not clear was why the spurious passband should be so much wider than the frequency range corresponding to the higher slow mode obtained by resonating the circuit. However, the slots can be inductive in several possible waveguide modes at higher frequencies depending on their excitation. That is, as the slots are cut on for higher order waveguide modes they are initially inductive and stay so until they are one-quarter guide wavelength deep. Also, they become inductive for lower order modes when their depth exceeds one-half guide wavelength. The structure is therefore capable of supporting surface waves almost continuously from the higher slow mode up to the peak of the triangle corresponding to the slot-to-slot pitch. These waves are much weaker than the slow wave modes observed when resonating the structure. The only evidence of their existence other than the low loss in a filter configuration has been the cluster of resonances at the apex frequency that has been observed on almost all periodic structures.

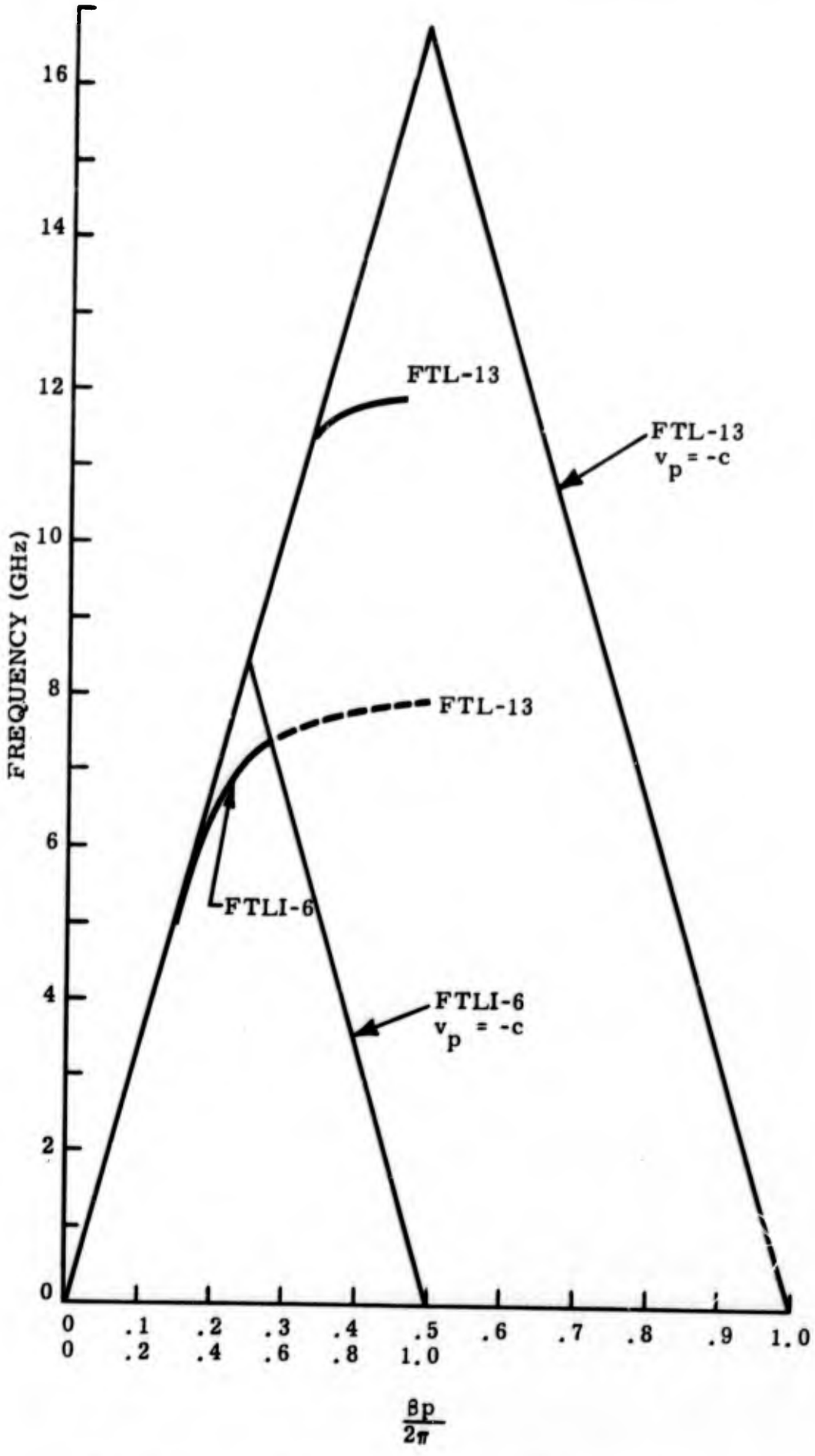

Figure 4-6. ω-β diagrams for the FTLI-6 and FTL-13.

Another important aspect of the design of the FTLI-6 is also shown by figure 4-6. The low values of γ in the operating band help to explain the passband losses encountered when bending the structure to eliminate the range of low stopband attenuation. The high losses at the upper edge of the passband can also be explained by the rapidly decreasing group velocity of the characteristic.

Therefore, it was appropriate to try to improve the thick ladder filter circuit before attempting to design transitions. The required improvements were:

1. Elimination of the low attenuation zone in the stopband.
2. Increased transverse separation constant γ.
3. Increased group velocity.

The design approach toward making these improvements was first to choose an appropriate stopband. Since it is generally desired to provide high attenuation of harmonic frequencies, the second harmonic should be placed above the apex frequency determined by the period of adjacent slots. This is shown on the normalized k-β diagram of figure 4-7, where the low frequency edge of a second harmonic band is at $kp/2\pi = 0.5$. The low end of the passband is therefore at $kp/2\pi = 0.25$. A desirable ladder characteristic which will have sufficiently high values of γ and v_g over the passband, as well as gradual slope, can then be sketched in. How well this curve could be realized would be determined by experiments on specific structures.

The above design approach represented a significant change in the concept of all filters based on periodic elements because it discarded the notion of an interdigital array of elements. If the elements are staggered alternately with respect to the axis, the passband will lie in the forbidden region based on the interdigital pitch, and will therefore suffer high loss. This is shown in figure 4-7 by the triangle based on interdigital pitch.

It was mentioned in the discussion of filter design in section II that structures with transverse phase variation apparently had a more linear phase characteristic than uniform structures (compare figure 2-11 with figure 2-6 or 2-7). In the case of ladder circuits or other periodic arrays of elements this appearance is due entirely to concentration on the k-β

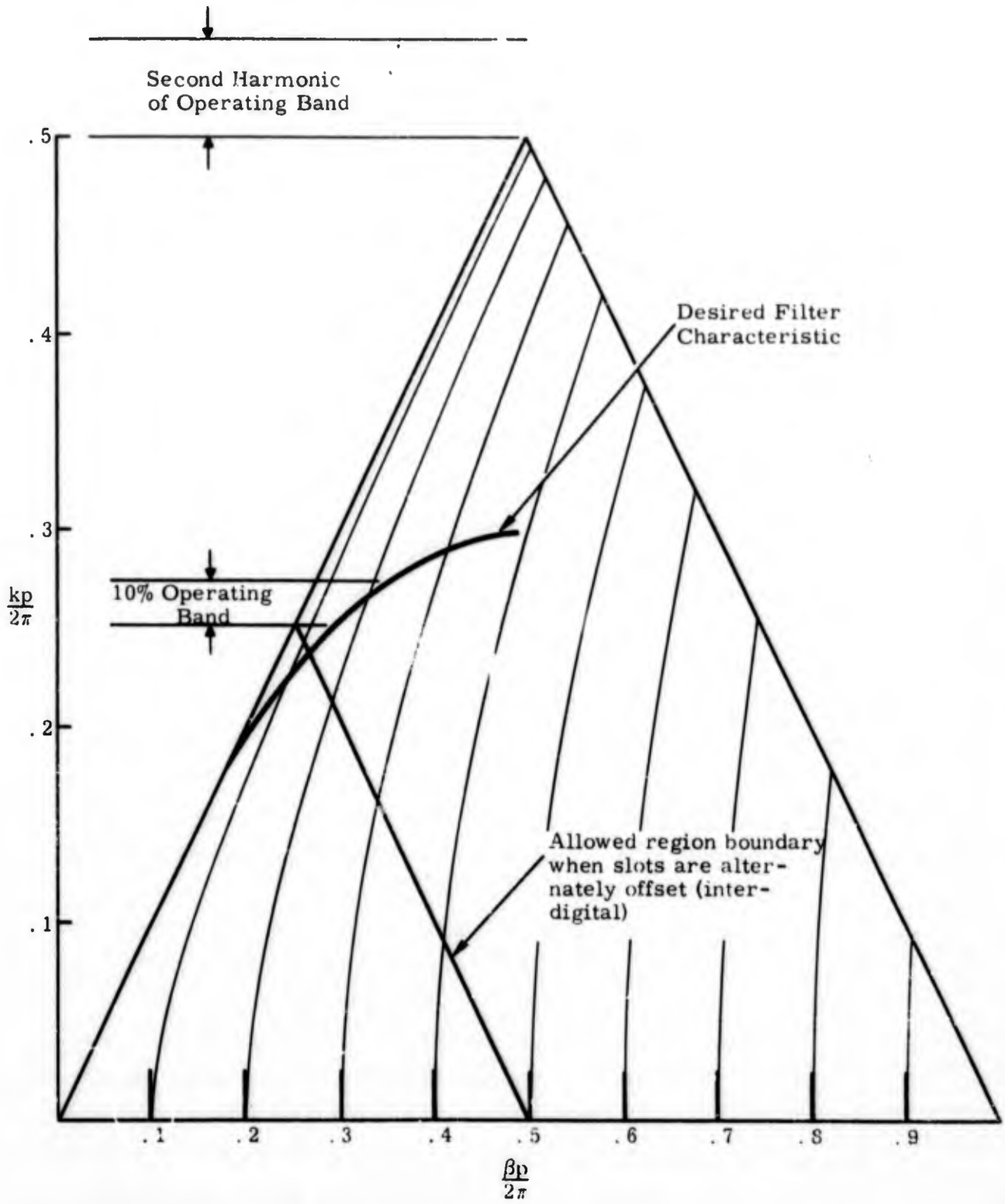

Figure 4-7. Diagram illustrating design of ladder filter for harmonic attenuation.

diagram based on interdigital pitch. When the k-β characteristic of an interdigital array is compared with that of a uniform array of the same elements with the same spacing of adjacent elements, as in figure 4-6, it can be seen that the k-β characteristics are really the same. At any frequency in the usable passband the absolute value of γ is the same for both arrays. This is reasonable when one considers that γ is determined in part by the inductive reactance of an element, and both arrays are composed of the same elements.

Discarding the interdigital concept and adopting the design approach of placing the second harmonic band above the apex of the k-β triangle led to the following conclusions:

1. For a given application, the pitch of any ladder structure is determined by the lower limit, f_1, of the passband

$$\frac{c}{4f_1} = \frac{\lambda_1}{4} \leq p \leq \frac{c}{2f_1} = \frac{\lambda_1}{2} \qquad (4.20)$$

2. Since the circuit cannot propagate in any mode at harmonic frequencies, it need be bent only enough to isolate the transition apertures from direct radiation and from reflections from the absorbers. The severe bending to eliminate propagating modes which occurred on the FTLI-6 is no longer needed and the passband loss due to bending can be reduced.
3. The sharp cutoff of the interdigital structures will not be achieved. However, since this characteristic was obtained by sacrificing a portion of the usable passband, it was not a real advantage.
4. The elements of the array can be optimized for the most desirable k-β characteristic without the restrictions imposed by the interdigital arrangement. This removal of restrictions also permits greater latitude in designing the elements for high power capability and low loss in the passband. It appears that the desired improvements will be aided by consideration of the surface impedance of an element.

V. COUPLED LINE JUNCTION STUDIES

A. GENERAL

The fourth junction of the functional block diagram of a transition (figure 3-2) was included because it might be of use in either or both of two possible circumstances:

1. When an efficient transition from the closed slow wave circuit directly to the open slow wave filter circuit would be difficult whereas an intermediate open slow wave circuit may permit more efficient launching.
2. When the junction may enhance filter effectiveness either by virtue of its own configuration or by permitting the use of an intermediate slow wave circuit.

It was pointed out in section III. D how a tandem junction could serve under the above circumstances. The possibility that coupled line junctions might also be of value was considered from the beginning of the program. They seemed to be of particular value in enhancing filter effectiveness. This is shown in figure 5-1(b) where two one-sided, slow wave structures are coupled so as to prevent much of the energy radiated from the structure and the transmitting horn aperture from reaching the receiving horn either directly or by reflection from the absorbers. Experiments with specific circuits were performed to demonstrate the value of coupled line junctions in filters.

In order to explain the concepts underlying the experiments, a brief discussion of coupled lines is helpful. By coupled lines is meant lines having common fields or currents for a given length in the direction of propagation. Consider first the case where the coupling is uniform, i.e., one segment of the coupling zone is the same as any other. Then, if the coupling is loose, permitting calculations based on the electrical characteristics of either line in the absence of the other, the fractional power transferred, F, from one line to another is given by Cook, et al (ref 7) as

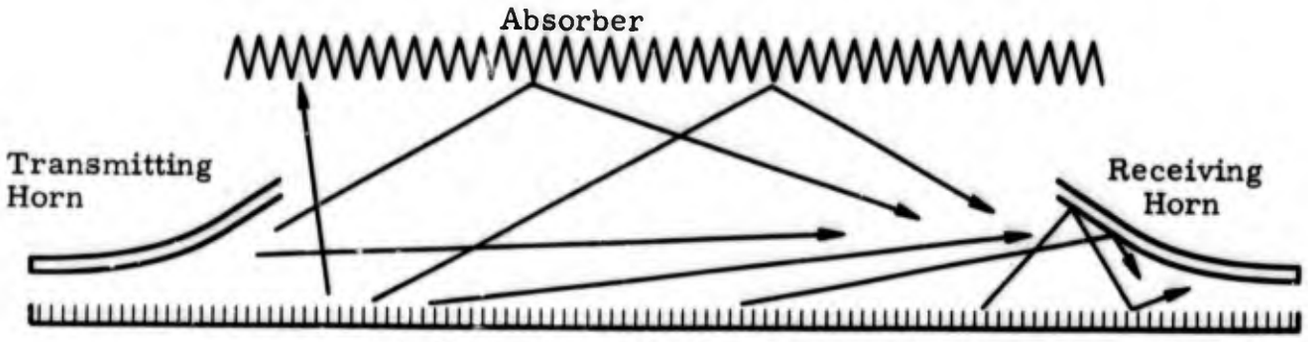

(a) Without coupled line junction.

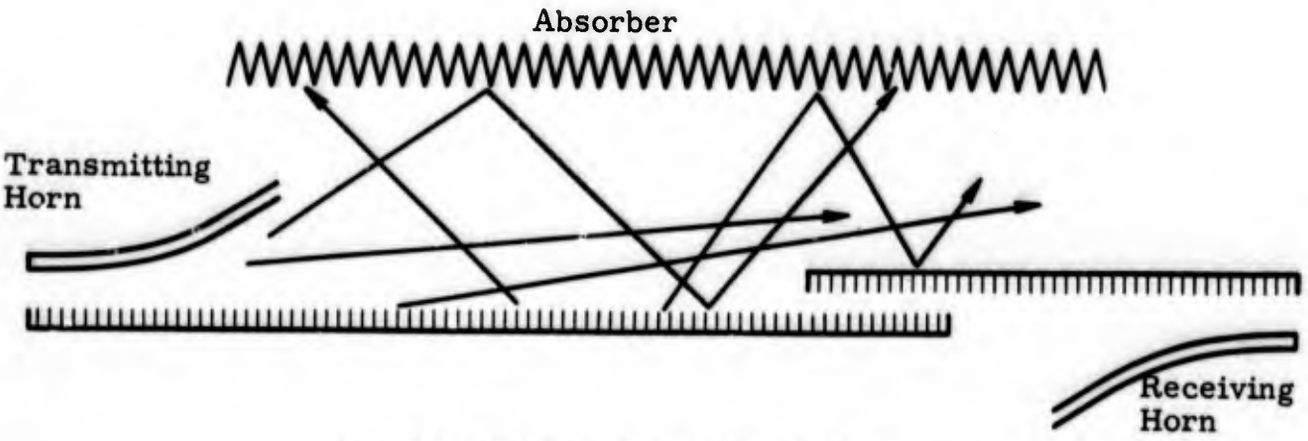

(b) With coupled line junction.

Figure 5-1. Schematic showing advantage of coupled line junction in filtering circuits.

$$F = \frac{\beta_c^2}{\beta_b^2} = \frac{\beta_1 \beta_2 (b + x)^2}{\left(\beta_1 - \beta_2\right)^2 + \beta_1 \beta_2 (b + x)^2} \tag{5.1}$$

where β_1 and β_2 are the phase constants of the individual lines. b and x are the capacitive and inductive coupling coefficients, respectively, and depend on the geometry of the coupling zone. β_c is the coupling phase constant and is defined by

$$\beta_c = \sqrt{\beta_1 \beta_2}\,(b + x) \tag{5.2}$$

β_b is the "beat" phase constant given by

$$\beta_b^2 = \left(\beta_1 - \beta_2\right)^2 + \beta_c^2 \tag{5.3}$$

The transfer of power is periodic along the length of the coupling zone, as is shown in figure 5-2, with "beat" wavelength $\lambda_b = 2\pi/\beta_b$.

When $\beta_1 = \beta_2$, the fractional power transfer is unity. The net amount of power transferred, τ, from one line to the other depends on the length L of the coupling zone and is given by Louisell (ref 8) for the case of equal phase velocities as

$$\tau = \sin^2 \frac{\pi L}{\lambda_{b_o}} \tag{5.4}$$

where

$$\lambda_{b_o} = \frac{2\pi}{\beta_c} = \frac{2\pi}{\beta_1 (b + x)} = \frac{2\pi}{\beta_2 (b + x)} \tag{5.5}$$

Therefore, a 3 db coupler will be one-quarter of a "beat" wavelength long, while a 0 db or 100% coupler will be one-half "beat" wavelength long. Such couplers are inherently narrowband because the beat wavelength changes with the wavelength of the coupled lines (equation 5.5). This in itself does not render this class of coupler unsuitable for application in a filter because when equation 5.4 is solved for 98 percent transfer (0.1 db loss) the resultant

bandwidth is about 12 percent. This may be sufficient for a particular radar application.

Because the coupling coefficients must be small for loose coupling, the "beat" wavelength and consequently the coupling zone will be long (equation 5.5).

When the restriction on loose coupling is removed, the analysis of uniform coupling becomes more difficult, but Miller (ref 9) has shown that the power transfer is still periodic over the coupling zone, and that 100 percent power transfer still requires lines with equal phase constants. However, the fractional power transfer between lines of different phase constants can be near unity if the ratio of the difference in phase constants to the coupling coefficient is small, provided the ratio of the difference in attenuation constants to the coupling coefficient C is also small. This is shown in figure 5-3 for the case where $\alpha_1 = \alpha_2$. C corresponds to the sum of b and x of the discussion of loose coupling. Cx is the product of coupling coefficient and coupling length. Figure 5-3 implies that lines with widely differing phase constants can be coupled with a high fractional power transfer if the coupling is made tight enough, and further, that the length required for maximum transfer decreases as the coupling coefficient increases.

For the particular case of the tightly coupled uniform helices of opposite sense and equal phase velocity, shown in figure 5-4, reference 7 shows that ideally a net power transfer of 99 percent can be obtained over a bandwidth in excess of 2:1. In practice (which was mainly concerned with traveling wave tube helices) the net power transfer was not smooth but varied erratically to as low as 96.7 percent. Since this may be due to mechanical irregularities, it does not rule out the use of this junction in a filter. However, this junction does not appear to offer any great advantage to filter design because after one has made the transition from coaxial line to the helix, there is no need to couple to a similar helix since it will not help improve filter effectiveness by isolation of the transmitting and receiving apertures.

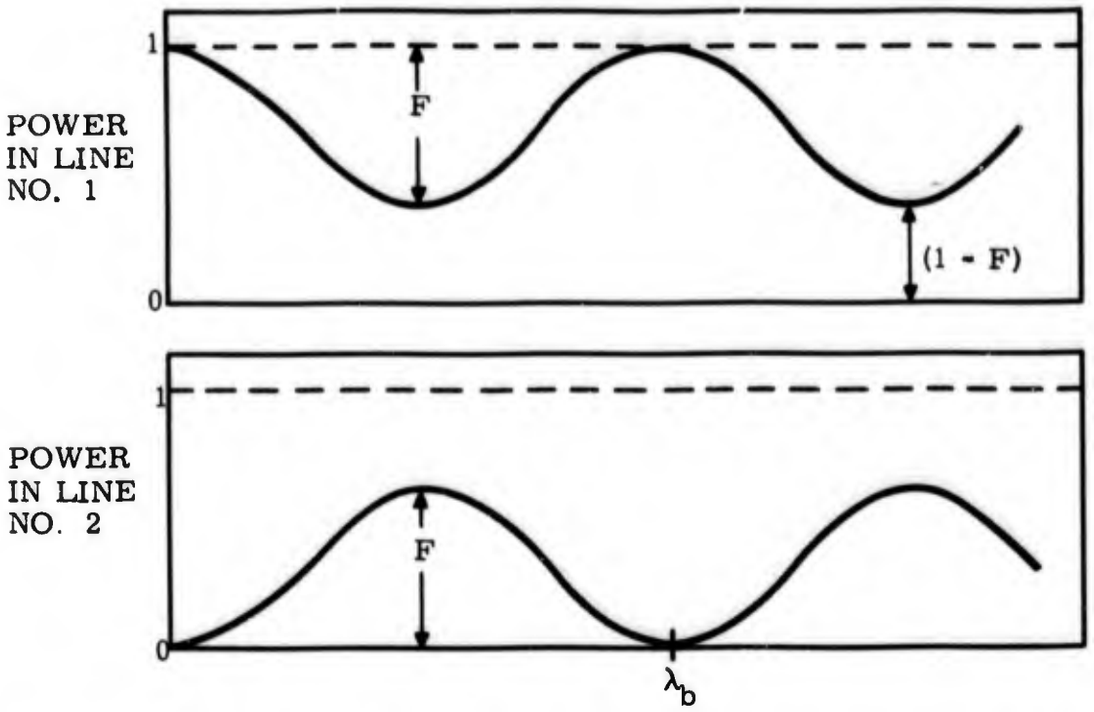

Figure 5-2. Incomplete power transfer resulting from coupling two lines having different phase velocities.

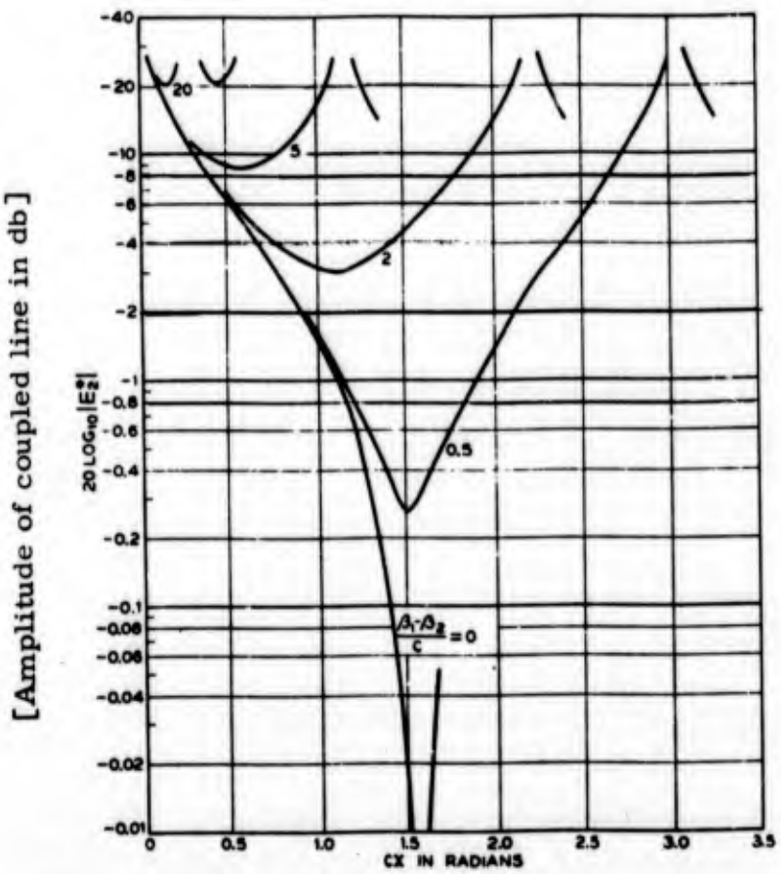

Figure 5-3. Undriven line wave amplitude versus CX with unequal phase constants and equal attenuation constants. The curves are periodic for larger values of CX. (Reprinted from ref 9 by permission of the AT&T Co.)

Thus far the discussion has been restricted to uniform coupling, which theoretically permits 100 percent coupling of lines of different phase constants only over narrow frequency ranges, and then only when the coupling coefficient is considerably greater than the difference in phase constants. Nonuniform coupling may be exploited to provide broadband junctions by varying the phase constants in the coupling region. This is depicted in figure 5-5 where the two lines with different phase constants enter the coupling region in which their phase constants are tapered so that the difference is reversed at the end of the coupling region. If this variation of the phase constants is properly adjusted, for any given input frequency ω, there will be a region such as that shown by $A(\omega)$ in which $\beta_1(\omega) = \beta_2(\omega)$. Efficient coupling will occur in this region. $A(\omega)$ should be about one-half local beat wavelength long for efficient coupling. Because the coupling coefficient will generally vary with frequency, the length $A(\omega)$ will also have to vary with frequency if broadband 100 percent coupling is to be achieved.

A realization of this type of coupler by Cook (ref 10) is shown in figure 5-6. The phase velocity of the inner helix is low at the left and high at the right; the outer helix has the opposite variation of phase velocity. Cook developed such a coupler for a 4 GHz traveling wave tube and demonstrated substantially 100 percent coupling over a bandwidth in excess of three octaves; the coupler length was 2 in. The values of the phase constants were not given.

While the coupler of figure 5-6 may not be of use in a filter for the same reason as the one-half beat wavelength coupler of figure 5-4, the principle of nonuniform coupling might well be applied to junctions between different open periodic circuits whose configurations will allow some benefits to filter effectiveness.

B. EXPERIMENTS

The first coupling experiment was between identical thick ladder circuits and was performed in order to determine:

1. The bandwidth limitations of uniform coupling
2. The improvement in filter performance, particularly stopband

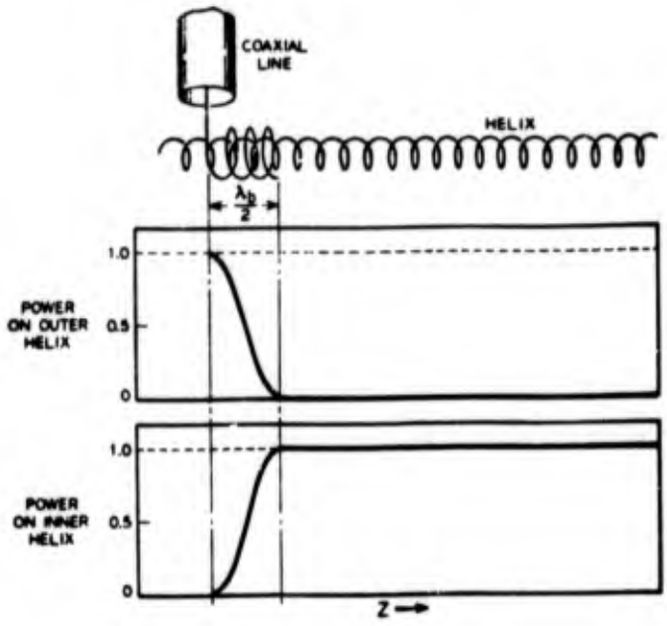

Figure 5-4. Helix coupler proposed by R. Kompfner demonstrating 100 percent coupling. (Reprinted from ref 7 by permission of the AT&T Co.)

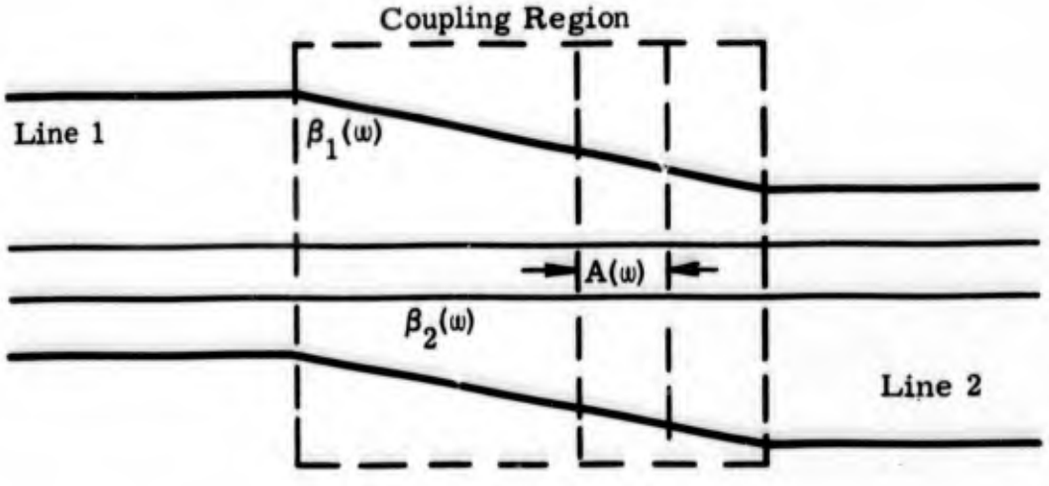

Figure 5-5. Broadband coupler employing nonuniform coupling.

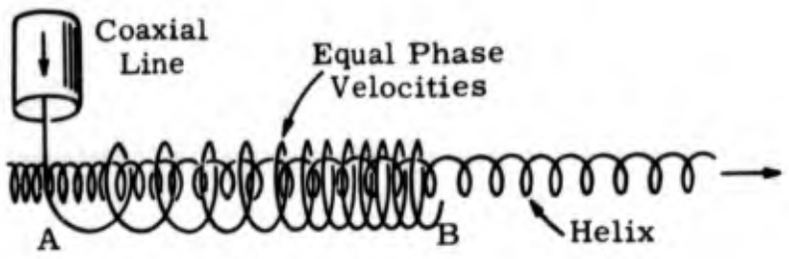

Figure 5-6. Helix coupler employing nonuniform coupling (after Cook, ref 10).

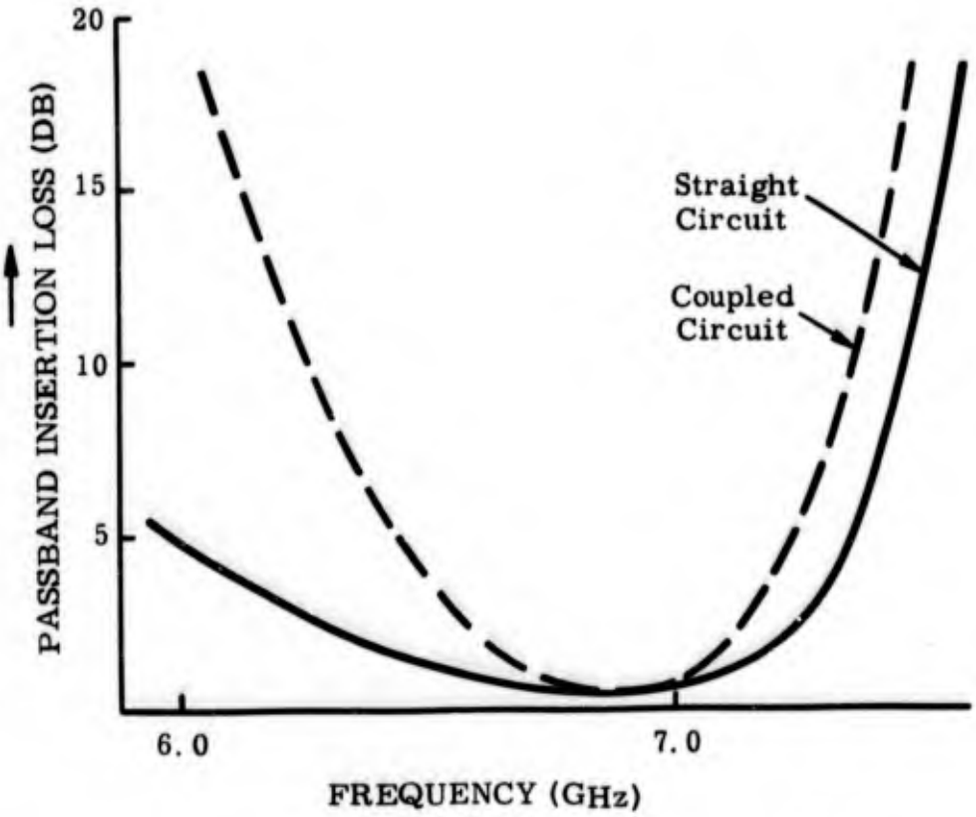

Figure 5-7. Insertion loss of coupled thick ladder.

attenuation, that could be obtained by employing a coupled junction between identical circuits.

The test setup was basically similar to figure 5-1. The thick ladder circuit and transitions were parts of FTLI-6 shown in figure 4-3. Nearly complete power transfer was achieved over a narrow bandwidth (figure 5-7) with 0.75-in. spacing between the circuits and a 2-in. coupling region. These were optimum dimensions. Variation in spacing and coupling region length produced the general trends predicted by the general studies of uniform coupling. Whether the narrow bandwidth was entirely due to the frequency sensitivity of the coupling or to other factors was not determined. One such factor could be the low value of γ at low frequencies which requires a large field volume. The abrupt beginning of the coupling zone might have caused reflection and scattering of these fields with consequent loss. Further, the transverse phase variation of the interdigital slot pattern (the use of which was dictated by the availability of the FTLI-6 filter) may have had an effect on the measurements.

Stop band attenuation increased about 10 db generally. Although some stray radiation could still be directed toward the receiving horn through the coupling gap, the major portion of this radiation was eliminated, showing the advantage to filter effectiveness provided by a coupled junction.

An experimental setup to determine the ability to couple from a thick ladder to a thin ladder is shown in figure 5-8. Such a junction might be employed as a transition to a thin ladder circuit. This is because of the relative ease of launching a slow wave on a thick ladder circuit which is one-sided, compared to the thin ladder circuit which requires the establishment of opposite field configurations on its two sides. Also the transition to a thick ladder can be made quite broadband and capable of handling high power. The fields on both sides of a thin ladder circuit are basically similar to those on the surface of a thick ladder circuit. For this reason a thin ladder was fabricated that had phase velocity characteristics similar to the FTLI-6, as shown in figure 5-9. Note that the characteristics of the thick and thin circuits are identical up to a frequency of about 6.9 GHz. The insertion loss of this circuit compared to that of the filter with a direct connection is shown in figure 5-10.

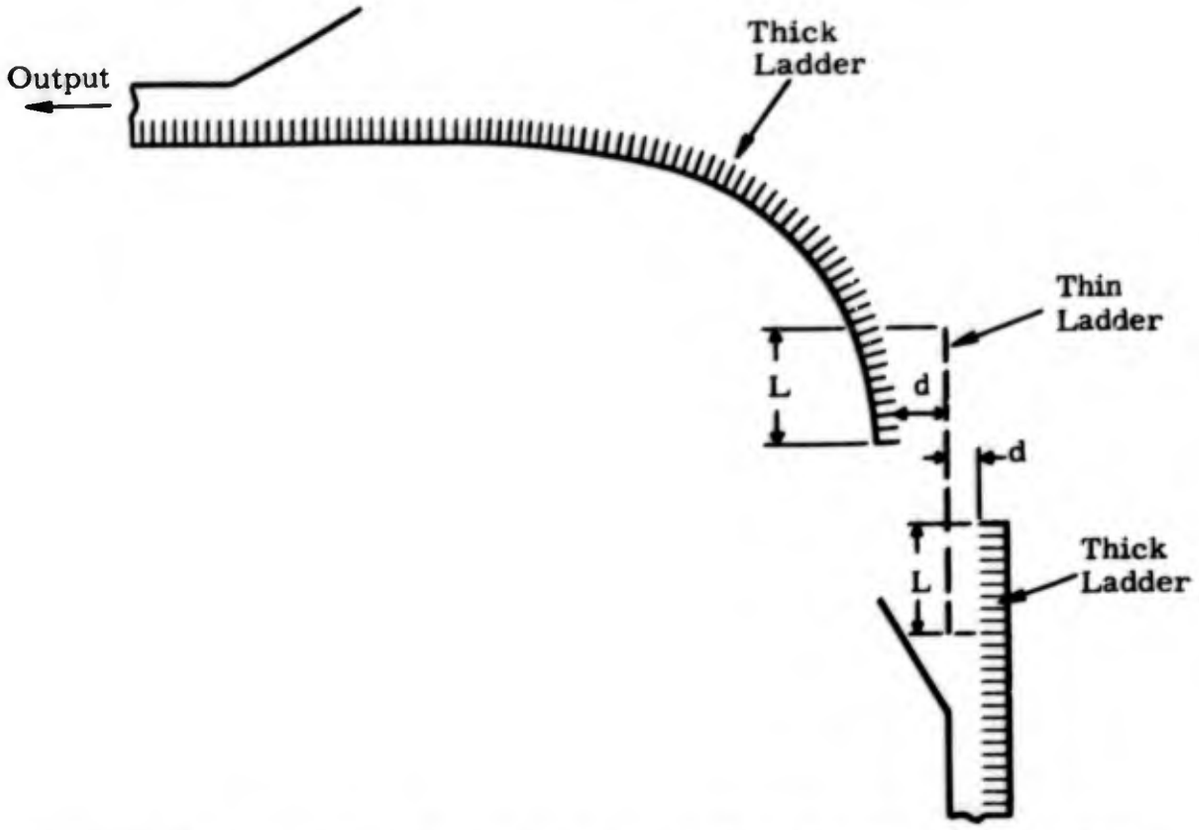

Figure 5-8. Thick interdigital to thin interdigital ladder coupling test configuration.

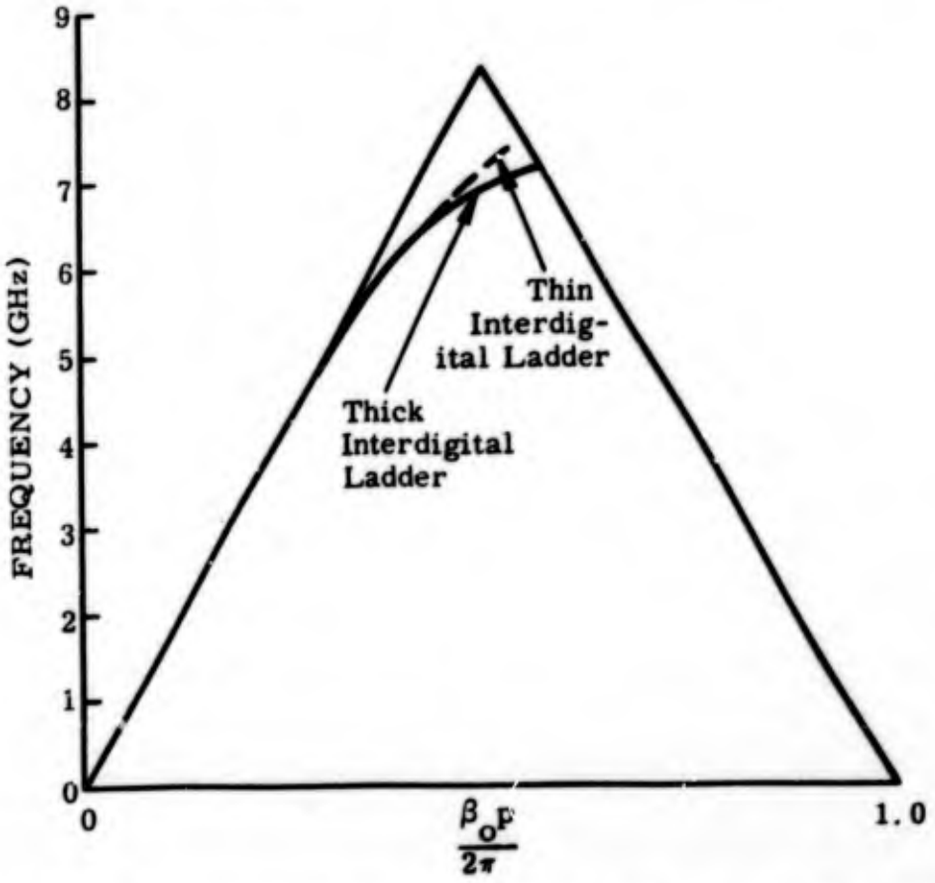

Figure 5-9. ω-β characteristics of the thick and thin interdigital ladder circuits employed in test configuration of figure 5-8.

The bandwidth of nearly complete coupling is about the same as for the coupled thick ladders (cf figure 5-7). However the loss is considerably greater above 7.0 GHz which probably relates to the disparity in phase velocities indicated in figure 5-9. The attenuation of the coupled configuration is about 0.5 db greater than that of the directly connected filter below 6.9 GHz. This 0.5 db difference can be considered coupling loss; and is attributed, first, to reflections and scattering due to the blunt edge of the thin ladder, and second, to the portion of the fields on the thick ladder that extend to the opposite side of the thin ladder in the coupling region. These fields are in the opposite direction to those of a thin ladder, and therefore, are detrimental to coupling.

To eliminate this effect, the spacing (d) in the coupling area was increased. However, to keep the coupling constant and high, the length L had to be increased to compensate for the increased gap. The passband insertion loss was improved slightly; however, the coupling area became quite long. It should be noted that there are two coupled line junctions in the schematic of figure 5-8. The results did show, however, that if the end effects were eliminated, successful coupling for transition applications can be obtained.

A practical transition by Chu and Kilcoyne (ref 11) utilizing coupling is shown in figure 5-11. The helix propagates in the -1 mode over the frequency range of interest. The helix is coupled to a circularly polarized HE_{11} mode dielectric rod. The field configuration of this mode is nearly identical to the -1 mode on a helix; therefore, good coupling efficiency to that mode should result provided the phase velocities are the same. The circularly polarized HE_{11} mode on the dielectric rod is the result of a TE_{11} circular waveguide mode that has been circularly polarized. Since the configuration and materials in this transition all have high power capability, a useful transition should result.

The fundamental mode velocity of the designed helix is approximately one-fifth the velocity of light so all slow wave modes higher than the -1 mode are eliminated from the allowed region as is shown in figure 5-12. The passband of this circuit was designed for the 2.7 to 2.9 GHz frequency

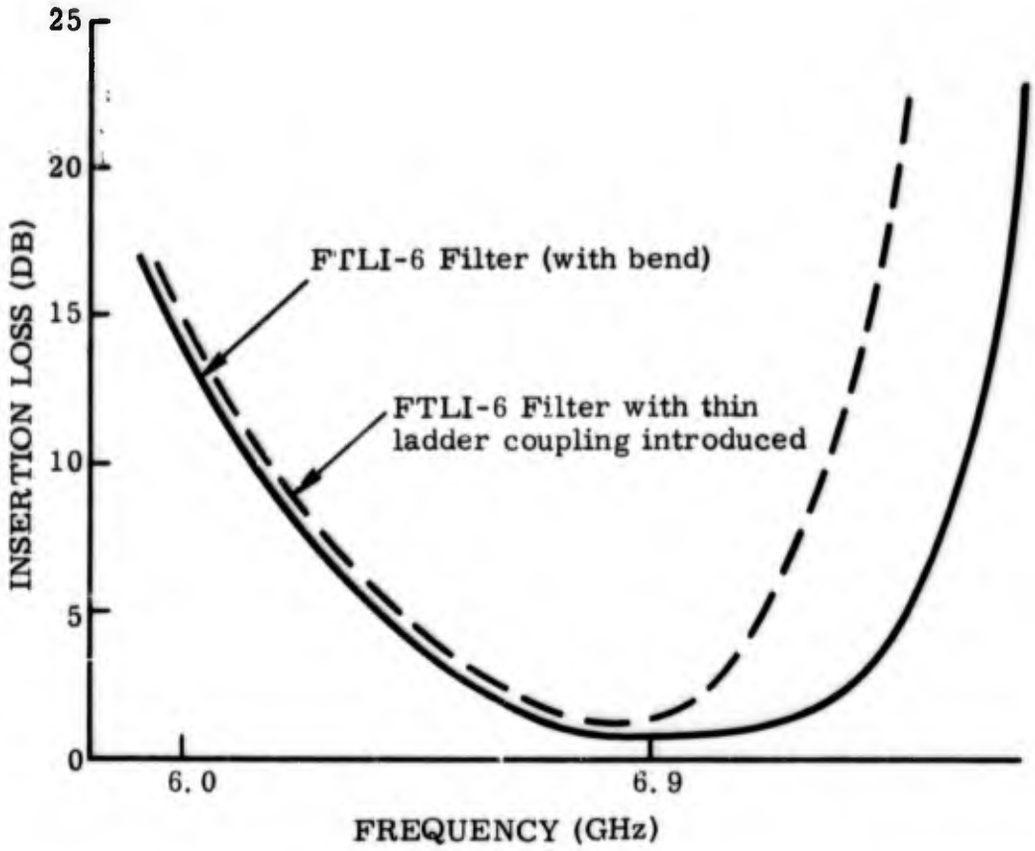

Figure 5-10. Thick ladder to thin ladder coupling insertion loss measurements.

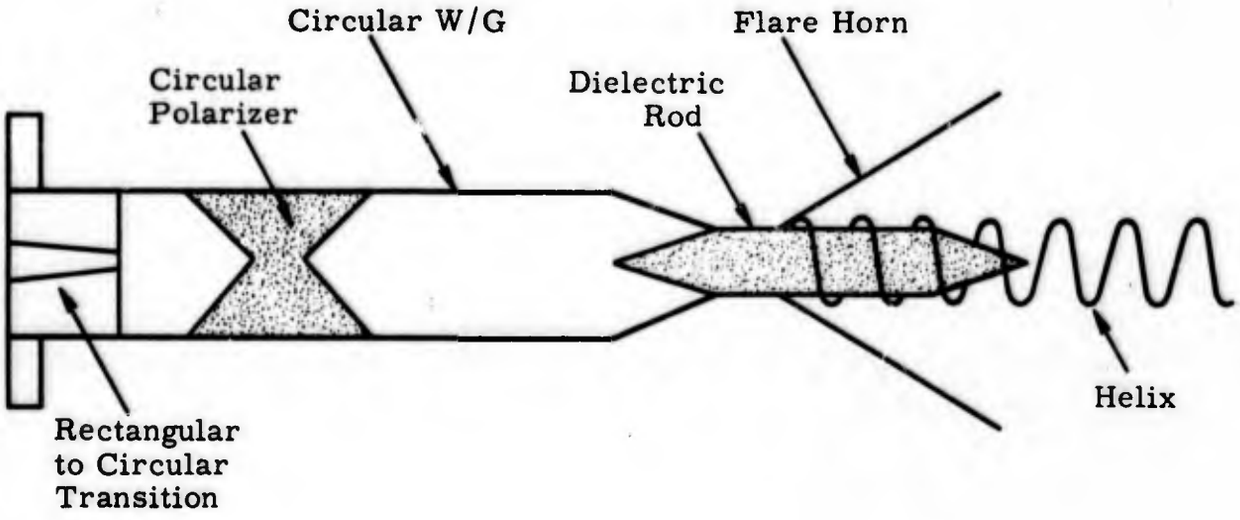

Figure 5-11. Dielectric rod to helix transition.

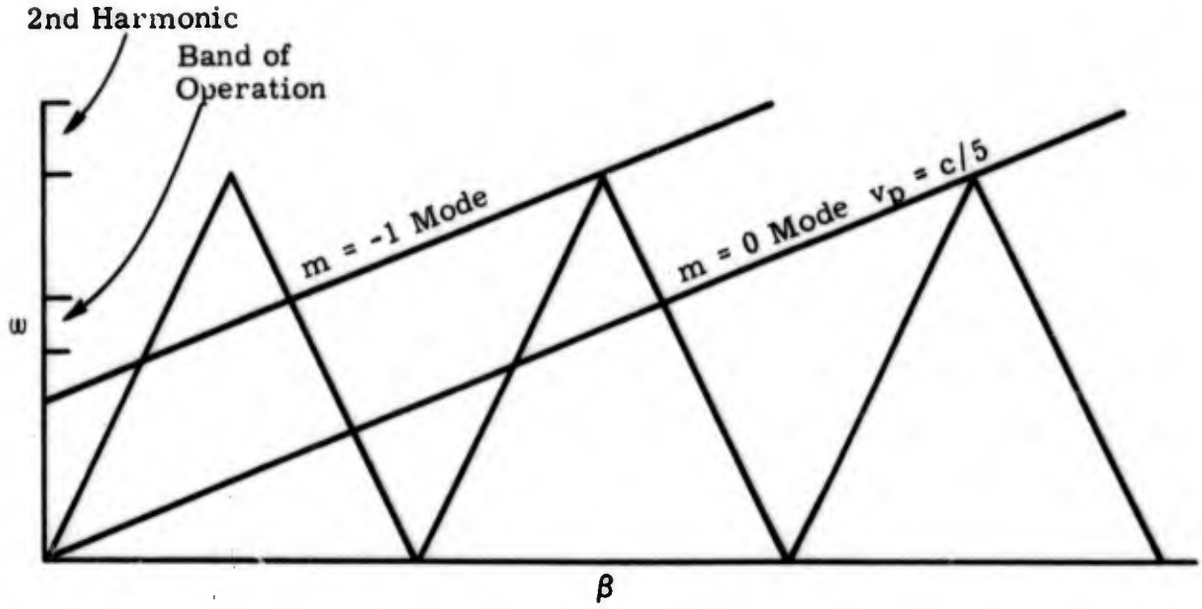

Figure 5-12. ω-β diagram for helix of figure 5-11.

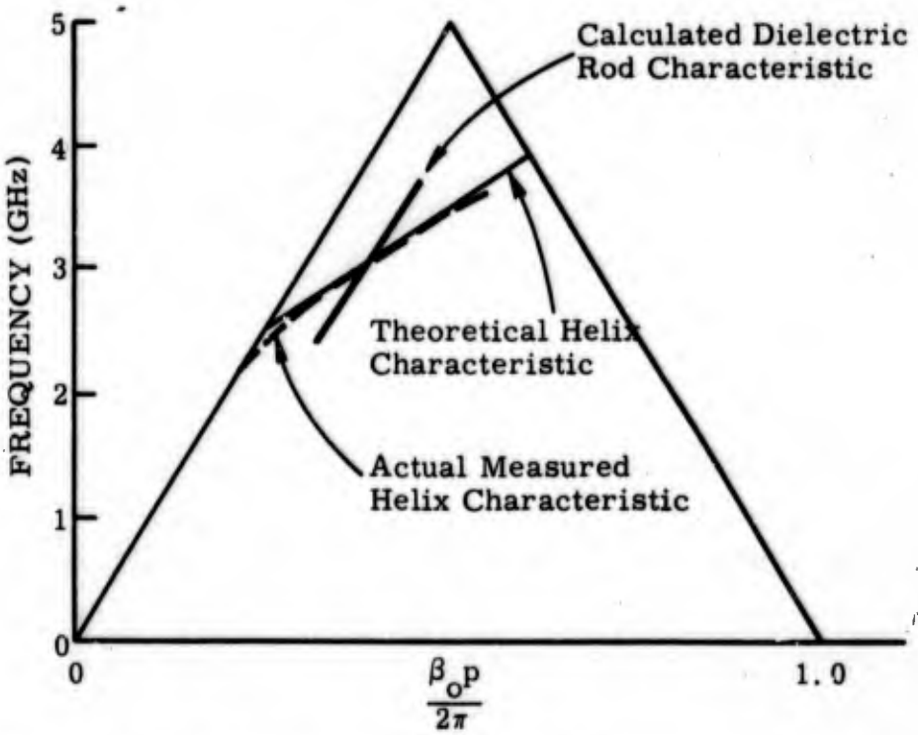

Figure 5-13. ω-β characteristics for the dielectric rod to helix transition.

range of the FPS-6 radar. An apex frequency of 5 GHz was selected, resulting in a required pitch of 1.18 in. for the helix. This pitch then, together with the required velocity, fixes the helix inside diameter at 1.58 in.

Once the diameter and operating frequency are known, the required dielectric constant of the rod for equal helix and rod phase velocities can be calculated. Our circuit required $\epsilon = 4$. The theoretical $\omega\beta$ characteristic together with the actual measured helix characteristic and the calculated dielectric rod characteristic are plotted in figure 5-13. Note that the characteristics cross at a frequency of approximately 3 GHz. This then is the frequency at which 100 percent coupling should be obtained.

An entire helix filter utilizing an 8-ft helix transmission line and two transitions of the type shown in figure 5-11 was fabricated. Passband insertion loss measurements were made and are plotted in figure 5-14. Note that the curve shows a definite frequency at which maximum coupling is obtained. This is the frequency at which the helix and dielectric rod have the same phase velocities. This bandwidth could probably have been increased by varying the pitch of the helix and utilizing nonuniform coupling. The insertion loss of 2 db could also be reduced by utilizing this method of coupling. This was not tried, however, because of other successful modifications made to this transition that resulted in the higher order mode helix transition discussed in section VI. D of this report.

C. SUMMARY

Coupled line junctions can improve filter effectiveness by increasing the isolation of the transmitting and receiving apertures and thereby increasing the stopband attenuation. This effect can be produced by a junction employing uniform coupling of identical open periodic circuits. The coupling region in such a junction must be one-half beat wavelength long for 100 percent transfer from one line to the other. Coupling of 100 percent will only be obtained over a narrow frequency range which increases as the coupling coefficient is increased until limited by scattering from end discontinuities or by power handling considerations.

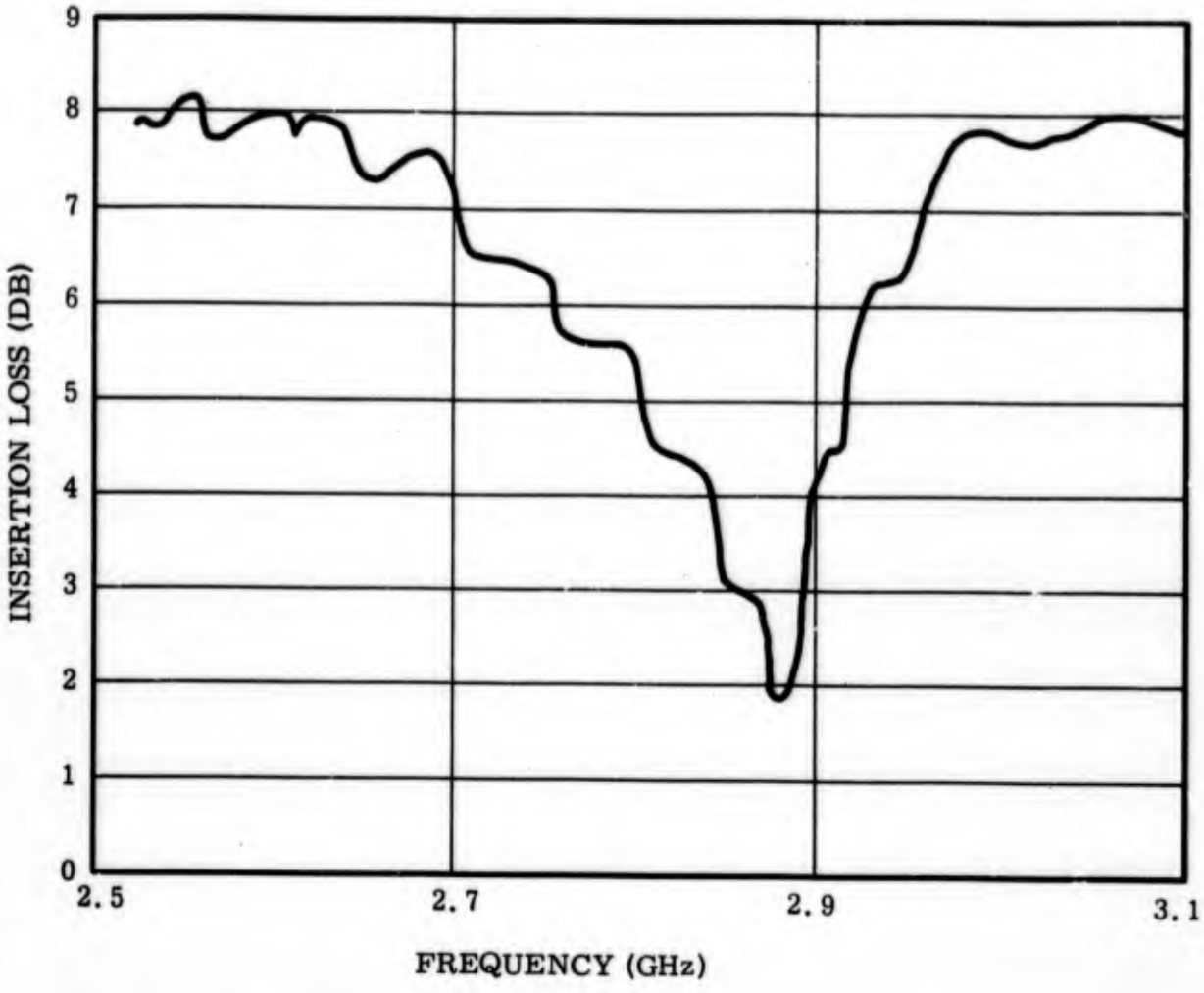

Figure 5-14. Insertion loss of -1 mode helix filter employing dielectric rod transitions of figure 5-11.

Dissimilar circuits can be coupled if necessary for transition efficiency. If the two lines have the same phase velocity over a sufficiently wide frequency range, then uniform coupling should provide 100 percent net coupling with one-half beat wavelength coupling zone. The bandwidth of 100 percent coupling should be the same as for identical circuits and should depend on the magnitude of the coupling coefficient in the same way. In practice, however, dissimilar circuits will not usually have the same $\omega\beta$ characteristic so the bandwidth of 100 percent coupling will be less than that of coupled identical circuits. Also, the different field configurations of dissimilar circuits may limit the bandwidth of a junction employing uniform coupling.

Nonuniform coupling involving the tapering of the phase velocities of the lines, or the coupling coefficient or both, appears to be necessary for 100 percent coupling of dissimilar circuits over useful frequency ranges. Such coupling may also permit the transformation of the field configurations.

VI. HELIX FILTERS AND TRANSITIONS

A. HELIX FILTERS

The basic design requirements for the wire helix filter circuit were explored in the previous program (ref 2). These requirements are illustrated by the k-β diagram of figure 6-1. The ideal phase velocity of a helix is given by

$$\frac{v_p}{c} = \frac{\text{pitch}}{\text{line length per pitch}} = \frac{p}{\sqrt{p^2 + (\pi D)^2}} = \sin \Psi \qquad (6.1)$$

where D is the diameter of the helix and Ψ is the pitch angle. The ratio v_p/c must be at least one-third if the operating band is to propagate in the fundamental (m = 0) mode. Lower ratios permit the existence of one or more higher order slow wave modes in the allowed region. This condition will permit spurious passbands which can occur at or near harmonics of a signal propagating in the fundamental mode. The helix characteristics are actually curved as shown in figure 6-1. The location of the operating point is limited by considerations of the desired stopband. Consider a helix with an ideal phase velocity of c/3. If attenuation of the second harmonic and higher frequencies is desired, then the second harmonic frequency should be placed no lower than $kp/2\pi \approx 0.23$. The fundamental would then be at $kp/2\pi = 0.115 = p/\lambda_o$. If it is desired to attenuate spurious outputs between the fundamental and the second harmonic, the operating point can be raised accordingly. However, as the operating point is raised above $kp/2\pi = 0.175$, the group velocity becomes lower than the phase velocity and gradually decreases to very low values above $kp/2\pi = 0.22$. As was mentioned before, a low group velocity causes high resistive loss in the slow wave structure. However, at $kp/2\pi = 0.22$, $\gamma p/2\pi = 0.6$ which implies very tight binding of the slow wave to the structure with consequent low losses in the surrounding absorber, relatively easy bending, and efficient launching. At the low end of the operating range $\gamma p/2\pi$ is 0.23 which implies greater losses outside of the structure. However, experience has indicated that these losses can

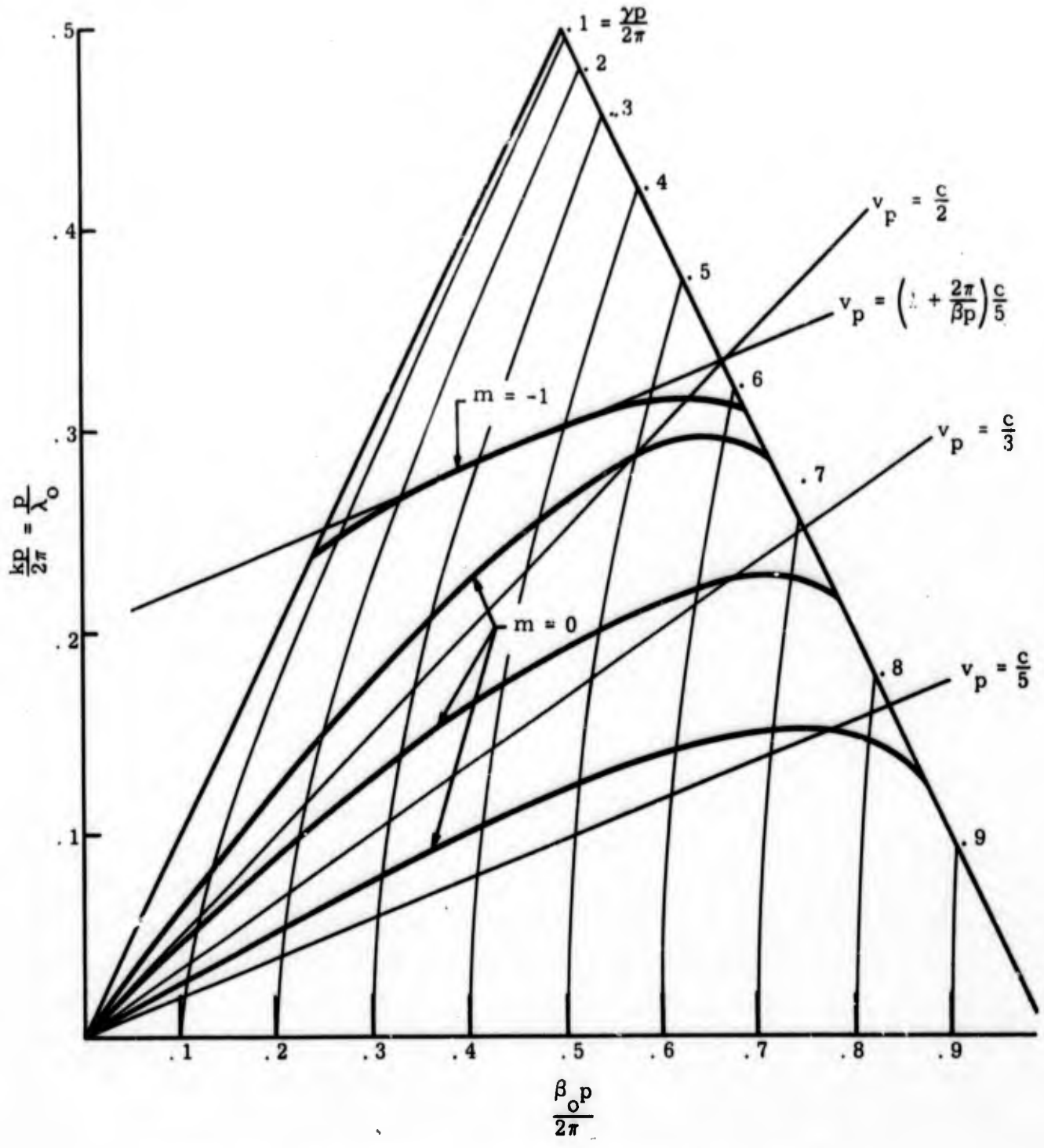

Figure 6-1. Normalized k-β characteristics of helix filters.

be kept to acceptably low levels by means of appropriate absorber location, aperture size, and bend radius, and that these dimensions are mechanically acceptable.

Clearly, the k-β characteristic of the wire helix provides considerable latitude in filter design. The possibility of using faster helices increases this latitude further. The uppermost m = 0 curve in figure 6-1 is that of a helix designed to have $v_p/c = 0.5$. Such a helix was used in the breadboard filter FH-15 which demonstrated the feasibility of high power open periodic filters in the previous program. The group velocity of this helix is about 65 percent higher than that of the $v_p = c/3$ helix at comparable operating points – accordingly, its loss should be lower. The lowest operating point on the characteristic which will permit attenuation of the second harmonic corresponds to $kp/2\pi = 0.15 = p/\lambda$. At this point $\gamma p/2\pi = 0.20$, and since the pitch of the fast ($v_p = c/2$) structure is 0.15/0.115 as great as that of the slow ($v_p = c/3$) structure for the same value of k, the magnitude of γ will be lower by 0.20 x 0.115/0.23 x 0.150, or a factor of 0.67. The choice of a helix for a given application will therefore be a compromise dictated by the amount of intrinsic resistive loss that can be tolerated and the need for high γ for efficient launching and small filter dimensions.

This was done for the FPS-6 application in the development of the fundamental mode helix filter employing right angle transitions and is described, along with the specific filter design, in section VI. E, although the factors affecting the helix design would be applicable to filters employing other types of transitions. Suitable power handling capacity is also required for filter helices, and this subject is also treated in section VI. E for the FPS-6 application.

It was mentioned earlier that the helix is different from periodic circuits composed of uniform elements in that it has a transverse component of phase variation with respect to the axis. It is similar in this respect to interdigital arrays of elements. As a consequence of the transverse phase variation, the ω-β characteristics of both helices and interdigital structures are asymmetrical with respect to the $\beta_o = \pi/p$ axis. But the helix has the property of being completely uniform, i. e., one transverse cross section

of a helix is like any other. In this sense the helix is not periodic – or it can be described as periodic with respect to a coordinate system but not with respect to itself. The implications of this statement are many and exploring them all seemed to be beyond the scope of this project. One implication that did seem to bear looking into is that a characteristic impedance similar to that of a uniform transmission line can be defined in terms of the fields of the predominant spatial harmonic. This is in contrast to more markedly periodic structures such as ladders (cf sec IV. B).

An expression for transverse power voltage impedance was developed by Chu (ref 12) for an open wire helix

$$K_t = (K_t)_o R_t \tag{6.2}$$

where

$$(K_t)_o = \frac{1}{4}\sqrt{\frac{\mu}{\epsilon}}\ \frac{1}{S\pi} \tag{6.3}$$

and

$$S = \beta\, a \cos \psi \tag{6.4}$$

In the above expressions, the various symbols have the following meanings:

a	=	mean helix radius
ψ	=	helix pitch angle
β	=	ω/c
$(K_t)_o$	=	developed sheath helix impedance
R_t	=	correction factor dependent on helix pitch and wire size

The factor R_t is shown in figure 6-2 as a function of wire diameter to pitch for various values of S. The impedance values for typical fundamental mode filter helices ranged from 150 to 200 ohms. This would seem to indicate that when matching a filter helix to a coaxial line that the impedance of the latter should be higher than the usual 50 ohms. It must be kept in mind, however, that Chu's expression relates to an open helix. If a helix

is enclosed, its transverse power voltage impedance may well be different, depending on the closeness of the outer conductor. It should also be kept in mind that merely equating the magnitude of similarly defined impedances in two lines does not guarantee a matched junction. It is also necessary to ensure that common fields exist at the junction. The fields on a helix propagating even the fundamental slow mode may be hard to align with dominant mode transmission lines.

B. COAXIAL LINE TO HELIX TRANSITIONS

The development of transitions from coaxial line to helix filters was a project goal and as such received attention early in the program. It was at first envisioned that such transitions would find their sole application in filters for systems employing coaxial line. Because of the need to meet the project goal of developing filters suitable for high power radars such as the FPS-6, which employs rectangular waveguide, attempting to achieve a transition to coaxial line gradually became a secondary effort. However, some basic design principles were studied and experiments were performed. The possibility of employing a coaxial line configuration in a transition from rectangular waveguide was also considered.

An important point regarding transitions to coaxial lines is the wide range of coaxial line dimensions that might be encountered. In the design of a 50-ohm or 75-ohm coaxial line transmission system, two factors must be considered: first, the frequency of operation which determines the maximum line size for purely TEM mode propagation; and second, the peak or average power, whichever is significant, which determines the minimum line dimensions. Since the dimensions of a filter helix are determined mainly by the operating frequency, two broad classes of transitions should be considered:

Class 1. Helix dimensions comparable to the system coaxial line dimensions.

Class 2. Helix dimensions larger than the system coaxial line dimensions.

Class 1 pertains to high power high frequency applications where the coaxial transmission line is made as large as possible to transmit the fundamental power without breakdown. The operating frequency is therefore close to the cutoff frequency of the first higher order mode (TE_{11}) in the coaxial line. The center conductor of a 50-ohm line in such applications has approximately the same diameter as an appropriate filter helix.

Class 2 pertains to applications where the coaxial line is relatively small compared to a wavelength, which is another way of saying that the operating frequency is considerably below the cutoff frequency of the TE_{11} coaxial mode. A low frequency system of moderate power, such as a UHF radar, typifies this case.

When a coaxial line configuration is employed in a transition from rectangular waveguide to a helix, the coaxial line to helix transition would probably be in class 1, since it would usually be desired to have the coaxial line power capability approaching that of the waveguide.

An attempt was made to measure the impedance of helices enclosed in a tube and joined abruptly to a coaxial line. In these tests S-band helices were joined to the inner conductor of a 1-5/8 in. coaxial line as shown in figure 6-3, and the outer conductor of the coaxial line was extended to enclose the helix. The resulting measurements of helix impedance over a large frequency range at the junction were considered anomalous in that they indicated the helix impedances were lower than the coaxial line rather than three or four times higher as predicted by the calculations based on reference 12. The measurements were also considered not too meaningful because it was believed that the slow mode was not launched on a helix at this type of junction since the transverse electric fields of the TEM coaxial mode had not been transformed into the largely longitudinal fields on the helix. In other words, the energy must have been transmitted through the junction in some sort of fast mode, or so it was thought. Later on it was found that the helices used in these experiments were excessively lossy and also that the termination probably was defective. Further, the impedances calculated for the helices in accordance with reference 12 did not take into account

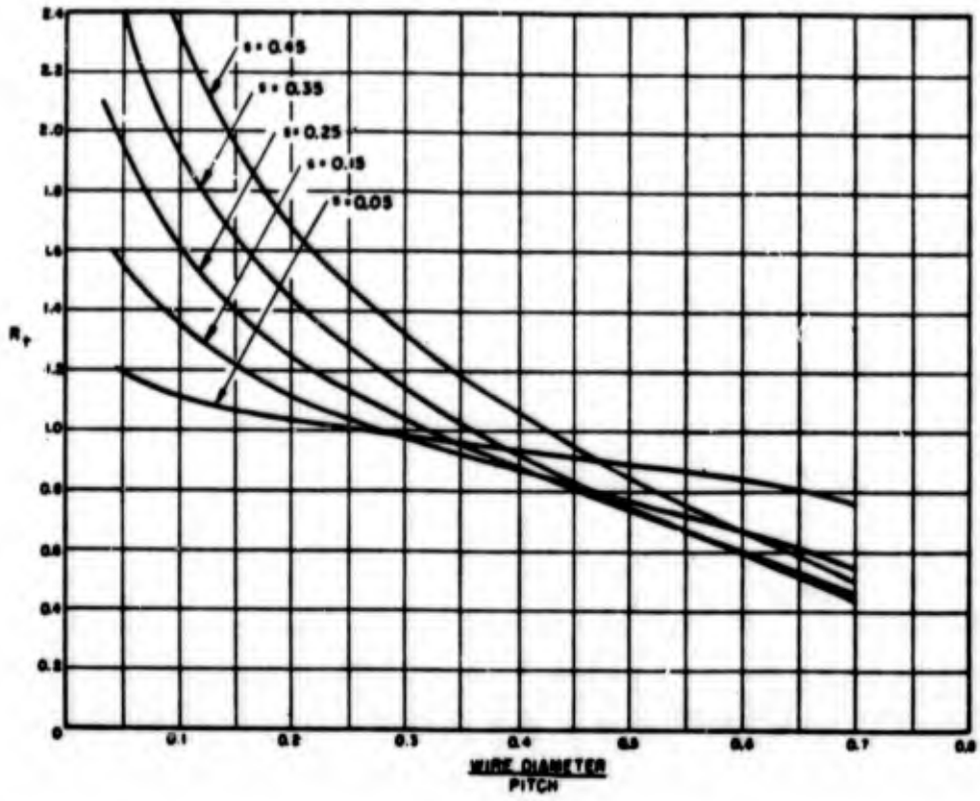

Figure 6-2. Effect of wire diameter on the transverse impedance of a helix. (Reprinted from ref. 12 by permission of the Am. Institute of Physics.)

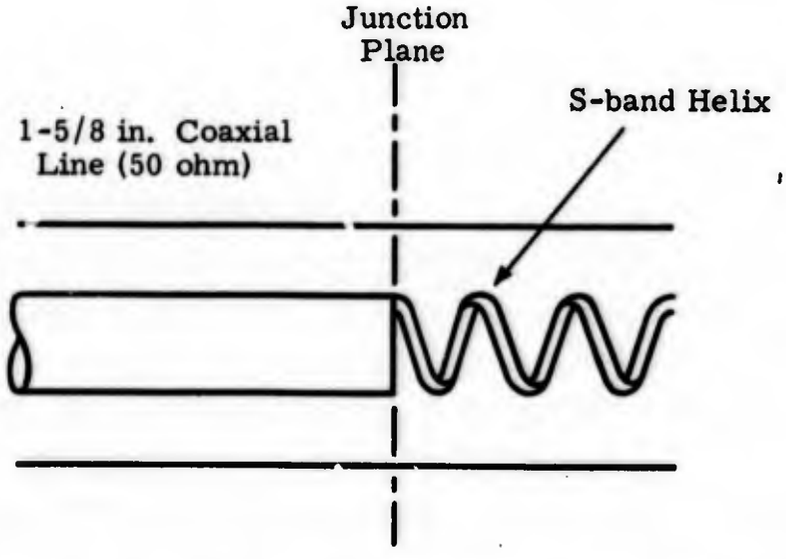

Figure 6-3. Abrupt junction of helix and coaxial line (Class 1).

the presence of an enclosing conductor. These considerations might explain away the anomalies and justify re-examination of this type of transition.

Perhaps a more important reason for re-examining the junction of figure 6-3 is the development of the general transition concept of section III. It was pointed out that at any junction it is necessary to have either unique propagating modes on both sides of the junction, or to discriminate against the unwanted modes. The configuration of figure 6-3 permits only the TEM mode in the coaxial line over the desired operating frequency range. In the helix region the same outer conductor dimensions also prevent the existence of the lowest order waveguide or coaxial mode. Since the junction permits continuous currents, the only mode capable of propagation in the enclosed helix region is one derived from the incident TEM mode. Therefore, the condition of unique propagating modes on both sides of the junction with adequate coupling between them appears to be met. Accordingly, it should be possible to utilize the junction of figure 6-3 in a class 1 coaxial line to helix transition. If the characteristic impedances of the two modes at the junction are truly mismatched, it should be possible to match the junction by a change in dimensions on either side (while maintaining the condition of unique modes) or by an appropriate tuning element. The match so obtained might be limited in bandwidth.

A modification of the above class 1 junction is shown in figure 6-4. In this junction the center conductor is gradually transformed into a helix by grooving it spirally with increasing depth at the helix pitch and then gradually removing its center. Although this transition was originally proposed during the previous program as a means of avoiding the launching of a fast mode, its function is primarily one of impedance matching when the modes are unique at both ends of the transition. A transition of this type was designed for an S-band helix, but its manufacture was held in abeyance because the helix was lossy. A transition for the final helix design was not fabricated because of the completion of the program. However, from the data of the previous program (ref 2, pp 6-16) this should provide a broadband impedance match and with an appropriate outer conductor should permit launching the desired slow mode with no loss due to conversion to a fast mode. It is, of course, necessary to make a gradual transition from the enclosed helix to the open

helix so as to avoid conversion to higher order modes and consequent scattering. The design of a useful helix is given in section VI. E, together with an empirical horn design. The design of the coaxial line to helix junction is seen as straightforward once proper impedance measurements have been made.

The stopband VSWR of either of the above transitions is impossible to predict. Harmonic energy can propagate in the coaxial line in possibly many modes, depending on the frequency, and the amount of reflected energy will depend on the relative modal content and the polarization of the modes. However, the in-line configuration of the transitions should tend to minimize the amount of reflection. It should be kept in mind that the center conductor supports in the system transmission line will tend to reflect or scatter higher order modes to about the same degree as these transitions. When these transitions are employed in a filter for use in a rectangular waveguide system, the level of reflected power will probably be higher because of the waveguide to coaxial line transition since such transitions usually involve a right angle junction and a short circuit.

No experimental work was done on class 2 transitions because they are inappropriate for high power microwave radars. However, some basic designs were studied. One design that appears feasible is shown in figure 6-5 in which the center conductor joins the helix at the pitch angle. For suitable helix dimensions, the enclosing conductor dimensions can be such as to prevent the propagation of waveguide modes or higher order coaxial line modes in the enclosed helix region. The junction between the small coaxial line and the enclosed helix region requires transforming the TEM coaxial mode into the TEM mode of a wire over a plane. Since the dimensions of both the coaxial line and the enclosed helix region are restricted, the only consideration in this junction is minimizing reflections. If the operating bandwidth is narrow, a more or less abrupt junction with tuning elements can be used. A broadband junction will require a gradual transformation. In either case, the design of the junction is straightforward and requires no more than basic transmission line techniques.

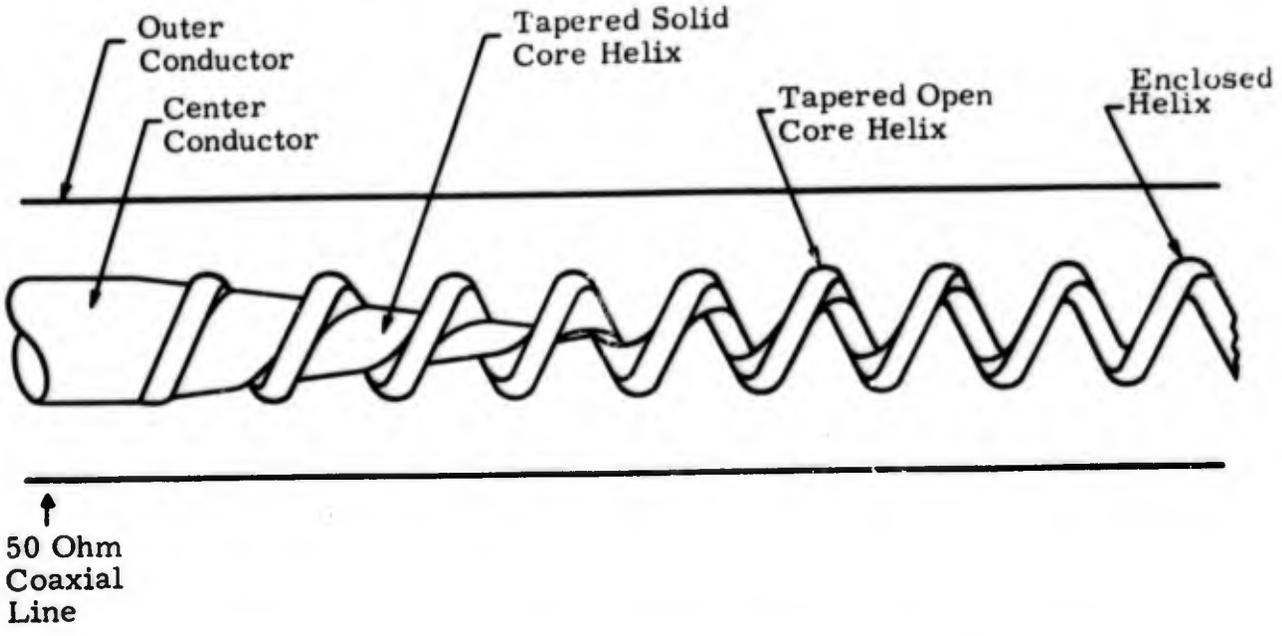

Figure 6-4. Tapered velocity transition between helix and coaxial line (Class 1).

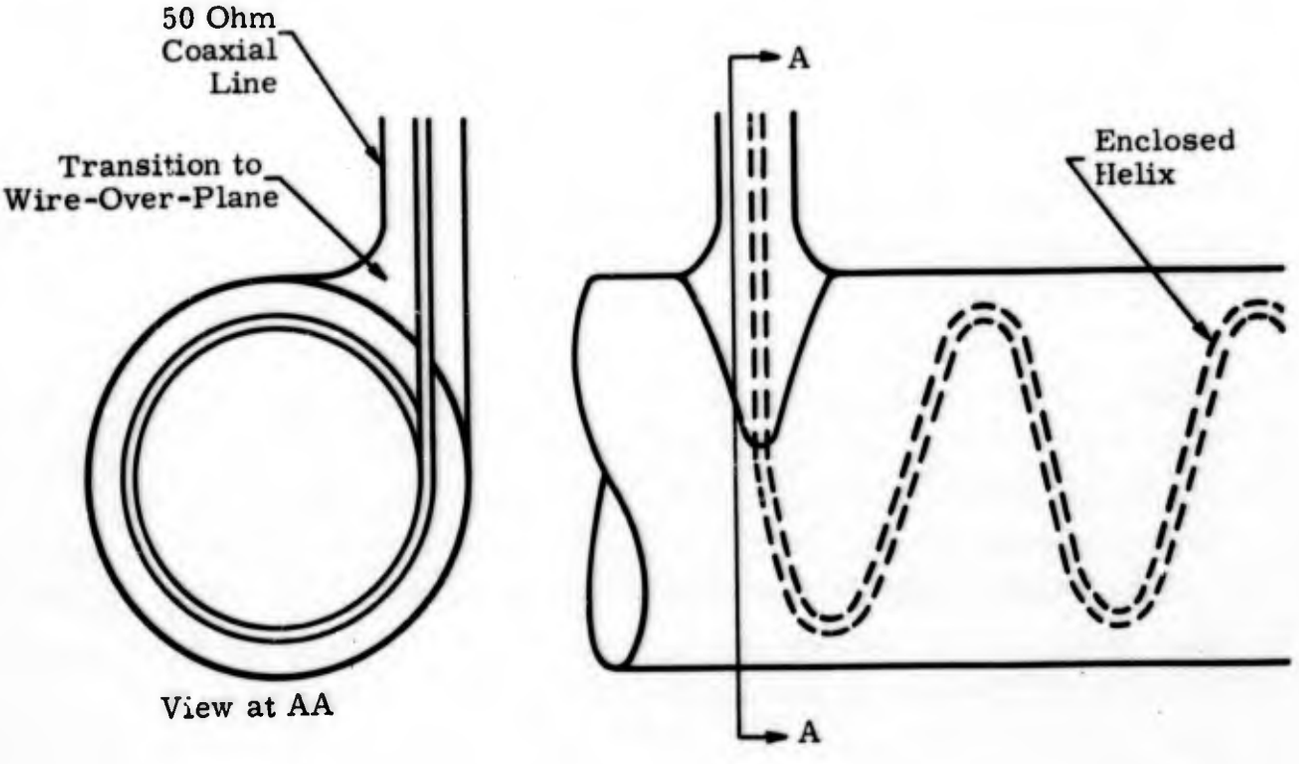

Figure 6-5. Transverse class 2 junction of coaxial line and helix.

In summary, coaxial line to helix transitions can be readily designed and built by following the basic concept of a transition as given in section III. Assuming that a suitable helix design is known, the key to the transition design is ensuring that unique modes exist at each junction. The transformation from the enclosed helix to the open helix must be done gradually enough to prevent conversion of the desired mode to fast modes as the dimensions of the enclosing conductor increase.

C. FUNDAMENTAL MODE HELIX TRANSITION EMPLOYING TM_{01} CIRCULAR MODE

The TM_{01} circular mode is the first higher order mode occurring in circular waveguide. It has an average longitudinal electric field that has its maximum amplitude at the axis of the waveguide as shown in figure 6-6. Since the fundamental mode of a helix has a predominantly longitudinal electric field, the use of the TM_{01} circular mode as a means of coupling energy to the helix was suggested early in the program. A potential advantage of a transition employing the TM_{01} mode is high power capacity resulting from the large outer conductor diameter required for the propagation of this mode. A variety of transitions to the TM_{01} circular mode from dominant mode rectangular or circular waveguide is treated by Ragan (ref 13 pp 379-405). Most of these transitions have fairly "open" dimensions making them suitable for high power applications and also indicating that they would have relatively low reflectivity at harmonic frequencies propagating in higher order modes.

Although the general transition studies and the general coupling studies had barely begun when this transition was proposed, it was anticipated that two significant problems would have to be solved. The first problem was the possible existence of the TE_{11} circular mode in the junction area. The presence of the helix could cause conversion to the TE_{11} mode, and this energy would therefore be lost. However, it had been shown in the previous program (ref 2; pp 6-14) that the coupling between a helix and the TE_{11} mode was weak, and it was hoped that it could be made weak enough to prevent significant loss. The second problem was the great difference in phase velocity between the slow helix mode and the fast TM_{01} circular

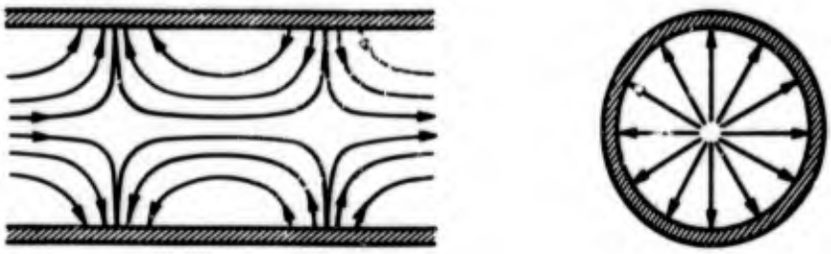

Figure 6-6. Electric fields of TM_{01} mode in circular waveguide.

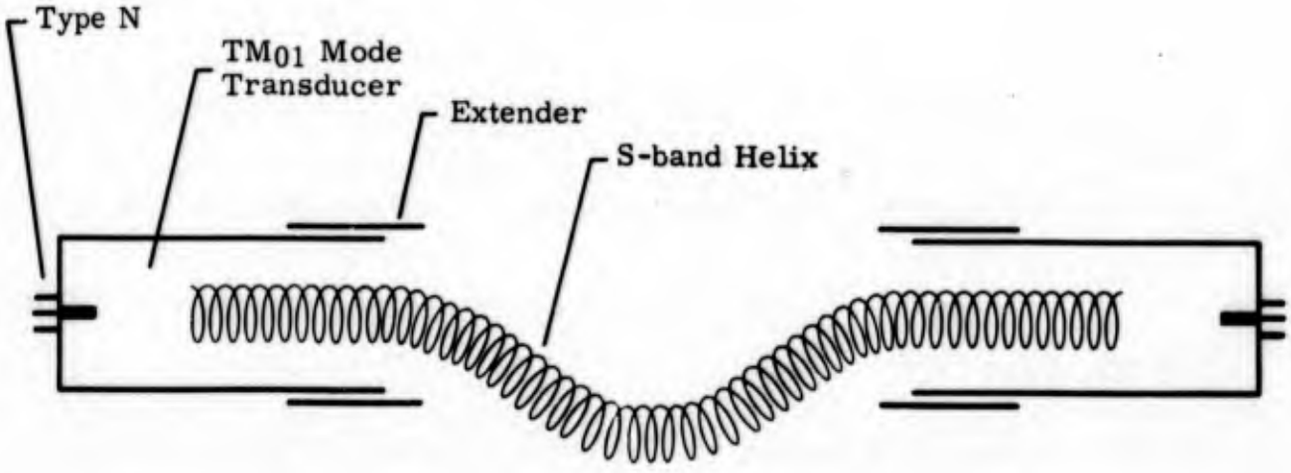

Figure 6-7. Schematic of TM_{01} mode to helix coupling experiment setup.

waveguide mode. The preliminary studies of uniform loose coupling indicated that the periodic fractional power transfer would be much less than unity for such disparate phase velocities.

An experiment was performed to determine how much energy could be coupled to a helix from the TM_{01} circular mode. Figure 6-7 shows a schematic diagram of the test arrangement. The TM_{01} mode launchers are low power transducers with type N fittings. The pipe diameter was 4.43 in. so that the TM_{01} cutoff frequency is the same as that of the TE_{10} mode in WR-284 S-band rectangular waveguide. The central probe was made a quarter guide wavelength long at 2800 MHz. The loss and reflection of these transducers when butted together is shown in figure 6-8. Electric probe measurements around the periphery of the pipe in the frequency range from 2700 MHz to 2900 MHz indicated that the TM_{01} mode existed with no admixture of TE_{11} or TE_{21} modes which have cutoff frequencies of 1.56 GHz and 2.59 GHz, respectively. It should be noted that no horns were used; they are not needed because in the large diameter pipe the helix is practically in free space.

The optimum transmission loss of the arrangement of figure 6-7 is shown in figure 6-9. The increasingly high loss above 2.7 GHz is believed to be due to the helix used, which in other tests was found to be lossy at higher frequencies because of low group velocity and the proximity of the forbidden region, as well as to the increasing disparity of the phase velocities. A significant finding is that the transmission loss varied in a periodic manner as the pipe extenders were moved longitudinally. This is to be expected in uniform coupling because the net power transfer depends on the length of the coupling region.

Since nonuniform coupling can generally provide greater net coupling and operating bandwidth than uniform coupling, a helix with tapered diameter ends was tested. A view of the transition zone is shown in figure 6-10. The tapered diameter of the helix causes a gradual decrease in the phase velocity of the helix wave from the velocity of light down to the final helix phase velocity. Tests were performed in which it was possible to vary the length of the coupling region. The optimum insertion loss is shown in figure 6-11.

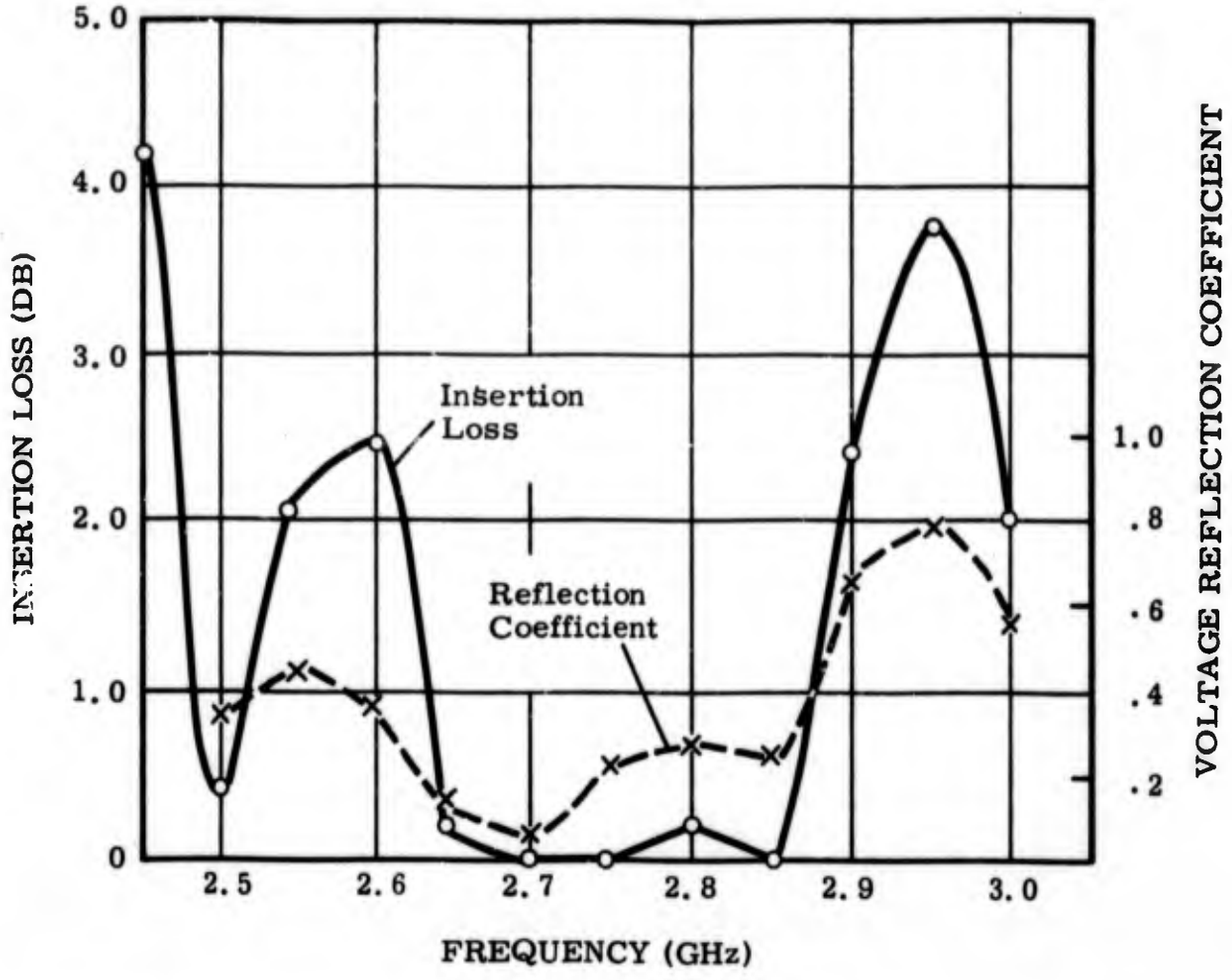

Figure 6-8. Loss and reflection of TM_{01} mode launchers.

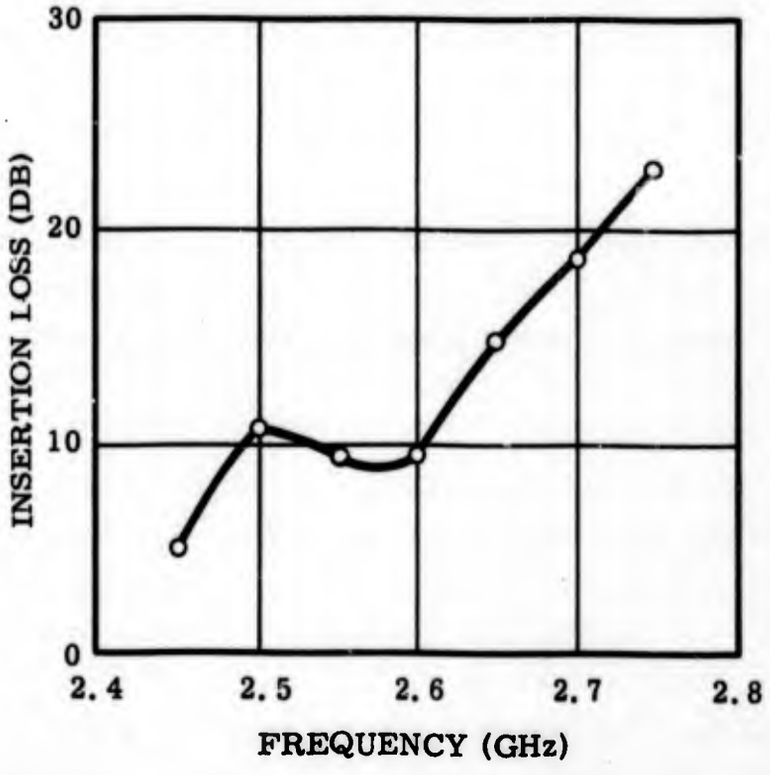

Figure 6-9. Optimum insertion loss of uniform coupling between helix and TM_{01} mode.

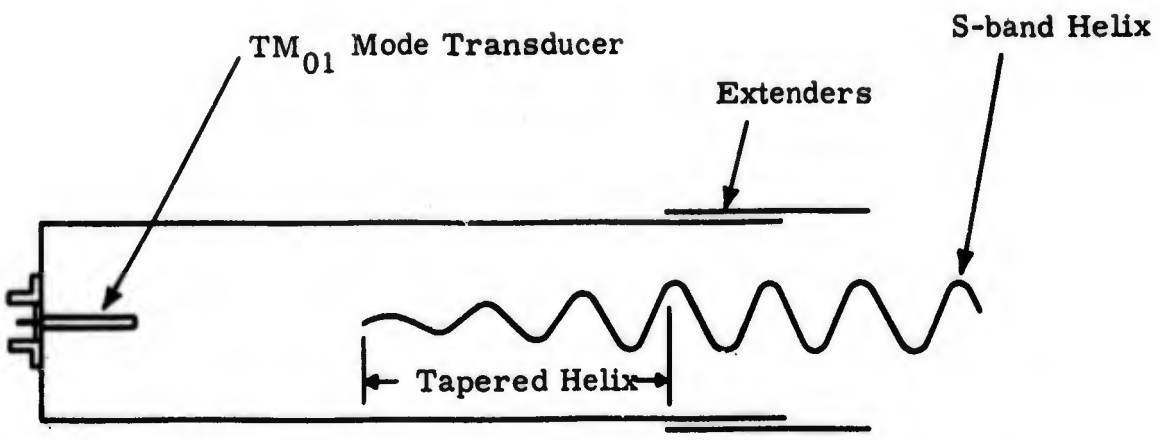

Figure 6-10. TM_{01} to helix transition employing tapered helix (nonuniform coupling).

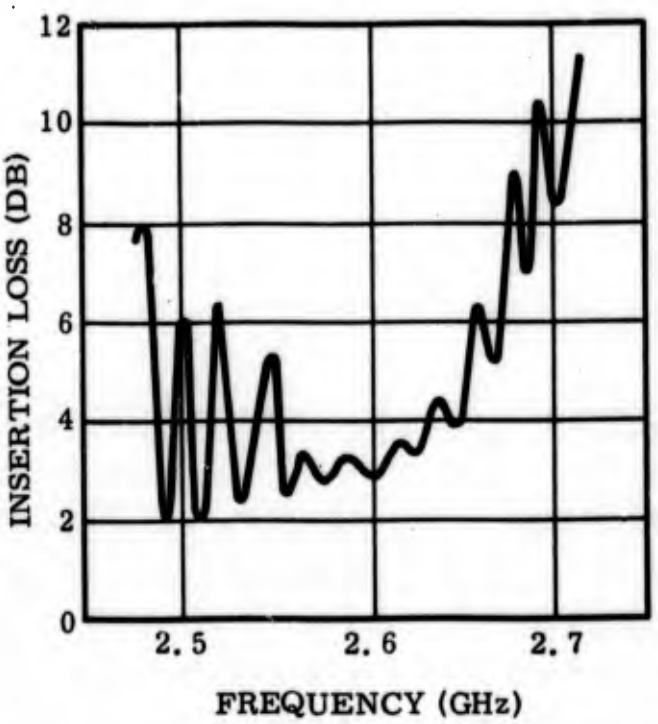

Figure 6-11. Loss of filter with tapered helix transition.

Tapering the helix clearly decreased the transmission loss. However, the net transmission at any frequency still varied periodically with the length of the coupling region. This indicated that the desired result of nonuniform coupling, which is to permit the transfer of energy from one line to the other and then prevent its return by decreasing the coupling while increasing the phase velocity difference, was not achieved. It should be noted that the conditions for the very broadband nonuniform coupling described in section V have not been met. The phase velocities of the two modes are never equal. However, the coupling is the tightest where the velocities are closest, i.e., at the beginning of the taper which is in the region of maximum electric field intensity. This probably accounts for the improved transmission.

It might be possible to make further improvements in the transmission loss and bandwidth of this coupler by using a different taper. For example, the coaxial or fast portion of the taper might be made longer or shorter or of different wire diameter so as to obtain tighter coupling and greater net power transfer in this zone, and the helix velocity might be changed with more or less rapidity. However, there was no assurance that any improvements would be sufficient to meet the project goals, and no further work was done. Another factor in this decision was the necessity of designing high power TM_{01} mode launchers of high modal purity.

D. HIGHER ORDER MODE HELIX FILTER EMPLOYING CIRCULARLY POLARIZED TRANSITION

1. BACKGROUND. The dielectric rod to higher order mode -1 helix of Chu and Kilcoyne (ref 11) was studied first as an experiment in coupled line junctions. These studies, which showed the narrowband coupling behavior typical of uniform coupling of lines having different phase velocities, are described in section V. In an attempt to apply the concept of this device to a practical filter, the necked down portion of the outer conductor of figure 5-11 was eliminated in order to obtain coupling fields on the outside of the helix. The resultant coupling was about the same as before, probably because most of the fields are concentrated in the dielectric rod. The need for the dielectric rod was questioned, since it was felt that the circularly polarized TE_{11} mode should couple to the helix nearly as well as the dielectric

rod HE_{11} mode, particularly if nonuniform coupling was employed. Accordingly, the dielectric rod was replaced with a tapered helix of uniform pitch, as shown in figure 6-12. This resulted in less than 1 db loss over the entire 20 percent operating range of the helix and indicated that a useful filter could probably be developed.

2. FILTER COMPONENT DESIGN AND ASSOCIATED EXPERIMENTS.

a. ω-β Characteristic. The design of a harmonic filter utilizing the m = -1 higher order mode of a helix is completely restricted by the ω-β characteristic of the helix. Figure 5-12 is the ω-β characteristic of a helix including the m = -1 mode employed in the filter. First the pitch of the helix is chosen so as to locate the apex of the triangle (allowed region) just below the second harmonic. This is done to keep all harmonics in the forbidden region thereby not allowing any spurious frequencies located below the apex of the triangle from traveling on the circuit and resulting in low harmonic loss. The pitch is determined by

$$p \text{ (in inches)} = \frac{5.9}{\text{apex frequency in GHz}} \qquad (6.5)$$

Since the filter will have transitions to S-band waveguide (WR-284), the lowest passband frequency is 2.5 GHz which fixes the apex frequency of the triangle at 5 GHz. This then from equation 6.5 determines the pitch of the helix to be 1.18 in.

The phase velocity of the helix is then chosen to be as low as possible in order to obtain maximum bandwidth and must still be kept high enough in order to keep the m = -2 mode from appearing in the top of the triangle, resulting in higher order passbands on the circuit. This minimum phase velocity is one-fifth the velocity of light. Because of mechanical tolerances, a slightly higher phase velocity of 0.21c was chosen in order to assure rejection of the m = -2 mode. This, using equation 6.6, results in a mean helix diameter of 1.785 in.

$$\tan \psi = \frac{p}{\pi D} \qquad (6.6)$$

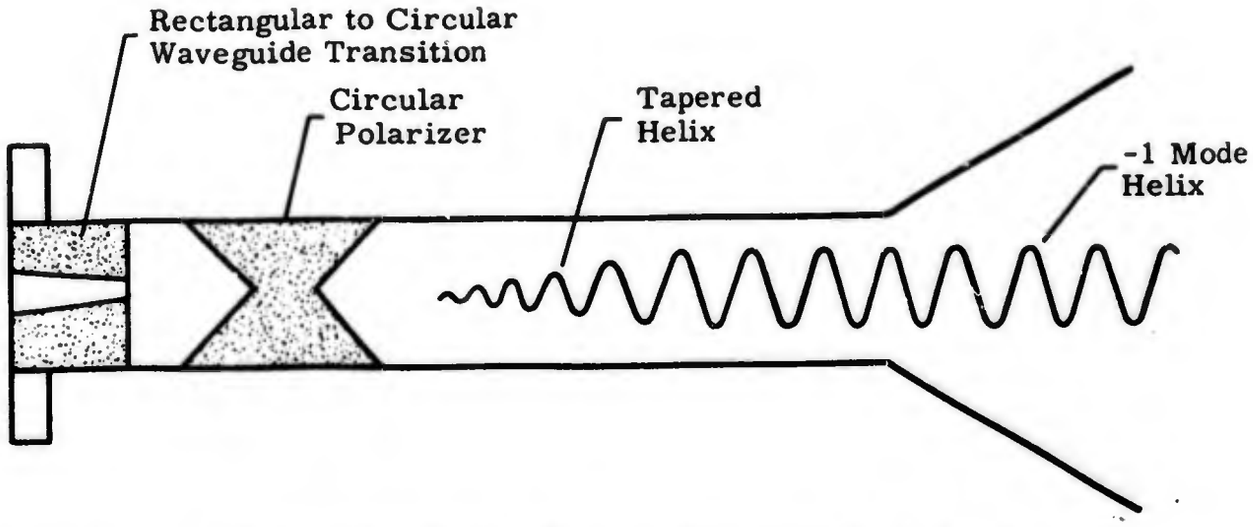

Figure 6-12. Rectangular waveguide to -1 helix in-line transition employing tapered helix.

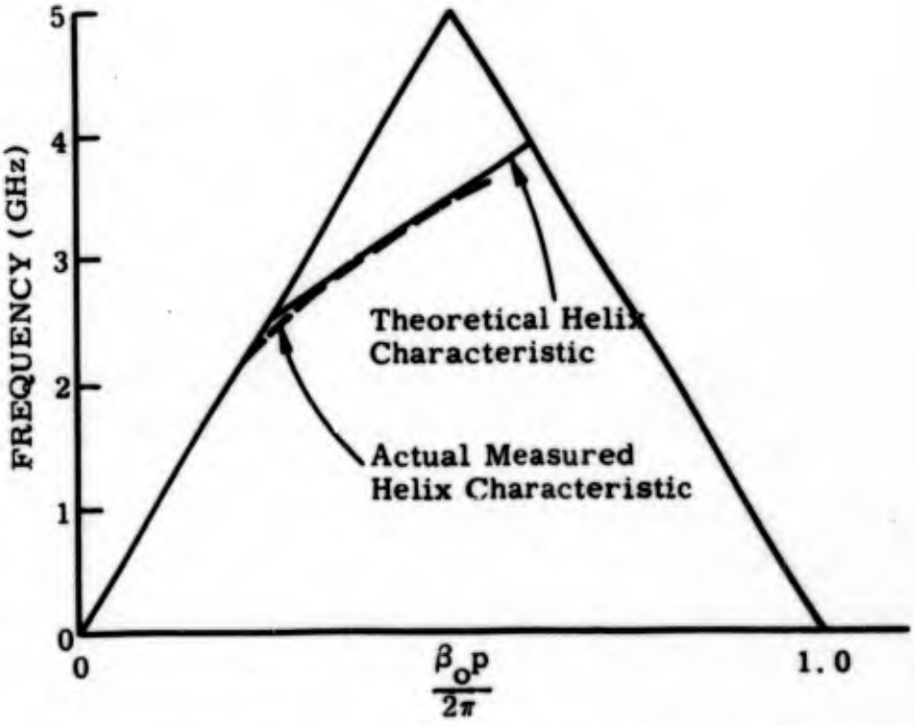

Figure 6-13. ω-β characteristic of -1 mode helix with 1.785 in. mean diameter and 1.18 in. pitch.

where ψ = pitch angle

p = pitch

D = mean diameter

Once the pitch and diameter of the helix are known, the physical size of the helix is fixed. Two helixes were purchased for experimental purposes, both having p = 1.18 in. and D = 1.785 in.; however, the wire thicknesses were 0.150 and 0.250 in. Curves of ω-β for both helices were found to be the same. The curve is plotted in figure 6-13 and shows excellent correlation between the theoretical and actual measured data. The frequency band of the FPS-6 radar, which is 2.7 to 2.9 GHz, is located on the lower portion of the curve.

b. Transitions and Polarizers. The field configuration required to feed the m = -1 mode helix is that of a circularly polarized HE_{11} mode on a dielectric rod, or that of a circularly polarized TE_{11} mode in circular waveguide. The latter was chosen for simplicity and potentially lower loss.

The first portion of the transition was from rectangular to circular waveguide in the dominant mode (TE_{10} rectangular to TE_{11} circular). Two methods were tried: first, a relatively short dielectric transformer described by Olin (ref 14) and, second, a conventional rectangular to circular taper. Both are shown in figure 6-14. Tests indicated that even though the match of the dielectric transformer was sufficient (less than 1.2 to 1.0) its insertion loss of 0.1 db was not acceptable. Therefore, the conventional taper was used.

The circular waveguide diameter was 3.025 in. which is a convenient size both in electrical characteristics and availability. For this diameter the TM_{01} circular waveguide mode, which is the first higher order mode, cannot exist below a frequency of 3.0 GHz. This is just above our upper passband frequency which is 2.9 GHz, making this size circular waveguide ideal for operation without over-moding and yet as close as possible to this cutoff frequency to make the λ_g in the passband as short as possible. The cutoff frequency for the dominant TE_{11} mode is 2.285 GHz.

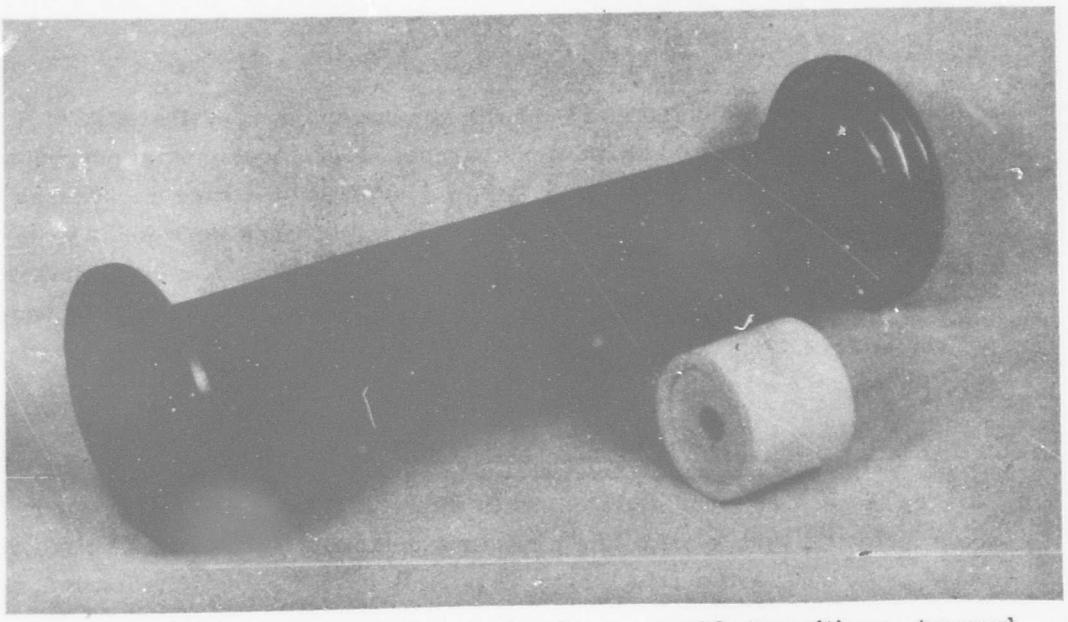

Figure 6-14. Rectangular to circular waveguide transitions: tapered and dielectric.

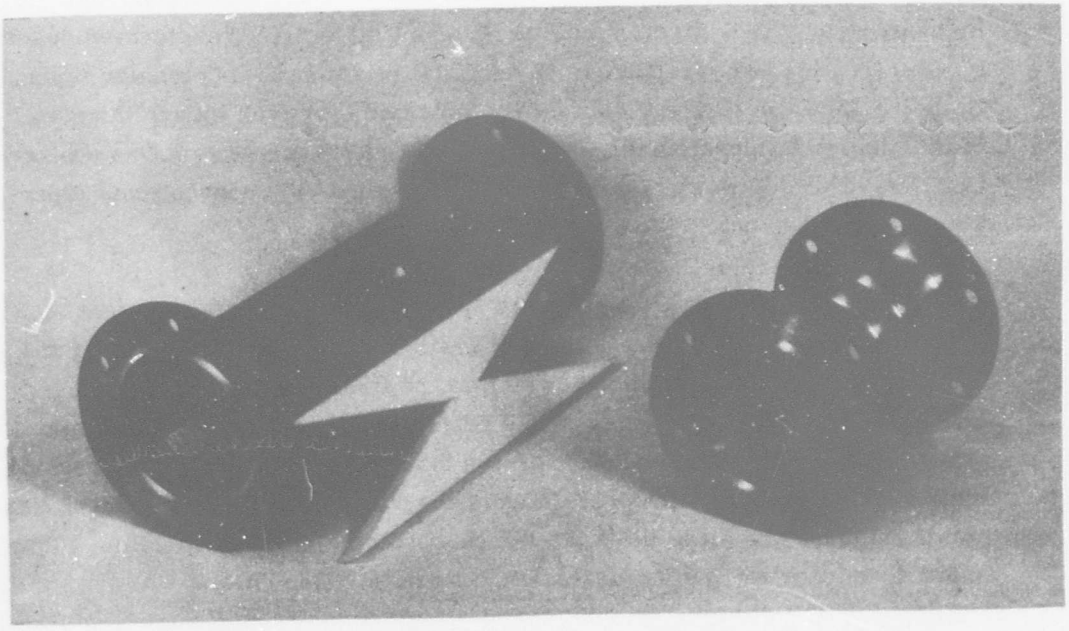

Figure 6-15. Circular polarizers: dielectric and pin type.

The second portion of the transition circularly polarizes the TE_{11} circular waveguide mode. Again two methods were used: first, a dielectric wedge at an angle of 45 deg to the incident wave, and, second, a 6-pin brass polarizer. Both devices are described by Ragan (ref 13, pp 269-379) and are shown in figure 6-15. Measurements showed that although the VSWR of the brass polarizer was less than 1.2 to 1.0, the combination of both polarizers was periodically as high as 1.4 to 1.0 making them unusable. For the filter application, therefore, the Teflon dielectric polarizers were used even though their total insertion loss was about 0.2 db. Match in this case was considered more important. Dimensions for the polarizer are given in figure 6-16.

c. Helix Taper. Several tapers were fabricated for matching the helix to the circularly polarized waveguide. These included constant diameter variable pitch, constant pitch variable diameter, and variable pitch variable diameter. Of these, the most successful taper was the simplest one: constant pitch variable diameter.

Three of these are shown in figure 6-17. Length of taper was varied from 8 to 16 in. with no change in match or efficiency noted. For this reason the shorter taper was used for filter application.

d. Flare Horn. Once the energy is on the enclosed helix circuit, the outer conductor must be removed to get to the open periodic filter configuration. This is accomplished with a gradually tapered flare horn. The length of the horn is 10 in., which is two helix wavelengths at 2.7 GHz.

The horn opening is a function of γ at this frequency. The height must be adequate to intercept almost all of the energy propagating along the circuit. The energy which is not intercepted constitutes passband loss. This loss was set at 0.01 db, corresponding to fields 26 db from their value at the surface. The height h can be calculated from equation 6.7 and is found to be 4 in.

$$\text{voltage ratio} = e^{-\gamma h} \qquad (6.7)$$

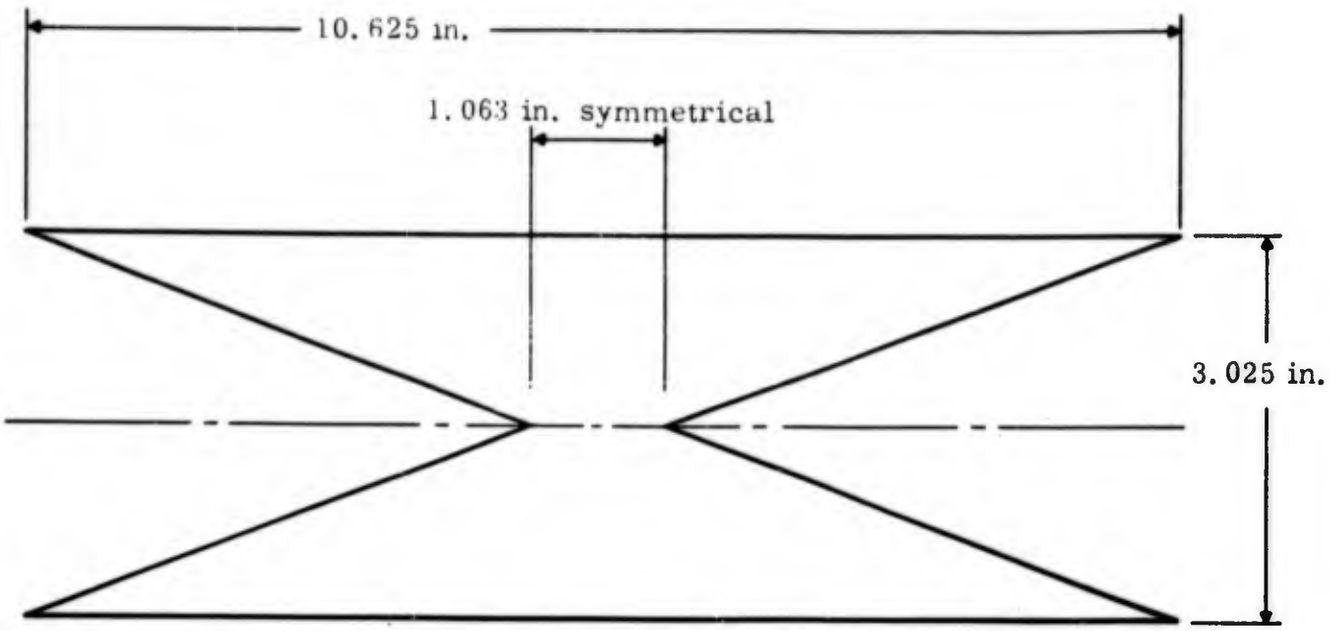

Material: Teflon 0.537 in. thick

Figure 6-16. Teflon circular polarizer.

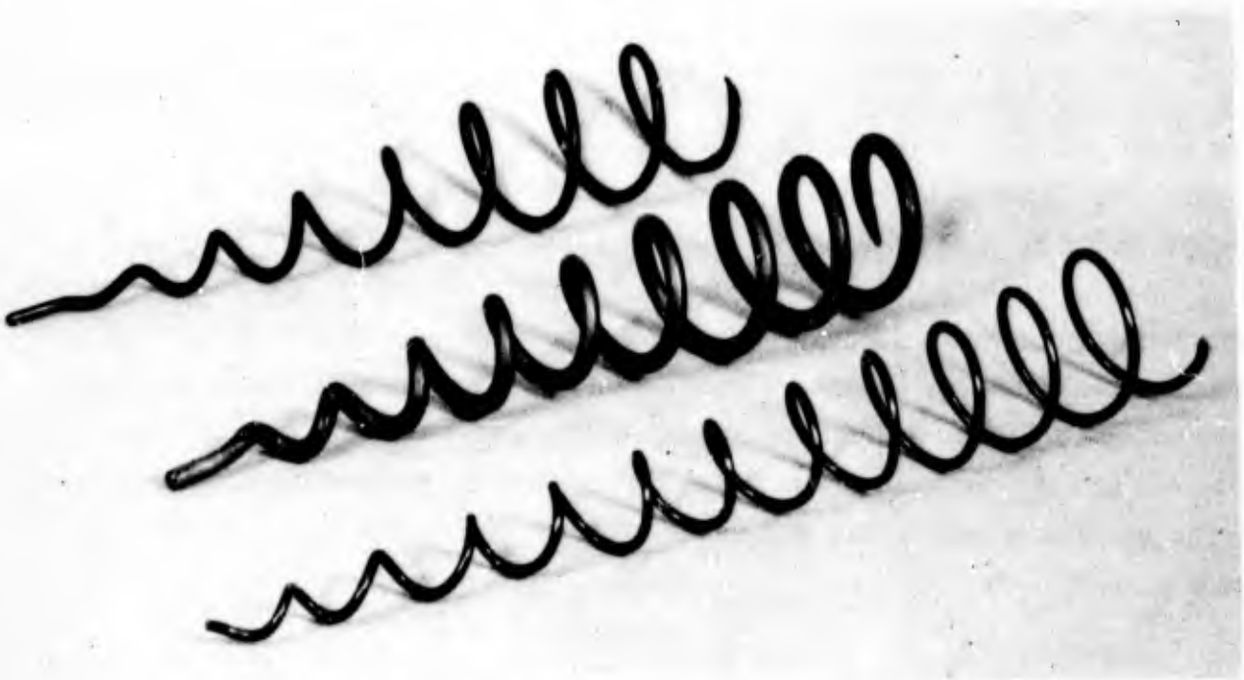

Figure 6-17. Constant pitch tapered diameter helices transitions.

where

voltage ratio (26 db) = 0.05

γ at 2.7 GHz = 0.3 nepers/cm

With the helix outer diameter of approximately 2 in. and a radial distance of 4 in. around the helix, the horn opening was 10 in.

The above values determined the flare horn dimensions and one has only to be careful to make the blend between the circular waveguide and the horn taper as gradual as possible to provide a minimum discontinuity. A 9-inch radius blend was used between the circular waveguide and the taper, making the total length of the horn about 12 in.

e. Bend Radius. Minimum bend radius for the helix circuit is a major consideration since it determines the length of the helix which in turn determines the filter's physical size.

The minimum γ is 0.3 nepers/cm for 2.7 GHz which is the lowest frequency in the passband. v_p/c at this frequency is 0.85. Both of these values are obtained from figure 6-13. These values together with the value h calculated for the flare horn are the only requirements needed to solve for the minimum bend radius using the design criteria of reference 2 pp 7-3 to 7-5. This radius is

$$r = \frac{h}{\frac{c}{v_p} - 1} \approx 22 \text{ in.}$$

f. Power Capability. Several high power experiments were performed on the FPS-6 transmitter to determine the power capability of this filter.

First the tapered transitions together with the circular polarizers were placed back to back and tested in an unpressurized condition at a frequency of 2.795 GHz. Breakdown occurred at 1.59 Mw. This result, scaled to the FPS-6 radar system at 30 psig pressure, indicates a power capability of 11 Mw, which is entirely satisfactory for the filter's use.

Next a short section of helix with tapers on both ends was placed in a section of waveguide between the transitions and polarizers. This test showed the actual filter power capability since the most critical location for breakdown is in the enclosed helix section. The 0.150 in. wire diameter helix was first tested and breakdown occurred at 725 kw unpressurized. This value is equivalent to 5 Mw peak power under FPS-6 pressure conditions.

Next the 0.250 in. wire diameter helix was tested and breakdown occurred at 925 kw or 6.5 Mw peak power at 30 psig pressure, which indicated that the filter was probably suitable for the FPS-6 radar without any increase in waveguide pressure. This increase in power breakdown level shows the advantage of using larger radius wire size. The higher order mode filter has a 60 percent higher power capability compared to the fundamental mode helix filter to be described in section VI. E.

3. FILTER CONSTRUCTION AND TEST DATA. A design sketch indicating the approximate physical size of the higher order mode filter is shown in figure 6-18. The clearance around the helix allows for 3 in. thick absorbers for the harmonic attenuation. The weight of this filter including absorbers and a reenforced container designed for 30 psig, was calculated to be close to 300 lb. This is the filter's main disadvantage since it is actually the size of an L-band leaky wall filter. Its performance, however, exceeds several leaky wall filters in series which makes its size and weight by comparison not too unreasonable.

The container for this filter was not fabricated, however electrical data for this configuration was obtained. Figure 6-19 shows the insertion loss of the complete filter with minor ripples smoothed out. The passband loss varies between 0.5 and 0.6 db. The dielectric polarizer contributes about 0.2 db. The remainder of the loss is probably due to scattering from the helix, resistive loss in the helix, and coupling loss between the circularly polarized TE_{11} mode and the helix. Attempts to measure the helix loss by using different helix lengths were inconclusive.

Also included in figure 6-19 is curve B which is the same circuit with a more severe bend. Note that the insertion loss of the frequencies with

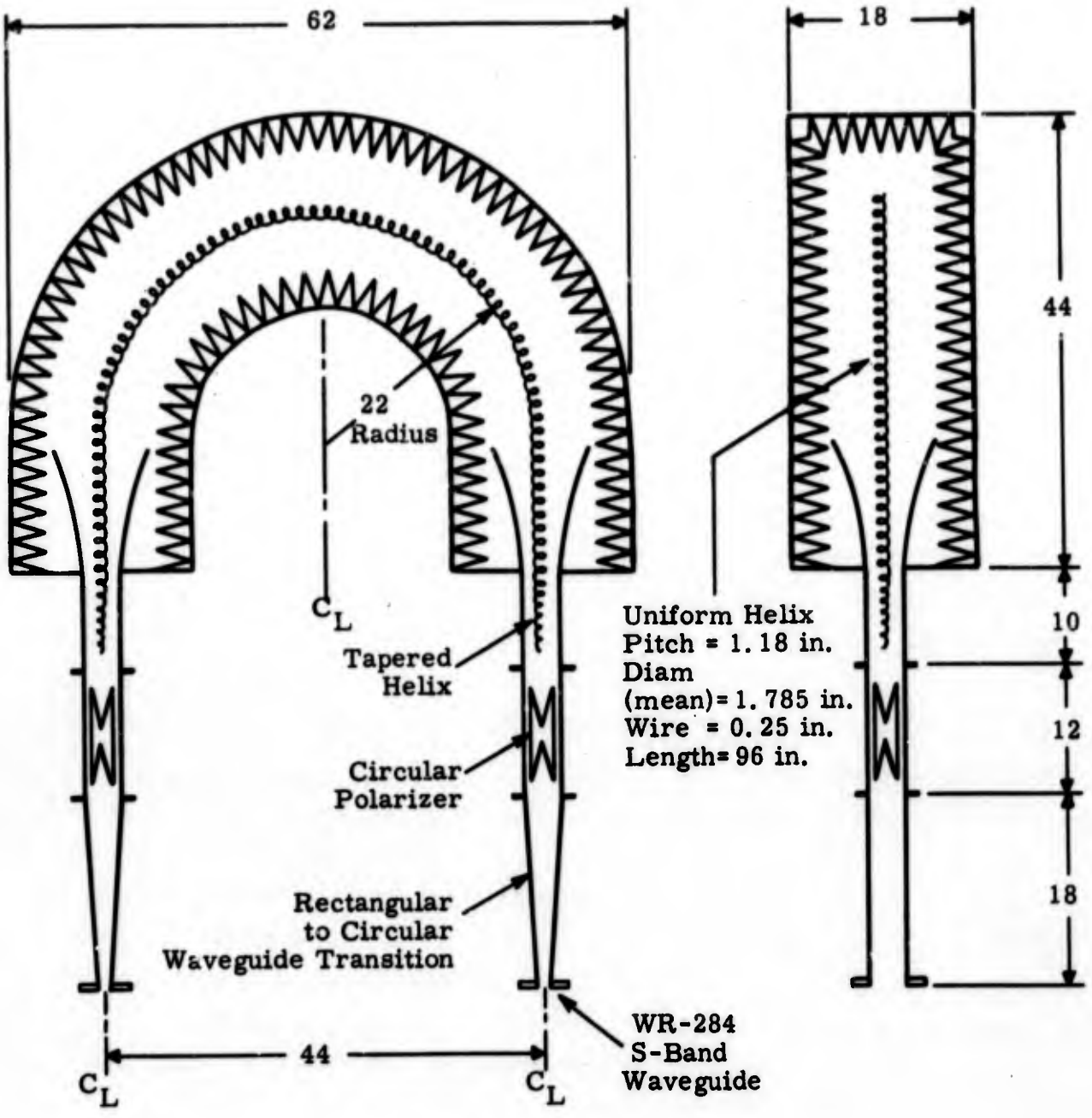

Dimensions are in inches.

Figure 6-18. Approximate dimensions of higher order mode filter.

a lower γ is increasing and begins to affect the lower part of our passband. This increase therefore determines the smallest radius bend and indicates the validity of the design calculations.

The VSWR of the passband for this filter is shown in figure 6-20. This VSWR is under 1.28 from 2.6 to 3.0 GHz which is over twice the bandwidth required for the FPS-6 transmitter. This VSWR is under 1.15 over much of this bandwidth and a match of this value should be obtainable over the FPS-6 frequency range by external matching techniques. However, such a matter was not attempted.

In addition to passband characteristics, stopband attenuation data were taken for both TE_{10} and TE_{01} modes through the 4th harmonic. These data are shown in figure 6-21. The cutoff characteristic is closer to the upper passband edge frequency of 2.9 GHz than that of the fundamental mode helix because of the limited bandwidth of permissible operation on the ω-β curve. The insertion loss increases from 1 db to at least 50 db within 100 MHz. The insertion loss is greater than 50 db throughout all the harmonics. Lower attenuation was measured in a range just below 5 GHz which is where the apex of the ω-β diagram is located (figure 6-13). This is the problem region that had been anticipated in the design of the helix and was the reason for locating the apex just below the second harmonic.

4. SUMMARY. The performance of the higher order mode helix filter indicates its suitability for use in radar systems. It has a passband VSWR comparable to other waveguide components. Its passband insertion loss of about 0.6 db is higher than that of most present day filters, but its stopband attenuation is far superior, particularly at high harmonic frequencies. However, attempting to achieve comparable performance with leaky wall filters would involve increased passband loss.

The main disadvantage of this filter is its size, particularly when compared to the fundamental mode helix filter, which has comparable stopband performance. The -1 mode helix has generally lower values of γ compared to the fundamental mode helix, resulting in a larger cross section and bending radius. The transitions are also quite long which could hinder its application

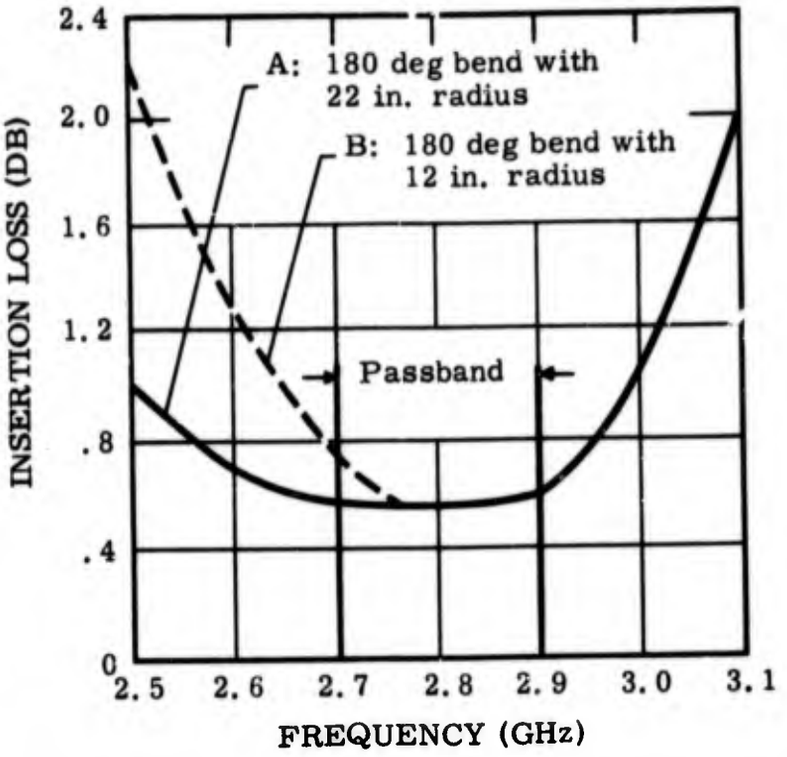

Figure 6-19. Passband insertion loss of higher order mode helix filter.

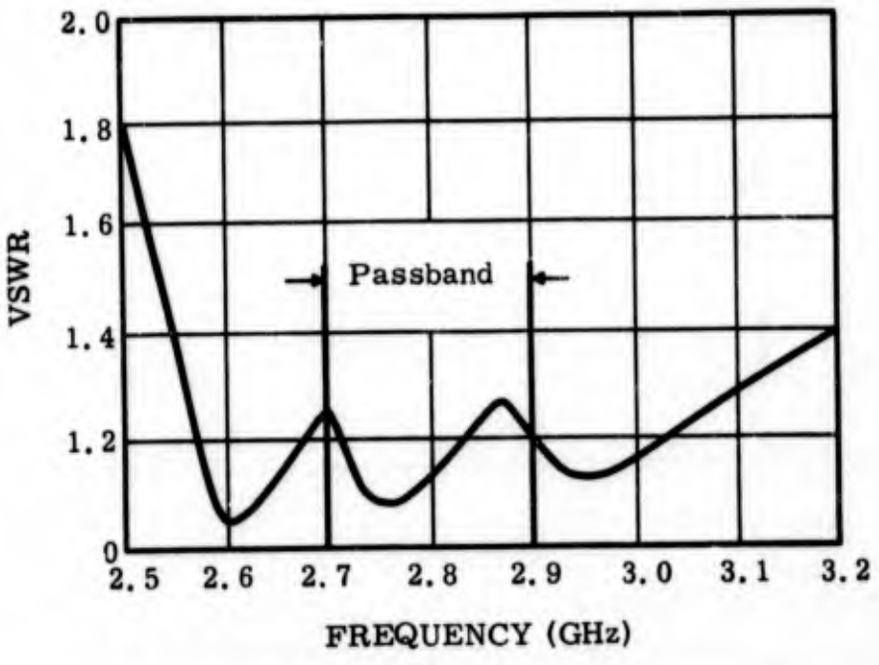

Figure 6-20. VSWR of higher order mode helix filter.

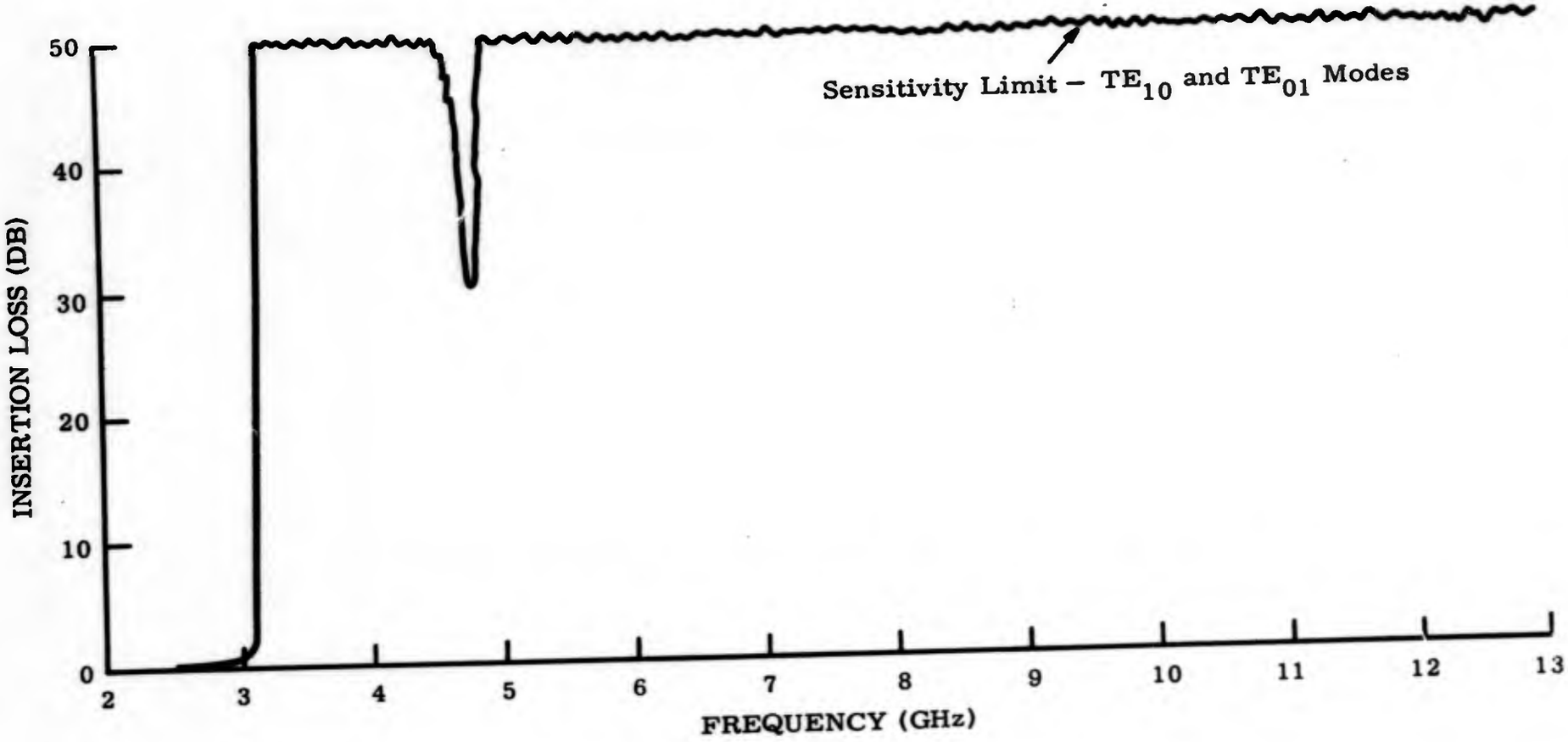

Figure 6-21. Stopband insertion loss of higher order mode helix filter.

in some radar systems. Some reduction in transition length can be achieved. The tapered transitions between the rectangular and circular waveguides could certainly be shortened (perhaps to 6 in. or less) since both lines are propagating only in the dominant mode, and the extremely broadband match provided by the long tapers is not needed.

The in-line configuration of the transitions has the probable advantage of causing relatively little stopband reflection, although this was not measured. Right angle transitions to rectangular waveguide similar to those used on the fundamental mode helix were tested. The total filter loss was about 0.8 db, indicating the feasibility of this approach. However, the in-line transition approach was a demonstration of the feasibility of nonuniform coupling, as well as having the probable advantage of lower stopband reflectivity. The main reason for continuing the in-line transition approach was because of the demonstrably high power capacity, which justifies the consideration of this filter as a solution to the problem of harmonic radiation in radar systems.

E. FUNDAMENTAL MODE HELIX FILTER WITH RIGHT ANGLE TRANSITIONS TO RECTANGULAR WAVEGUIDE

1. BACKGROUND. The feasibility of using the lowest order or fundamental propagating mode of a wire helix in a useful filter was demonstrated on the previous program, during which an operable prototype filter in L-band was built. This developmental filter, FH-15, is shown in figure 6-22. The prototype filter did, however, suffer from a number of shortcomings, among which were ranges of low attenuation in the stopband, narrowband match, rather high passband insertion loss, and poor power handling capability.

These shortcomings were attributed mainly to the transition from rectangular waveguide to the helix, the design of which was based on traveling wave tube experience. Since the feasibility of the basic right angle transition design had been demonstrated, it was believed that design improvements might enable it to achieve project goals. It was recognized that some of the shortcomings of the FH-15 might have been the result of the choice of helix dimensions, particularly as they affect the design and performance of the

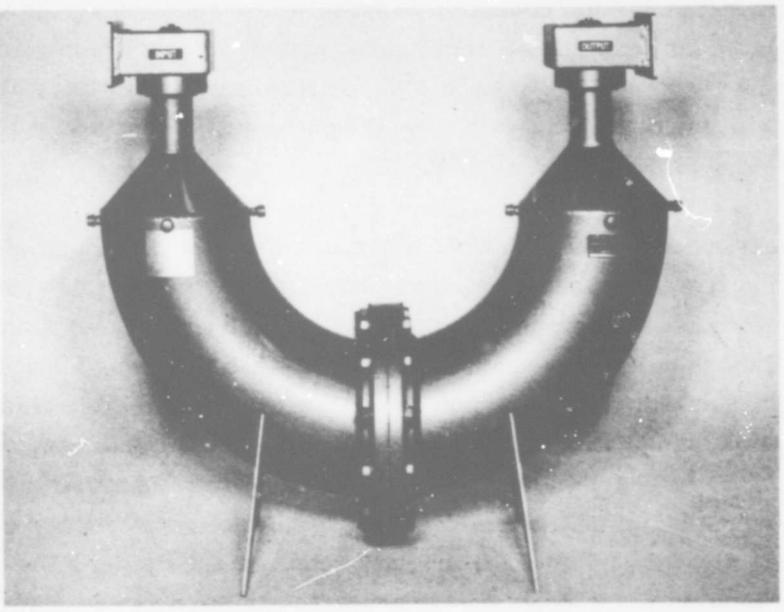

(a) Photograph.

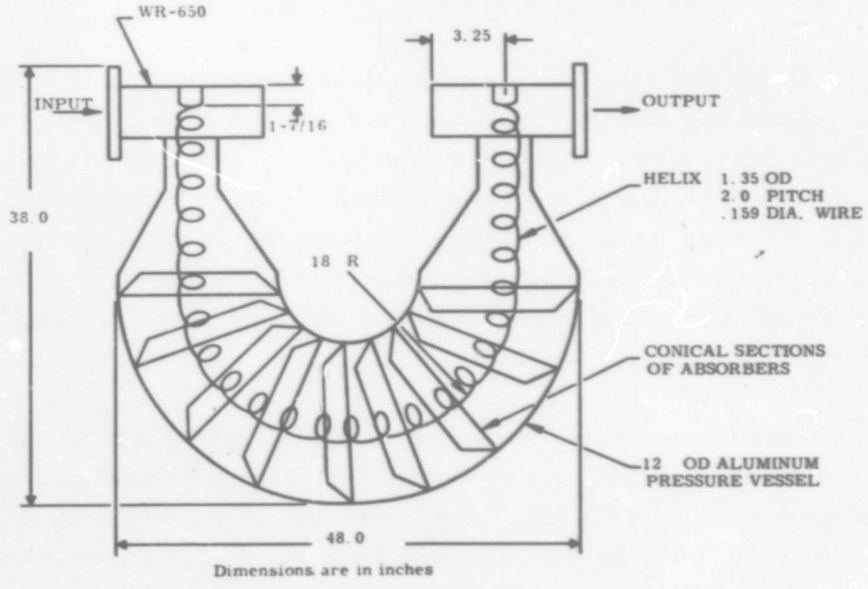

(b) Dimensions.

Figure 6-22. Fundamental mode helix filter FH-15.

transition. Accordingly, investigations of helix characteristics were carried on along with experiments aimed at optimizing the dimensions of the right angle transition between the helix and rectangular waveguide.

2. HELIX DESIGN. Since launching efficiency and loss due to bends and absorbers all improve with increasing γ, a general rule that γ should be made as large as possible was adopted at the beginning of the program. Figure 6-1 shows that γ increases as the pitch angle (given by $\sin^{-1} v_p/c$) decreases. For a given pitch angle or speed, γ is higher the closer the actual helix velocity approaches the geometric design velocity before the group velocity reaches zero. Accordingly, the first helix designs placed the 2.7 to 2.9 GHz operating band of the FPS-6 rather high on their k-β characteristics (normalized to pitch). The dimensions of two of these helices are given in table 6-1 under the designations "Fast" and "Slow." Their k-β characteristics are shown in figure 6-23. When these helices were tested in a filter configuration, however, excessive passband insertion loss was observed. The source of this excess loss was at first unexplainable. Further experiments and theoretical considerations lead to the conclusion that they were being operated far too high up on the k-β diagram. The group velocity at these operating points is decreasing rapidly and since attenuation is inversely proportional to group velocity, the increased loss is to some extent explainable. It is possible that at operating points too close to the forbidden region the circuit is more sensitive to inadvertent distortions. Once this realization became apparent, helices were designed for operation lower down on the k-β characteristic to obtain acceptable insertion loss levels. Parameters of the helix used in the final prototype helical filter are included in table 6-1, and its k-β characteristic is shown in figure 6-23.

It is apparent that the final helix design operates appreciably lower on its k-β characteristic (normalized to pitch) compared to the earlier designs. The group velocity is also higher and more nearly equal to the phase velocity for this helix. While the final helix operates at slightly lower γ than previous ones, the value of γ is much higher than can be obtained with other periodic circuits. For example, it is at least twice as high as that obtainable with the thick ladder circuit. The power handling capability of helices was

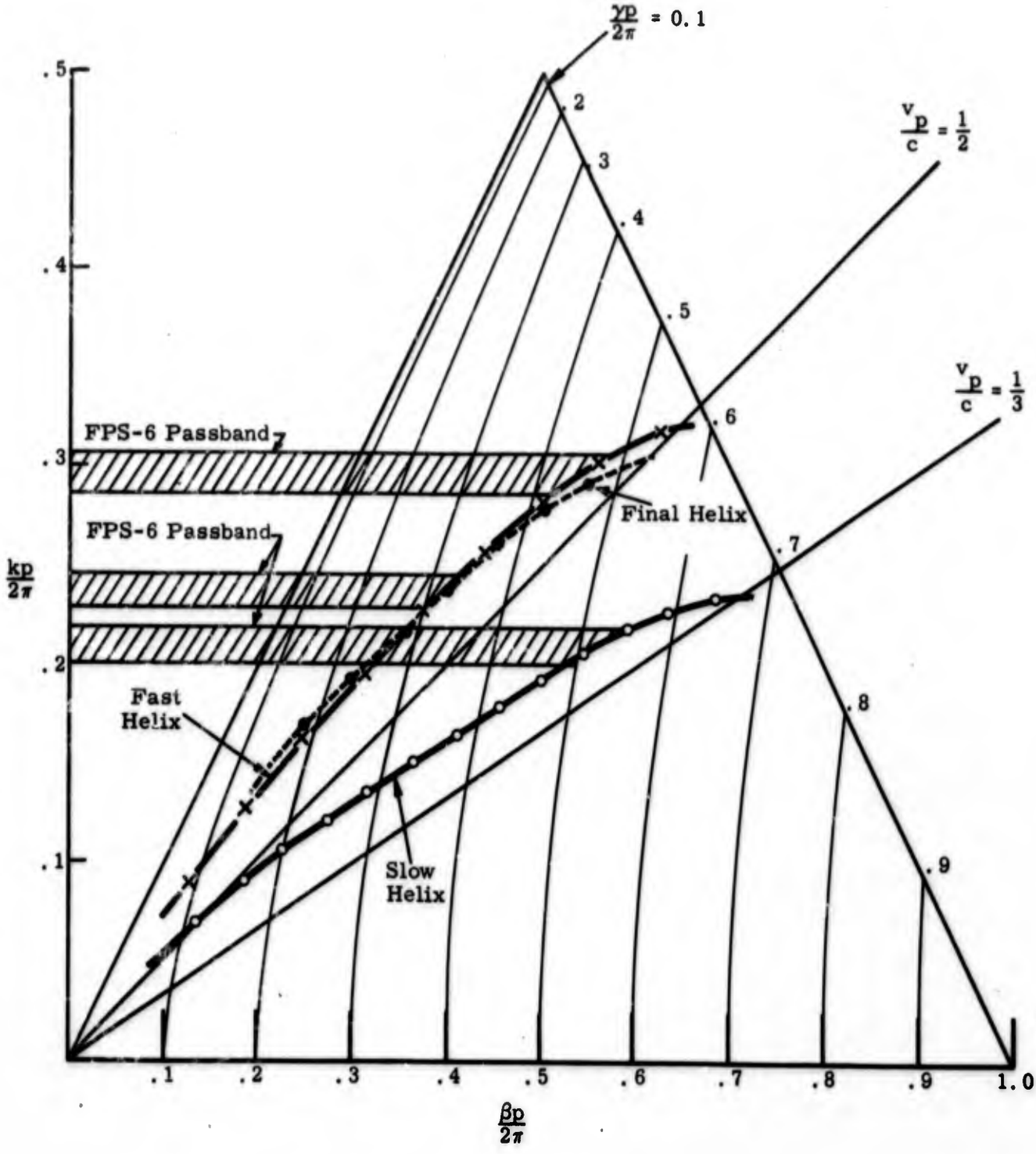

Figure 6-23. The k-β diagram of S-band helices.

Table 6-1. S-Band Filter Helix Parameters

Designation	$\frac{v_p}{c}$ approx	Pitch Angle (deg)	Pitch (in.)	ID (in.)	OD (in.)	Wire Diam (in.)	Operating Point at 2.8 GHz: $\frac{kp}{2\pi} = \frac{fp}{c}$ approx	$\frac{\beta p}{2\pi}$ approx	$\frac{\gamma p}{2\pi}$ approx	γ (nepers/in.)
Fast	.55	30	1.25	.562	.812	.125	.295	.53	.45	2.26
Slow	.35	20.5	0.885	.625	.875	.125	.22	.55	.51	3.62
Final	.60	31	1.00	.380	.700	.160	.237	.39	.31	1.95

analyzed and is included as appendix A. While many assumptions were required for the analysis, the results are felt to be indicative of what is to be expected of various helices. High power testing indicated that the results are at least of the correct order of magnitude.

To determine the effect of wire size on the propagation characteristics of helices, two helices otherwise similar to the fast and slow helices of table 6-1 but with twice the wire diameter were fabricated. It had been thought that using larger wire diameters would raise the k-β curve, resulting in a faster helix, which would allow operation at a point having a more favorable group velocity. Tests showed that the k-β curves for these helices are faster at low frequencies and slower at high frequencies. In other words, the actual k-β curve of a thick wire helix departs further from the design velocity line than a thin wire helix of the same mean diameter and pitch. However, larger wire diameters might provide greater mechanical stability, improved power handling capability and, perhaps, lower resistive loss. It might also permit liquid cooling of the helix from within.

Choosing the correct helix dimensions for a given application requires a certain amount of engineering judgment. It would seem that the slowest permissible helix, i.e., a helix having a design phase velocity of one-third of the speed of light would be better for filter applications than a somewhat faster helix because of its higher γ. However, when helices of different phase velocities are compared on the same basis, as for example in figure 6-24 where the pitches of three helices are determined by placing the second harmonic frequency at the beginning of the helix forbidden region, it can be seen that the slowest helix requires the finest pitch. Solution of equation 6.1

for these three cases shows that the mean diameter increases as the speed decreases. The operating points dictated by figure 6-24 are the lowest that can be allowed in a useful harmonic filter. Therefore, this condition corresponds to the widest possible operating range. However, when helices were designed in accordance with figure 6-24, it was found that they were so small that they could not be fabricated in the available facilities. This necessitated using coarser pitch designs. For a given helix speed, the coarser the pitch, the larger the helix diameter, and consequently, the higher the power capacity for a given wire diameter. It was pointed out before, however, that the pitch must not be so coarse as to introduce high loss due to proximity of the helix forbidden region. When a compromise operating point was chosen, i. e., one not so high on a pitch-normalized k-β diagram as that of the "Fast" and "Slow" helices of table 6-1, but higher than that dictated by placing the helix cutoff at the second harmonic (such as in figure 6-24), it was found that the $v_p = c/2$ helix design appeared to have higher power capacity than the $v_p = c/3$ helix.

The "Final" helix of table 6-1 was therefore a compromise among the following factors:

1. Passband loss and filter size considerations requiring sufficiently high γ
2. Passband loss considerations requiring a sufficient frequency interval between the operating range and the helix cutoff
3. The general trends of power handling capacity
4. Feasibility of helix fabrication

These factors may not be the same for all applications. However, it is believed that the "Final" helix design should be suitable for most microwave radars. It is of interest to note that the helix design of the FH-15 filter and the final helix of table 6-1 are very similar, having approximately the same speed and operating point with respect to wavelength.

3. TRANSITION DESIGN. When the right angle waveguide to helix transition is analyzed in terms of the general transition block diagram of figure 3-2, it can be seen that no intermediate fast wave line is employed, so that the waveguide to enclosed helix junction performs the functions of

junctions 1 and 2. That is, it modifies the fields of the rectangular waveguide dominant mode and also provides a coupling mechanism between these fields and the enclosed helix. No intermediate open slow wave circuit is employed so junction 4 of the block diagram is eliminated. The function of junction 3 is performed by the flare or horn. Because of the inherently high γ of the helix, the design of the horn is relatively simple and uncritical. The desired improvements must then come about through modifications to the waveguide to enclosed helix junction.

Improvements in power handling capability were expected to result from the following modifications:

1. Use of a spherical or doorknob antenna instead of a basically cylindrical antenna
2. Use of a relatively large tube diameter

These modifications were incorporated in test pieces for a program of measurements intended to maximize the bandwidth of low VSWR. The measurements were planned to include a wide range of dimensions for all parts of the junction. This approach was chosen because of the difficulty of analyzing the complex geometry of the junction. In particular, it was seen that the fields on the helix were hard to describe analytically or even to visualize. The field configuration for the fundamental helix mode depends not only on the phase velocity but also on the choice of operating point. For example, the phase shift between turns of a helix operated high on its pitch normalized k-β characteristic may be about 180 deg, while for a low operating point (i.e., finer pitch) the phase shift per turn might be only 100 deg. A good deal of empirical data was taken for various combinations of junction dimensions employing the "Fast" and "Slow" helices of table 6-1. The conclusions of this study are summarized as follows:

1. The junction can be matched over the FPS-6 radar operating range, but not appreciably more.
2. The tubing diameter should be two to three times the helix diameter.
3. Helix orientation is important, with the broadest band matches obtained when the helix starts in the center of the guide, facing the waveguide opening.

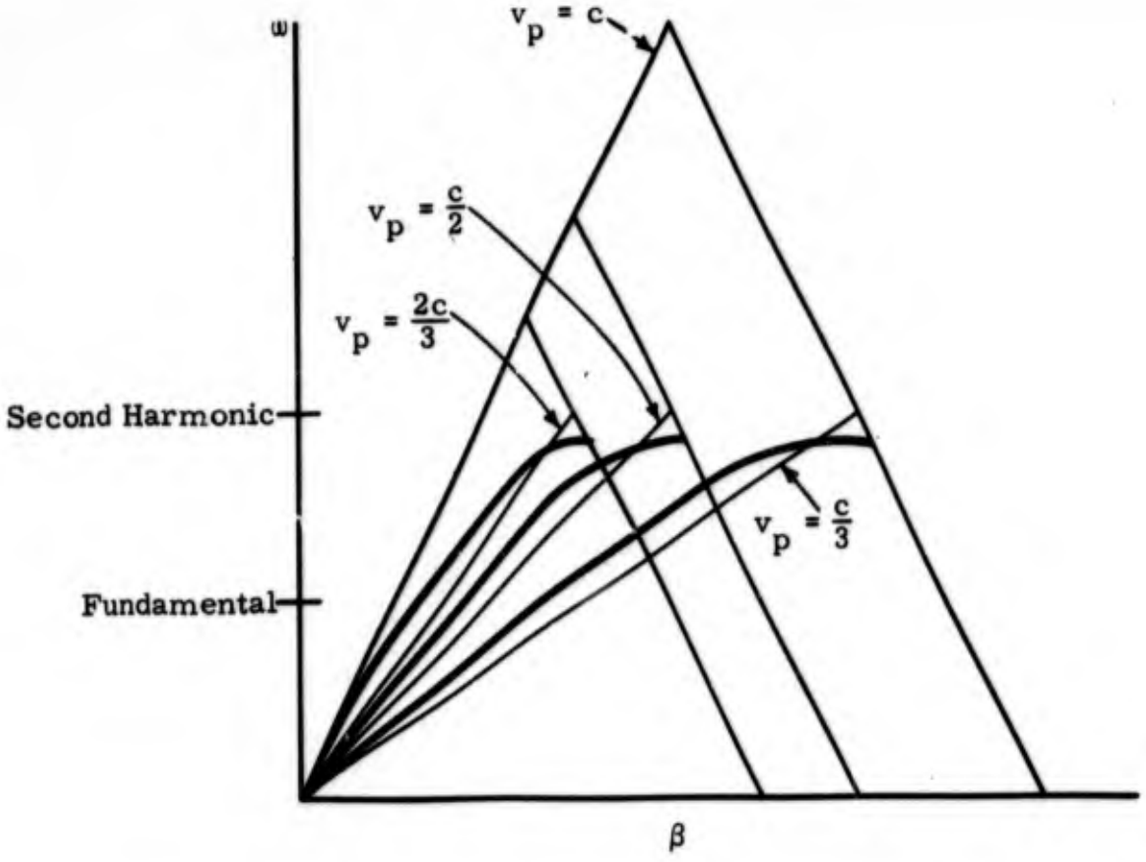

Figure 6-24. ω-β characteristics of maximum bandwidth helices.

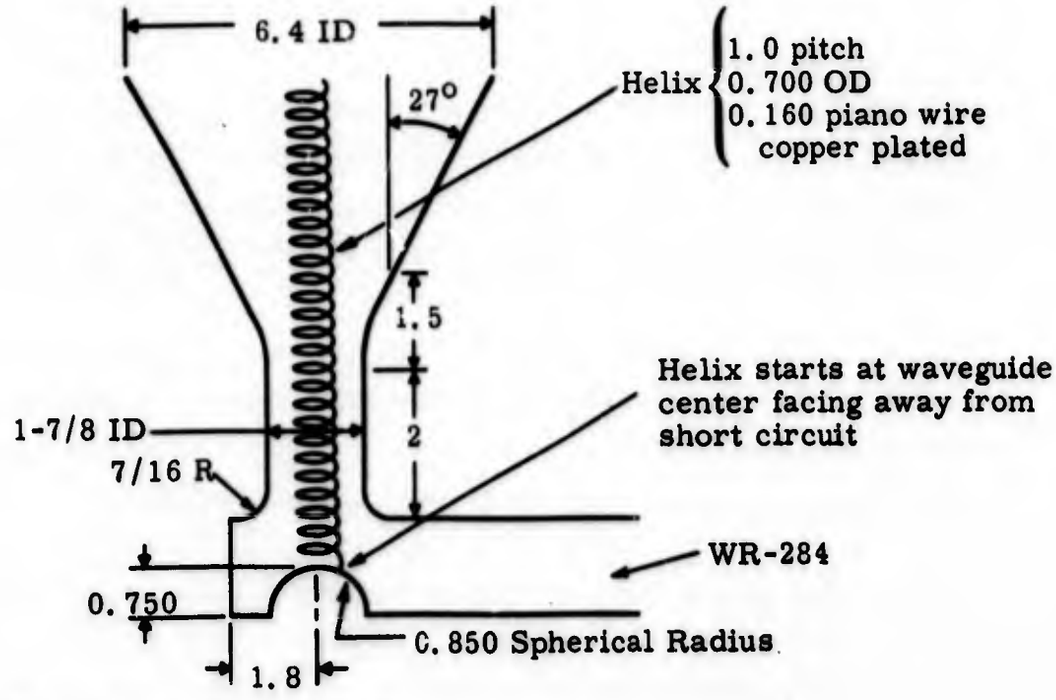

Dimensions are in inches.

Figure 6-25. Dimensions of final waveguide to helix transition.

4. The required precision in locating the waveguide short circuit is least when the helix is oriented as described in item 3.
5. The match can be optimized by adjustment of the antenna height and shape, and by the use of inductive irises in the rectangular waveguide.

The above conclusions were applied to the matching of the transition incorporating the "Final" helix of table 6-1. The important dimensions of the transition are shown in figure 6-25. The VSWR of one transition with the helix terminated is shown in figure 6-26. The termination was found to be imperfect, so that the effects of fine adjustments or tuning irises were not clear. It should be noted that the tube enclosing the helix has a cutoff frequency of 40 GHz for the lowest order (TE_{11}) waveguide mode. Therefore, in the FPS-6 operating range the desirable condition of unique modes on both sides of the junction is realized, since the propagating fields in the enclosed helix transmission line must be supported by the helix.

Two waveguide to helix transitions as shown in figure 6-25 were conneeted by a length of 1-7/8 in. ID pipe and used as a high power breakdown test vehicle. For this test the horns from the closed helix to the open helix were not used. The test thus used a fully enclosed length of helix. This configuration broke down at 580 kw peak power at atmospheric air pressure. This figure can be compared to the 400 kw level at which breakdown occurred in the FH-15 filter. Considering that the new filter operates in S-band compared to the FH-15 operating in L-band the improvement in power handling capability wouldbe a factor of about 2.9. Scaling the 580 kw level to the FPS-6 radar operating pressure (30 psig) implies a power handling capability of 4.05 Mw which is not high enough for the nominal FPS-6 power level.

The breakdown in this transition appeared to occur between the spherical antenna dome and the first turn of the helix. No breakdown from turn to turn on the helix or from helix to the enclosing pipe was observed. The reason for the breakdown in this region is no doubt tied to the higher order modes necessary to satisfy the complex boundary conditions within this complicated geometry. Thus, the limiting factor is still the transition

region and not the helix itself. Efforts to improve the power handling capacity of this transition beyond the level measured were discontinued in view of the time schedule. The level is such that a useful filter for FPS-6 radar operation could be made provided high dielectric strength gas is used.

4. BREADBOARD FILTER DESIGN AND FABRICATION.

a. Electrical Design. The design of a filter usually requires a compromise between passband loss and stopband attenuation. Both quantities generally increase with filter length. Open periodic filters require bends to insure adequate stopband attenuation, and passband loss also depends on the radius and angle of bending. Therefore, in order to determine the breadboard filter configuration, it was necessary to consider both passband loss and stopband attenuation.

Passband insertion loss in this type of filter is made up of a number of contributions. The intrinsic loss of the helix, the launching efficiency of the transitions, transition mismatch loss, helix scattering loss, and absorber location all play an important role in determining the passband insertion loss of the filter. The intrinsic helix loss was measured in a filter configuration by first measuring a long helix and then repeating the measurement after removing a known length of helix. By this method the intrinsic loss of the helix was determined to be 0.033 db/ft. These tests were for an open helix with no absorbers, so that the effects of absorber location were eliminated. The final test configuration used a 4-ft long helix so that an estimate of transition launching efficiency can be made. The insertion loss of this filter was 0.3 db of which 4(.033) = 0.132 db is intrinsic helix loss. This leaves 0.300-0.132 = 0.168 db loss for the two transitions. This then gives us an estimate of transition launching loss of the order of 0.084 db per transition. This figure is within the 0.1 db objective specification of the present contract. These figures for intrinsic helix loss and launching efficiency of the transitions then will enable us to predict the passband insertion loss of the prototype filter. For reasons explained in the following section 8 ft of helix are required for the prototype filter. We thus expect

$$
\begin{aligned}
8(.033) &= 0.264 \text{ db} \quad \text{intrinsic loss} \\
&+ \underline{0.168 \text{ db}} \quad \text{launching loss} \\
&\quad 0.432 \text{ db} \quad \text{total loss}
\end{aligned}
$$

This figure does not include the effects of absorber and mismatch losses. It does, however, provide a minimum loss value to expect.

The FH-15 filter exhibited generally good stopband characteristics with the exception of some points of low attenuation at the 2nd harmonic band. To improve this characteristic it was decided to build a filter having a 360 deg bend. This together with more careful attention to absorbers should provide a filter with improved stopband characteristics. The decision to improve the stopband characteristics by going to a 360 deg bend required the helix length to be 8 ft. Some helix length might have been saved through going to a more complex geometric configuration, but the added complexities in assembly and parts making did not warrant this.

One of the most important considerations in absorber design for such a filter is the spacing between the circuit and the absorber so that negligible passband loss is introduced. The design of the absorbers in this respect is based on the work of the previous contract. From table 6-1, γ for our helix is 1.95 nepers/in. $\cong$ 0.77 nepers/cm. From figure 7-8 of reference 2 we determine the distance from the circuit so that the insertion loss should be less than 0.05 db. This number comes out to the order of 1-1/2 in. Since our helix OD is 0.700 in. we chose a 4 in. ID for the absorbers. This gives a 1.650 in. clearance from the helix which, then, should be adequate to ensure very little insertion loss addition due to absorbers. Another consideration is that of absorber material. Generally a good bulk absorber is the best. Other desirable characteristics include thermal characteristics, lightweight, and low reflectivity. Certain hardwoods have been used as microwave absorbers and of these oak is one of the better ones. Oak was chosen because of its hardness, machinability and freedom from pitch. A photograph comparing the initial absorber design with the final one is shown in figure 6-27. The one with the small hole is the result of a mistake in computation. The initial filter assembly used absorbers having the smaller

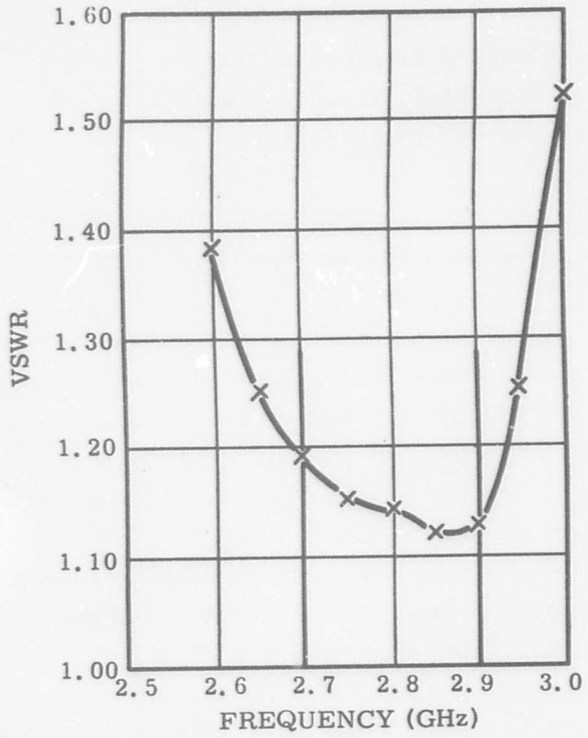

Figure 6-26. VSWR versus frequency of single transition of breadboard model filter.

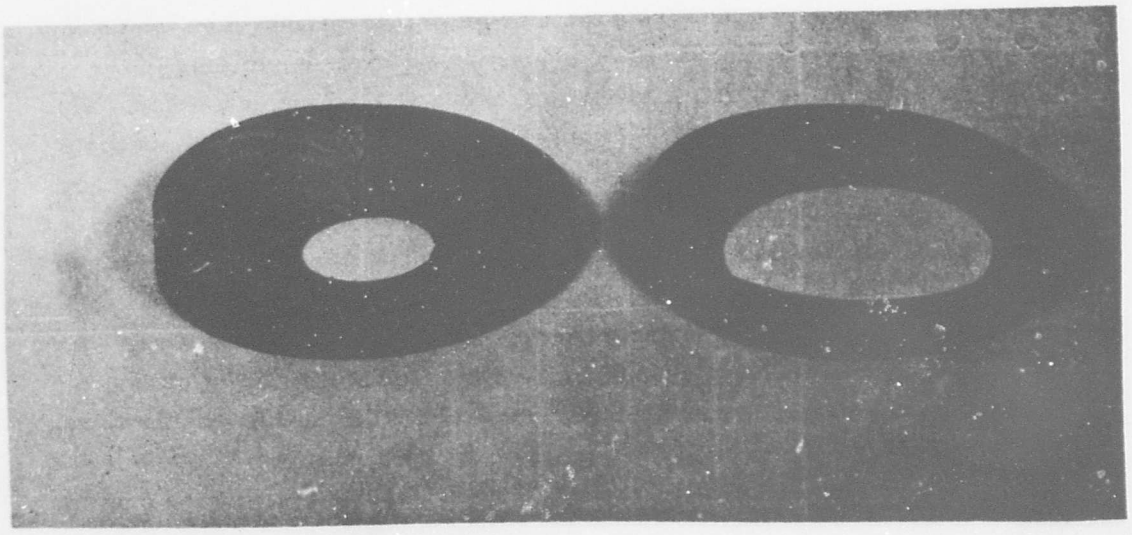

Figure 6-27. Photograph of oak absorber.

ID. The filter insertion loss turned out to be about 2.5 db. Recheck of computations revealed the error and the absorber ID was opened up to 4 in. This absorber configuration was used in the breadboard filter.

b. Mechanical Design. Mechanically there were several requirements that had to be met in order to complete the prototype filter. The filter had to be pressure tight so that high dielectric strength gas pressure could be maintained. Provision had to be made for the mating of pressure windows. A pressure bypass connection had to be made for maintaining system operating air pressure. A 360 deg bend was decided upon for improved stopband characteristics. Assembly procedures also had to be kept in mind.

To accomplish all of these requirements, thin wall stainless steel tubing was chosen for the pressure vessel. This material was chosen because commercially available bends could be obtained and because of its high strength to weight ratio and the ease of assembly using inert gas arc welding techniques. The pressure vessel is 6-5/8 in. OD x 0.109 in. wall 304L stainless steel and is comprised of four 90 deg elbows and a straight section. Two commercial reducers were used as the horns to complete the transitions. These were mated to the waveguides with an O-ring seal. The waveguides were provided with a welding flange for attaching the pressure windows. Figure 6-28 shows a photograph of the filter components before assembly. All assembly with the exception of the helix connection and the waveguide to horn connection was by inert gas arc welding. The waveguide to horn connection is made by an O-ring seal while the helix connection is made by bolting to the waveguide. The helix must remain centered in the absorber configuration, regardless of the filter mounting position, in order to prevent undue loss. The stiffness of the helix, which is made of steel piano wire, helps serve this purpose. As insurance, however, the helix was tied at several points to the absorbers using nylon string. Teflon string would have been better for high temperature characteristics, but was not available in time to meet the assembly schedule. Following assembly of the pressure vessel, the waveguide and helix connections were made, the windows were welded on, and the assembly was completed by attaching the pressure fittings. Figure 6-29 shows the physical

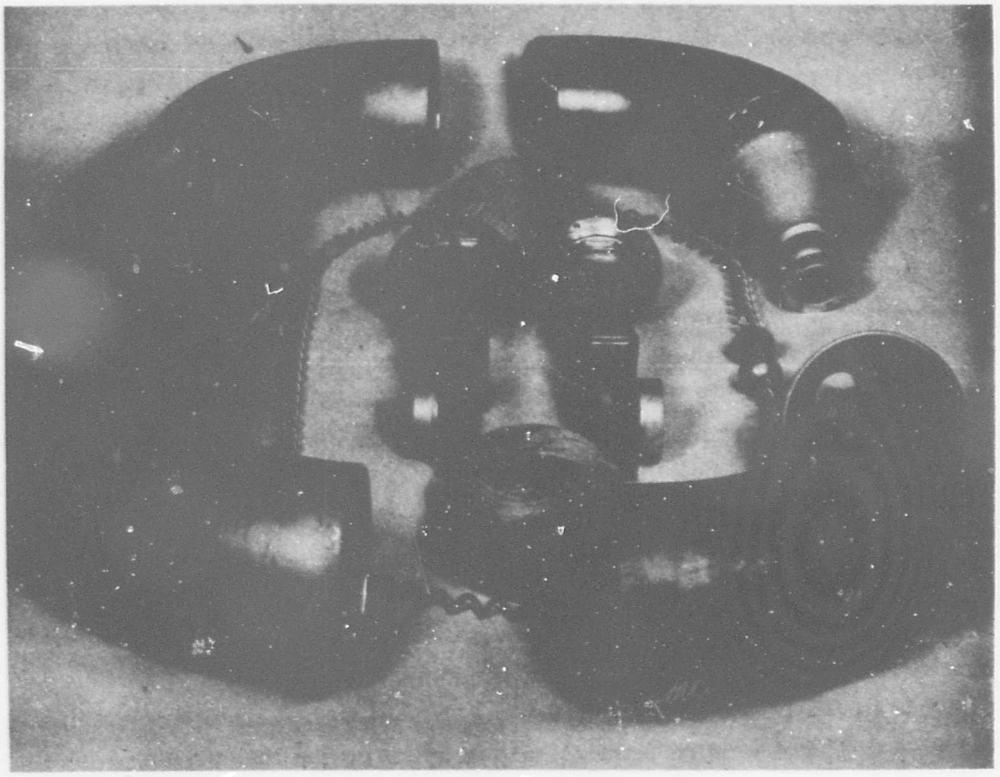

Figure 6-28. Photograph of breadboard filter parts.

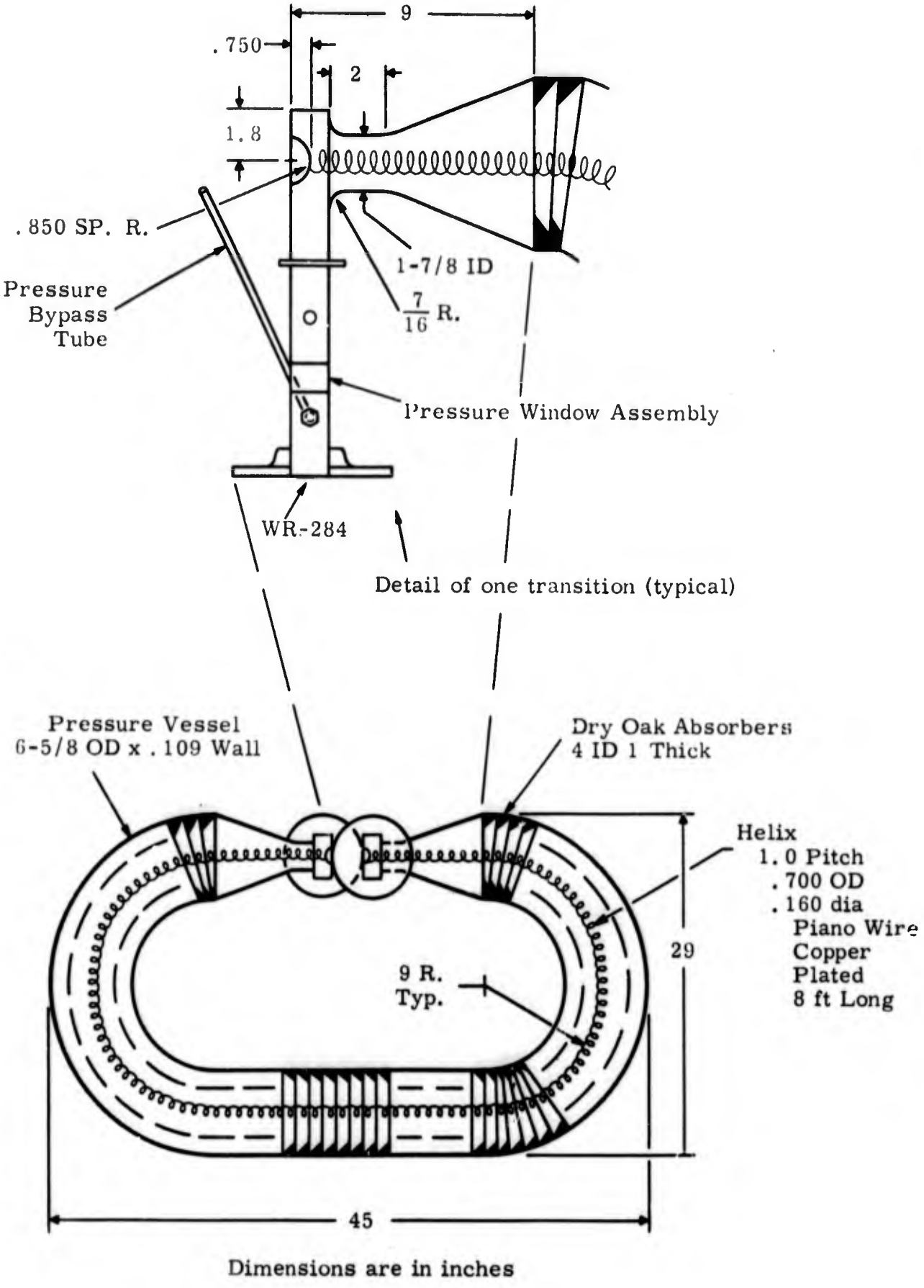

Figure 6-29. Physical dimensions of prototype helical filter.

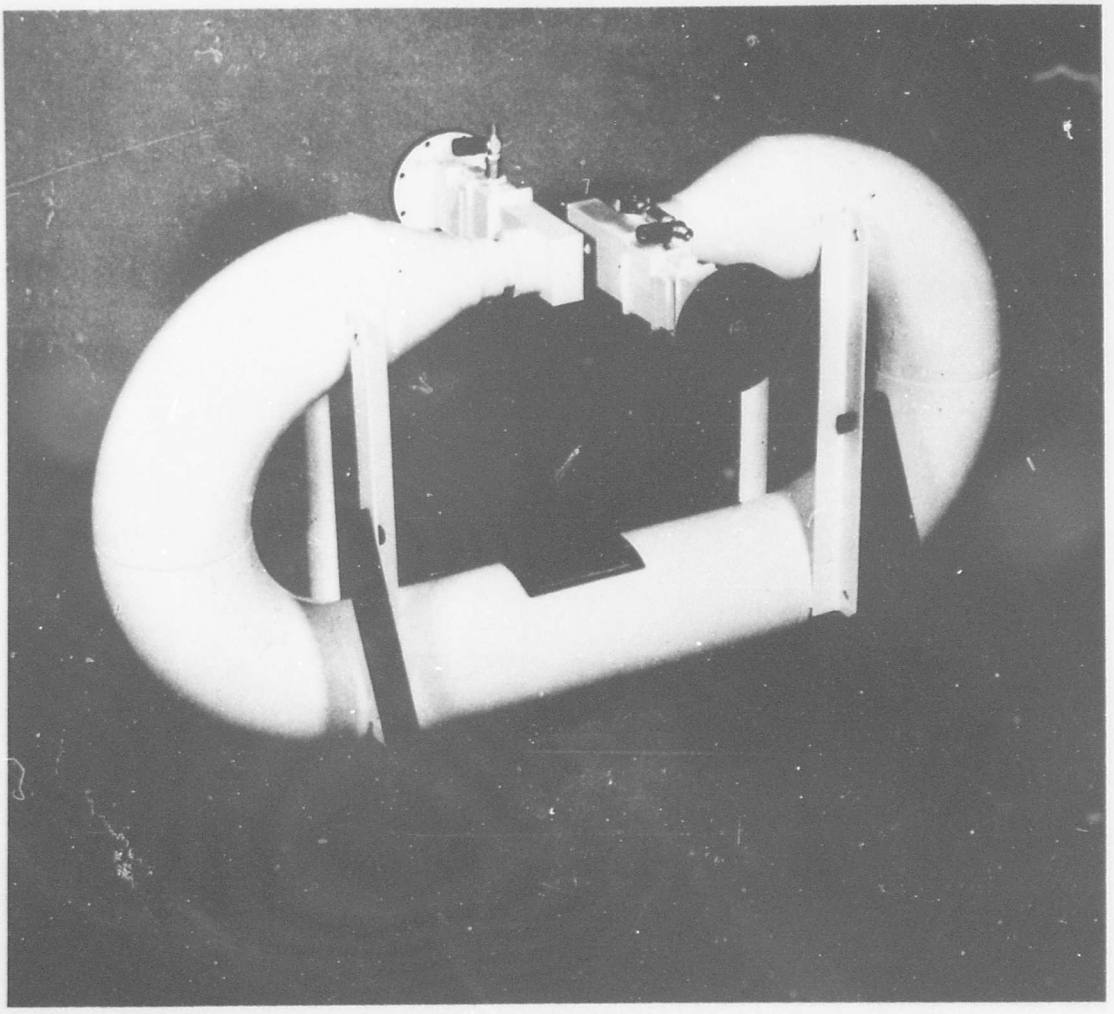

Figure 6-30. Photograph of completed breadboard filter.

dimensions of the final filter, and figure 6-30 is a photograph of the final filter after assembly and painting. The filter was then exhausted using a mechanical forepump and filled with Freon 116 to a pressure of 15 psig. This gas was used because of its low evaporating point which permits its use in cold climates. Its dielectric strength is less than that of Freon 12, but it was believed that it would be adequate with sufficient pressurization. The filter was then ready for tests.

c. Test Results of Breadboard Filter. Initial high power testing in the laboratory was done at a gas pressure of 6 psig. The filter at this pressure seemed to break down at a power level of 2.5 Mw. Raising the pressure to 15 psig enabled the filter to take the full power of our FPS-6 system. During field tests at RADC the filter was again taken to the maximum power of the field system and no breakdowns occurred. Considerable heating of the filter was observed in the field tests. This heating raised the gas pressure to approximately 30 psig but no deleterious effects were noted. The filter thus has demonstrated the ability to take the full peak and average power delivered in the FPS-6 system. On a power density basis this power level can be interpreted as fully meeting the objective power handling specifications of this contract.

A plot of passband VSWR versus frequency for the breadboard filter is shown in figure 6-31. Figure 6-32 compares the VSWR of the helix filter and the FH-15 filter, both without windows. The improvement in match is not as good as had been hoped for. The match is quite periodic indicating multiple reflections. Some improvement in bandwidth is apparent, however. The source of the periodicity of the match may in part be due to some helix pitch distortion due to the helix forming procedure. The interaction of these reflections with those of the two transitions and some contribution due to the pressure windows no doubt can account for the observed periodicity. The conclusion here is that the desired objectives in passband VSWR have not been realized. The experience of this program leads us to conclude that the passband VSWR for a fundamental helix filter employing right angle waveguide to helix transitions will be difficult to improve further. Improvements over narrow bandwidths can be made, but better broadband matches are difficult to obtain, particularly for high power applications, which tend to restrict matching techniques.

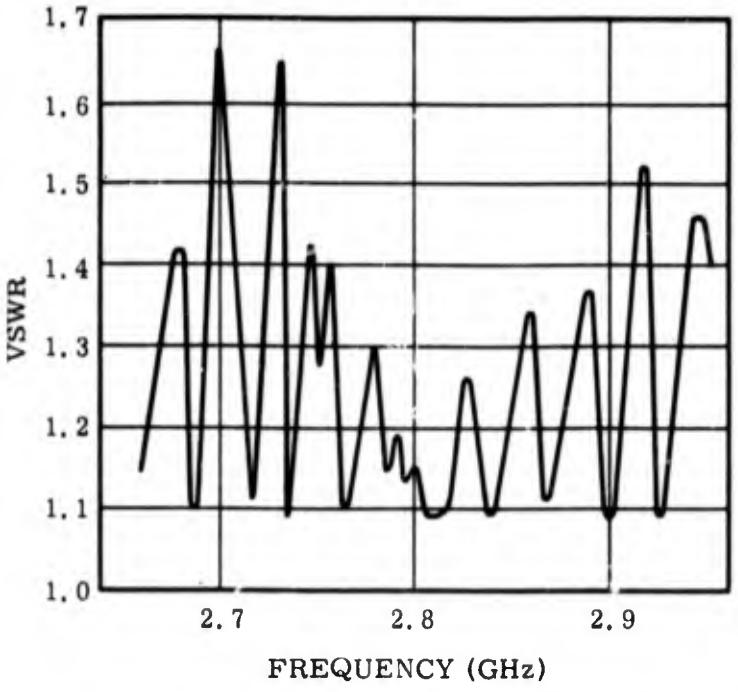

Figure 6-31. Passband VSWR fo breadboard model of fundamental mode helical filter.

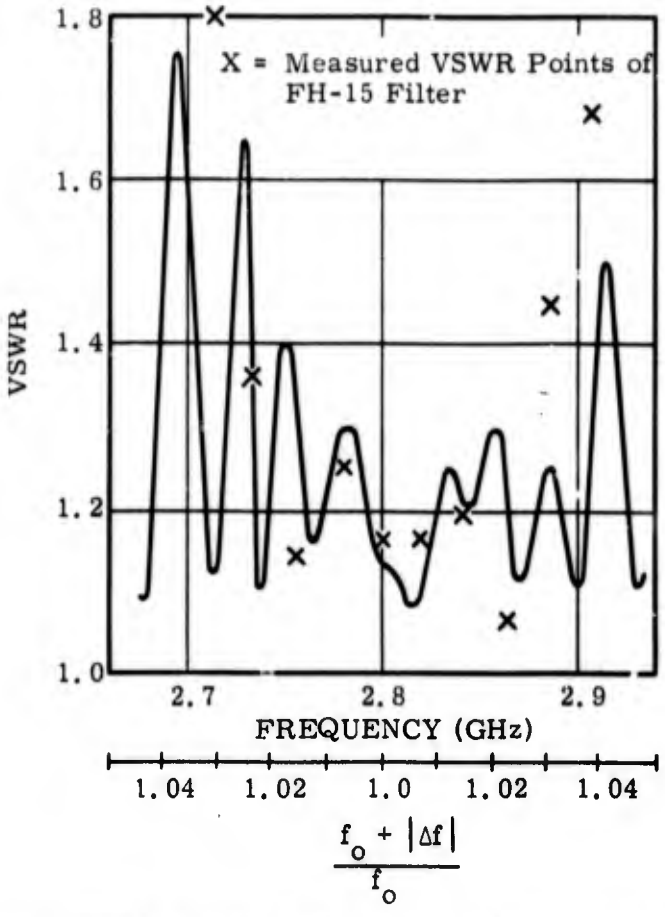

Figure 6-32. VSWR of breadboard model of fundamental mode helical filter without windows. Measured VSWR point of the FH-15 filter are also shown.

Plots of passband insertion loss for the completed filter with and without pressure windows are shown in figure 6-33. The predicted loss due to intrinsic helix loss and launching loss was about 0.4 db; figure 6-33 shows a loss slightly more than 0.6 db at best. This leads us to conclude that the absorbers contributed about 0.2 db of loss. This value is higher than predicted but not unreasonable when the possibility of the helix not being perfectly centered is considered. The helix no doubt was not perfectly centered and thus a somewhat higher loss contribution due to absorbers was the result. The pressure windows also contributed to the overall filter insertion loss to the extent of approximately 0.15 db. Thus the overall insertion loss is explainable and while higher than desired, the filter did function properly. The result of the insertion loss was considerable filter heating while in field tests. This heating, however, did not seem to degrade the filter performance and thus was tolerable. The loss itself was not detected in the field tests.

A plot of the overall attenuation characteristic of the final prototype filter as measured in the laboratory is shown in figure 6-34. The characteristic shows greater than 55 db attenuation for all harmonics from the 2nd through at least the 6th. There are some spikes down to 40 db for frequencies below the 2nd harmonic frequency range. These spikes, it is felt, are due to insufficient radial thickness of the absorbers. These characteristics would probably have been better if an 8 in. diameter pressure vessel had been used instead of the 6 in. one. This would have allowed more radial thickness for absorbers and should improve attenuation at the lower end of the stopband. The overall stopband characteristics are good, and show significant improvement over those obtained with FH-15. Stopband VSWR data were not taken because the fabrication and testing schedule did not allow time for it.

The field tests tended to confirm the laboratory tests. The measured power at the receiving site is plotted in figure 6-35, with and without the filter. No harmonic energy could be detected with the filter installed. Spurious outputs near the fundamental frequency were attenuated in varying degree, depending on their proximity to the fundamental. These tests were a clear demonstration of the effectiveness of the filter in "cleaning up" the output spectrum of the radar.

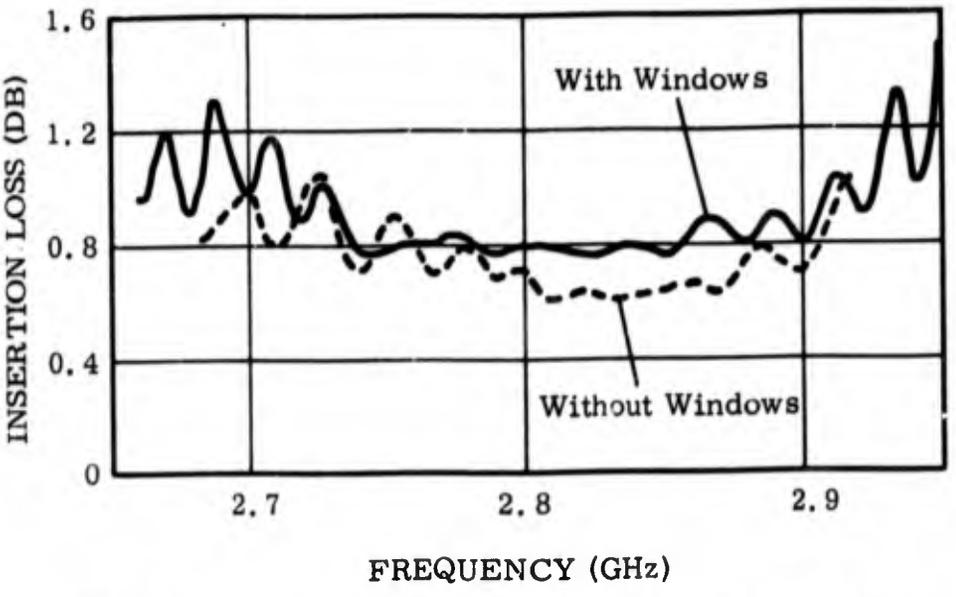

Figure 6-33. Passband loss of breadboard model of fundamental mode helical filter.

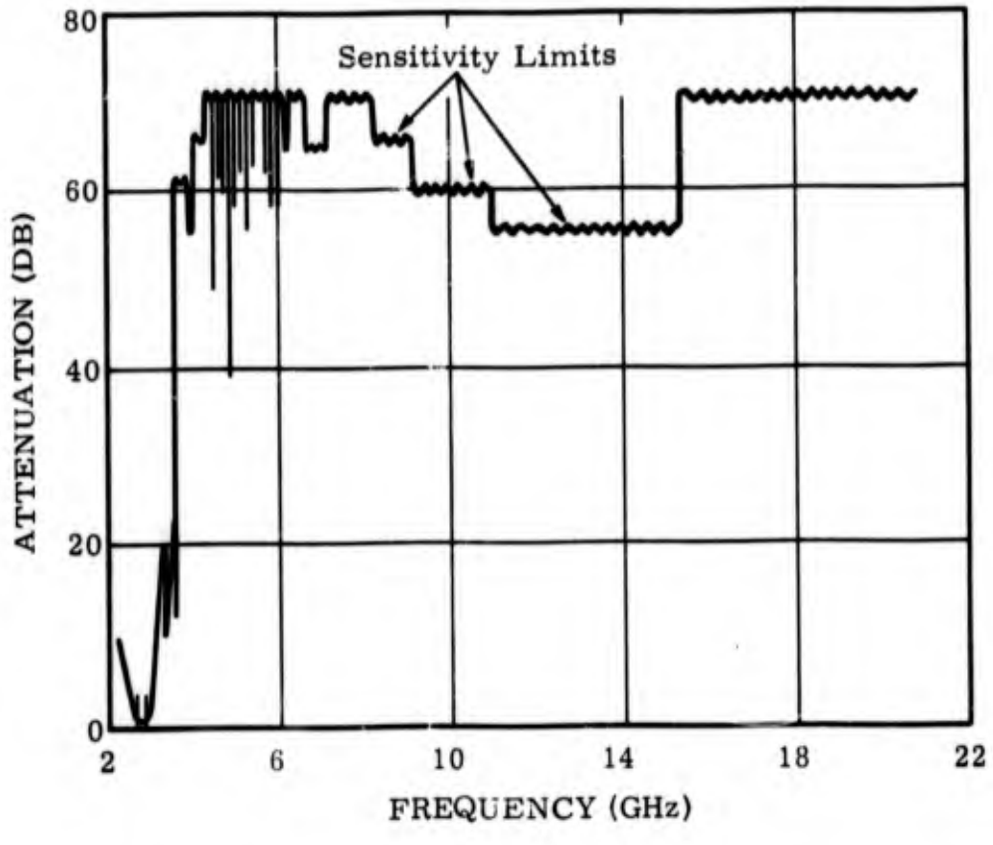

Figure 6-34. Fundamental mode helix filter attenuation – TE_{10} and TE_{01} modes.

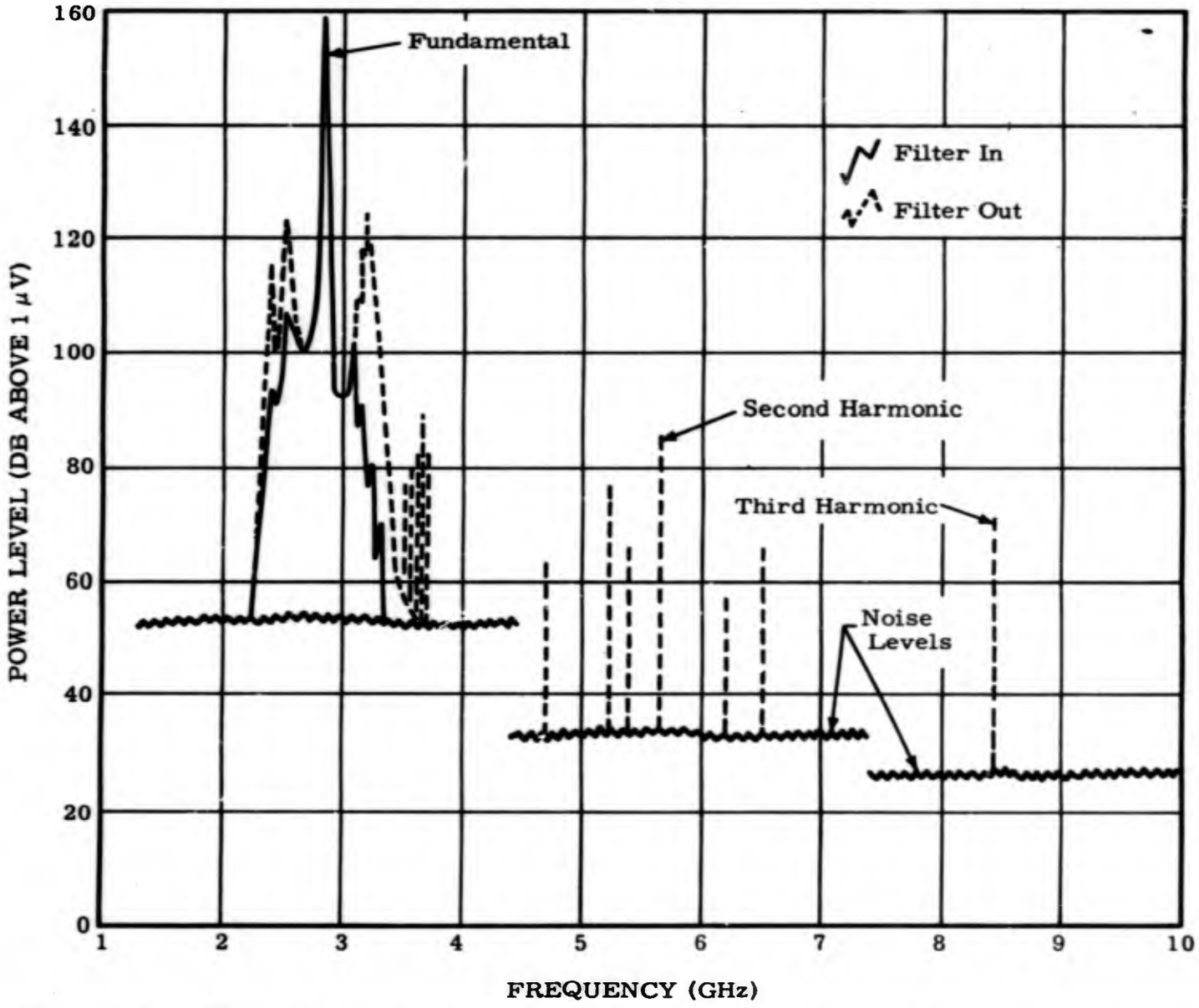

Figure 6-35. Field measurements of output spectrum of an FPS-6 radar with and without breadboard filter.

5. SUMMARY. Although the right angle waveguide to helix transition appears to be inherently narrowband and of relatively low power capacity, its simplicity, ruggedness and compactness permitted the realization of an operational filter that is effective in reducing the level of spurious outputs of high power radars. In the course of improving this transition, useful information regarding the design of fundamental mode helix filters was gathered: in particular, the factors affecting the choice of helix dimensions were determined.

VII. LADDER FILTERS AND TRANSITIONS

A. GENERAL

The general filter studies of section IV led to the following conclusions regarding the use of ladder structures (or more generally, periodic arrays of identical elements) as filters:

1. To ensure attenuation of all harmonic frequencies without excessive bending and consequent passband loss, the pitch of the structure should be between a quarter wavelength and a half wavelength at the lowest passband frequency.
2. Application of item 1 above rules out interdigital or alternately staggered arrays of elements since the passband will be in the forbidden region based on the interdigital pitch.
3. The elements of the array can be optimized for the most desirable k-β characteristic, i.e., a characteristic having high γ and group velocity in the passband, as shown in figure 4-7. Consideration of surface impedance may assist in achieving high γ.

Since the previous program treated so many different circuits without, by any means, exhausting the field, the above conclusions were of value in deciding which circuits should receive the most attention on the present program. If a particular structure could not provide the desired k-β characteristic, it could be discarded. The decision as to which of the remaining circuits should be studied could then be based on circuit simplicity, ease of construction, transition design, high power capability, and overall filter configuration. It appeared that complex structures (considered either mechanically or electrically) should not be studied until the potentialities of simpler circuits had been explored, unless an immediate advantage to one of the other considerations was evident. Such an advantage was never clear during the course of the program, so only simple circuits such as the thin ladder and the thick ladder were studied, to the exclusion of ring plane circuits, ring bar circuits, thick one sided zigzag circuits, and the

like. Certain of these circuits may one day be found to be particularly suited for filter applications – at that time it would be expected that the design principles derived from experience with simpler circuits could be applied.

The program plan required the study of transitions to several classes of slow wave structures. When the above listed conclusions were first arrived at, they seemed to apply to all of these classes except the helix, which is obviously not a periodic array of identical elements. Further thought led to another exception – the interdigital open slot ladder of figure 2-12. This circuit was first conceived as an interdigital arrangement of the uniform open slot ladder of figure 2-8. However, it is basically different in that the fields propagate along both edges. The conclusions regarding ladder structures could not be applied to the interdigital open slot ladder because if the slots are uniformly aligned, the structure loses its identity. This structure will be discussed in this section even though it differs from other ladder structures in that it must be interdigital. The design and testing of Yagi array, thin ladder, and thick ladder filters will also be described.

B. INTERDIGITAL OPEN SLOT LADDER

At the beginning of the investigation of interdigital open slot ladders, it was wondered how the k-β characteristic could be optimized. The characteristic of figure 2-12 appears to be capable of improvement with respect to linearity and bandwidth. Little was known about its design parameters, particularly the dependence of the k-β characteristic on the amount of slot displacement (figure 4-21 of reference 2 shows the characteristics of interdigital open slot ladders for various slot length to pitch ratios, but the relative displacement is constant). The frequency of zero group velocity was known to be about 13 percent below the calculated slot resonant frequency for the case where the displacement is equal to half the slot length, provided the pitch is not so coarse as to place the resonant frequency in the forbidden region. An experiment was run in which the slot and web width were equal and with the displacement increased so that the length of the tab was equal to the width of the web. The resulting normalized k-β

characteristic is shown in figure 7-1 as curve I. The frequency of zero group velocity is now 9 percent lower than the calculated resonance frequency. When the corners of the tab were fully rounded, which would be done for power handling capacity considerations, curve II resulted. The frequency of zero group velocity is almost exactly equal to the slot resonant frequency. This is reasonable when it is considered that the capacitive loading at the end of the slot has been decreased. But of possibly more interest is the fact that curve II could have been predicted to some extent by a phase velocity line corresponding to

$$\frac{v_p}{c} = \frac{\text{pitch}}{\text{line length per pitch}} \tag{7.1}$$

where the line length is measured along the centerline of the conductor. The bowing of the curve can be at least partially explained by considering that at low frequencies the currents will hug the inside curves of the structure with a resulting higher phase velocity. As frequency increases, the surface current path will lengthen. This suggests that if the line width is reduced so that the effective line length per pitch is more nearly equal at both high and low frequencies, the k-β characteristic should lie closer to the phase velocity line with consequent improvement in γ and group velocity.

This train of reasoning is illustrated in figure 7-2, which shows hypothetical k-β characteristics for four circuits whose dimensions have been adjusted so that they all have the same zero group velocity frequency. Curve D, representing a structure made from wire, is almost the same as that of a wire zigzag line, and also approaches that of a helix having the same design velocity.

The point of this discussion is that the interdigital open slot ladder, when optimized for desirable k-β characteristics, reduces to a geometric velocity circuit, which we will refer to as a sinuous line. As such, it is more analogous to a helix than it is to a ladder circuit, whether interdigital or uniform. Since it is so similar to a helix, the transitions from system transmission lines should be conceptually similar. The TEM line of

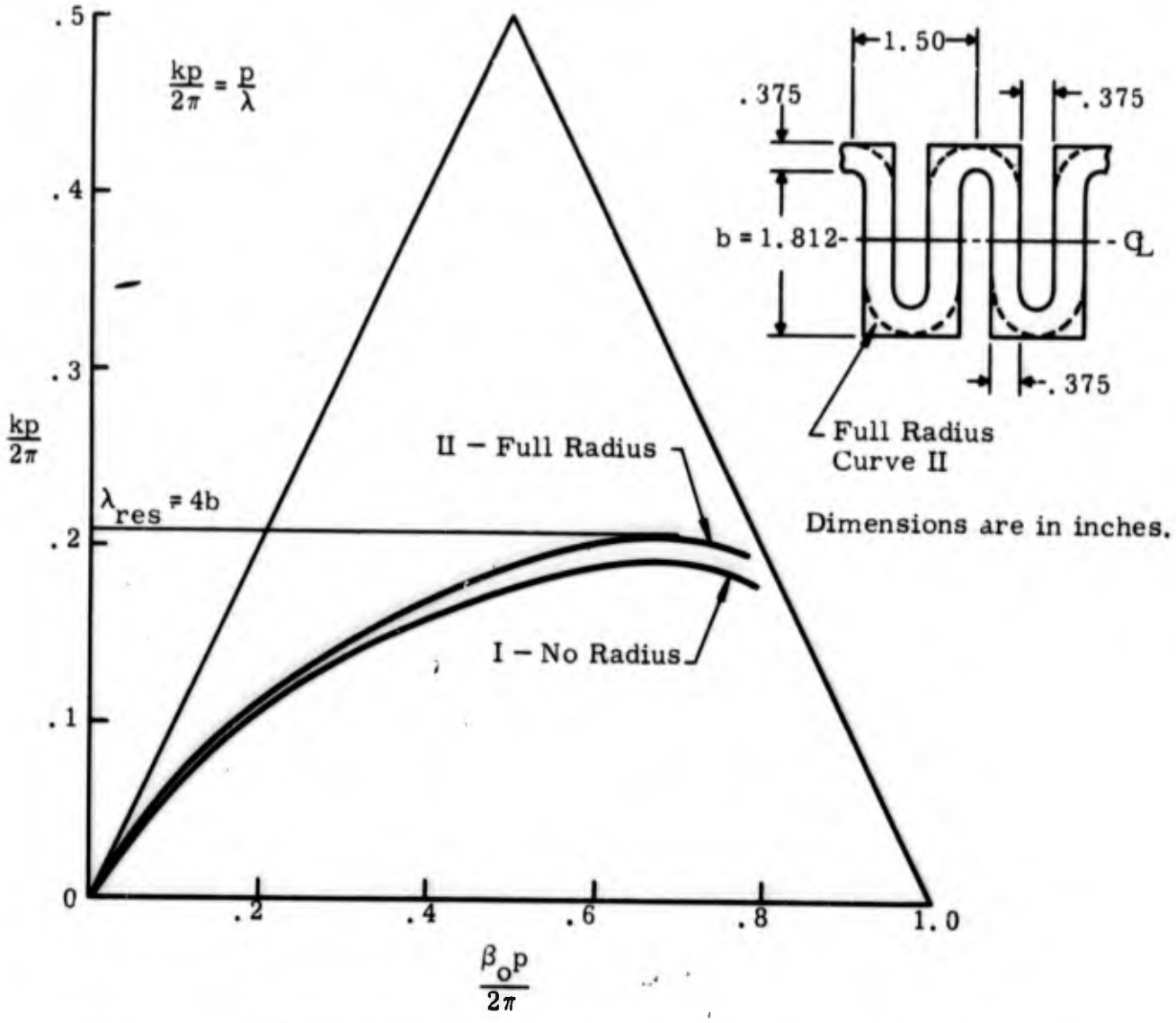

Figure 7-1. Normalized k-β curves of interdigital open slot ladder with and without full outer radius.

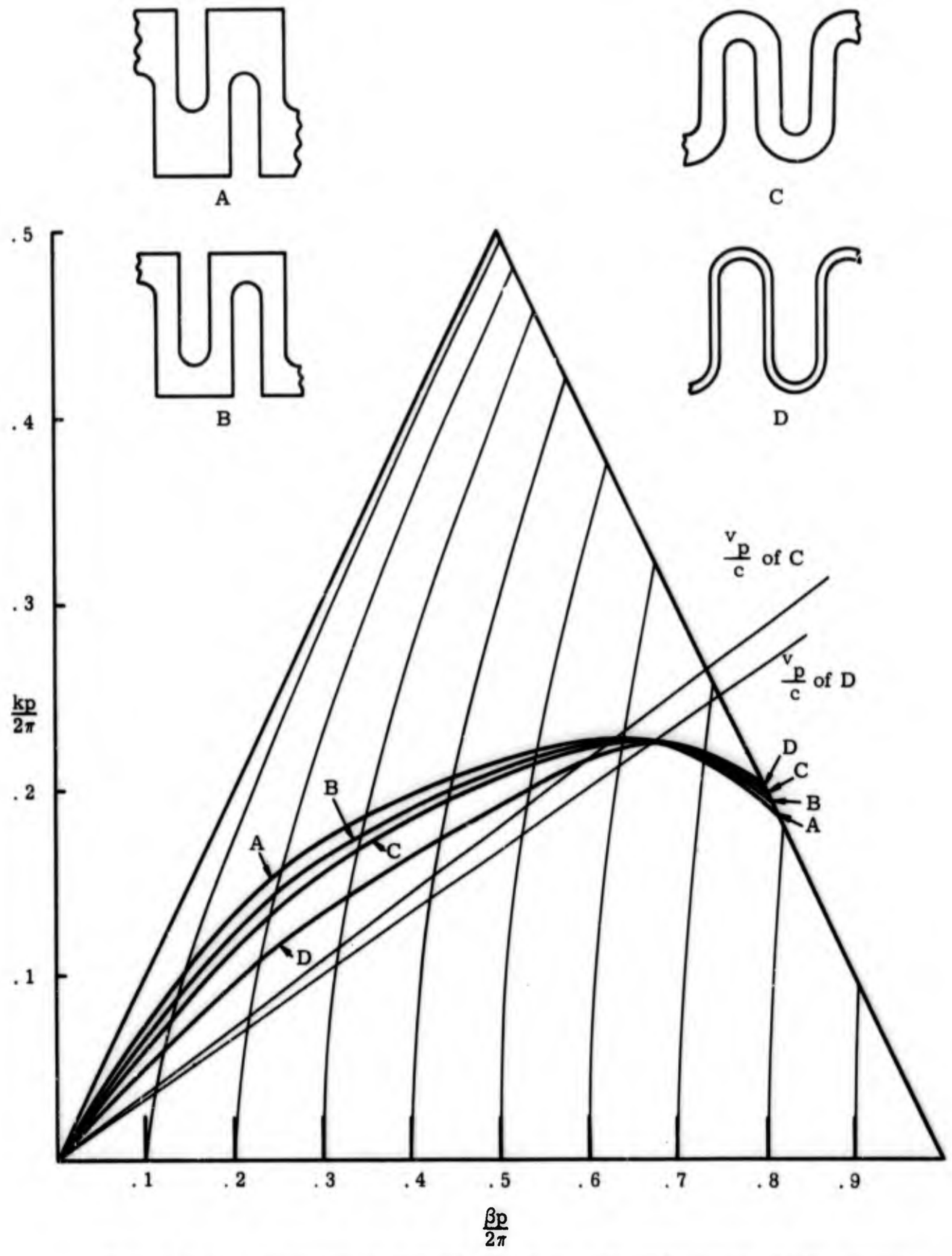

Figure 7-2. Evolution of sinuous line from open interdigital ladder circuit.

figure 7-3 is appropriate for a class 1 (cf, section VI. B) transition to a sinuous or zigzag line. The inner conductor can be abruptly joined to a closed sinuous line and matched over a narrow frequency range, or the transition can be made gradually as shown. The dimensions of the outer conductor should be such as to ensure that only TEM modes can propagate on either side of the junction. The use of this configuration will require a transition to standard coaxial line or waveguide. In the case of a system employing coaxial line, use of a sinuous line as a filter circuit therefore complicates the overall transition problem, compared to a helix filter circuit.

A class 2 transition between a sinuous line and a coaxial transmission line should be no more difficult than a class 2 transition to a helix. Figure 7-4 shows a possible configuration.

Since the sinuous line is so similar to the wire helix in electrical characteristics, the choice between these two filter circuits for a given application would probably be determined by consideration of power handling capacity, the type of system transmission line, and mechanical simplicity. Since the advantages in these considerations appeared to lie with the helix filter, it was decided not to design filters employing sinuous lines (or zigzag lines, or interdigital open slot lines). The knowledge obtained from designing transitions to helices should be generally applicable to the analogous circuits.

C. YAGI FILTER

Rather late in the program a transition design by Ehrenspeck and Poehler (ref 15) was found that appeared to be promising for filter application. The slow wave structure was a periodic array of short posts perpendicular to a ground plane. The filter configuration is shown in figure 7-5. Its advantage to filter applications is that the apertures are in the ground plane; therefore, little or no bending should be required to prevent stopband energy from radiating in appreciable amounts from the input to the output. According to Ehrenspeck and Poehler, a flare horn is not required for high launching efficiency. It can be seen, therefore, that the launching mechanism

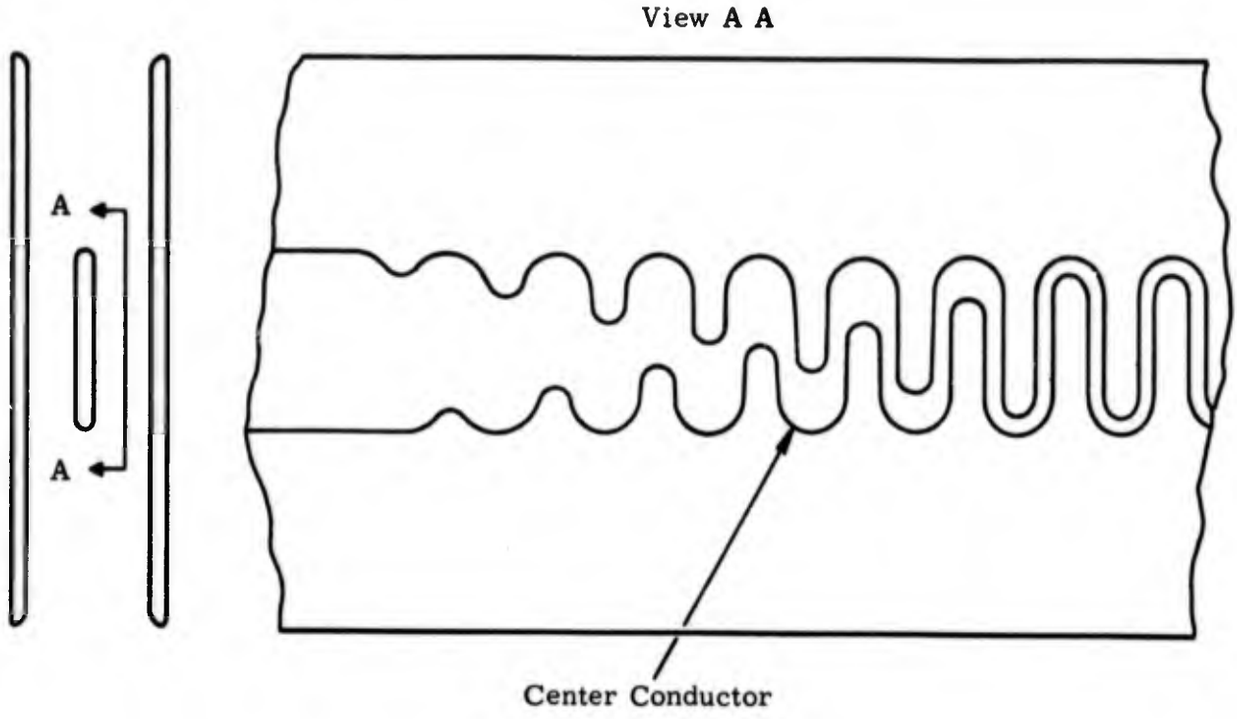

Figure 7-3. Class 1 transition from TEM line to closed sinuous line.

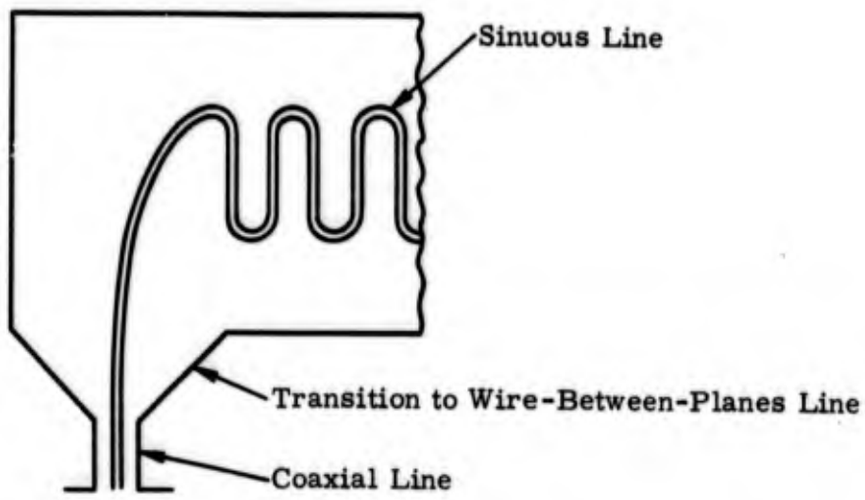

Figure 7-4. Class 2 transition between coaxial line and closed sinuous line.

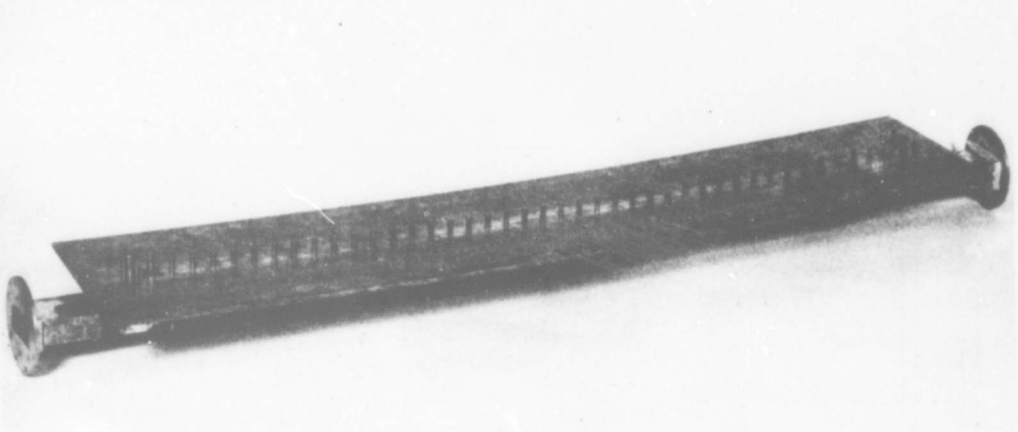

Figure 7-5. Photograph of Yagi filter.

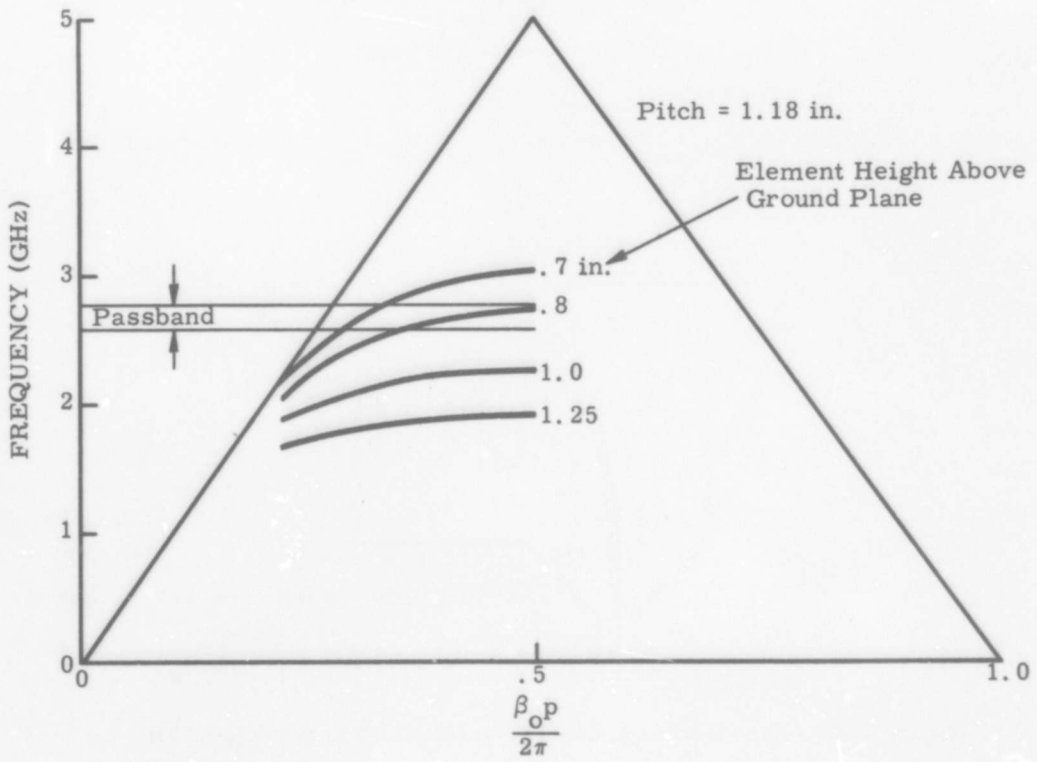

Figure 7-6. ω-β characteristic of Yagi structure.

involves the radiation of passband energy. The directionality of the radiation is provided by the array of stubs behind the launching antenna. The transition, therefore, is different from all of the others studied on this program in that it represents the special case of figure 3-2 (general transition block diagram) where the closed periodic structure is of zero length.

The filter pitch was chosen for attenuation of the FPS-6 radar second harmonic. An ω-β diagram for this structure is shown in figure 7-6. The characteristic is similar to that of a ladder and indicates that adequate bandwidth can be achieved with a post height of about 0.75 in.

Initial filter insertion loss measurements are shown in figure 7-7. The solid line curve is taken with the filter in the same configuration as shown in figure 5-1. Notice that the launching efficiency in the passband is very poor, resulting in an insertion loss of 5 db. The VSWR was below 1.2 over most of the passband. The stopband, however, rises sharply to 50 db and stays above this level even where clutter is normally found in the region of the apex on the ω-β diagram.

Horns plus an enclosure were added to the feed structure on both ends of the filter (as shown in figure 7-8) with insertion loss characteristics obtained as shown by the dotted line in figure 7-7. Note that the launching efficiency is improved to reduce the total filter passband insertion loss to just under 2 db. Insertion loss in the stopband, however, is greatly reduced down to a level of 30 db at various frequencies. This confirms the theory that horns tend to direct and catch harmonic energy, thereby reducing stopband insertion loss.

This experiment also tends to confirm the belief that a transition employing radiation in the passband suffers too much loss for high power radar applications. A gradual transition from a closed periodic circuit to an open periodic circuit appears to be necessary.

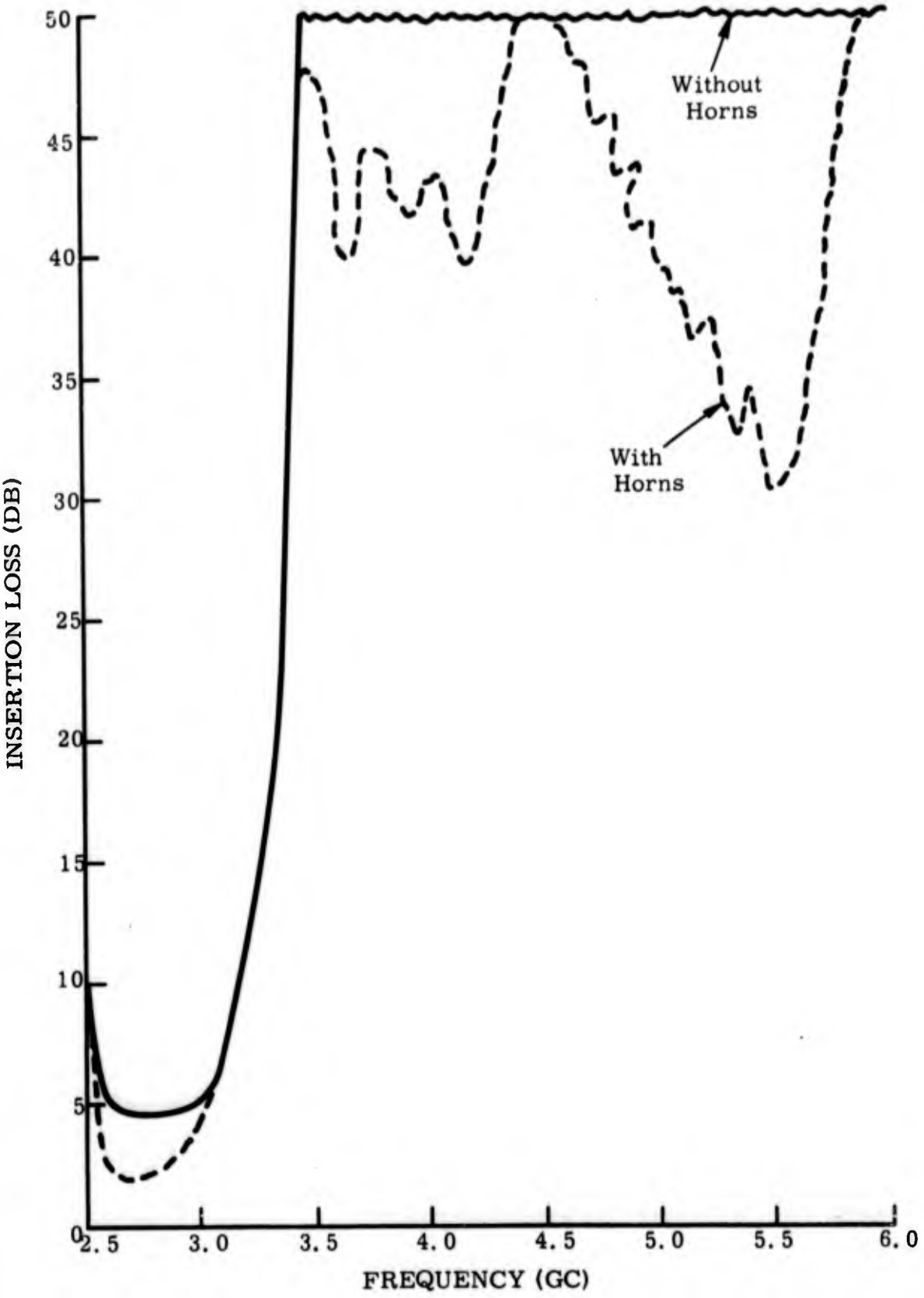

Figure 7-7. Yagi filter characteristics.

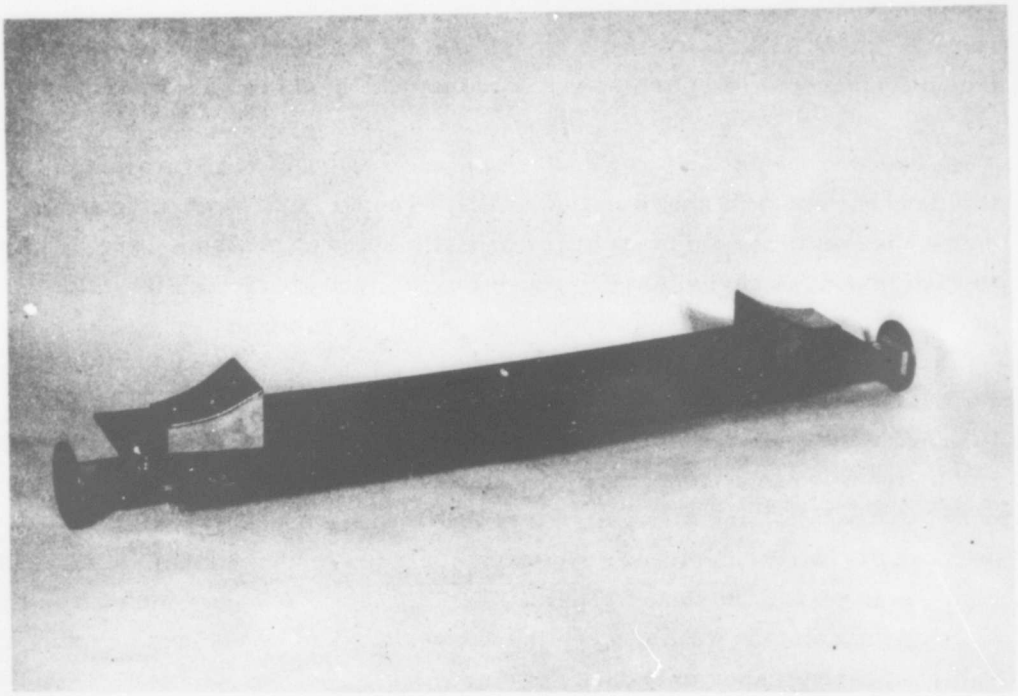

Figure 7-8. Periodic Yagi filter with horns.

D. THIN LADDER FILTER

The thin ladder circuit was one of the first slow wave structures proposed for filter applications by White and Birdsall (ref 1). The k-β characteristics had been investigated under the previous program (ref 2) and filter configurations built. These filters suffered from transition design problems. Because of the simplicity of the circuit and the existence of an interesting transition scheme, an attempt was made to design and build a filter.

The proposed transition was based on the electric field configuration of thin ladder, which is shown in figure 7-9. The electric field components perpendicular to the surfaces of the opposite sides of the ladder are opposed to each other. A device (or component) capable of producing this field orientation will be required to feed this ladder structure.

An E-plane folded hybrid T such as that shown in figure 7-10 can be used to provide the required electric field orientation. With the E arm terminated and a signal fed into the H arm, the energy will divide equally and come out of the parallel arms 180 deg out of phase with each other. If the wall between the two waveguides is slotted to form the ladder circuit, a successful high power transition should result. The impedance problem introduced by slotting the common wall between the waveguides can be avoided by using a sufficiently long taper to reduce the discontinuity.

A second method of providing the required field orientation is by transitioning to the TEM mode geometry shown in figure 7-11. This can be done by means of a mode transducer functionally similar to a waveguide to coaxial line junction. The center conductor can now be slotted symmetrically about its center line, starting with a tapered slot pattern for impedance matching. However, since the folded hybrid approach appears to have higher power capacity, and is more suited to a waveguide system, this approach was followed.

The first step in designing the filter was to determine the appropriate ladder dimensions. The conclusions of section IV regarding the design of ladder filters for harmonic attenuation were applied. Thin ladder k-β data

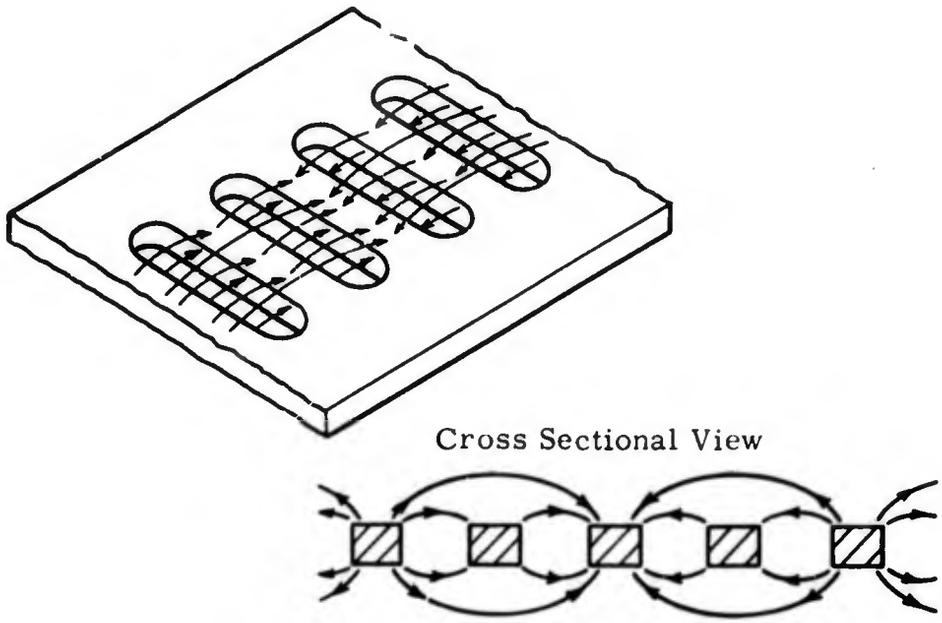

Figure 7-9. Electric fields about a thin ladder.

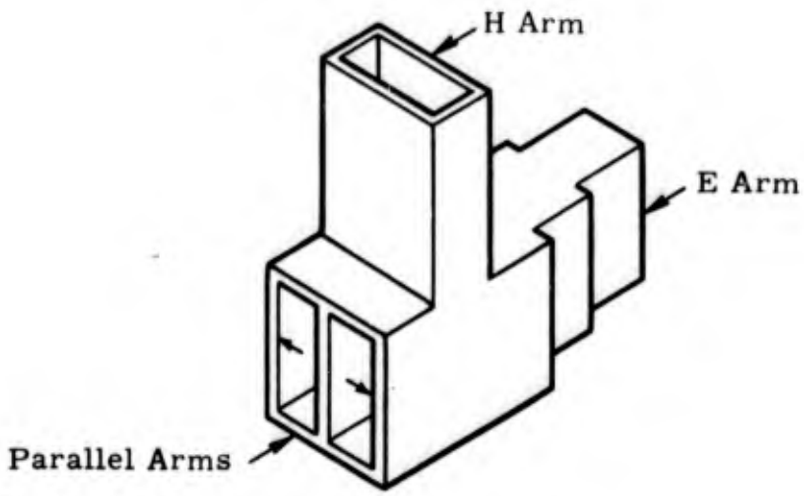

Figure 7-10. E plane folded hybrid T.

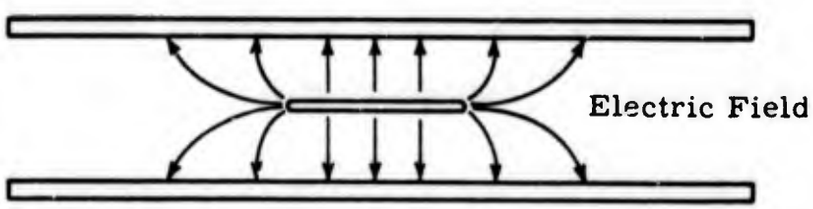

Figure 7-11. TEM mode suitable for making a transition to a thin ladder.

from the previous program were plotted to determine how closely the desired characteristic of figure 4-7 for a second harmonic filter could be approached, and also to determine the effect of circuit dimensions. These data are shown in figure 7-12. It appears that the ratio b/p should be about 0.8. Increasing w/p tends to raise the frequency at which $v_g = 0$ for slots with a given b/p. Therefore w/p should be maximized in order to achieve the maximum values of v_g over the operating band. Of course, w/p is limited by practical considerations of mechanical strength and power handling capability. The webs between the slots should probably be made no narrower than the thickness of the ladder.

The operating range of 5.4 to 5.9 GHz was chosen because of the availability of folded hybrid tees in this range. These hybrids were in WR-137 waveguide size. The pitch of the circuit should be so spaced that the location of the apex frequency of the ω-β diagram is slightly below the second harmonic of the lowest frequency in the passband. This would be a frequency of less than 10.8 GHz (2 x 5.4). Since we have had filter rejection problems on previous filters in the area of the apex of the ω-β diagram, it was decided to go low enough in frequency to provide better performance. For convenience the pitch was made 0.6 in. resulting in an apex frequency of 9.84 GHz. Figure 7-12 indicates that the slot length (2b) would be about 0.96 in. However, figure 7-12 does not take into account the effect of the enclosing waveguide which would be used in the transition. This is best shown by the ω-β curves of figure 7-13 which represent a ladder circuit on which side plates have been introduced. Note that as the side plates are moved in toward the slots, the cutoff along the $\beta p/2\pi = 0$ line rises in frequency. This continues until the plates are separated from one another by the length of the slot. The resulting ω-β curve is a straight horizontal line of no bandwidth. This means as wide a feeding waveguide as practical must be used to feed the circuit in order to obtain maximum bandwidth.

From figure 7-13 it can be seen that the upper limit of the k-β curve is located at approximately $kb/2\pi = 0.23$. By solving this equation for a frequency just above the upper limit of the passband or 6000 MHz, we find that the minimum length of the slot (2b) is 0.906 in.

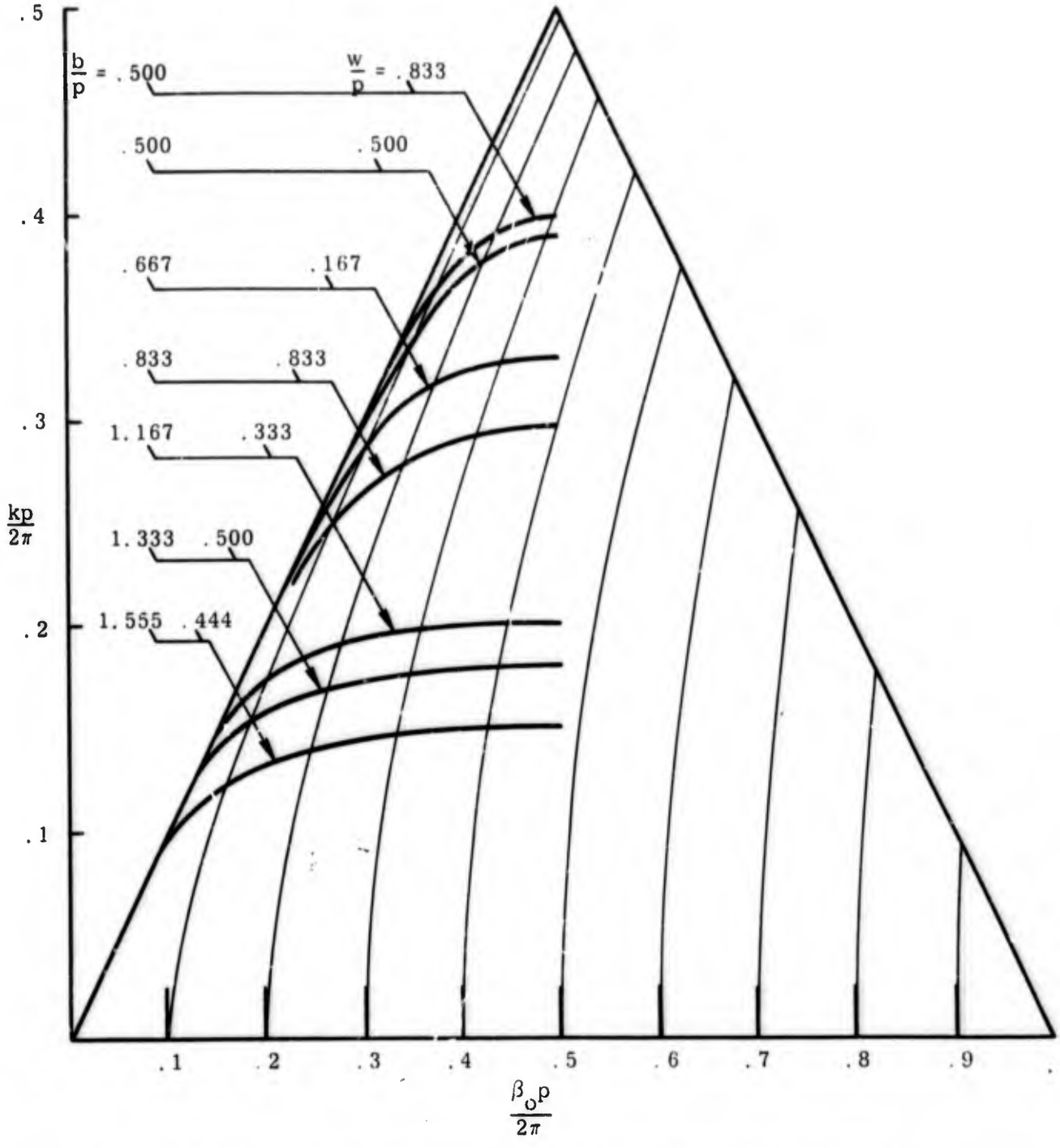

Figure 7-12. Normalized κ-β curves for thin ladder circuits.

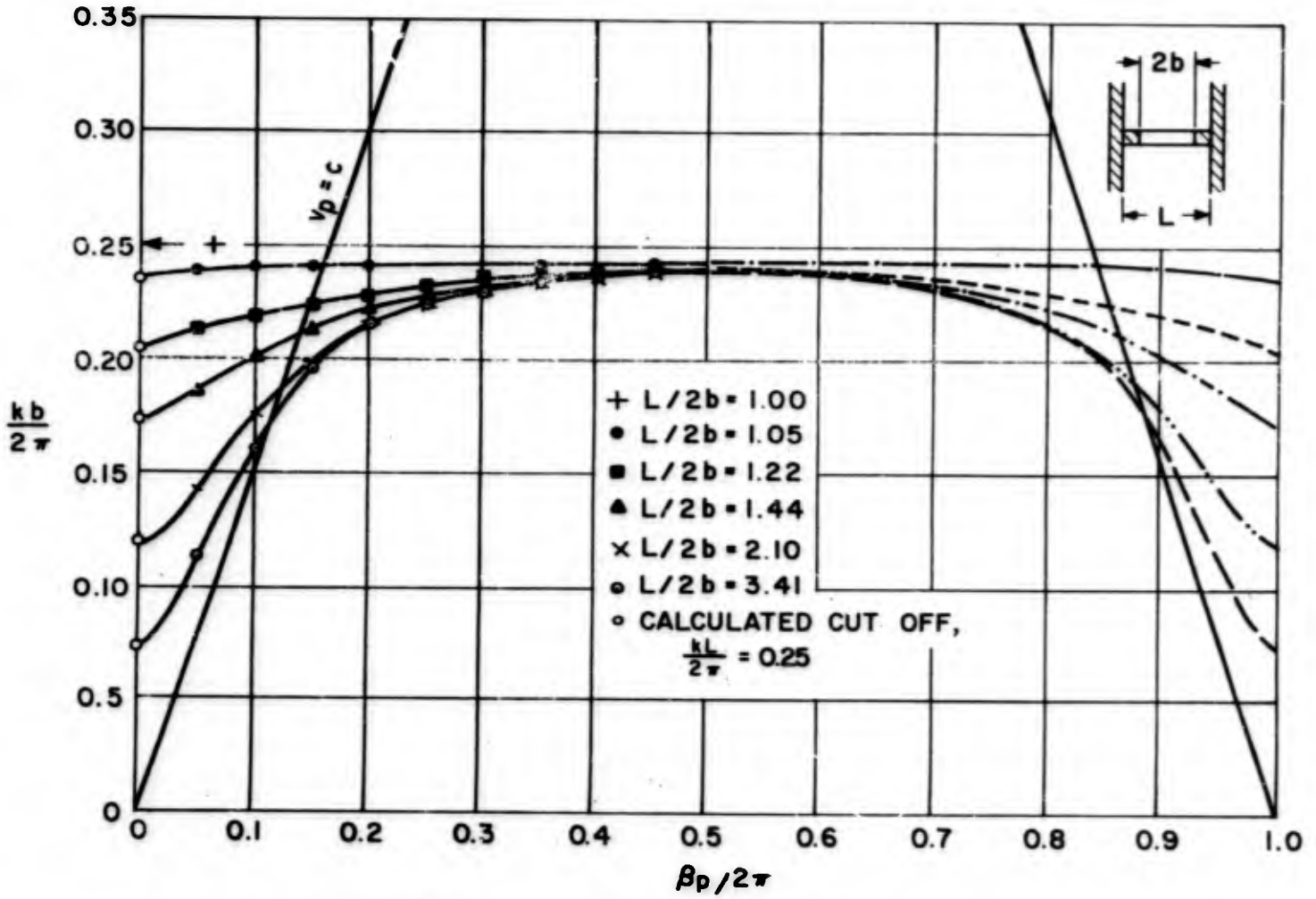

Figure 7-13. Propagation characteristics of a thin ladder with vertical side plates.

The width of the slot should then be made as large as possible to obtain best bandwidth and power capabilities. A value of 0.5 in. was chosen, being just under the 0.6 in. pitch spacing.

Since round corners were to be used on the ladder slots and the calculations are for a rectangular slot, a correction had to be made. The new length utilizing full radius slots can be determined by Cohn's relation (ref 16).

$$b = \frac{\lambda_c + 0.429\ w}{4} \qquad (7.2)$$

The slot length of 0.906 in. when corrected for radius results in a slot 1.00 in. long. This completes the design of the ladder circuit which will have full radiused slots 1.00 in. long, 0.5 in. wide, with a 0.6 in. pitch. The slot length of 1.00 in. corresponds very closely to the value estimated from figure 7-8 which was based on experimental data taken on ladders with fully radiused ends.

The f-β characteristic of the open ladder is shown in figure 7-14. The results show the location of the curve to be 100 MHz below the theoretical design. This is an error of about 1.6 percent which is primarily due to the difference in the physical characteristics between our ladder and those from which the design curves were plotted. Time did not permit the fabrication of a new ladder having a higher resonant frequency whose f-β characteristic would approach the optimum more closely.

In order to ensure maximum bandwidth in the transition, WR-187 waveguide was used to enclose the thin ladder. This waveguide has a dominant mode cutoff of 3.155 GHz. The first higher mode is cut off up to about 6.31 GHz which is above the upper frequency limit of the passband. The use of this waveguide required a transition from the WR-137 waveguide of the folded hybrid tee. This is shown in figure 7-15.

A ladder taper approximately 6 in. long is used in the common waveguide wall in order to provide an impedance match to the ladder circuit. A flare horn was used to effect a transition from the closed to the open periodic circuit. The height and width of this horn is determined by the minimum

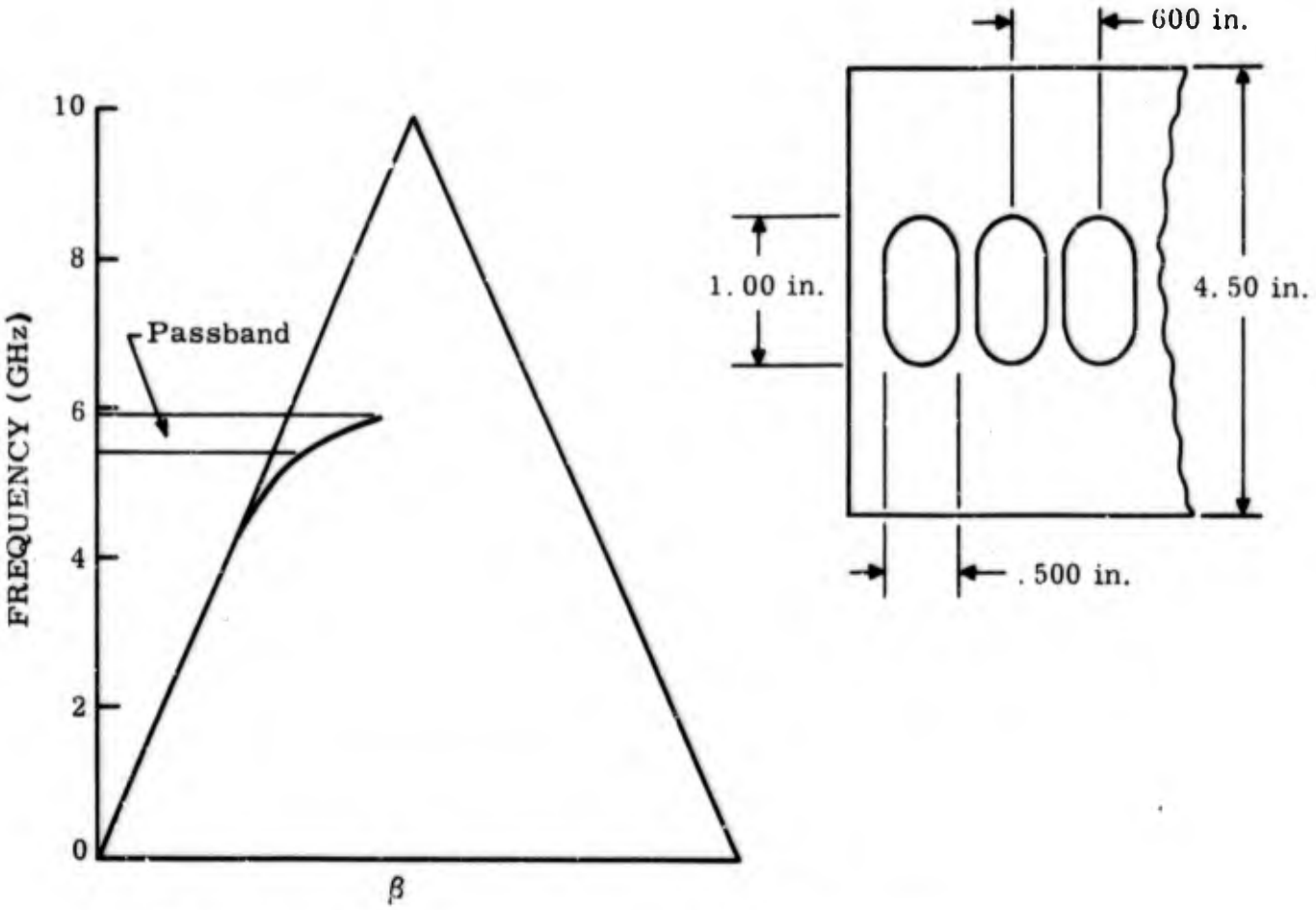

Figure 7-14. f -β characteristic of thin ladder filter.

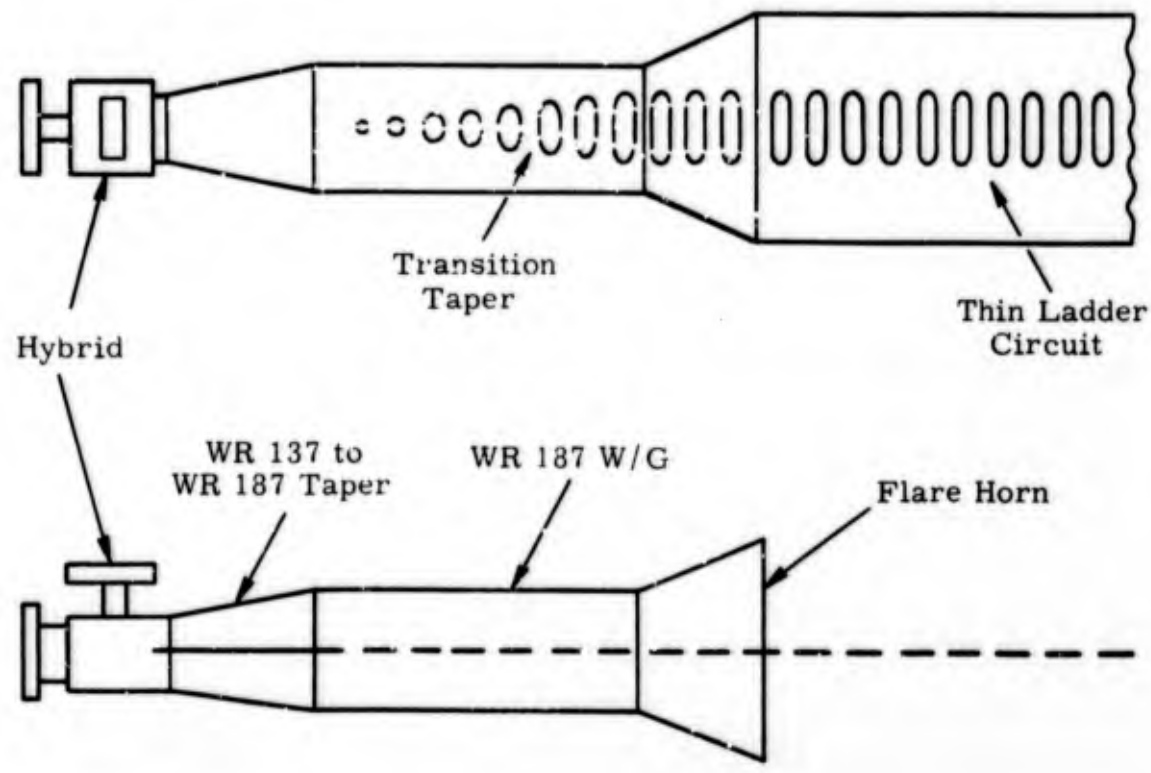

Figure 7-15. Transition from rectangular waveguide to thin ladder circuit using folded hybrid Γ.

γ of the circuit which is estimated to be 0.8 nepers/in. The width, therefore, can be calculated to be

$$w = \frac{3.62}{\gamma} = 4.5 \text{ in.} \qquad (7.3)$$

and the height of the horn is found to be 2 in. These calculations were based on design relationships presented in section VII of reference 2.

A filter was fabricated in accordance with the above design and is shown in figure 7-16.

The passband loss varied between 1.5 and 2.0 db from 5.0 to 5.5 GHz while the VSWR went as high as 1.7 periodically in the passband.

The stopband characteristics of this filter were measured up to a frequency of 15 GHz. The data are shown in figure 7-17 for a straight filter circuit. Note that once again a "hole" in the characteristic due to spurious clutter is indicated. This "hole" is again located just below the second harmonic where the apex of the ω-β diagram of the circuit is located. The narrow zones of low attenuation at higher frequencies are believed to be due to radiation from the horns or from the circuit. No absorbers were used in the test and, consequently, energy could have been reflected from the surroundings.

Several attempts were made to eliminate the "hole" in the stopband response. First a bend of 70 deg was made in the structure with almost no change noticed. In order to isolate the source of the energy from the receiver horns, the horns on the outside of the bend were completely covered, and a metal shield was placed 2 in. away from the circuit on the inside of the bend, as in figure 7-18(a). Little or no effect was noted, and it was concluded that the energy was bouncing or propagating along the inside surface very close to the metal ground plane.

A 90 deg twist was then made in the circuit and the hole still extended down to 35 db. As a final test, the circuit was bent into an S shape as shown

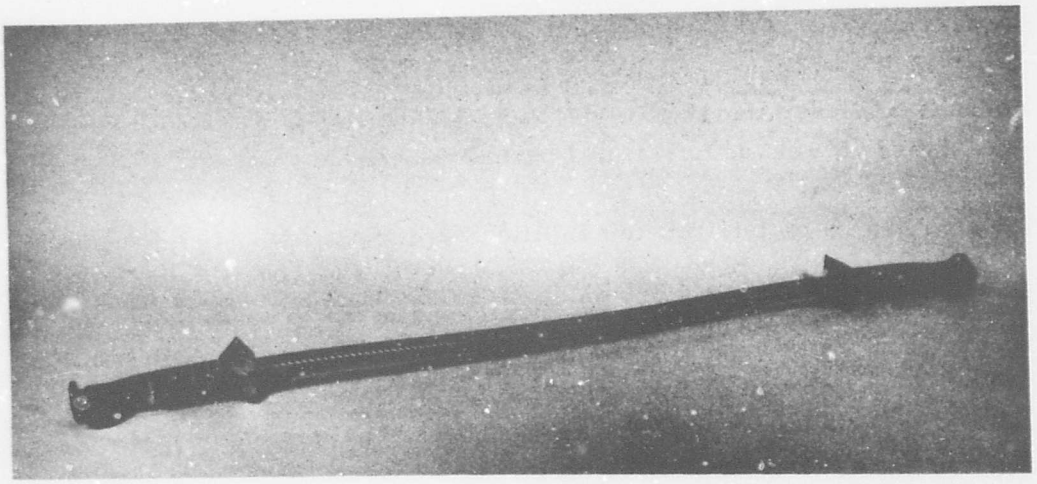

Figure 7-16. Thin ladder filter with transitions of figure 7-15.

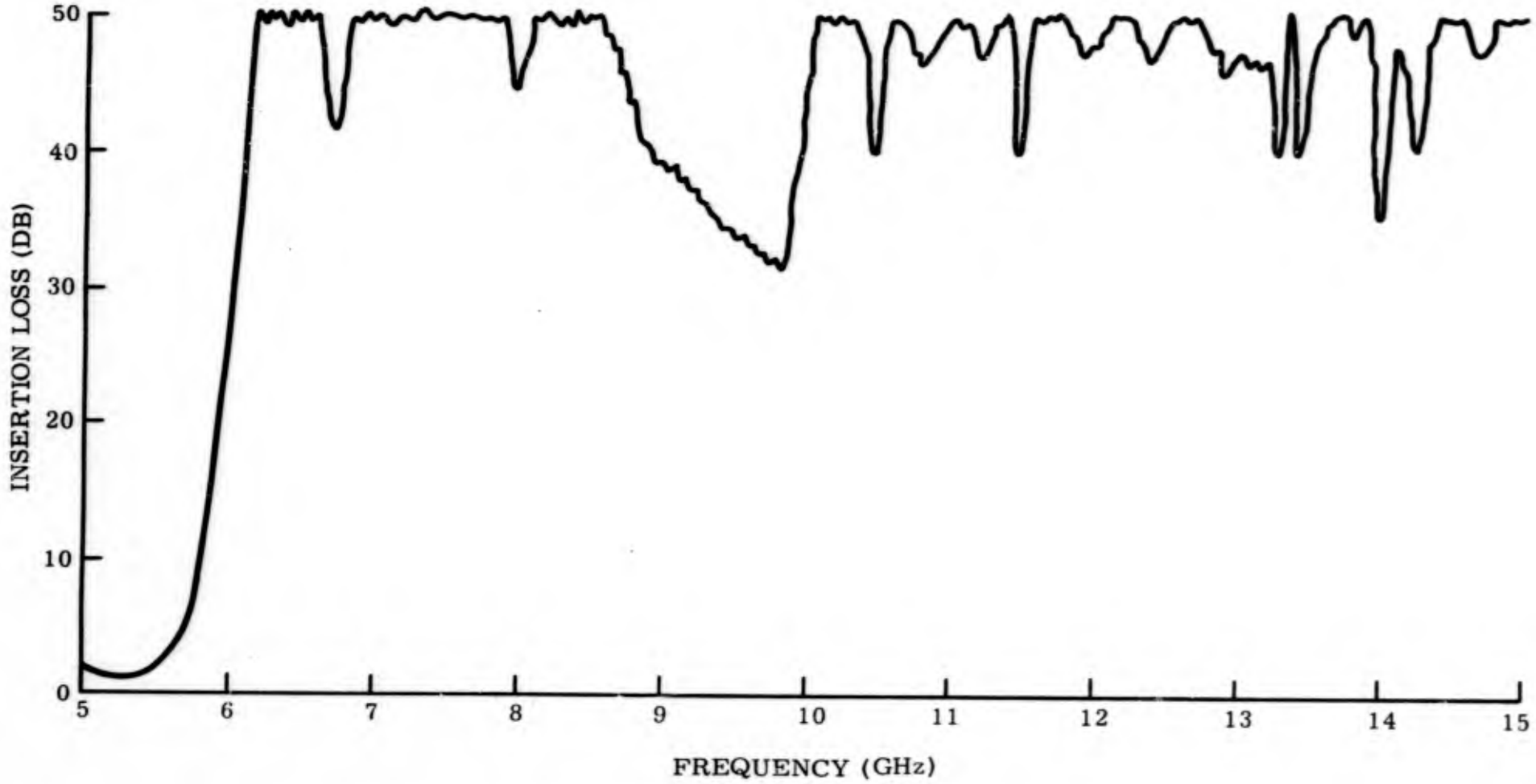

Figure 7-17. Insertion loss of thin ladder filter.

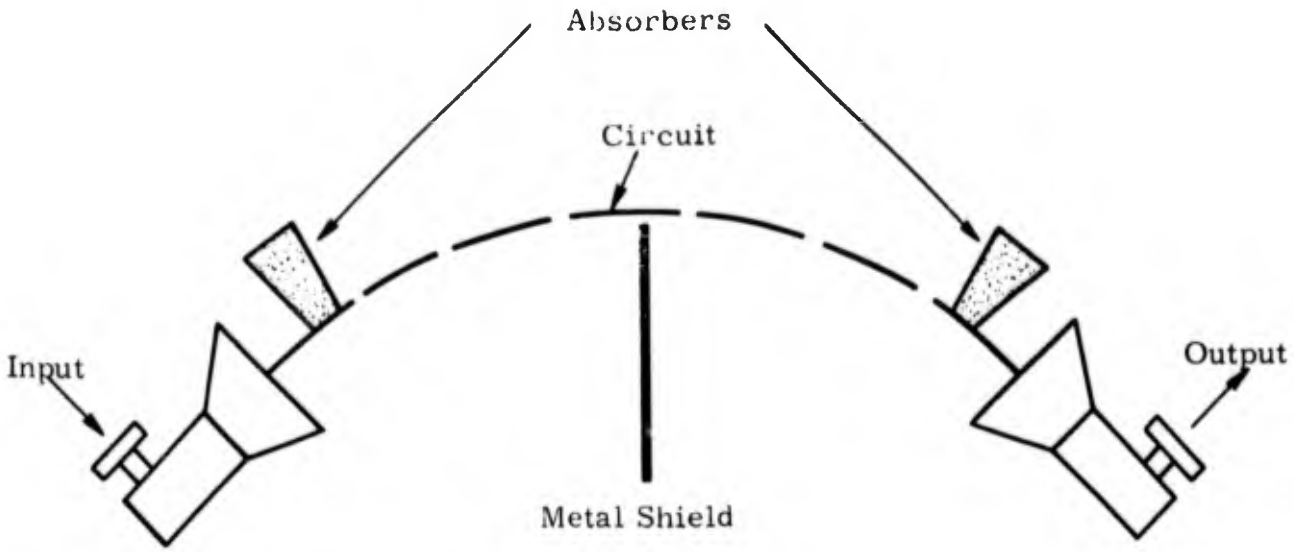

(a) 70^{o} bend.

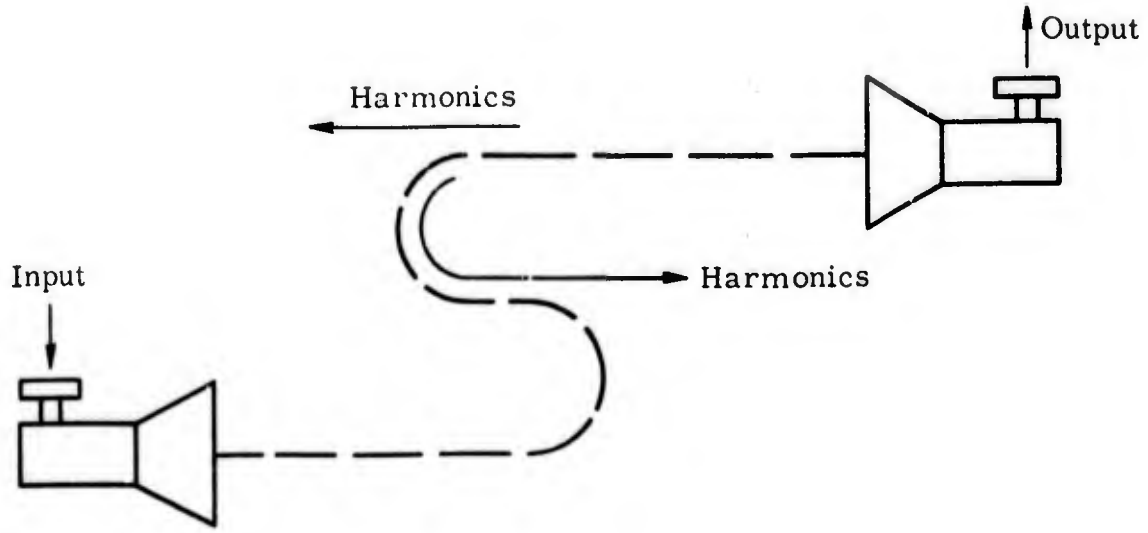

(b) "S" bend.

Figure 7-18. Modifications to thin ladder filter for elimination of stopband "hole."

in figure 7-18(b). This isolated both sides of the circuit, and the stopband rejection including the hole was increased to greater than 45 db.

The difficulty in suppressing the hole indicates that it is due to end fire radiation of a leaky wave structure, i.e., the energy propagates on the structure with a complex phase propagation constant and a forward direction of radiation. However, since the hole is below the second harmonic, it is of little importance in a harmonic filter.

The stopband measurements on the thin ladder filter indicate that the property of "two-sidedness" is a disadvantage in filter applications because it makes it difficult to isolate the receiving and transmitting apertures. This difficulty would probably have been more severe if absorbers had been used because of the increased level of reflected energy.

The filter model served to illustrate the feasibility of the folded hybrid junction transition. The narrow bandwidth with respect to passband losses is probably due to two basic causes. First, the high loss above 5.5 GHz is probably the result of not optimizing the ladder k-β characteristic. Its cutoff frequency was lower than expected, as was mentioned before. A new ladder with smaller slots would probably have yielded better results. Second, the transition could be improved in the light of experience obtained on the thick ladder filter. The flare horn began with a sharp discontinuity. Because of the low γ of ladder circuits, particularly at low frequencies, such discontinuities can cause loss by scattering. A gradual transition was found to be necessary for the thick ladder filter which has comparable values of $\gamma\ \lambda$. A reduction in height of the waveguide enclosing the thin ladder may also improve the VSWR.

Because of the stopband shortcomings of the thin ladder filter, no improvements were made to the transition once its feasibility had been established. Instead, the effort on ladder filters was restricted to the thick ladder filter which appeared to have higher power handling capability and potentially better isolation between the apertures.

E. THICK LADDER FILTER AND TRANSITION

1. GENERAL. The thick ladder filter was the subject of much study under the previous program because, of all the slow wave circuits, it seemed to have the highest power handling capacity. Its main shortcoming was high loss even in a very narrow passband range. This loss was due to the open filter circuit and to launching loss in the transition. The required bending for adequate second harmonic attenuation caused additional loss. The loss mechanisms were complementary, as was shown in figure 4-5. The launching efficiency of the basically simple transition design was closely related to γ, and appeared to have been optimized. The thick ladder filter, therefore, seemed to have inherently high loss and narrow bandwidth unless a different transition design could provide higher efficiency at the low frequencies where γ was low. In this connection it had been speculated that the existing simple transition design was deficient because it permitted energy to remain in a fast mode in the closed thick ladder region rather than coupling to the desired slow mode, and that some form of phase velocity matching was required to provide this coupling. However, this concept ran counter to experience obtained in designing reactive filters, in which a well matched junction is achieved between a fast transmission line and a closed filter structure having a much lower phase velocity without any consideration of phase velocity.

The general transition studies reported in section III indicated that the problem of coupling to an undesired slow mode could be avoided by ensuring that propagation occurred in a unique mode wherever possible. Adequate launching efficiency requires that the aperture be made large enough so that the fields across it sufficiently resemble the fields on the open periodic structure, and that the transition from the closed region to the open region, which necessarily involves the consideration of multimode propagation, be made sufficiently gradual as to avoid conversion to fast modes. The general filter studies (section IV) indicated that the design of ladder filters could be improved to provide higher harmonic attenuation without excessive bending and consequent passband loss by making the pitch or period larger than a half wavelength at the lowest harmonic frequency, and that the dimensions of the elements could then be adjusted to yield an optimum k-β characteristic.

The design program of the thick ladder filter follows these general concepts.

2. DESIGN STUDIES. There are four main dimensions in the uniform thick ladder shown in figure 7-19. The pitch, p, is determined by the desired stopband frequency. The slot length, 2b, determines the lower cutoff frequency of the structure, i.e., the lowest frequency at which the slot becomes inductive. The slot depth, ℓ, determines the upper cutoff frequency, i.e., the frequency at which the slot is resonant. This occurs when ℓ is approximately one quarter guide wavelength. The slot width, w, does not explicitly determine the cutoff characteristics of the ladder, but it must obviously have some effect on the shape of the k-β characteristic because if w were nearly zero, there would be very little stored energy per pitch. Therefore, from the concept of surface impedance, w should be made large so as to make the surface as inductive as possible for a given choice of b and ℓ. The width of the ground plane has little effect on the filter characteristic if it is greater than 3b.

The first step in the design of a filter is the choice of pitch, which must be at least a half wavelength at the lowest frequency to be attenuated. For a harmonic filter, the pitch will then be between a quarter wavelength and a half wavelength at the lowest frequency of the passband. This provides considerable latitude. However, the pitch cannot be exactly a half wavelength at the lowest passband frequency because the bandwidth would be zero. The upper frequency limit of the passband must also be considered. It was shown on the previous program that the k-β characteristic of an array of elements is flattened as the pitch becomes coarser, and that zero group velocity occurs below the apex of the allowed region triangle, even though the elements may be resonant at a high frequency (ref 2, pp 4-3 to 4-6). It seemed that the greatest bandwidth for a given element would be achieved if the pitch were made as fine as possible, i.e., for a harmonic filter, if the pitch were made a little more than a quarter wavelength at the lowest passband frequency. The reason for making the pitch slightly longer than the minimum length is to ensure attenuation of the lower portion of the second harmonic band.

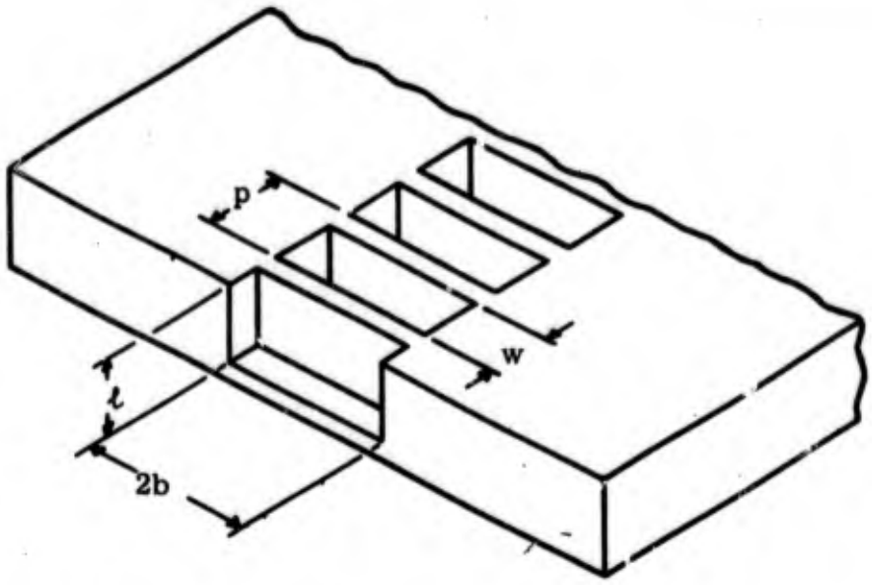

Figure 7-19. Uniform thick ladder.

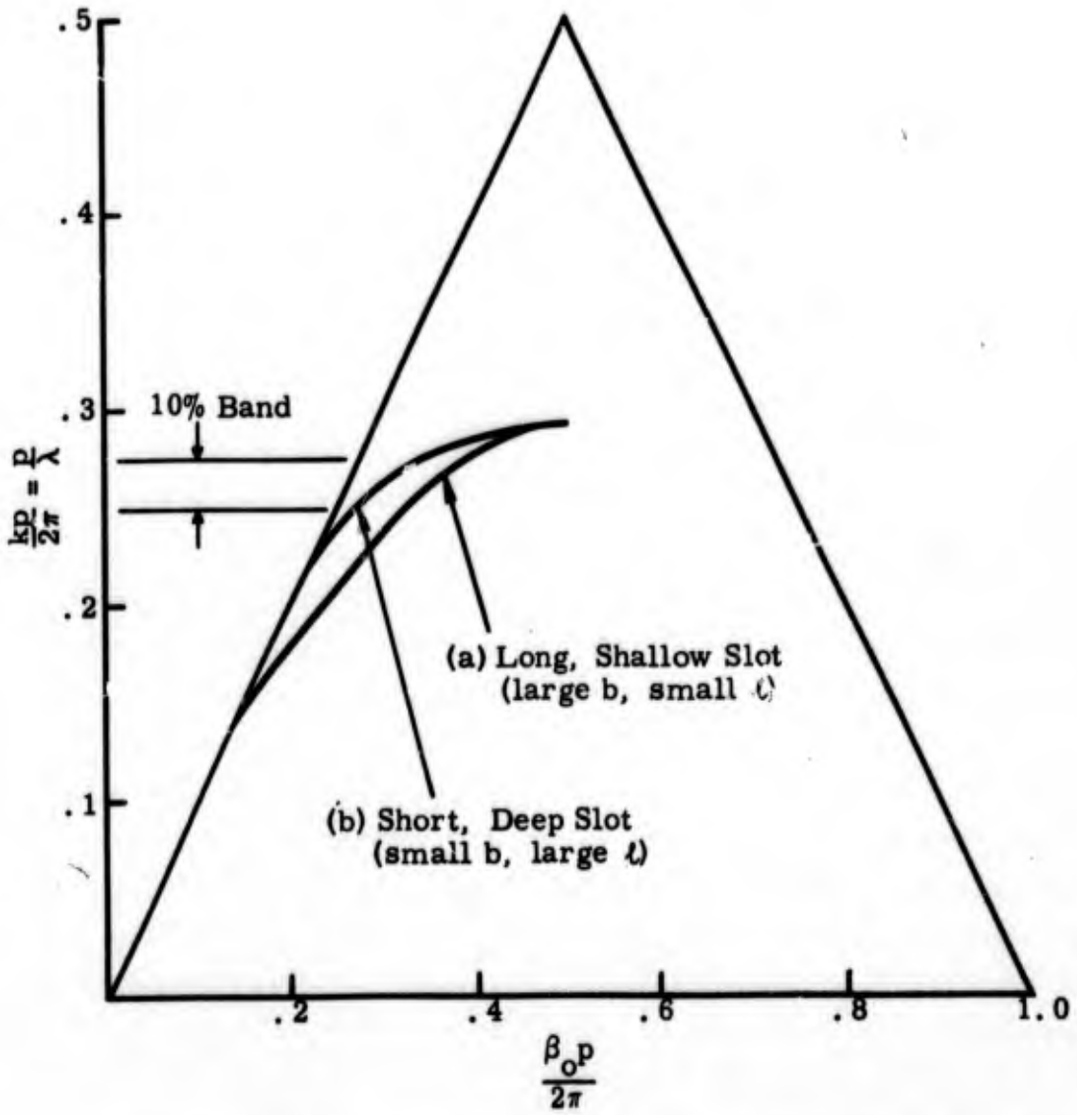

Figure 7-20. Normalized k-β diagram of thick ladder showing effect of b and ℓ.

Since the desired k-β characteristic should provide high values of γ and v_g over the passband, the effects of the dimensions b and ℓ on these characteristics were investigated. Figure 7-20 shows the general trends of the pitch normalized k-β characteristics for different slot configurations. A 10 percent operating band starting at $kp/2\pi = 0.25$ is assumed. Curve (a), for a long shallow slot, is relatively linear and has greater group velocity and γ than curve (b) for a short deep slot having the same frequency of zero group velocity. The greater slot depth for curve (b) is a consequence of the greater guide wavelength. Curve (a) is apparently superior, indicating that dimension b should be as large as possible. However, it was felt that the slot length should be restricted sufficiently to prevent the existence in the slot of the TE_{20} mode in the passband. For the 10 percent bandwidth of figure 7-20, the maximum value of b is therefore determined by

$$\frac{kp}{2\pi} = 0.275 = \frac{p}{\lambda_{c_{20}}} = \frac{p}{2b} \tag{7.4}$$

This in turn fixes the lower cutoff frequency of the ladder at $kp/2\pi = 0.1375$. Figure 7-21 shows the hypothetical pitch normalized k-β chracteristics of two ladders whose pitch and slot length were designed in accordance with the above discussion. Curve (a), for the shallow slot (small ℓ), is more linear and should suffer less intrinsic loss because of its higher group velocity. Curve (b), for the deeper slot, has higher values of γ in the passband and should, therefore, suffer less transition and bending loss for a given filter configuration. It was mentioned that the slot width w is relatively uncritical, but that it should be made as large as possible for maximum inductive reactance and hence maximum γ. Curve (c) in figure 7-21 shows the probable effect of using a small value of w in the deep slots. The cutoff frequencies will be the same, but γ will be lower and the curvature more pronounced.

Since the optimum slot depth cannot be determined by examination of the k-β characteristic, testing in a filter configuration is required. Accordingly, filter designs for the FPS-6 application were begun.

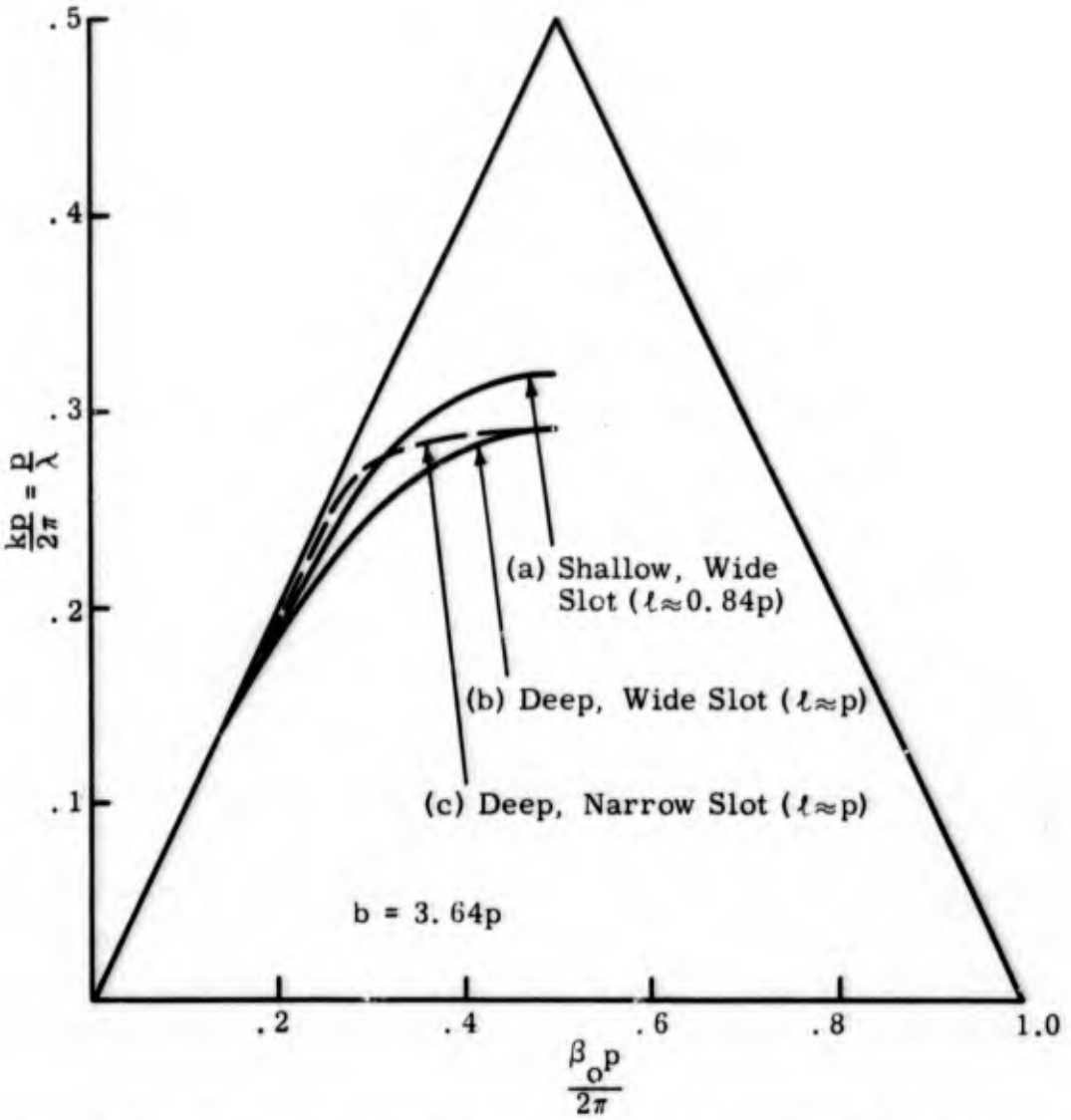

Figure 7-21. Normalized k-β diagram showing effect of ℓ and w for fixed b.

The operating range of the FPS-6 radar is from 2700 MHz to 2900 MHz. The lowest second harmonic frequency is, therefore, 5400 MHz. The pitch was set at 1.100 in., corresponding to a half wavelength at 5370 MHz, although it was not known whether this choice would provide high attenuation at 5400 MHz. The pitch normalized passband range is, therefore, $0.2515 \leq kp/2\pi \leq 0.2702$. The slot length 2b was made 3.700 in. because of available materials. This corresponds to a lower cutoff frequency of about 1595 MHz and places the TE_{20} cutoff at approximately 3190 MHz. A test ladder with a slot depth of 0.785 in. was constructed. Its pitch normalized k-β characteristic is shown in figure 7-22 as curve (a). $\gamma\lambda$ is about 70 percent higher than for the FTLI-6, primarily because of the relatively larger slot width, although the group velocity at the high end of the passband is about the same.

The first test transitions were planned to follow the design of those of FTLI-6 in that the slot depth was tapered for a good impedance match. The horn was designed to begin tangent to the inside surface of the enclosing waveguide as is shown in figure 7-23. Before constructing the filter, VSWR measurements were made of the tapered depth ladder enclosed in waveguide as shown in figure 7-24. The VSWR increased rapidly at 2800 MHz, which was at first thought to be an indication of rapidly changing impedance in the enclosed thick ladder. This change in impedance, which was apparently greater than the linearly tapered ladder could match, was presumed to be the result of the decreasing group velocity. This suggested the fabrication of a new ladder with shallower slots, which was started immediately, or reducing the impedance by decreasing the spacing between the enclosing waveguide and the ladder.

Another possible cause of the high VSWR is mode conversion. This possibility was indicated when a section of the ladder was covered with a full height waveguide and resonated in order to determine the phase characteristic. Spurious resonances appeared at and above 2750 MHz. These resonances are probably due to higher order modes in the composite waveguide (slot depth and full height waveguide taken together, ignoring the webs between the slots). The TE_{01}, TE_{11}, and TM_{11} modes can all exist within the passband range. Conversion of the incident energy in the VSWR test to any of these modes with

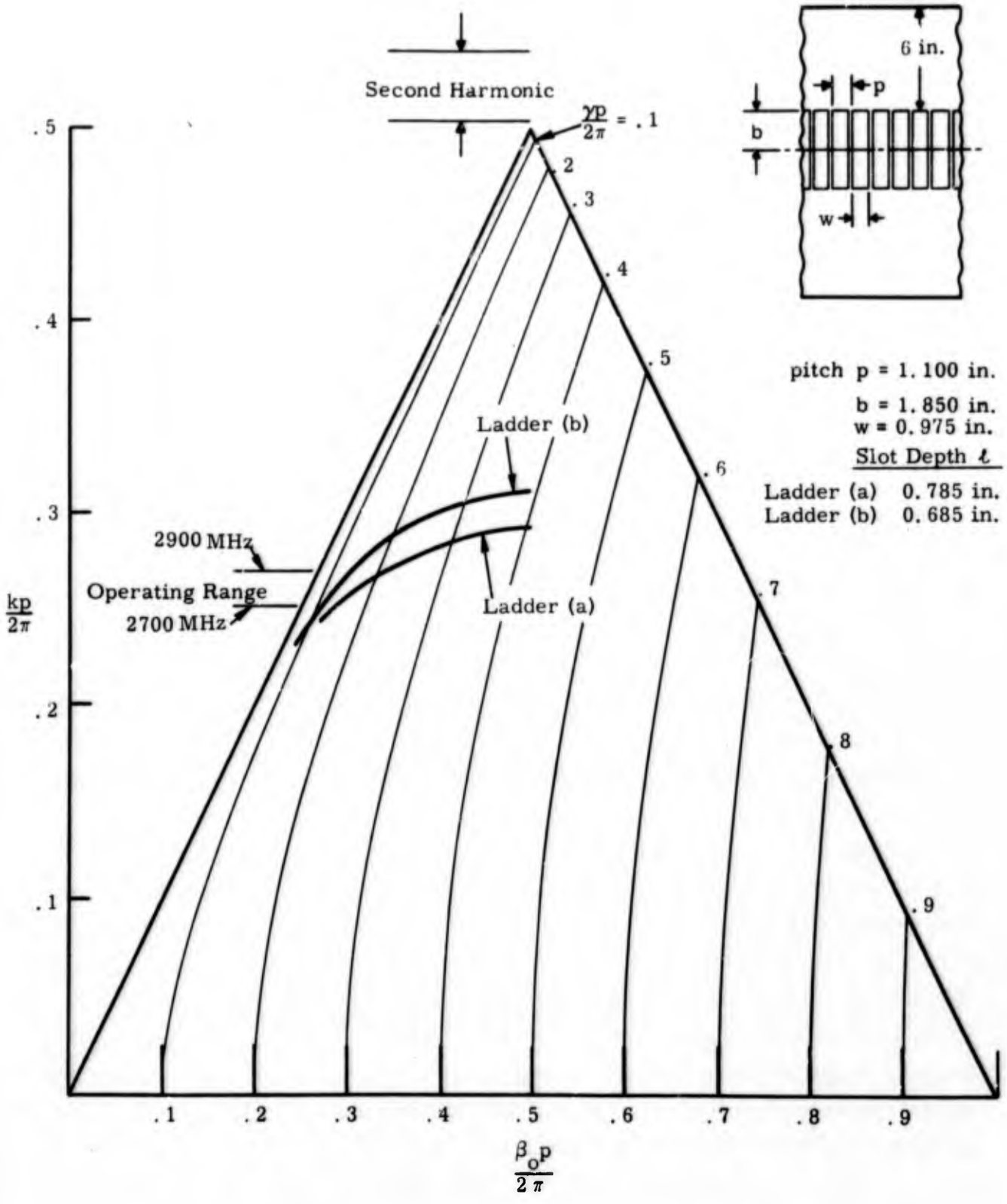

Figure 7-22. Normalized k-β characteristic of two thick ladders.

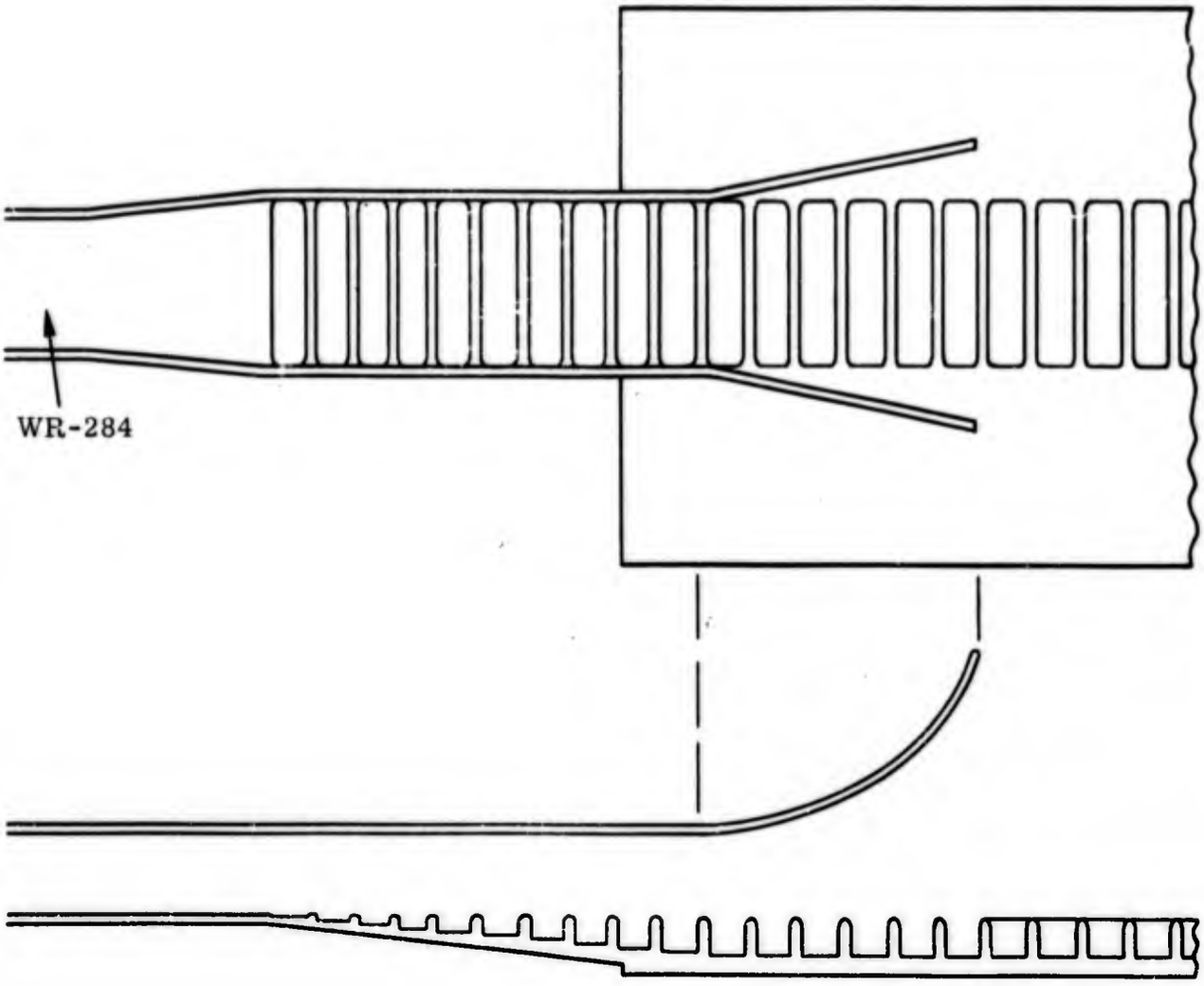

Figure 7-23. Preliminary design of transition to thick ladder (a) of figure 7-22.

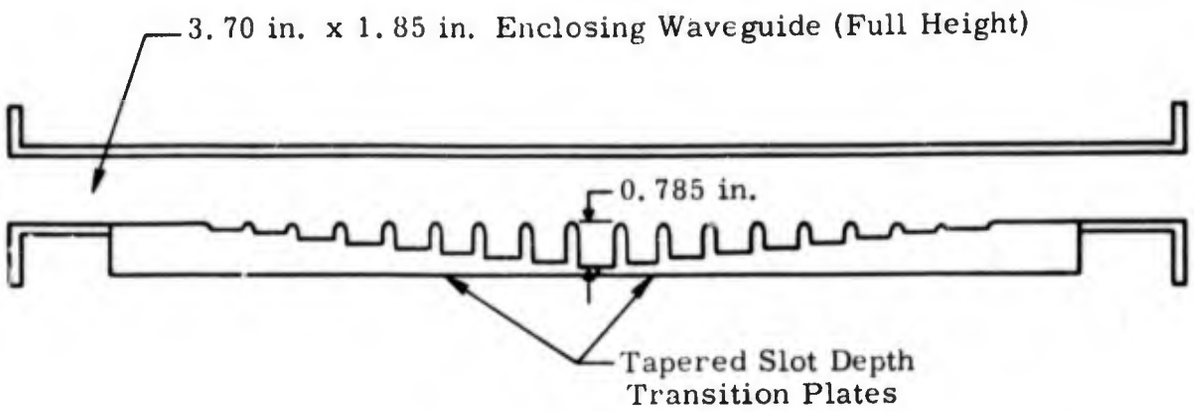

Figure 7-24. Tapered slot depth transition plates arranged for VSWR measurement.

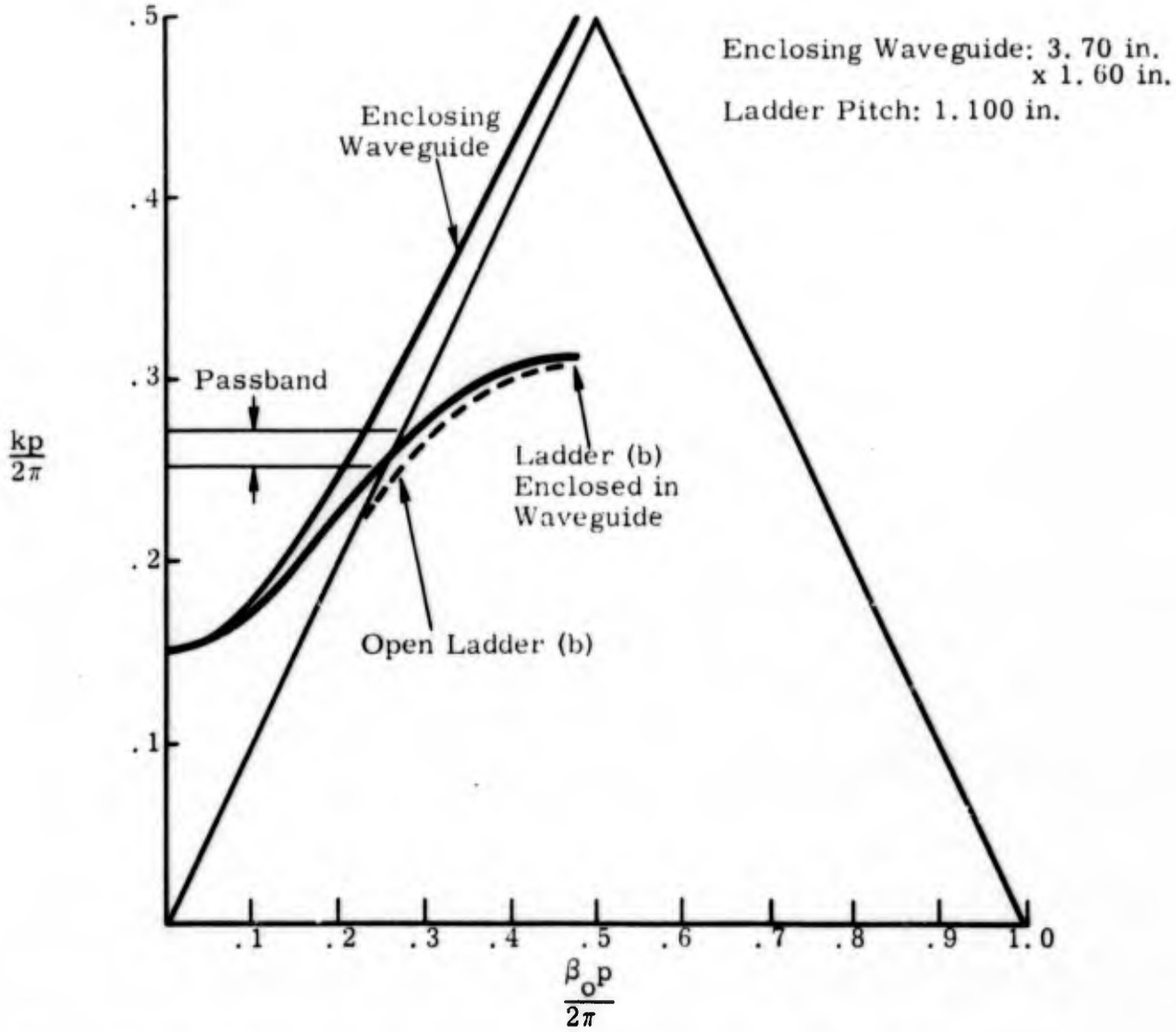

Figure 7-25. Comparison of propagation curves of ladder (b) enclosed in reduced height waveguide with open ladder and enclosing waveguide.

subsequent reflection could account for the high VSWR. Simply because the higher order modes appear to be present when the closed ladder is resonated does not mean that the modes are necessarily launched in the tapered transition. However, this possibility exists.

The pitch normalized k-β curve for the shallower slot ladder is shown as curve (b) in figure 7-22. While $\gamma\lambda$ for this curve is only 30 percent higher than that of the FTLI-6, the group velocity is about 0.5 c, or about 67 percent higher. When this ladder was enclosed in a full height waveguide and resonated, the first spurious resonances occurred slightly above the middle of the design passband. A 14 percent reduction in the height of the enclosing waveguide then moved the spurious responses to well above the passband. Figure 7-25 shows the measured propagation characteristic of the closed ladder.

Impedance measurements were made on a short section of ladder (b) enclosed in waveguide as shown in figure 7-26. Difficulty in making a good termination in the short space available required measurement of the VSWR of two junctions rather than one. However, the VSWR of one junction could be estimated from the resulting Smith chart plot. High VSWRs and an irregular plot were encountered in the upper half of the passband when the enclosing waveguide was full height. This indicated that it is not only desirable but necessary to suppress the higher order waveguide modes. The 14 percent reduction in enclosing waveguide height resulted in a regular impedance plot. The impedance appeared to be fairly constant at 1.4 times the waveguide impedance over the passband.

Although this was an encouraging result and indicated that a broadband tapered slot depth transition could be achieved, an attempt was made to achieve an abrupt match between the closed ladder and the reduced height waveguide. Since the impedance of the closed ladder is higher than that of the waveguide, the ladder should be moved closer to the enclosing waveguide wall. Doing this with the structure of figure 7-26 seems inadvisable since there would then be a large capacitive obstacle at the junction which would probably lower the power handling capacity. Instead, a test piece was constructed as shown in figure 7-27. Now the ladder begins in

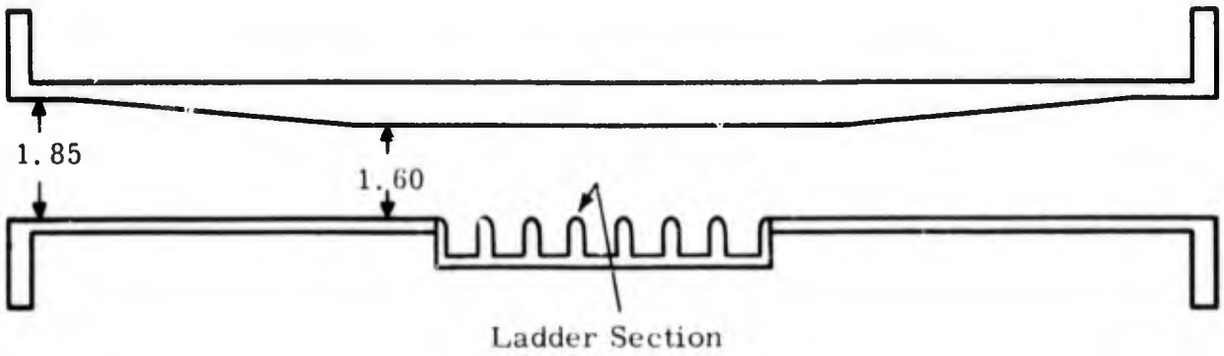

Figure 7-26. Test piece for closed ladder impedance measurement. Ladder begins at center of web.

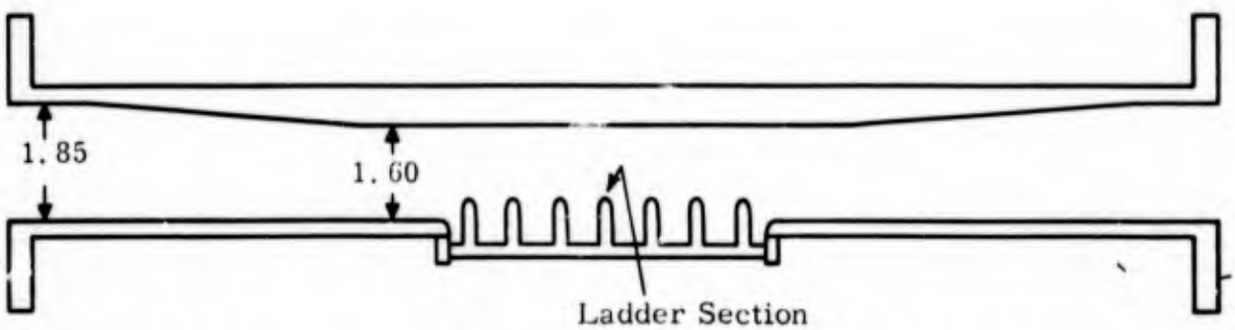

Figure 7-27. Test piece for closed ladder impedance measurement. Ladder begins at center of slot.

the middle of a slot. Provision was made for adjusting the depth of insertion of the ladder into the waveguide. With a ladder insertion depth of 0.27 in. the real part of the impedance matched the waveguide impedance at the center of the operating band. A small inductive iris was required to match out excess capacitance at the junction. The VSWR of the structure of figure 7-27 was less than 1.10 over the design passband. It should be noted that two junctions contribute to the VSWR.

With the achievement of this abrupt impedance match, it was decided to abandon the tapered slot depth transition between the waveguide and the closed ladder because of the saving in overall transition length.

The structure of figure 7-27 was tested on an FPS-6 transmitter in the laboratory. The spacing between the ladder and the waveguide wall was 1.33 in. Breakdown occurred at a peak power level of 0.69 Mw at atmospheric pressure and 0.0072 duty. Burns could be seen on the first three webs, and on the rounded end of the waveguide at the junction, with maximum burning on the first web. No burns could be seen on the waveguide wall. This might have been an indication of corona due to excessive currents on the webs with subsequent breakdown between the webs. In any event the breakdown power level was disappointingly low, and the solution seemed to be an increase in web thickness. Accordingly, new ladders were designed with fully rounded quarter-inch webs. While this work was in process, tests of ladder and transition loss were started.

Since a match had been achieved between dominant mode waveguide and a closed thick ladder propagating in a unique slow mode, attention was concentrated on the horn design. The first horn design tested is shown in figure 7-28(a). The horn aperture was made large to reduce the amount of lost energy due to finite size to a negligible level (less than 0.001 db according to figure 3-9). The loss measurements with and without an 18 pitch straight section are shown in figure 7-29. The curves represent smoothed values. The actual data varied around the curves because of the measurement technique, which was measurement of the short circuited VSWR, and the proximity of the horns, which permits periodic reinforcement or cancellation of the energy propagated on the circuit by radiated energy. Nevertheless,

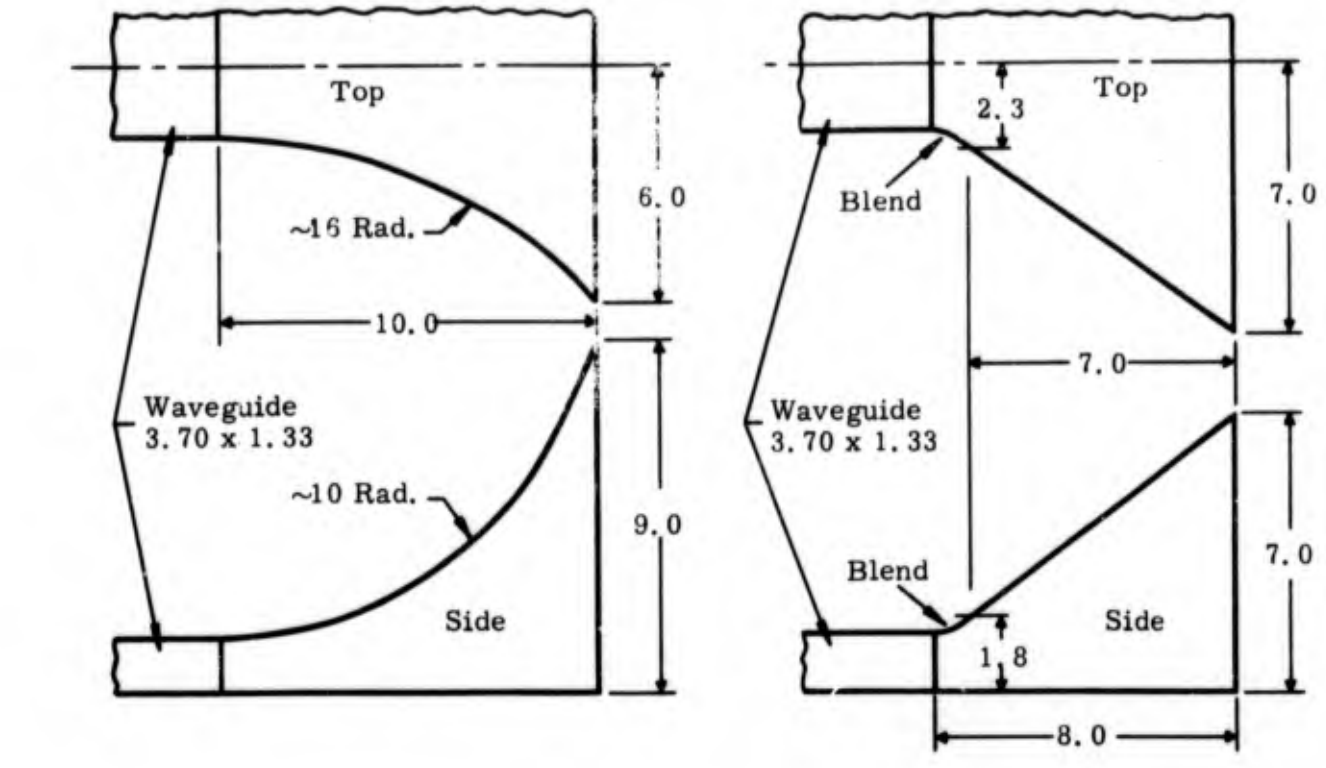

(a) (b)

Dimensions are in inches.

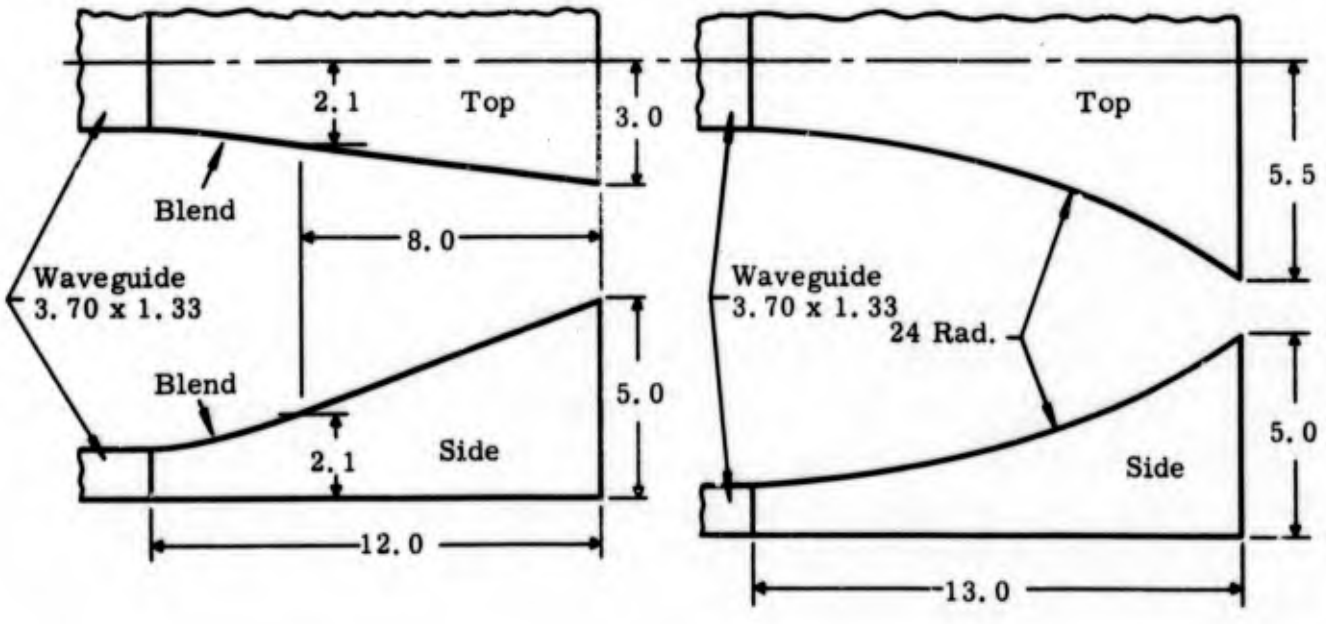

(c) (d)

Figure 7-28. Test horns.

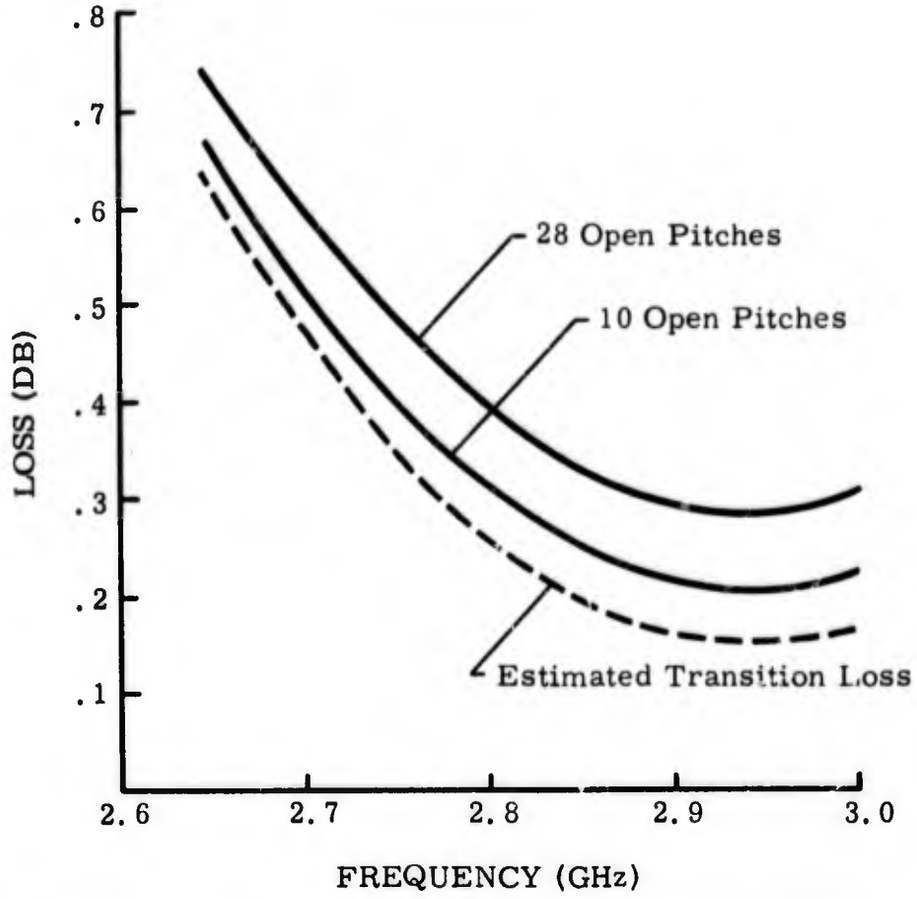

Figure 7-29. Filter loss with horns of figure 7-28(a).

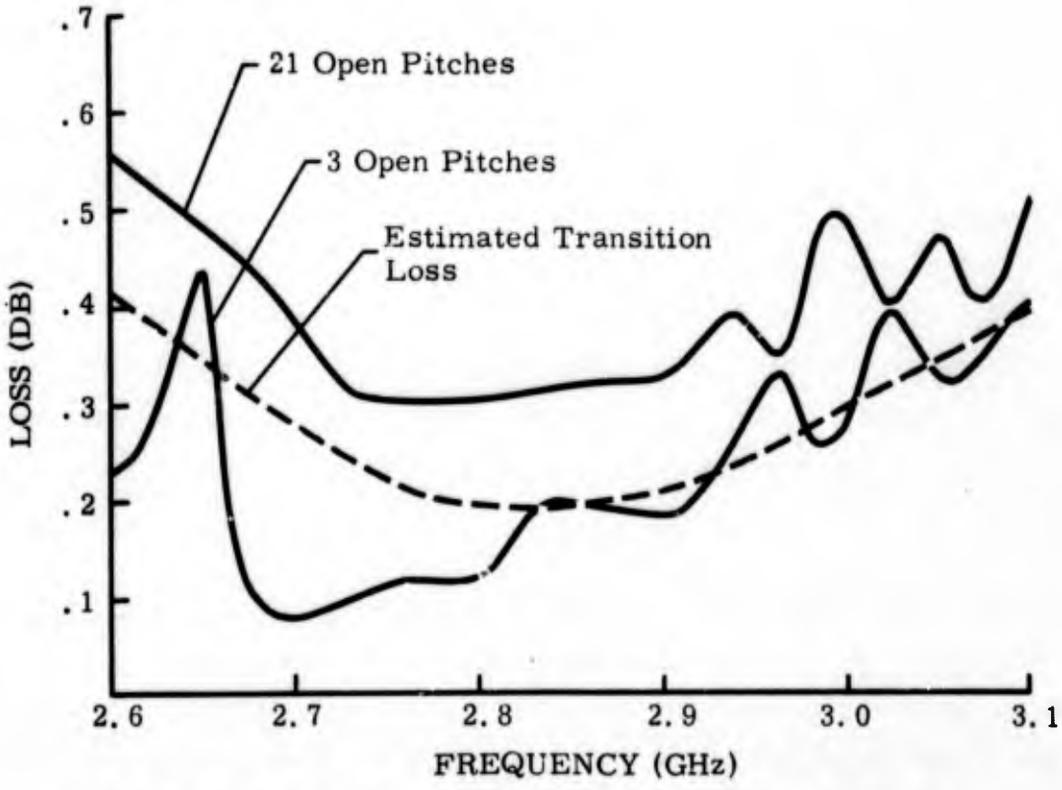

Figure 7-30. Filter loss with horns of figure 7-29(d).

these curves permitted a rough estimate of the loss due to the transitions which is also shown in figure 7-29. This transition loss is roughly comparable to the FTLI-6 transition loss shown in figure 4-5, but it is somewhat broader band, i.e., it does not increase as rapidly with decreasing frequency and γ.

The approximately 0.1 db loss due to the 18 pitch straight section is fairly constant over the measurement band rather than increasing rapidly with frequency as the FTLI-6 ladder loss does (figure 4-5). This could be attributed in part to the remoteness of the forbidden region, which is quite close to the operating band of the FTLI-6.

The transition loss shown in figure 7-29 was believed to be due to a too rapid increase in the horn dimensions. The horns shown in figure 7-28(b) were then tried. These horns are comparable in scale dimensions to those of the FTLI-6 but differ in having a blended junction with the enclosing waveguide. The loss measurements were about the same as before which seemed to indicate the need for an even more gradual change in horn dimensions. Accordingly, the aperture was made smaller to permit a more gradual taper as shown in figure 7-28(c). The aperture height should still contribute relatively little loss (less than 0.01 db) on the basis of finite size. The results at first were worse than before which almost led to the conclusion that the horn design had indeed been optimized on the FTLI-6. However, in order to see if the aperture width had been made too narrow, the sides of the horn were extended about 3 in. along the line of the taper, with a large improvement in transmission. New horns were built to the design shown in figure 7-28(d), which has greater aperture width and the same aperture height as the horn of figure 7-28(c). The length was increased slightly to ensure that the change in horn dimensions was sufficiently gradual.

The loss of these horns was measured by substitution, both with and without an 18 pitch straight ladder section, and is shown in figure 7-30. The waviness of the trace without the 18 pitch section is probably due to radiation at low frequencies, since the horn apertures were only 3 pitches apart. At high frequencies the waviness is probably due to the instrumentation. Smoothing

these curves permitted a rough estimate of the loss due to the transitions which is also shown in figure 7-29. This transition loss is roughly comparable to the FTLI-6 transition loss shown in figure 4-5, but it is somewhat broader band, i.e., it does not increase as rapidly with decreasing frequency and γ.

The approximately 0.1 db loss due to the 18 pitch straight section is fairly constant over the measurement band rather than increasing rapidly with frequency as the FTLI-6 ladder loss does (figure 4-5). This could be attributed in part to the remoteness of the forbidden region, which is quite close to the operating band of the FTLI-6.

The transition loss shown in figure 7-29 was believed to be due to a too rapid increase in the horn dimensions. The horns shown in figure 7-28(b) were then tried. These horns are comparable in scale dimensions to those of the FTLI-6 but differ in having a blended junction with the enclosing waveguide. The loss measurements were about the same as before which seemed to indicate the need for an even more gradual change in horn dimensions. Accordingly, the aperture was made smaller to permit a more gradual taper as shown in figure 7-28(c). The aperture height should still contribute relatively little loss (less than 0.01 db) on the basis of finite size. The results at first were worse than before which almost led to the conclusion that the horn design had indeed been optimized on the FTLI-6. However, in order to see if the aperture width had been made too narrow, the sides of the horn were extended about 3 in. along the line of the taper, with a large improvement in transmission. New horns were built to the design shown in figure 7-28(d), which has greater aperture width and the same aperture height as the horn of figure 7-28(c). The length was increased slightly to ensure that the change in horn dimensions was sufficiently gradual.

The loss of these horns was measured by substitution, both with and without an 18 pitch straight ladder section, and is shown in figure 7-30. The waviness of the trace without the 18 pitch section is probably due to radiation at low frequencies, since the horn apertures were only 3 pitches apart. At high frequencies the waviness is probably due to the instrumentation. Smoothing

this trace and applying the estimated ladder loss of about 0.1 db for 18 pitches yields the dashed curve which represents the estimated transition loss. It should be noted that the insertion of ladder sections may involve losses due to misalignment or poor junctions, and that these losses would not necessarily be representative of a well assembled filter. The assembly of the horn by welding caused a dishing in of the top of the horn so the desired shape was not completely achieved. However, figure 7-30 does indicate a great improvement in transition efficiency. The loss is less than 0.1 db per transition over a wide frequency range, which meets the project goal.

The VSWR was measured for each of the loss tests and was found to be essentially the same as that determined by the test piece of figure 7-27 regardless of the horn configuration. This was as expected because all of the horns began gradually. In this respect the transition designs meet the project goal of 1.06 VSWR. Two bends had been constructed using the thin web design. These bends were designed according to the criteria developed on the previous program (ref 2, pp 7-3 to 7-6). Loss measurements were taken with these bends. Figure 7-31 shows the loss obtained with a 25-in., radius bend 25 pitches long. Two horns of the type shown in figure 7-28(d) were used, and the measurements were taken both with and without an 18 pitch straight section, which introduced approximately 0.1 db loss that was consistent with previous measurements. Subtracting the estimated transition loss from the measured data results in the actual loss of the bend. This was far in excess of the predicted loss, which is the sum of the relative bending loss calculated in accordance with reference 2 and the loss corresponding to the length of the bend (approximately 0.14 db). The reason for this disparity is that the previous theory in effect treats all loss as occurring at the beginning of the bend and does not take into account the magnitude of the central angle of the bend, only the radius and the circuit γ. Therefore, the same relative bending loss is predicted regardless of whether the bend is short or long in terms of arc length. This seemed intuitively wrong. Since bent circuits were being designed for the thick web ladder, it was essential to determine the permissible bending radius and arc length, lest the resulting filter be useless because of excessive loss. Since time did not permit a theoretical study of bending loss an

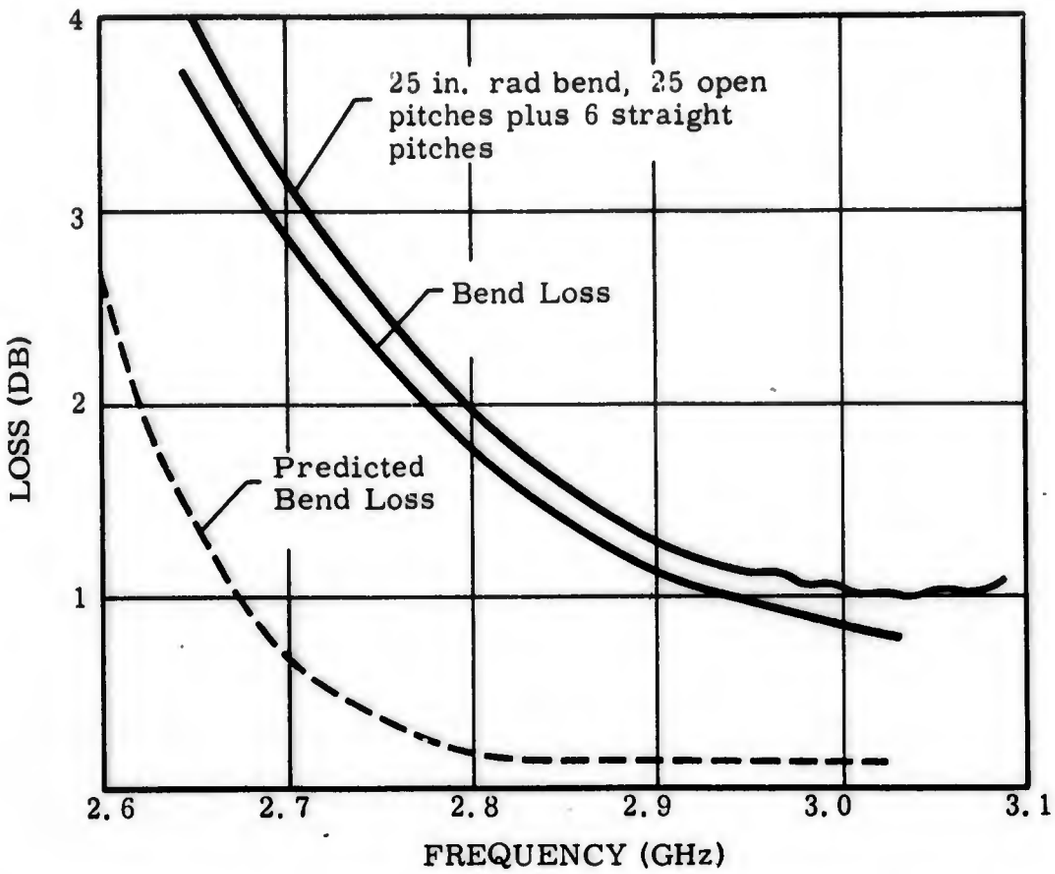

Figure 7-31. Measured bend loss compared to predicted loss.

empirical approach was followed. The loss data of figure 7-31 and corresponding data for a 13-in. radius bend of 18 pitches were compared. A dimensionless function was sought which would agree with the two sets of data, taking into account the variation of the transmission constants with frequency as well as the dimensions. The following equation seemed to fit the observed loss

$$\text{Bending Loss} = e^{\left[-0.8\sqrt{\frac{R\gamma}{\theta}}\left(\frac{\gamma}{k}\right)^3\right]} \qquad (7.5)$$

where R is the bending radius and θ is the angle of bending. This equation was used to predict the loss of a 96-in. radius bend having an arc length of 60 in. This bend would be sufficient in a filter configuration to position apertures 5-in. high out of sight of each other. The predicted bending loss decreases smoothly from 0.58 db at 2.7 GHz to 0.13 db at 2.9 GHz. This was considered excessive, and therefore, the design of the thick web ladder was modified by decreasing the slot depth to 0.735 in. in order to increase γ, particularly at the low frequency end of the band. The k-β characteristic of this design is approximately midway between the curves of figure 7-22. The relatively small increase in web thickness seemed to have little effect. With this ladder design the predicted bending loss was 0.22 db to 0.08 db over the passband. This still seemed marginal for good filter performance. However, it was recognized that equation 7.5 was based on very little data. Accordingly, parts were ordered for two bends of 96 in. radius and only 39.60 in. arc length (36 pitches). If the actual bending loss turned out to be higher than predicted, then one bend and a straight section might be used to provide the desired isolation between the horn apertures.

An enclosed test ladder was constructed to determine the spacing required for a good impedance match and to test high power capability. The test piece operated without breakdown on the laboratory FPS-6 transmitter up to a peak power level of 1.31 Mw at 0 psig. This time burns could be seen on the waveguide wall opposite the webs. The spacing between the ladder and the wall was 1.30 in. The optimum matching dimension was found to be 1.40 in. This would indicate that the breakdown level in the matched test piece would be about 1.4 Mw. Since the FPS-6 system is pressurized

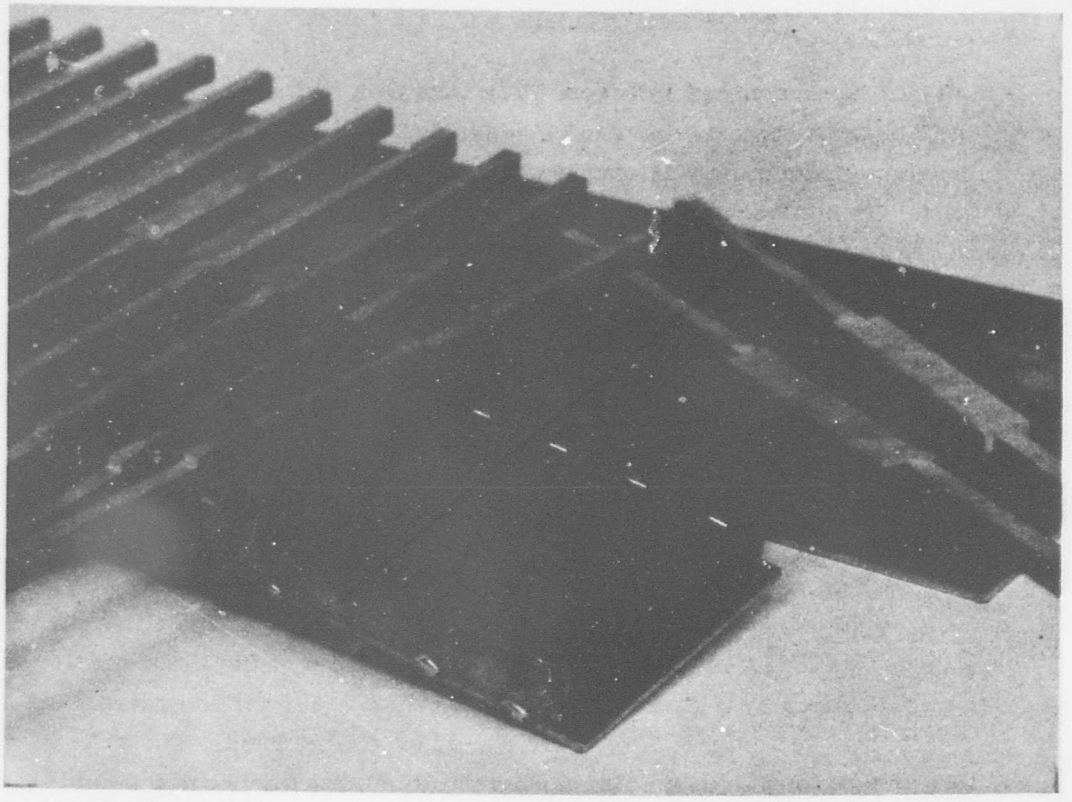

Figure 7-32. Pre-brazing assembly of thick ladder filter.

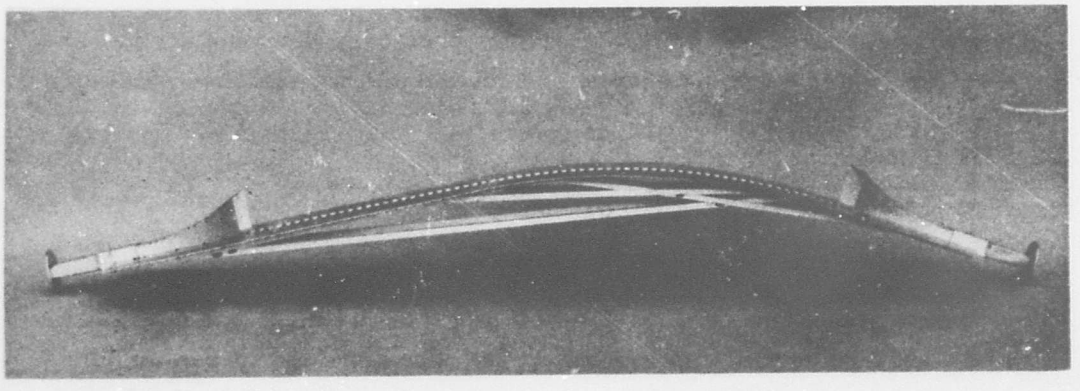

Figure 7-33. Completed thick ladder filter assembly.

to 30 psig, the measured breakdown level indicates that the transition should be suitable for system application without either an increase in system pressure or the use of a high strength dielectric gas.

The new thick web parts were received in the last month of the program, and sections were quickly assembled and brazed. Figure 7-32 shows a detail of the pre-brazing assembly. The horn has the same design dimensions as that of figure 7-28(d). A photograph of the completed filter assembly is shown in figure 7-33. Figure 7-34 shows the important dimensions. The filter was designed to incorporate the ladder and ground planes as part of an enclosing assembly strong enough to permit pressurization. The trusses were added to permit handling and testing prior to construction of the rest of the pressure container.

Passband loss was measured without absorbers. The results are shown in figure 7-35. The loss was 0.4 db or less over the passband, and the filter could be applied for even wider passbands. The loss contributions of the various parts of the filter are hard to determine because of the difficulty encountered in aligning the parts. Eliminating this source of error would have required repeated assemblies and tests which time did not permit. However, if the transitions perform only as well as that estimated in figure 7-30, the losses in the open ladder, including the bending loss, are considerably lower than previous measurements and calculations would indicate. In all probability the transition performance was improved because of better assembly. The average slot depth on straight sections was 0.740 in. and on the bend it was 0.750 in. instead of the design value of 0.735 in. The bend radius was 108 in. instead of 96 in. These deviations may account in part for the low loss. They indicate that a slightly deeper slot may work even better.

The VSWR of the filter is shown in figure 7-36. The maximum VSWR in the FPS-6 operating range is 1.28 at 2.71 GHz but this is the highest value over the remainder of a 600 MHz or 20 percent range. This is not as good as the match obtained with the test piece and appears to be due to dimension changes during the welding assembly and to the increased slot depth. There should be no difficulty in obtaining a good match.

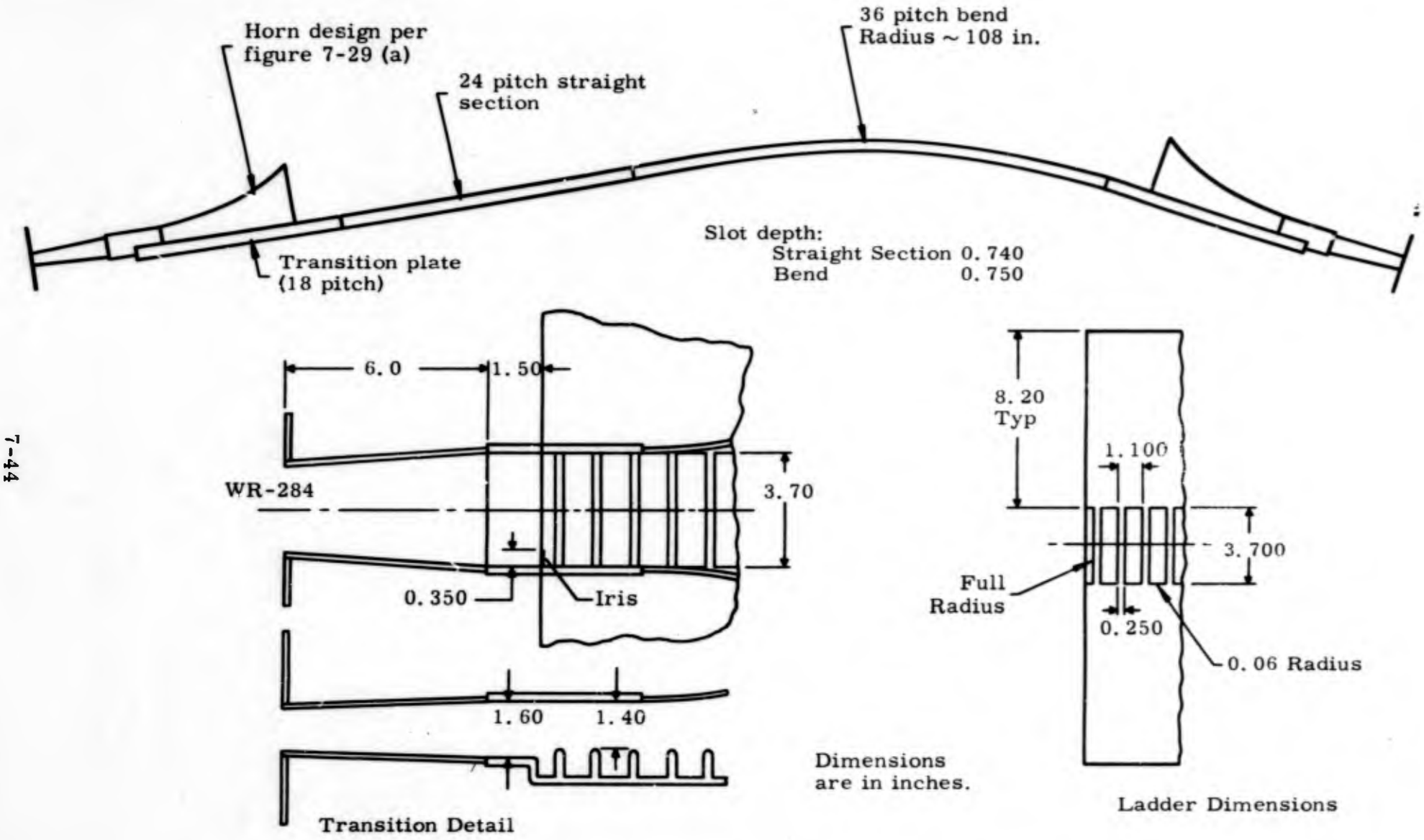

Figure 7-34. Dimensions of completed thick ladder filter assembly.

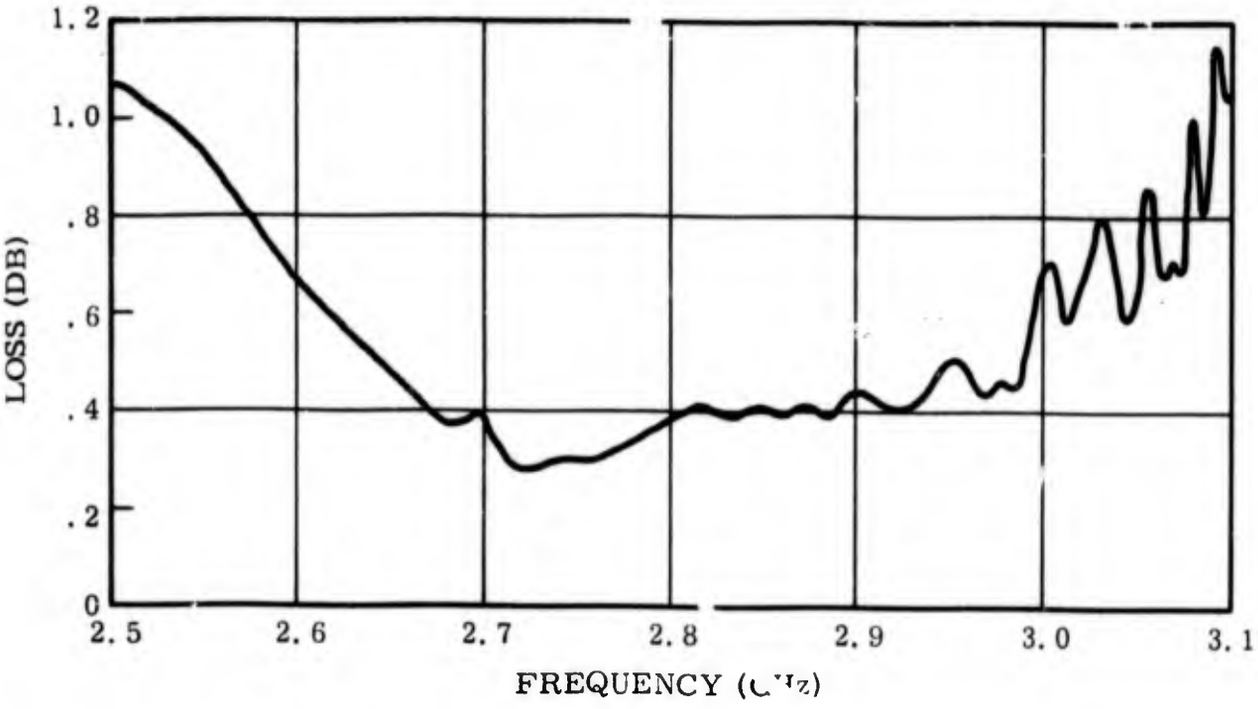

Figure 7-35. Passband loss of thick ladder filter.

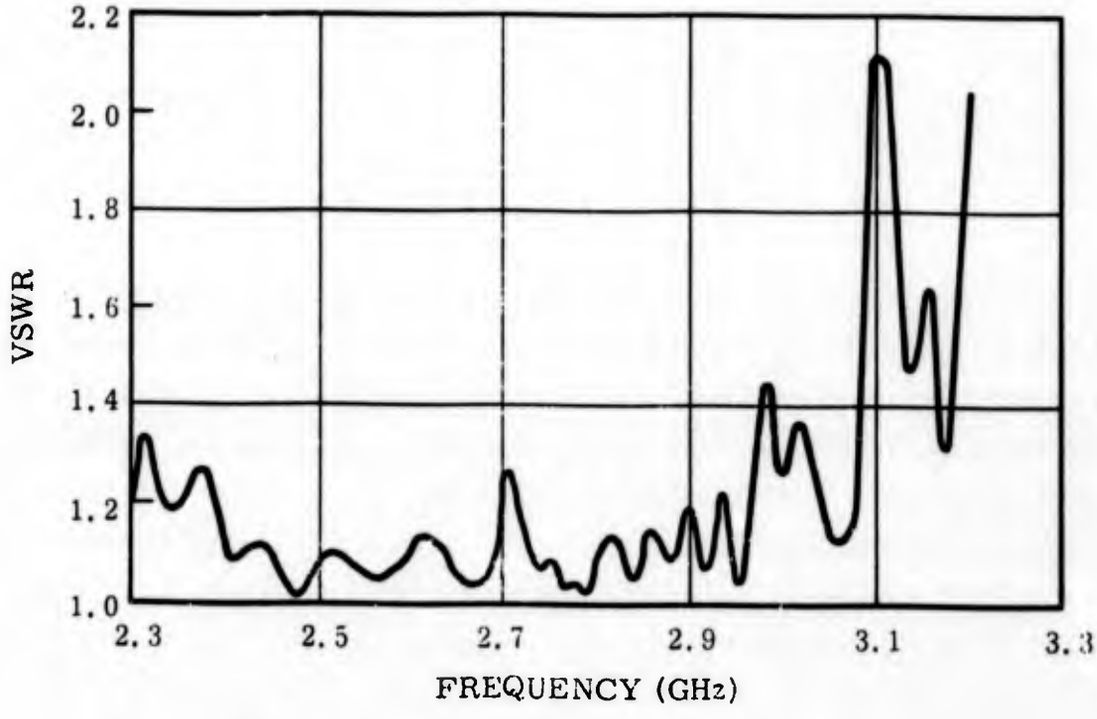

Figure 7-36. Passband VSWR of thick ladder filter.

Stopband attenuation of the TE_{10} and TE_{01} modes was measured and is shown in figure 7-37. It can be seen that high attenuation is achieved 0.3 GHz (about 10 percent) above the passband. The low attenuation spike corresponding to the apex of the allowed region triangle occurs at 5.3 GHz which indicates that the pitch was sufficiently coarse for second harmonic attenuation. These measurements were made without an absorbing medium or a container. When absorbing material was placed around the filter, the attenuation level decreased due to reflections. This was not unexpected since this effect has been noticed on every ladder filter. It is a natural consequence of the low γ of ladder filters which prohibits the severe bending required to provide a high degree of isolation between the apertures. This problem had been given some thought and it seemed that the first approach should be to provide an absorber that looks as much like free space as possible. Since the spurious energy radiating from the ladder or from the transmitting aperture will probably have fields in all directions, the absorber should attenuate fields in any direction. This implies that the absorbing medium should have bulk resistivity as opposed to films or thin vanes which attenuate some field orientations more than others. Redwood spears were tried in the hope that if the impedance mismatch to an incident plane wave were too severe, the spears would tend to scatter the energy. However, the reflections from an array of redwood spears were very noticeable in terms of increased transmission at stopband frequencies. Moving the array about showed that the energy was radiated in lobes from the aperture – the most distinct lobe being in a direct line from the throat of the horn. Carbon impregnated sponge rubber spears were also tried with the same result. These spear arrays had been designed for low reflection at L-band frequencies. However, the poor results indicated that a finer spear structure would not help too much. What is apparently required is a material which is so "soft" in the microwave sense, that incident waves see neither a resistive nor a dielectric-constant mismatch. A hair or very open sponge material would seem to be suitable. Preliminary experiments using rubberized horsehair sprayed with aquadag indicated that this approach may be valid. These homemade absorbers did not provide sufficient attenuation to prevent reflections from a conductor concealed behind them until the material was 6 in. thick or more. Heavier carbon loading might increase their attenuation, but it is possible that the impedance mismatch

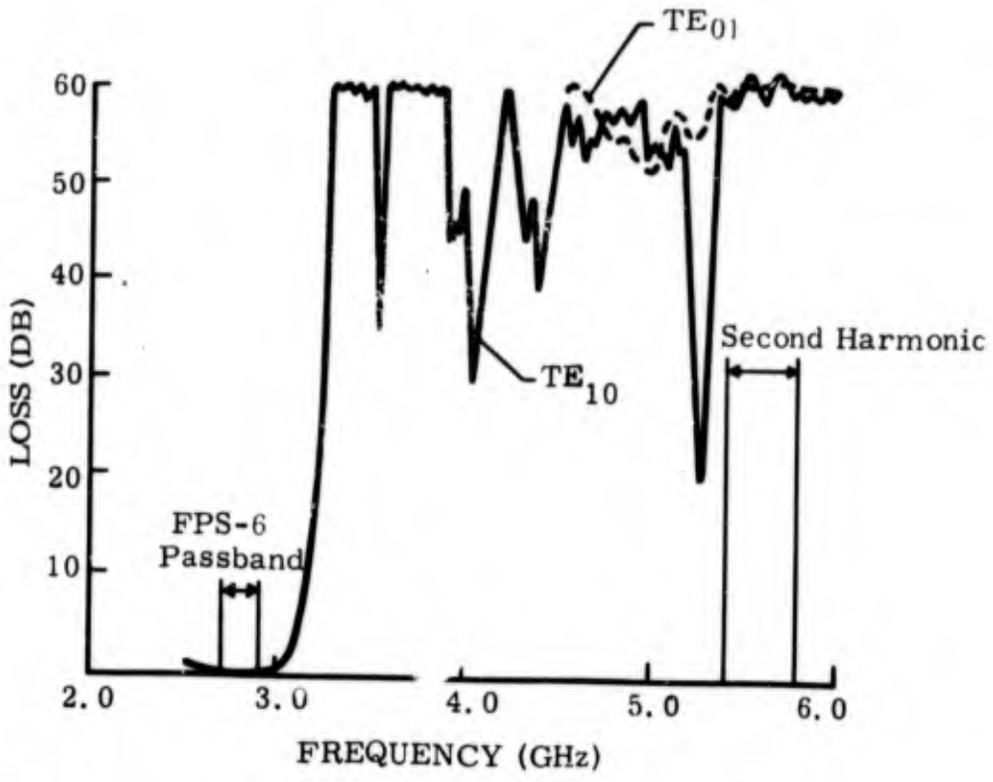

Figure 7-37. Attenuation of thick ladder filter without absorbers.

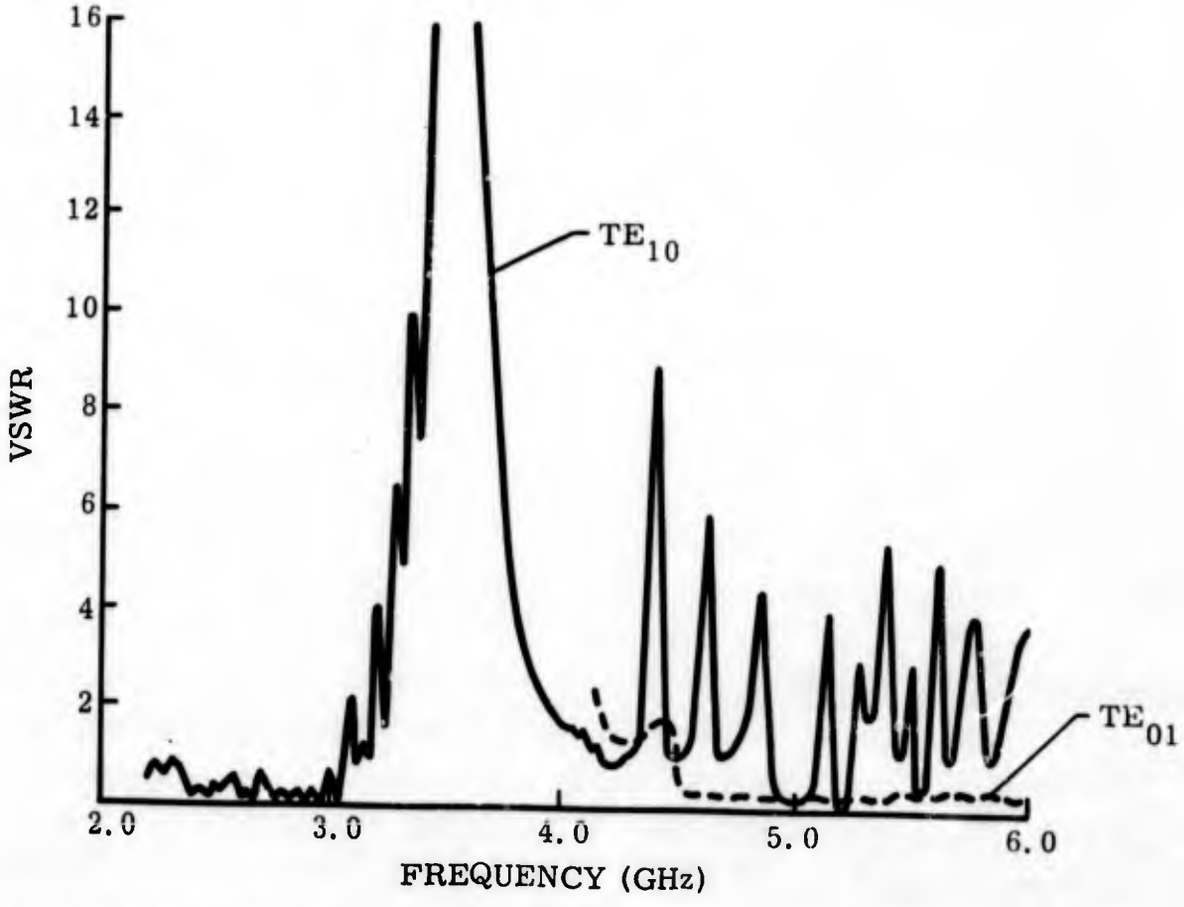

Figure 7-38. Passband and stopband VSWR of thick ladder filter.

may then become more severe, resulting in a higher reflection level. Graduated bulk resistivity may be the answer. The absorbers that have been mentioned might be objected to on the basis that they are only suitable for low power. However, the low loss achieved with the thick ladder filter and the large volume into which this lost energy is scattered indicates that the power absorbed by any given part of the absorbers need not be too high for organic materials. The location of the absorbers, as well as their material, should probably be taken into consideration in the design of a useful ladder filter. With respect to passband loss, it appears that no excess loss is introduced if the absorbers are located outside the transition aperture.

Stopband measurements above 6.0 GHz were not made because all previous experience with open periodic structures indicates that the loss will remain high except for the effects of reflection from the absorbers or the container. However, the stopband VSWR was measured in the TE_{10} and TE_{01} modes up to 6.0 GHz and is shown in figure 7-38. The TE_{10} mode VSWR is generally low except for periodic spikes every 500 MHz or so. These spikes are probably caused by the closed ladder, but no analysis was performed. The TE_{01} mode VSWR is negligible above 4.6 GHz. These results represent an improvement over those obtained with the FTLI-16, an L-band filter developed under the previous program and using transitions similar to the FTLI-6 (ref 2, pp 8-4). The improvement is somewhat surprising because the previous transitions were more "open," that is, the enclosing waveguide was full height and the slots were relatively small. It is conjectured that the tapering of the slot depth in those transitions caused a broadband effect. If so, the decision to use an abrupt junction had an unforeseen favorable consequence.

3. SUMMARY. The development of the thick ladder filter followed the basic concepts of the general periodic filter and transition studies and represents a verification of their validity. In particular, application of the general periodic filter concepts resulted in a ladder structure having a very wide operating band resulting from the use of large slots having sufficiently high values of γ at low frequencies, and by the use of a uniform array of slots, rather than an interdigital array, which permitted a high upper cutoff frequency without the excessive loss due to having a forbidden

region near the passband. The design procedure also results in high attenuation at the second harmonic, due to the choice of pitch, without excessive bending.

Application of the basic transition concept, primarily the concept of separating the functions of the various junctions, led to a transition design which utilized most of the basic ladder bandwidth. Separation of functions permitted the obtaining of a good match, which is a basic microwave art, without having to be concerned about high launching efficiency, which was provided by a different portion of the transition. Achieving high launching efficiency, even for relatively low values of γ, was aided by the treatment of the horn as a transformer for a closed slow mode rather than as an antenna.

The thick ladder filter and its transitions, therefore, demonstrated low loss and VSWR over a wide passband, with high power handling capability, and high attenuation of the harmonics if suitable absorbers of moderate power capacity can be designed.

A particular shortcoming of the thick ladder filter is its size. Its cross section is large, resulting from the circuit size and the low values of γ, compared to the fundamental mode helix, which are typical of any periodic array of elements. Its length is great, partly because of the transition horn, and partly because of the large bending radius and line length required to isolate the transition apertures. It is believed that the horn length is near minimum for high launching efficiency. The tapered waveguide transition could probably be reduced at least 50 percent without sacrifice of bandwidth by means of standard design procedures. It appears that significant shortening could come about only by the use of a coupled junction, such as that shown in figure 5-1, to provide greater horn isolation. The experiments of tight coupling of identical thick ladder circuits indicate that such a coupled junction might be achieved without excessive sacrifice of bandwidth.

VIII. CONCLUSIONS AND RECOMMENDATIONS

The work of this project was comprised of the following parts:

General studies

1. Transitions (section III)
2. Filters (section IV)
3. Coupled lines (section V)

Design studies of specific circuits

4. Helix filters (section VI)
5. Ladder filters (section VII)

Each of these parts is discussed below.

1. TRANSITION STUDIES (section III). The design of transitions is aided by the conceptual separation of functions. This leads to a block diagram which, in its most general and apparently useful case, includes an enclosed periodic structure. The highest launching efficiency over the greatest frequency range is obtained when the periodic structure is continuous through an aperture which is sufficiently large that the fields on the closed periodic structure are almost the same as those on the open periodic structure. Making a transition from a fast transmission line to a closed periodic structure can be treated as an ordinary impedance matching problem, especially if only one mode can propagate on either side of any junction. The critical part of the overall transition is the change from the narrowly enclosed periodic structure to the large aperture. This change must be gradual enough to maintain the desired slow mode without conversion to fast modes as the enclosing dimensions increase, with consequent loss by radiation.

2. FILTER STUDIES (section IV). The impedance of periodic structures was studied. It was concluded that an impedance formula based on either the predominant spatial harmonic or an equivalent circuit would not be

valid at both ends of a period structure enclosed by a conductor whose distance from the periodic structure varies from very close to quite remote. However, the trend of impedance change in such a region may perhaps be predicted. A general design procedure for harmonic filters employing ladders or periodic arrays of identical elements was necessary before transitions could be designed. These procedures involved spacing the elements so that second harmonic frequencies cannot propagate in any mode. This eliminates the need for excessive bending to provide high attenuation of harmonic frequencies with consequent passband loss. It also eliminates staggered or interdigital arrays from consideration as filters. The elements of the array can then be optimized for the most favorable k-β characteristics in the passband.

3. COUPLED LINE STUDIES (section V). Coupled line junctions can be employed to provide more efficient transitions or for improved filter performance. Uniform tight coupling of identical circuits appears to be feasible and may serve the purpose of improved filter performance. Nonuniform coupling can be employed where it will assist the transition function. It appears to be particularly useful when coupling dissimilar periodic structures, and led to the design of specific filter configurations.

4. HELIX FILTER STUDIES (section VI). Transitions between helices and coaxial lines may be divided into two classes: those in which the coaxial line dimensions are comparable to the helix dimensions (class 1), and those in which the coaxial line is considerably smaller than the helix (class 2). In both cases the application of the general transition studies, particularly the requirement that the propagating modes at any junction be unique, leads to useful transitions.

A filter configuration employing a helix propagating in the fundamental spatial harmonic mode and utilizing nonuniform coupling to a higher order waveguide mode was investigated. The transitions showed the potential usefulness of nonuniform coupling but indicated that considerable effort would be required to achieve low loss over adequate bandwidths.

A filter configuration employing a helix propagating in the second (m = -1) spatial harmonic mode and utilizing nonuniform coupling to the circularly polarized dominant mode in circular waveguide was designed and tested. This filter demonstrated good stopband attenuation and the lowest passband loss yet attained in any helix filter. The operating bandwidth was adequate for radar applications. The transitions demonstrated higher power capability than any other helix transition and would be suitable for high power radar application without increasing the dielectric strength of the medium. Its main disadvantage was its size which was due in part to the relatively great length of the transitions.

An operational filter utilizing a helix operating in the fundamental spatial harmonic mode was constructed. Its transitions were similar to the right angle, waveguide-to-helix transition used on the breadboard filter developed on the previous program. These transitions provided only slightly improved performance with respect to passband width and VSWR. The passband power capacity was considerably improved, but the transition breakdown level is still a limiting factor in this filter configuration and required that the filter be filled with a high dielectric strength gas. The passband loss of the filter was about 0.8 db, of which less than 0.2 db was contributed by the transitions. In spite of this loss and the consequent heating, the filter operated satisfactorily in an FPS-6 radar. No deterioration of radar performance was encountered; no breakdowns occurred; and spurious outputs, except for those too close to the fundamental frequency, were eliminated. Study of the loss mechanisms indicates that the passband loss could be lowered by about 0.2 db by a better method of supporting the helix.

5. LADDER FILTER STUDIES (section VII). Ladder filters were studied and designed following the guidelines of the general filter studies with the exception of the interdigital open slot ladder, which was shown to be analogous to a helix, particularly when its k-β characteristic is optimized. The Yagi filter (array of posts on a ground plane) was studied because of the possibility of obtaining low passband loss using transitions that had no closed periodic structure. The transitions assisted in obtaining high stopband attenuation but their passband loss was excessive, providing another instance of the failure of launchers employing radiation in the passband.

A thin ladder filter was constructed which showed the feasibility of its transitions. Better passband performance could probably have been obtained had the ladder dimensions been optimized, but stopband attenuation measurements showed that the "two-sidedness" of this structure is a disadvantage in filter applications.

A thick ladder filter for FPS-6 radar application was designed following the guidelines of the general filter studies and the general transition studies. The critical part of the transition design was determining the correct shape of the horn for minimum radiation. The filter configuration was determined in part by the dimensions of the required bend. A new design procedure was required to ensure that the loss due to bending was acceptable in high power radars. The transition demonstrated a peak power capacity of 1.3 Mw at atmospheric pressure, which was the highest power capacity of any of the transitions developed on the program and appoaches that of waveguide. The loss of the filter was about 0.4 db over the FPS-6 operating range, and the transition was well matched over a 20 percent frequency range. The stopband VSWR was generally low. High attenuation was measured in a stopband extending upward in frequency from below the second harmonic. However, the very limited bending that a ladder filter can be subjected to requires that the stopband absorbers be practically reflectionless. Development of such absorbers having moderate power absorption capacity is required for attaining the full stopband attenuation this design is capable of. The use of a coupled junction employing tight, uniform coupling should also provide high stopband attenuation and result in a shorter filter.

IX. REFERENCES

1. C. K. Birdsall and R. M. White, "Experiments with Forbidden Regions of Open Periodic Structures: Application to Absorptive Filters," IEEE Trans MTT, vol 12, No. 2, pp 197-202, March 1964.

2. R. H. Stone, et al, Suppression of Spurious Emissions, RADC-TDR-64-227, Contract AF 30(602)-2955, General Electric Company Palo Alto Tube Operation, TIS-R64ELM247-4, May 1964.

3. L. Young, "Waveguide 0-db and 3-db Directional Couplers as Harmonic Pads," Microwave J, May 1964.

4. H. M. Barlow and J. Brown, Radio Surface Waves, Oxford, Clarendon Press, 1962.

5. S. A. Schelkunoff, Electromagnetic Waves, New York, Van Nostrand, 1943.

6. R. E. Collin, Field Theory of Guided Waves, New York, McGraw-Hill, 1960.

7. J. S. Cook, R. Komphner, and C. F. Quate, "Coupled Helices," Bell System Tech J, vol 35, p 127, 1956.

8. W. H. Louisell, "Analysis of the Single Tapered Mode Coupler," Bell System Tech J, vol 34, p 853, 1955.

9. S. E. Miller, "Coupled Wave Theory & Waveguide Applications," Bell System Tech J, vol 33, p 661, 1954.

10. J. S. Cook, "Tapered Velocity Couplers," Bell System Tech J, vol 34, p 807, 1955.

11. T. S. Chu and N. R. Kilcoyne, "The Excitation of a Dielectric-Rod Antenna by a Helix," IEEE Trans PG Ant and Prop, p 416, July 1961.

12. C. M. Chu, "Propagation of Waves in Helical Wave Guides," J Appl Phys, vol 29, No. 1, pp 88-99, Jan 1958.

13. G. E. Ragan, ed., Microwave Transmission Circuits, Rad Lab Series, vol 9, New York, McGraw-Hill, 1951.

14. I. D. Olin, "Dielectric Transformers," Electronics, p 146, Dec 1955.

15. E. W. Ehrenspeck and H. Poehler, "A New Method for Obtaining Maximum Gain from Yagi Antennas," IRE Trans PG Ant and Prop, pp 379-386, Oct 1959.

16. S. B. Cohn, "Bones from the Technical Graveyard," Microwave J, p 15, Nov 1961.

APPENDIX A

HELIX BREAKDOWN

INTRODUCTION. RF breakdown in the helical slow wave circuit is considered. Expressions are derived for various electric field components for the helix made of finite diameter round wire. The maximum values of the electric fields occurring next to the helix wires are related to the dimensions of the helix, the frequency, and the power flow along the circuit. These expressions are evaluated for a number of different helix filter designs. Peak breakdown powers are obtained for fundamental mode operation, using the assumption that the breakdown field is 30 kv/cm, an order of magnitude value characteristic of air at standard temperature and pressure. Average power has not been considered here, as power limitations due to average heating (and only radiation cooling) have been treated elsewhere by Bryant and White (ref 1).

RELATING THE SHEATH HELIX TO THE WIRE HELIX. As a first approximation one may consider the fields on a sheath helix, i.e., an infinitesimally thin cylinder which conducts current only at an angle ψ with respect to the normal to its axis. On such a structure the field expressions are particularly simple, no spatial harmonics exist, the different modes are uncoupled, and expressions for the relevant impedances have been computed and are readily available in the literature, e.g. Pierce, (ref 2).

A realistic calculation, however, must take account of the actual periodicity of the helix and the fact that the helix wires have a finite diameter. Connection between the actual case and the idealized sheath model can be made (for helices subject to certain dimensional restrictions) by the use of Chu's (ref 3) analysis and calculations. This analysis, involving conformal transformation of circular or elliptical wire helices into equivalent developed tape helices, permits appropriate corrections to be made to the sheath helix results. Results are immediately applicable to the fundamental mode of operation. Additional computation is required for modes other than the fundamental; only the fundamental is discussed here.

Connection between the properties of the actual wire helix and the sheath helix is made via normalizing ratios derived by Chu (ref 3). For a given impedance K_i (such as the transverse impedance or the longitudinal impedance on the helix axis or at its periphery) a factor R_{K_i} relates the impedance K_i of the developed wire helix to the corresponding impedance K_i of the developed sheath helix. R_{K_i} is defined as

$$R_{K_i} \equiv \frac{(K_i) \text{ developed wire helix}}{(K_i) \text{ developed sheath helix}}$$

If one then assumes (with Chu) that the ratio of the impedance of the true wire helix to that of the true sheath helix is the same as the ratio of the impedance of the developed wire helix to the developed sheath helix, one obtains the true impedance by multiplying the factor R_{K_i} times K_i for the true sheath helix. In this way, formal connection can be made between the properties of the idealized sheath helix and those of a true wire helix.

FIELDS ON THE SHEATH HELIX. Two electric fields, normal to the helix wires, might be considered as possible causes of breakdown. One of these is the radial electric field, E_r, given inside and outside the helix by Pierce (ref 2), appendix 2, equations 24, 30

$$|E_r(a)| = B \frac{\beta}{\gamma} I_1 (\gamma a) \qquad \text{(inside)}$$

$$|E_r(a)| = B \frac{\beta}{\gamma} \frac{I_o (\gamma a)}{K_o (\gamma a)} K_1 (\gamma a) \qquad \text{(outside)}$$

where a is the helix radius, B is an amplitude constant, β is the axial propagation constant, γ is the radial separation constant, and I_o, I_1, K_o, and K_1 are modified Bessel functions of the first and second kinds, of orders 0 and 1. The other field of interest is the electric field in the cylindrical surface directed normal to the direction of conduction,

$$|E_n(a)| = \frac{B I_o (\gamma a)}{\cos \psi}$$

The preceding equation is obtained by adding the projections of the axial and circumferential fields in a direction normal to those in the direction of

conduction, viz,

$$E_n = E_z \cos \psi - E_\phi \sin \psi$$

where $E_z = B\, I_o(\gamma a)$

$$E_\phi = -B\, I_o(\gamma a)\left(\frac{1}{\cot \psi}\right)$$

In order to evaluate the amplitude factor B for a given sheath helix it is convenient to refer to the interaction impedance on the axis of the helix, at $r = 0$,

$$K(0) \equiv \frac{E_z^2(0)}{\beta^2 P},$$

where P is the power flow along the z axis*. B is given in terms of K(0) by

$$B = \frac{E_z(0)}{I_o(0)} = [K(0)\beta^2 P]^{1/2},$$

where we have used the fact $I_o(0) = 1$. K(0) is given in terms of the helix dimensions by

$$K(0) = (\beta/\beta_o)(\gamma/\beta)^4\, F^3(\gamma a)$$

where β_o = free space propagation constant and F(γa) is the function defined and plotted by Pierce (ref 2) in figures 3 and 4.

The ratio of the fields $(E_r)_{\text{inside}}/(E_r)_{\text{outside}}$ is equal to $I_1(\gamma a)K_o(\gamma a)/I_o(\gamma a)K_1(\gamma a)$, shown in figure 1. For the range of γa useful in the present filter design, the radial field outside is considerably larger than that inside, so we shall not consider further the field inside the helix.

---

*K(0) as originally defined by Pierce (ref 2) has been used rather than the later definition $E_z^2(0)/2\beta^2 P$ because computed values of Pierce will be used later here.

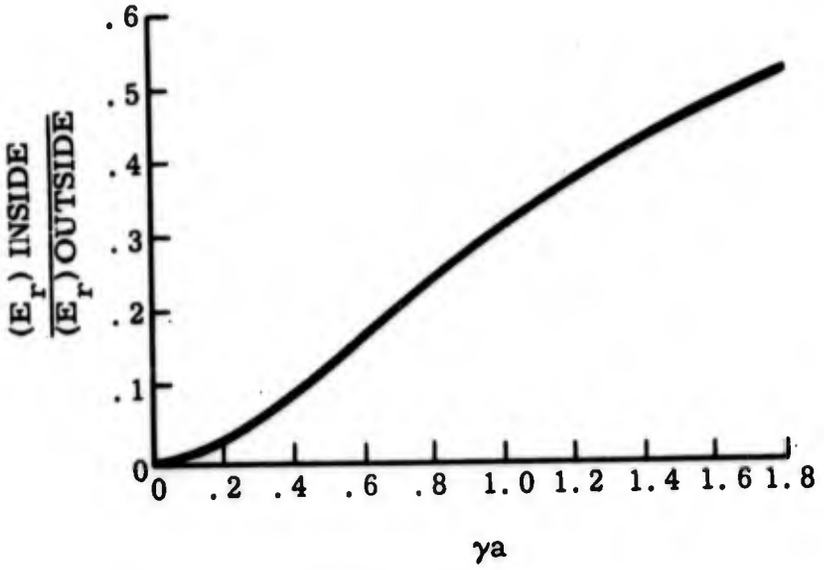

Figure 1. Ratio of radial field inside to radial field outside sheath helix versus γa.

Equating the fields (E_r) outside and E_z to a breakdown field E_b results in the following expressions for breakdown power as given by the sheath helix fields:

$$P_{br} = \frac{E_b^2}{K(0)\,\beta^2\,I_o^2(\gamma a)} \cdot \left(\frac{\gamma}{\beta}\right)^2 \frac{K_o^2(\gamma a)}{K_1^2(\gamma a)} \qquad (E_r) \text{ outside field}$$

$$P_{bn} = \frac{E_b^2}{K(0)\,\beta^2\,I_o^2(\gamma a)} \cdot \cos^2 \Psi \qquad (E_n) \text{ field}$$

CORRECTIONS TO THE SHEATH HELIX FIELDS. Chu's analysis of propagation on helices is based on a developed helix model; he states that the results should be essentially free of error due to neglect of dispersion and of the unequal distribution of current on the conductors inside and outside the mean diameter provided:

1. helix circumference is several times guide wavelength $[2\pi a > \lambda_o(v/c)]$

2. thickness of the helix wire is small compared to helix radius a. These conditions are not satisfied by all helices having possible use in filters, as will be seen later. But for helices which do meet these conditions we may correct the power levels obtained for a sheath helix as follows.

The normalizing factor R_T applies to the transverse helix impedance, K_T, defined for the sheath as (Pierce, ref 2, p 30)

$$K_T = \frac{V_T^2}{2P}$$

where $V_T = -\int_a^\infty E_r dr$ = transverse helix voltage.

The normalizing factor R_T thus is equal to the factor by which $E_r^2(a)$ must be multiplied to yield the true square of the radial field at point B on the true helix. Thus the power for breakdown due to the radial fields on the true helix is given by

$$P_{br}^1 = \frac{E_b^2}{K(0)\, R_T\, \beta^2\, I_o^2(\gamma a)} \cdot \left(\frac{\gamma}{\beta}\right)^2 \frac{K_o^2(\gamma a)}{K_1^2(\gamma a)}$$

The normalizing factor R_K applies to the interaction impedance on the axis of the helix. The field $E_z^1(0)$ for a true wire helix is given by

$$E_z^1(0) = [K(0)\, R_k\, \beta^2\, P]^{1/2}$$

The point A (fig. 2) on the developed wire helix transforms to A^1 on the tape, and an exponential field decay away from the developed circuit is assumed. The maximum field normal to the true wire, lying in the cylindrical surface containing the helix, will occur at A; hence the corrected field E_n^1 will be

$$E_n^1(a) = [K(0)\, R_k\, \beta^2\, P]^{1/2}\, I_o(\gamma a)/\cos \psi$$

and the corresponding breakdown power will be

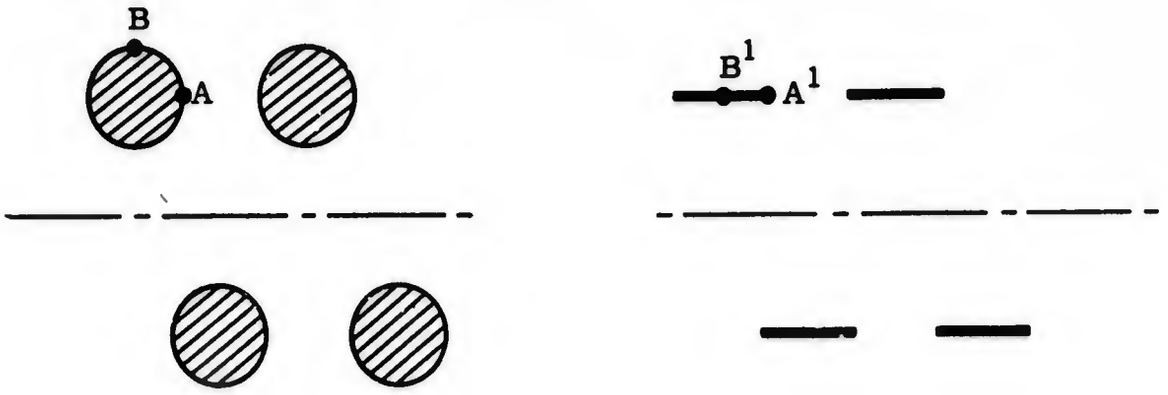

Figure 2. True wire and developed tape helices showing corresponding points.

$$P_{bn}^{1} = \frac{E_b^2}{K(0)\, R_k\, \beta^2\, P\, I_o^2(\gamma a)} \cos^2 \psi$$

The breakdown power for a helix could be determined by substituting into the equations for P_{br} and P_{bn} and taking the smaller of the two values. The maximum power handling capability would be obtained by adjusting helix parameters so that $P_{br}^{1} = P_{bn}^{1}$.

If (γa) and ψ were held constant, as well as β and $(\frac{\gamma}{\beta})$, breakdown would be equally likely between the wires and in the radial direction provided

$$\frac{R_T}{R_k} = \frac{1}{\cos^2 \psi} \left(\frac{\gamma}{\beta}\right)^2 \frac{K_o^2(\gamma a)}{K_1^2(\gamma a)}$$

The ratio on the left is a function of the ratio wire diameter/pitch, as well as the parameter s, where

$$s = \beta_o a \cos \psi$$

For round wires with wire diameter/pitch less than 0.5, an increase in diameter results in a decrease in R_T, increase in R_k, and a decrease in R_a, the normalizing factor for attenuation. These trends are physically reasonable: as helix wires get larger there is an increasing concentration of electric field between wires and, for the same total energy storage, a decrease in the strength of the radial fields; at the same time there is a decrease in the current density on the wire surface and hence less attenuation.

For the helices examined for filter application it is not possible to satisfy the equation above with any wire diameter less than about half the pitch. For reference the ratio R_T/R_k is plotted for the extreme values of s in figure 3.

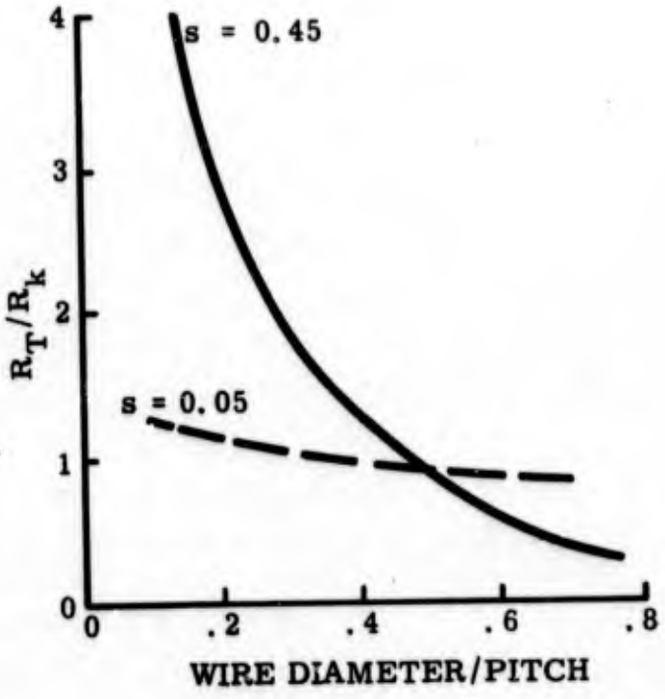

Figure 3. R_T/R_k versus wire diameter/pitch (based on figs. 6 and 11, Chu, ref 2).

RESULTS FOR SPECIFIC HELICES. Before computing P^1_{br} and P^1_{bn} for particular helices let us consider the two conditions listed earlier for applicability of the Chu analysis. For five helices of interest (identified

in tables A-I and A-II) comparison is made in table A-III to determine which helices satisfy the conditions (1) $2\pi a > \lambda_o(v/c)$, and (2) wire diameter < radius a.

Table A-I. S-Band Filter Helix Parameters

Designation	$\frac{v_p}{c}$ approx	Pitch Angle (deg)	Pitch (in.)	ID (in.)	OD (in.)	Wire Diam (in.)	Operating Point at 2.8 Gc: $\frac{kp}{2\pi} = \frac{fp}{c}$ approx	$\frac{\beta p}{2\pi}$ approx	$\frac{\gamma p}{2\pi}$ approx	γ (nepers/in.)
Fast	0.5	30	1.25	.562	.812	.125	.295	.53	.45	2.26
Slow	.35	20.5	.885	.625	.875	.125	.22	.55	.51	3.62

Table A-II. Helix Filter Designs for Operation at Lower $\frac{\gamma p}{2\pi}$

Helix	$\frac{v_p}{c}$ approx	Pitch Angle (deg)	Pitch (in.)	Mean Diam (in.)	Operating Point at 2.8 Gc: $\frac{kp}{2\pi} = \frac{fp}{c}$	$\frac{\beta p}{2\pi}$ approx	$\frac{\gamma p}{2\pi}$ approx	γ (nepers/in.)
1.	.645	40.2	1.125	.425	.267	.36	.24	1.34
2.	.5	30	.885	.488	.210	.36	.30	2.12
3.	.35	20.5	.520	.442	.123	.30	.28	3.39

Table A-III. Comparison of Helix Parameters

Helix	$2\pi a$ (in.)	$(\lambda_o)_{2.8\,Gc}(v/c)$ (in.)	Wire Diameter (in.)	Radius a (in.)
A	2.36	1.61	.125	.375
B	2.16	2.32	.125	.344
1	1.34	3.17	.125	.212
2	1.53	2.41	.125	.244
3	1.39	1.73	.125	.221

The first inequality is satisfied only by helix A, while the second inequality is satisfied by all the helices. For this reason values of P^1_{br} and P^1_{bn} are listed in table A-IV only for helix A as an indication of the possible severity of the reduction in power handling capacity. To compare the helices, the

values of K(0), P_{br}, and P_{bn} derived from sheath helix fields are listed in table A-IV.

Table A-IV. Power Handling Capabilities of Various Helices

Helix	K(0) (ohms)	P_{br} (10^6w)	P_{bn} (10^6w)	P^1_{br} (10^6w)	P^1_{bn} (10^6w)
A	47.0	1.74	3.04	0.74	6.75
B_1	68.2	2.46	6.37	--	--
1	53.1	2.16	15.8	--	--
2	102	1.68	5.41	--	--
3	136	0.78	2.04	--	--

The effect of R_T is generally to reduce the breakdown power level due to radial fields below P_{br}, and that of R_k is to increase the breakdown power level due to normal fields above P_{bn}. As noted earlier, an increase in the quantity wire diameter/pitch causes R_T to diminish and R_k to increase. For a value of about 0.4 for the ratio wire diameter/pitch, $R_T \approx R_k \approx 1$ and the breakdown power level would be equal to the values P_{br} as determined from the sheath helix fields. Thus, from the standpoint of breakdown, helices B_1 and 1 having large wire diameters appear most attractive, and they should have a breakdown power of about 2 to 2.5 x 10^6 watts under the conditions stated.

APPENDIX REFERENCES

1. J. H. Bryant and E. J. White, "Attenuation and Power-Handling Capability of Helical Radio-Frequency Lines," IRE-PGMTT, vol 1, no. 2, pp 33-38, Nov 1953 .
2. J. R. Pierce, Traveling-Wave Tubes, Van Nostrand, New York, 1950.
3. C. M. Chu, "Propagation of Waves in Helical Waveguides," J. Appl. Phys. vol 29, no. 1, pp 88-99, Jan 1958.

UNCLASSIFIED
Security Classification

DOCUMENT CONTROL DATA - R&D
(Security classification of title, body of abstract and indexing annotation must be entered when the overall report is classified)

1. ORIGINATING ACTIVITY (Corporate author) Varian Associates, 601 California Ave., Palo Alto, California 94304	2a. REPORT SECURITY CLASSIFICATION Unclassified 2b. GROUP N/A

3. REPORT TITLE
Transitions for Periodic Filters

4. DESCRIPTIVE NOTES (Type of report and inclusive dates)
Final Report - December 1964 to February 1966

5. AUTHOR(S) (Last name, first name, initial)
Rooney, John P.
Gerlack, Richard Z.
Mohr, Hans J.

6. REPORT DATE	7a. TOTAL NO. OF PAGES	7b. NO. OF REFS
May 1966	294	19

8a. CONTRACT OR GRANT NO.	9a. ORIGINATOR'S REPORT NUMBER(S)
AF30(602)-3556 b. PROJECT NO. 4540 c TASK NO: 454003 d.	66CA0260-4 9b. OTHER REPORT NO(S) (Any other numbers that may be assigned this report) RADC-TR-66-207

10. AVAILABILITY/LIMITATION NOTICES This document is subject to special export controls and each transmittal to foreign governments or foreign nationals may be made only with prior approval of RADC (EMLI), GAFB, N.Y. 13440.

11. SUPPLEMENTARY NOTES	12. SPONSORING MILITARY ACTIVITY
None	Rome Air Development Center (EMCVI-1) Griffiss Air Force Base, New York 13440

13. ABSTRACT

This report presents the results of a one year program for improvement of transitions between conventional transmission lines and periodic filters suitable for use on high power radars. General studies of transitions, filter design, and coupled periodic circuits are described. These studies were applied to a variety of filter structures and resulted in:

1. A novel higher order mode helix filter of high power capacity.
2. A helix filter that operated satisfactorily in tests on an FPS-6 radar.
3. A ladder filter with low loss and VSWR over a wide passband and high power capability.

The validity of the general studies was demonstrated and their conclusions can be extended to several applications of a variety of periodic structures.

DD FORM 1 JAN 64 1473

UNCLASSIFIED
Security Classification

UNCLASSIFIED
Security Classification

14. KEY WORDS	LINK A		LINK B		LINK C	
	ROLE	WT	ROLE	WT	ROLE	WT
RF Filter						
Open Periodic Filter						
Transitions						
Periodic Circuit						
Microwave Filter						
High Power						
Low Pass Filter						

INSTRUCTIONS

1. ORIGINATING ACTIVITY: Enter the name and address of the contractor, subcontractor, grantee, Department of Defense activity or other organization *(corporate author)* issuing the report.

2a. REPORT SECURITY CLASSIFICATION: Enter the overall security classification of the report. Indicate whether "Restricted Data" is included. Marking is to be in accordance with appropriate security regulations.

2b. GROUP: Automatic downgrading is specified in DoD Directive 5200.10 and Armed Forces Industrial Manual. Enter the group number. Also, when applicable, show that optional markings have been used for Group 3 and Group 4 as authorized.

3. REPORT TITLE: Enter the complete report title in all capital letters. Titles in all cases should be unclassified. If a meaningful title cannot be selected without classification, show title classification in all capitals in parenthesis immediately following the title.

4. DESCRIPTIVE NOTES: If appropriate, enter the type of report, e.g., interim, progress, summary, annual, or final. Give the inclusive dates when a specific reporting period is covered.

5. AUTHOR(S): Enter the name(s) of author(s) as shown on or in the report. Enter last name, first name, middle initial. If military, show rank and branch of service. The name of the principal author is an absolute minimum requirement.

6. REPORT DATE: Enter the date of the report as day, month, year; or month, year. If more than one date appears on the report, use date of publication.

7a. TOTAL NUMBER OF PAGES: The total page count should follow normal pagination procedures, i.e., enter the number of pages containing information.

7b. NUMBER OF REFERENCES: Enter the total number of references cited in the report.

8a. CONTRACT OR GRANT NUMBER: If appropriate, enter the applicable number of the contract or grant under which the report was written.

8b, 8c, & 8d. PROJECT NUMBER: Enter the appropriate military department identification, such as project number, subproject number, system numbers, task number, etc.

9a. ORIGINATOR'S REPORT NUMBER(S): Enter the official report number by which the document will be identified and controlled by the originating activity. This number must be unique to this report.

9b. OTHER REPORT NUMBER(S): If the report has been assigned any other report numbers *(either by the originator or by the sponsor)*, also enter this number(s).

10. AVAILABILITY/LIMITATION NOTICES: Enter any limitations on further dissemination of the report, other than those imposed by security classification, using standard statements such as:

(1) "Qualified requesters may obtain copies of this report from DDC."

(2) "Foreign announcement and dissemination of this report by DDC is not authorized."

(3) "U. S. Government agencies may obtain copies of this report directly from DDC. Other qualified DDC users shall request through

_____ ."

(4) "U. S. military agencies may obtain copies of this report directly from DDC. Other qualified users shall request through

_____ ."

(5) "All distribution of this report is controlled. Qualified DDC users shall request through

_____ ."

If the report has been furnished to the Office of Technical Services, Department of Commerce, for sale to the public, indicate this fact and enter the price, if known.

11. SUPPLEMENTARY NOTES: Use for additional explanatory notes.

12. SPONSORING MILITARY ACTIVITY: Enter the name of the departmental project office or laboratory sponsoring *(paying for)* the research and development. Include address.

13. ABSTRACT: Enter an abstract giving a brief and factual summary of the document indicative of the report, even though it may also appear elsewhere in the body of the technical report. If additional space is required, a continuation sheet shall be attached.

It is highly desirable that the abstract of classified reports be unclassified. Each paragraph of the abstract shall end with an indication of the military security classification of the information in the paragraph, represented as *(TS), (S), (C), or (U)*

There is no limitation on the length of the abstract. However, the suggested length is from 150 to 225 words.

14. KEY WORDS: Key words are technically meaningful terms or short phrases that characterize a report and may be used as index entries for cataloging the report. Key words must be selected so that no security classification is required. Identifiers, such as equipment model designation, trade name, military project code name, geographic location, may be used as key words but will be followed by an indication of technical context. The assignment of links, rules, and weights is optional.

UNCLASSIFIED
Security Classification